STUDIES OF ELECTRON CONTENT AT LOW LATITUDES

A THESIS

SUBMITTED FOR THE DEGREE OF

DOCTOR OF PHILOSOPHY

OF THE

GUJARAT UNIVERSITY

AHMEDABAD

BY

GAUTAM CHAND SETHIA

FEBRUARY 1980

PHYSICAL RESEARCH LABORATORY

AHMEDABAD 380009

INDIA

Dedicated

to

my uncle

LATE SHREE MULTAN MAL SETHIA

and

my father

LATE SHREE GHEWAR CHAND SETHIA

CERTIFICATE

I hereby declare that the work presented in this thesis is original and has not formed the basis for award of any degree of any university or institution.

(Gautam Chand Sethia)
Author

Certified by:

(R.G. Rastogi)

(H. Chandra)

Thesis Advisors

PREFACE

In the present investigations an attempt has been made to study some of the physical properties of the low latitude ionosphere and the plasmasphere. The study is based on the (a) ionosphere electron content derived from Faraday rotation measurements, made at a chain of stations covering almost entire Indian sub-continent during the period October 1975 - August 1976 using radio beacons from the geostationary satellite ATS-6 and (b) the plasmasphere electron content derived from simultaneous Faraday rotation and the group delay measurements made at a low latitude station Ahmedabad (23.0°N, 72.6°E, dip. lat. 18.6°N) during June, July 1976 and at a near equatorial station Ootacamund (11.4°N, 76.7°E, dip. lat. 3°N). It is worthwhile to note that the ionosphere electron content measurements using a geostationary satellite were made for the first time, at a chain of stations at low latitudes from magnetic equator to about 25°N dip lat. In addition the plasmasphere electron content measurements at low latitudes were not available so far; hence the current investigations on the plasmasphere form a new contribution to the subject. Various ionospheric and geophysical data have also been studied and used for interpretation, wherever necessary.

The total electron content (TEC) defined broadly as the number of free electrons in a column of unit cross-section extending through the ionosphere and above, can be measured by a

number of techniques out of which the Faraday rotation and the group delay techniques are of present interest. In the Faraday rotation technique, the angle of rotation of the plane of polarization of the radio wave is measured as it passes through the ionosphere whereas in the group delay technique, the difference in transit times of two radio waves, with different frequencies, across the medium is measured. It is important to note that the Faraday rotation angle is strongly dependent upon the longitudinal component of the earth's magnetic field whereas the dependence of the group delay on the earth's magnetic field is insignificant. The Faraday rotation technique, therefore, gives the ionosphere electron content N_F, upto an altitude of h_F (which is about 2000 km for low and mid-latitude stations and is about 1500 km for near equatorial station like Ootacamund) whereas the group delay technique gives the electron content N_T upto the satellite height. The difference in electron content measured by these two techniques i.e. $N_T - N_F$ gives the electron content above h_F, upto the satellite height along the ray-path. The electron content so obtained is usually termed as plasmasphere electron content (N_P). Keeping in view the errors involved in deriving N_F, for Ootacamund to ATS-6 geometry due to uncertainties in geomagnetic field models, the plasmasphere electron content has not been studied for this station. However, the difference of the N_T and N_F termed as the 'residual component' (N_R) for the Ootacamund measurements has been studied and may be considered as a rough

estimate of the plasmasphere content. The importance of the radio beacon studies of the plasmasphere has been realised only recently and not much work has undergone in this direction.

The lay-out of the thesis is as follows:-

The general introduction to the low and equatorial latitude ionosphere and the plasmasphere is given in the first chapter. Previous work about TEC studies at low latitudes and the plasmaspheric studies using in-situ and whistler measurements have been reviewed.

The second chapter describes the group delay and Faraday rotation techniques of electron content measurements. The calibration factors for these measurements, for the present satellite geometry have been described. Using actual electron density profiles over Kodaikanal and Jicamarca, the calculations of magnetic field factor calibration for Ootacamund to ATS-6 ray-path have been undertaken, and are described in detail. Lastly a description of the computations of elevation, azimuth, range, sub-ionospheric points and magnetic field factors, is given in the same chapter.

In the third chapter, the morphological studies like diurnal, seasonal, latitudinal and day to day variations of TEC at low latitudes has been described. A comparison has been made between electron contents N_F and N_T, obtained from Faraday rotation

and the group delay techniques respectively. The quiet time variations of the residual electron content (N_R) at Ootacamund and the plasmasphere electron content (N_P) at Ahmedabad, have been described and discussed in the same chapter.

The fourth chapter deals with the electron content studies in conjunction with the bottomside ionosonde data. The daily variation of equatorial TEC has been compared with the variations of many different parameters like equatorial N_mF_2, crest region TEC, topside electron content N_a, bottomside electron content N_b, slab-thickness τ, semi-thickness y_m, and the height of the peak F-region electron density h_m, etc. A detailed study of the slab-thickness of the equatorial ionosphere using both N_F and N_T data has also been undertaken and is described in this chapter.

The fifth chapter describes the influence of electrojet on the low latitude ionosphere. The role of electrojet in latitudinal distribution of TEC under different geomagnetic conditions and also in the anomalous semi-annual variation of TEC at low latitudes has been studied and discussed. Lastly the day to day variability of the low latitude ionosphere in conjunction with electrojet strength has been discussed.

The lunar tidal effects in the low latitude TEC and in the equatorial N_mF_2 and slab-thickness have been separated and studied in the sixth chapter. A brief summary of the previous work on lunar tidal effects in the F-region of the low latitude

ionosphere is also given in the same chapter.

The storm time effects on the low and equatorial latitude TEC and equatorial N_m have been described in the seventh chapter of the thesis. In addition the storm time effects on the residual electron content (N_R) at Ootacamund has been studied and discussed in terms of solar wind velocity and geomagnetic activity dependence of N_R.

The eighth chapter describes the numerical model for low latitude ionosphere TEC for different solar activity conditions. Its applications to satellite tracking systems have been described.

The conclusions of the present investigations are summarised in the last i.e. in ninth chapter. Some suggestions for the future work have also been included in this chapter.

It is sincerely hoped that the present work has made some contribution in the better understanding of the complex ionospheric and plasmaspheric processes; though it is being wished, keeping in view the Einstein's remark which says:

"Onething I have learned in a long life:
that all our science, measured against
reality; is primitive and childlike - and
yet it is the most precious thing we have".

(Gautam Chand Sethia)
Author

Certified by:

(R.G. Rastogi)

(H. Chandra)

ACKNOWLEDGEMENTS

The author expresses his deep sense of gratitude and indebtedness to Prof.R.G. Rastogi for introducing the author to the subject of this thesis and for his invaluable guidance, advice and encouragement throughout this study.

The author is sincerely grateful to Dr.H. Chandra for his active guidance, countless discussions and a number of constructive suggestions in the course of this work. The author owes him a special debt of thanks for his zeal in supervising the preparation of the thesis.

The author is thankful to Prof.M.R. Deshpande for encouragement, suggestions and many fruitful discussions during the course of this work. His willing encouragement helped the author a lot in getting through many critical moments.

The ATS-6 Ootacamund project was a joint undertaking of the Physical Research Laboratory, Ahmedabad, India and the Space Environment Laboratory, NOAA, Boulder, Colorado, USA. Thanks are due to Prof.K. Davies and his group for the collaboration and to Prof.G. Swarup and his group at the Radio Astronomy Centre, Ootacamund for facilities. The project was financially supported by NASA, USA and DOS, Government of India.

Thanks are due to Prof.J.A. Klobuchar for joint AFGL-PRL project of radio beacon studies at Ahmedabad and also to the authorities of all the ATS-6 collaborating institutions for their encouragement.

Thanks are also due to Mr.Banshidhar and Mr.N.M. Vadher for the installation and operation of the equipment at Ootacamund and also for developing and fabricating the polarimeters used at different collaborating institutions.

The ionospheric and the geomagnetic data from the Indian Institute of Astrophysics, Kodaikanal have been used quite extensively in the present work and for this thanks are due to Drs.J. Hanumath Sastri and B.S. Murthy.

Thanks are due to Prof.R.Raghavarao for providing the topside ionograms recorded at Ahmedabad.

Thanks are due to Profs. K.R. Ramanathan, D. Lal, S.P.Pandya and R.V. Bhonsle for the encouragement.

The author had wide ranging discussions on many scientific aspects related to the present work, with Prof.J.A.Klobuchar during his visit to PRL, Ahmedabad. The author renders his sincere thanks to him.

The scientific discussions with Profs.B. Buti, R.Raghavarao, R.P. Kane and J.S. Shirke are also thankfully acknowledged.

Thanks are due to Drs.K.N. Iyer, A.V. Janve and M.Singh for the fruitful discussions which the author had with them during their stay in PRL at various stages of ATS-6 data analysis. Sincere thanks are also due to my colleagues Dr.H. O. Vats, Mr.G.D. Vyas and Mr.V.P. Patel for many scientific discussions.

Thanks are also due to Miss Chhaya R. Shah, Mr.K. C. Patel and Mr M.V. Bhavsar for the excellent computational assistance provided to the author. The author also appreciates the willing assistance of Mrs. Bharati K. Bhatt, Mrs. Suchita D. Desai and Mrs. Manisha Pandya at all times of need.

It is a pleasure to thank Mr.P.S. Shah and his colleagues at PRL Computer Centre for their kind cooperation in data processing and analysis.

Thanks are also due to Mrs.R.R. Bharucha and other library staff for providing excellent facilities during the course of this work.

The painstaking job of elegantly typing the thesis was most efficiently done by Mr.P. Raghavan. The author records his sincere thanks and appreciation to him.

The author greatly appreciates the assistance of the following people at various stages of the preparation of the thesis: Mr.H.S. Panchal of Drafting Section for drafting and photo-stenciling the diagrams; Mr.C.B. Khopkar of Photography Section for printing the diagrams and Mr.Ghanshyam Patel for the efficient cyclostyling of the thesis.

The author also appreciates the excellent xerox work done by Mr.J.G. Vora and Mr.N.F.Khoja on many occasions.

Thanks are due to the Physical Research Laboratory administration for providing the author all possible help for the completion of this work.

It is my great pleasure to appreciate the friendly encouragement provided by my friends Ashok, Rajesh and Shyam. My special thanks are due to Paresh who provided his unceasing moral support during my initial phase at PRL.

I am deeply indebted to all the members of my family for their affection and encouragement.

I am most grateful to my wife, Meenu whose profound understanding and the moral support during many excruciating moments of anxiety and despair, proved to be invaluable. Finally it would be unjustified not to appreciate the refreshing moments provided by my little son Kapil, at many moments of need.

--- Gautam Sethia

LIST OF AUTHOR'S PUBLICATIONS

Papers Published in Journals:-

*1. Sethia G., M.C. Gupta and C.S. Sastry
Shadow pole contribution to the S-matrix in potential scattering
J. Phys. A. Math., Nucl. Gen., Vol.7, No.18, 2267-2272 (1974).

2. Deshpande M.R., R.G. Rastogi, H.O. Vats, J.A. Klobuchar, G. Sethia, A.R. Jain, B.S. Subbarao, V.M. Patwari, A.V.Janve, R.K. Rai, Malkiat Singh, H.S. Gurm and B.S. Murthy
Effects of electrojet on the total electron content of the ionosphere over the Indian sub-continent
Nature, Vol. 267 (5612), 599-600 (1977).

*3. Deshpande M.R., H.O. Vats, G. Sethia and B.S. Murthy
Daytime ionospheric scintillations associated with geomagnetic storms
Nature, Vol.268, 614 (1977).

*4. Jain A.R., M.R. Deshpande, G. Sethia, R.G. Rastogi, Malkiat Singh, H.S. Gurm, A.V.Janve and R.K. Rai
Geomagnetic storm effects on ionospheric total electron content in Indian zone,
Ind. J. Rad. & Space Phys., Vol.7, 111-118 (1978).

*5. Jain A.R., M.R. Deshpande, G. Sethia, R.G. Rastogi, Malkiat Singh, H.S. Gurm, A.V. Janve and R.K. Rai
Geomagnetic storm effects on ionospheric total electron content in Indian zone - Part II : Evidence of equatorial electrojet control through Fountain effect
Ind. J. Rad. & Space Phys., Vol.7, 254-261 (1978).

6. Sethia G., H. Chandra, M.R. Deshpande and R.G. Rastogi
A numerical model for low-latitude ionospheric TEC
Ind. J. Rad. & Space Phys., Vol.7, 149-151 (1978).

7. Sethia G., H. Chandra, M.R. Deshpande and R.G. Rastogi
Faraday rotation measurements at Ootacamund
Ind. J. Rad. & Space Phys., Vol.7, 153-154 (1978).

8. Sethia G., H. Chandra and R.G. Rastogi
TEC from group delay measurements near magnetic equator (Ootacamund)
Ind. J. Rad. & Space Phys., Vol.7, 312-314 (1978).

*These publications do not form a part of the thesis.

9. Sethia G., M.R. Deshpande and R.G. Rastogi
The solar wind influences plasmasphere electron content
Nature, Vol.276, No.5687, 482 (1978).

*10. Singh Malkiat, H.S. Gurm, M.R. Deshpande, R.G. Rastogi, G. Sethia, A.R. Jain, A.V.Janve, R.K.Rai, V.M. Patwari and B.S.Subbarao
Total electron content (TEC) at low latitudes
Proc. Ind. Acad. Sci., Vol. 87A, No.3, 47-55 (1978).

*11. Chandra H., A.V. Janve, G. Sethia and R.G. Rastogi
Equatorial F-region during counter electrojet
Ind. J.Rad. & Space Phys., Vol.8, 1-55 (1979).

*12. Chandra H. and G. Sethia
Estimates of tracking errors for low orbiting satellites
Curr. Sci., Vol.48, No.17, 769-770 (1979).

*13. Chandra H., Hari Om Vats, G. Sethia, M.R. Deshpande, R.G. Rastogi, J.H. Sastri and B.S. Murthy
Ionosphere scintillations associated with features of equatorial ionosphere
Ann. Geophys., Vol.35, No.3, 145-151 (1979).

14. Davies K., R.F. Donnelly, R.N. Grubb, P.V.S. Rama Rao, R.G. Rastogi, M.R. Deshpande, H. Chandra, H.O. Vats and G. Sethia
ATS-6 satellite radio beacon measurements at Ootacamund, India
Radio Sci., Vol.14, No.1, 85-95 (1979).

15. Rastogi R.G., G. Sethia, H. Chandra, M.R. Deshpande, K. Davies and B.S. Murthy
Total electron content and F-region electron density distribution near the magnetic equator in India
J. Atmos. Terr. Phys., Vol.41, 561-564 (1979).

16. Sethia G., H.Chandra and R.G. Rastogi
Equatorial electrojet control on the low latitude ionospheric total electron content (TEC)
Proc. Ind. Acad. Sci., Vol.88A, Part II, No.2, 87-91 (1979).

17. Sethia G., H. Chandra, R.G. Rastogi and B.S. Murthy
Daily variation of total electron content near magnetic equator
Curr. Sci., Vol.48, No.9, 377-379 (1979).

*18. Sethia G. and R.G. Rastogi
Total electron content measurements at Jaipur
Ind. J. Rad. & Space Phys., Vol.8, 32-33 (1979).

19. Sethia G., R.G. Rastogi, M.R. Deshpande and H. Chandra
Equatorial electrojet control of the low latitude ionosphere
J. Geomag. Geoelect. (1979) (in press).

*20. Sethia G., H. Chandra, M.R. Deshpande and R.G. Rastogi
On the effect of the partial solar eclipse of 29th April 1976 on electron content
Proc. Ind. Acad. Sci. (1979) (communicated).

Symposium Papers:-

21. Iyer K.N., M.R. Deshpande, G. Sethia and R.G. Rastogi
On the evaluation of ionospheric electron content using ATS-6 satellite beacons
Proc. Workshop on beacon satellite studies, PRL, Ahmedabad, pp.64-86 (1976).

22. Davies K., R.F. Donnelly, R.N. Grubb, P.V.S. Rama Rao, R.G. Rastogi, M.R. Deshpande, H. Chandra, H.O. Vats and G. Sethia
ATS-6 satellite radio beacon measurements at Ootacamund, India
Proc. Radio Beacon Symposium, Paper No.2, Florence, Italy (1978).

23. Deshpande M.R., R.G. Rastogi, Hari Om Vats, G. Sethia, H. Chandra, K. Davies, R.N. Grubb and J.E. Jones
Achievements of ATS-6 beacon experiment over the Indian sub-continent
Proc. Radio Beacon Symposium, Paper No.3, Florence, Italy (1978).

24. Rastogi R.G., M.R. Deshpande, G. Sethia, H. Chandra and H.O. Vats
On the ionospheric electron content over the Indian sub-continent
Proc. Radio Beacon Symposium, paper No.10, Florence, Italy (1978).

25. Sethia G., H. Chandra, M.R. Deshpande, R.G. Rastogi and P.S. Murthy
Total electron content from ATS-6 group delay measurements at Ootacamund, India
Proc. Radio Beacon Symposium, paper No.14, Florence, Italy (1978).

*26. Chandra H., Hari Om Vats, G. Sethia, M.R. Deshpande, R.G. Rastogi and J. Hanumath Sastri
Ionospheric scintillations associated with equatorial E-region
Proc. Radio Beacon Symposium, paper No.35, Florence, Italy (1978).

27. Klobuchar J.A., G. Sethia, Banshidhar, M.R. Deshpande and R.G. Rastogi
Plasmaspheric electron content measurements at Ahmedabad
Space Sci. Symposium, Waltair (1978).

28. Sethia G., H. Chandra, M.R. Deshpande and R.G. Rastogi
Radio beacon studies of equatorial electron content
Symposium on Low Latitude Aeronomical Processes, COSPAR, Bangalore (1979).

*29. Klobuchar J.A., R.G. Rastogi, H. Chandra, G. Sethia and M.R. Deshpande
A comparison of near equatorial electron content in the Indian and American longitudes
Symposium on Low Latitude Aeronomical Processes, COSPAR, Bangalore (1979).

30. Sethia G., H. Chandra, R.G. Rastogi and M.R. Deshpande
Lunar tidal oscillations in the low latitude ionosphere
Space Science Symposium, BHU, Varanasi (1980).

Scientific Reports:-

*31. Deshpande M.R., R.G. Rastogi, H.O. Vats, G. Sethia, H. Chandra, R.V. Bhonsle and H.S. Sawant
On ATS-6 Radio Beacon Studies
Scientific Report, Phys. Res. Lab. (1978).

CONTENTS

CHAPTER - I

INTRODUCTION TO THE LOW LATITUDE IONOSPHERE AND THE PLASMASPHERE

1.1 Introduction to the Ionosphere

The ionosphere is a region of the upper atmosphere which contains free electrons and ions. It begins at height of about 50 km with no well defined upper limits. The ions and electrons are most abundant at heights of around 300 km but they represent only one thousandth of the air density even at that level; so the ionosphere can be regarded as a weakly ionized plasma embedded in the earth's magnetic field. But as regards its practical utility and scientific interest, the ionization has attracted as much attention as the neutral air from which it is produced by the action of solar radiation. The most important property of the ionosphere is to reflect - under suitable conditions - long, medium and short waves used for broadcasting and radio communication.

The early investigations from radio sounding of the ionosphere (Breit and Tuve 1925, Appleton and Barnett 1925) had revealed the existence of distinct layers, conventionally designated as D (70 to 90 km), E (90 to 150 km) and F (150 to 500 km) regions whose reflecting properties and physical characteristics are distinct and show marked variations, partly systematic and partly irregular. A detailed description of various techniques of probing the ionosphere is given in the April issue of the Journal of Atmospheric and Terrestrial Physics, 1970.

1.1.1 Physics of the Equatorial Ionosphere

Once routine monitoring of the ionosphere had become widespread, soon it became apparent that certain aspects of the behaviour of the equatorial ionosphere differed greatly from the behaviour of the ionosphere elsewhere. It was also found that these differences were not determined by the geographic equator but by the dip equator.

The major influence of the Earth's magnetic field on the equatorial ionosphere (in E and F regions) arises because charged particles move more freely along the magnetic lines of force than across them. Near dip equator the magnetic field lines are horizontal (along N-S). Hence the ionization can be moved in a vertical or in an eastwest direction by electric fields only. It is known that electric fields are produced by the neutral winds attempting to blow the ionization across magnetic lines in the 100-110 km height range (the dynamo region). This electric field system drives the Sq (quiet Sun) current system. In practice it appears that the large-scale electric fields set up in the dynamo region some 10° to 15° in latitude away from the equator, travel up the highly conducting magnetic lines to appear virtually undiminished in the equatorial F-region (150 km and above).

The above mentioned Sq current system causes a diurnal variation of the geomagnetic field with a range, which depends on the latitude of the observation point relative to the Sq current

system. Ground based magnetometers when placed near the dip equator show an abnormally large amplitude for the daily variation of the horizontal component (H) of the earth's magnetic field (Chapman and Bartels 1940). Fig.1.1 (after Matsushita and Campbell 1967) illustrates the abnormally large diurnal range in H in the equatorial region. The enhancement is believed to be caused by an electric current flowing eastward in the dynamo region above the dip equator which has a width of about 500 km. The source of this current is the special geometry of the geomagnetic field at the dip equator which causes a vertical Hall polarization field resulting in enhanced conductivity in the eastward direction. This extra current known as the equatorial electrojet (Chapman 1951) causes several interesting phenomena in the equatorial ionosphere. The more details regarding the conductivities of the equatorial ionosphere are described in the next section.

1.1.2 Conductivity in the Ionosphere and the Equatorial Electrojet

An excellent review on the electrical conductivity of the ionosphere has been given by Chapman (1956). The presence of geomagnetic field makes the conductivity, anisotropic in nature. Charged particles, electrons and positive ions, move freely in the direction of the earth's magnetic field but are forced to spiral round the field lines with angular frequencies ω_e and ω_i respectively, and this reduces their mobility transverse to the

field. The ions and electrons also undergo collisions with frequency ν_i and ν_e respectively, which interfere with the movement of electrons along the field lines. If there are N electrons and ions per unit volume and their respective masses are m_e and m_i, the electrical conductivity σ_o (known as longitudinal conductivity) along the direction of the magnetic field is given by:

$$\sigma_o = N e^2 \left(\frac{1}{m_e \nu_e} + \frac{1}{m_i \nu_i} \right) \qquad (1.1)$$

and is the same as the conductivity in the absence of the field.

The Pederson conductivity σ_1, transverse to the field is

$$\sigma_1 = N e^2 \left[\frac{\nu_e}{m_e(\omega_e^2 + \nu_e^2)} + \frac{\nu_i}{m_i(\omega_i^2 + \nu_i^2)} \right] \qquad (1.2)$$

indicating that the electronic and ionic components of σ_1 are each smaller than σ_o by the factors $\nu^2/(\omega^2 + \nu^2)$ which vary with ν and hence with height. When the electric field is perpendicular to the magnetic field there will also be a Hall current flowing in the direction $(-E \times H)$ with Hall conductivity σ_2 given by

$$\sigma_2 = N e^2 \left(\frac{\omega_e}{m_e(\omega_e^2 + \nu_e^2)} - \frac{\omega_i}{m_i(\omega_i^2 + \nu_i^2)} \right) \qquad (1.3)$$

and the electronic and ionic components of σ_2 are seen to be smaller than those by σ_o by factors $\nu\omega/(\omega^2 + \nu^2)$.

Near magnetic equator, the Hall current is inhibited giving rise to a vertical polarization field. This gives rise to an

additional conductivity in the same direction as the normal Pederson conductivity (σ_1). The effective conductivity is known as the cowling conductivity σ_3, and is given by:

$$\sigma_3 = \sigma_1 + \frac{\sigma_2^2}{\sigma_1} \qquad (1.4)$$

If we assume a rectangular co-ordinate system such that the x-y plane coincides with the ground, the positive z axis is vertically upwards, the positive y direction is eastward and the positive x direction is south, the resultant conductivities along the co-ordinate axes can be shown to be:

$$\sigma_{xx} = \frac{\sigma_0 \sigma_1}{\sigma_0 \sin^2 I + \sigma_1 \cos^2 I} \qquad (1.5a)$$

$$\sigma_{yy} = \frac{\sigma_2^2}{(\sigma_0 \tan^2 I + \sigma_1)} + \sigma_1 \qquad (1.5b)$$

$$\sigma_{xy} = \frac{\sigma_0 \sigma_2 \sin I}{\sigma_0 \sin^2 I + \sigma_1 \cos^2 I} \qquad (1.5c)$$

Where I is the magnetic dip angle. At the magnetic equator $I = 0$, and

$$\sigma_{xx} = \sigma_0 \qquad (1.6a)$$

$$\sigma_{yy} = \sigma_1 + \frac{\sigma_2^2}{\sigma_1} = \sigma_3 \qquad (1.6b)$$

$$\sigma_{xy} = 0 \qquad (1.6c)$$

Graphs showing the variation with altitude of the conductivities σ_1, σ_2 and σ_3 have been calculated for typical ionospheric conditions by Chapman (1956) and are shown in Fig.1.2a,b (after Chapman and Raja Rao 1965). The cowling conductivity, σ_3, is the most important near the magnetic equator and takes large values within a comparatively narrow range of heights near 100 km, thus justifying the assumption that the dynamo region approximates to a bounded slab. Further consideration of the above equations shows that values of σ_{yy} within a few degrees of the equator are greater by an order of magnitude than elsewhere, leading to a large intensification of the Sq currents in these regions. The equatorial electrojet can thus be regarded as a logical consequence of the dynamo theory of Sq when the anisotropic electric conductivity of the ionosphere is taken into account.

1.1.3 Important Features of the Equatorial F-region

a) The Equatorial Anomaly:- The F_2 region in the equatorial latitudes is marked by two distinct features (i) Daily variation of the critical frequency (f_oF_2) shows peaks in the morning and late evening with a valley near noon, generally known as midday bite-out (Berkner and Wells 1934, Maeda 1955). (ii) Latitudinal plot of noon f_oF_2 against magnetic dip shows two maxima around 30° dip with a trough around magnetic equator (Appleton 1946), generally known as the Appleton anomaly or the equatorial anomaly. Both the midday bite-out and the equatorial trough in f_oF_2, illustrated in Fig.1.3 (after Rajaram 1977), are explained in terms

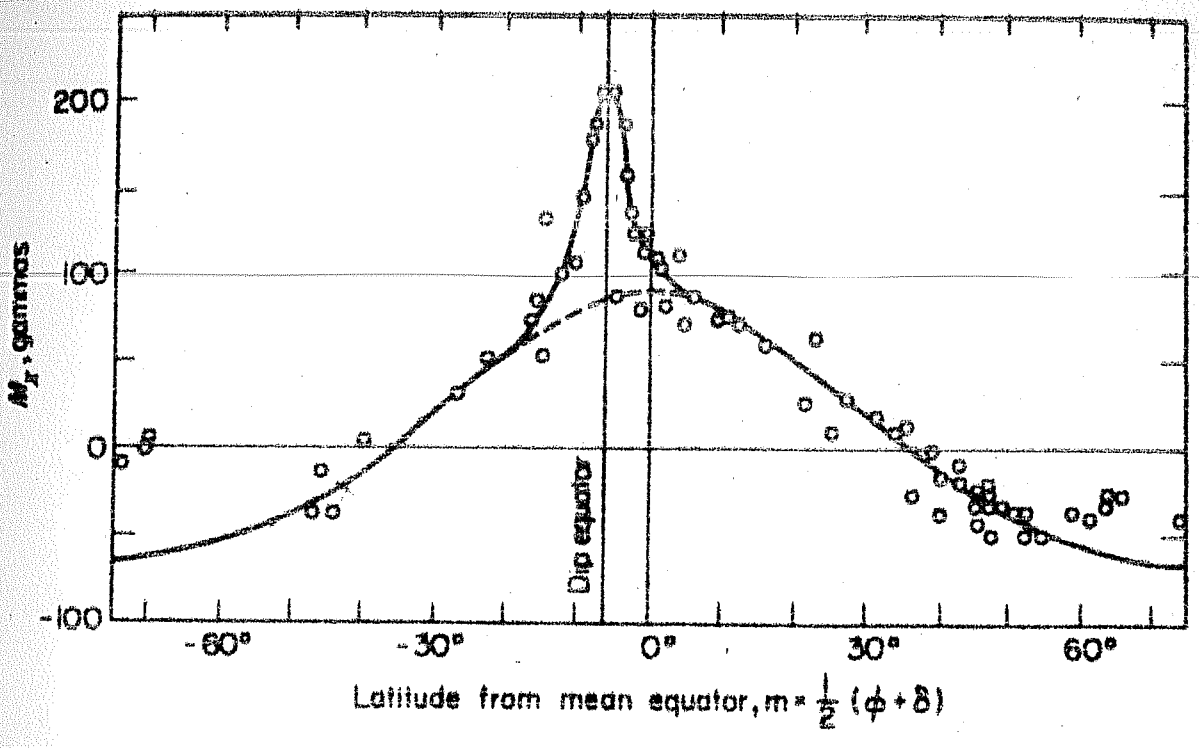

Fig.1.1 Variation of the daily range in H field with latitude measured from the mean equator indicating the abnormally large range in the equatorial electrojet region (after Matsushita and Campbell 1967).

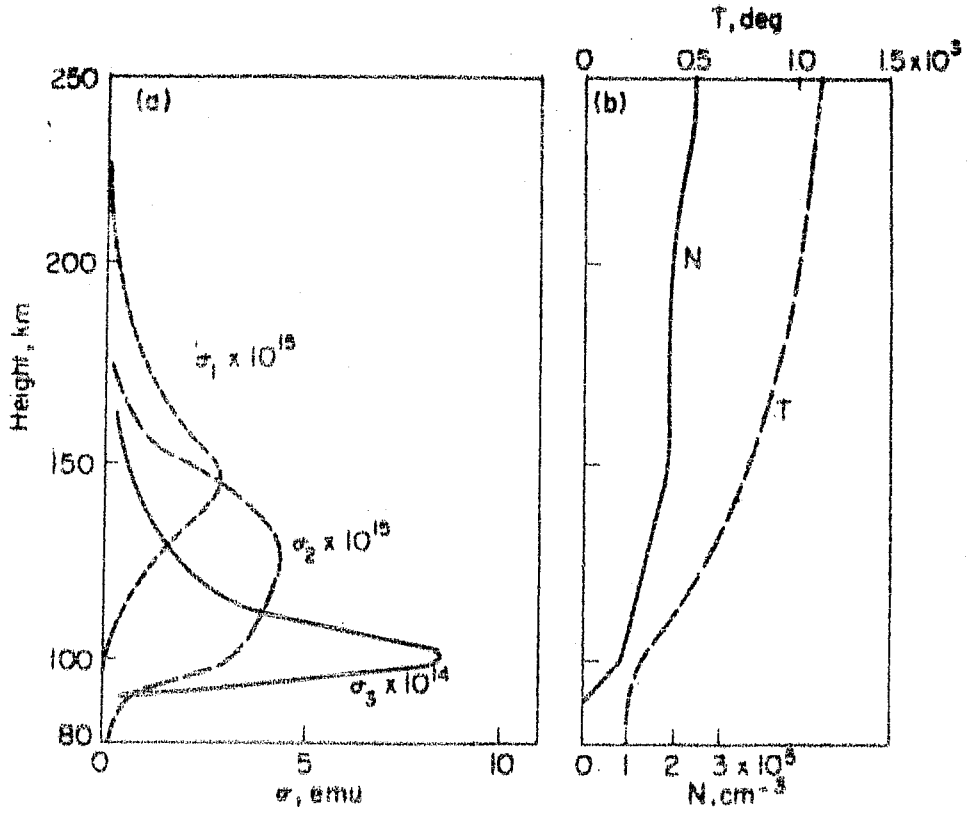

Fig.1.2 Variation of Pederson σ_1, Hall σ_2, and Cowling σ_3 conductivities with height (shown at a) for an ionosphere in which electron density N, and tempera-

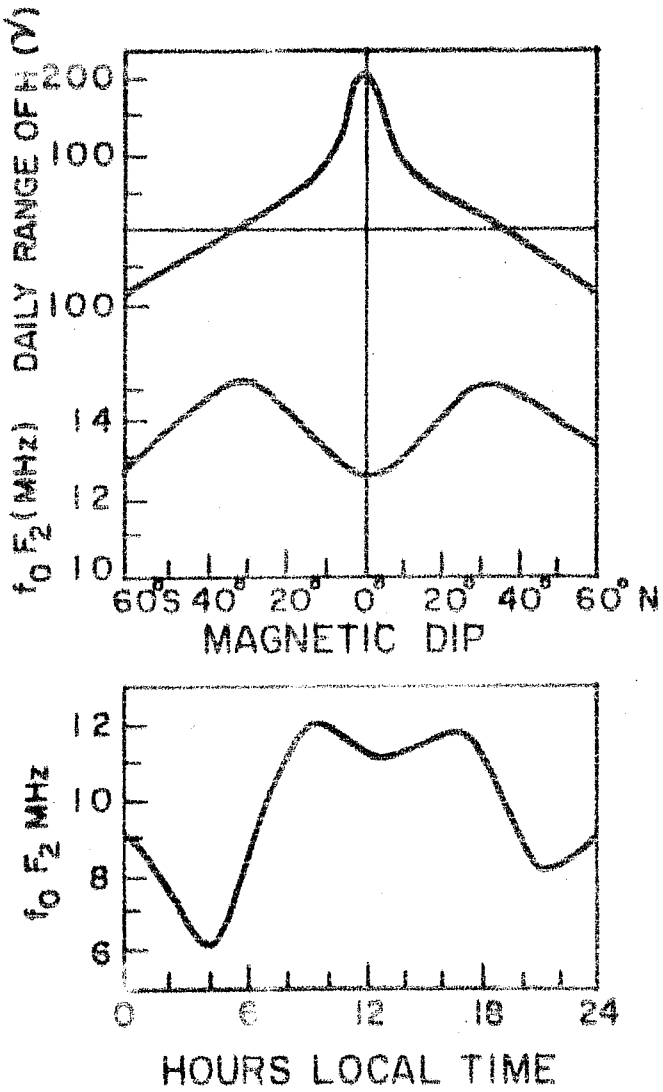

Fig.1.3 Schematic diagram illustrating some prominent effects of the equatorial electrojet (after Rajaram 1977).

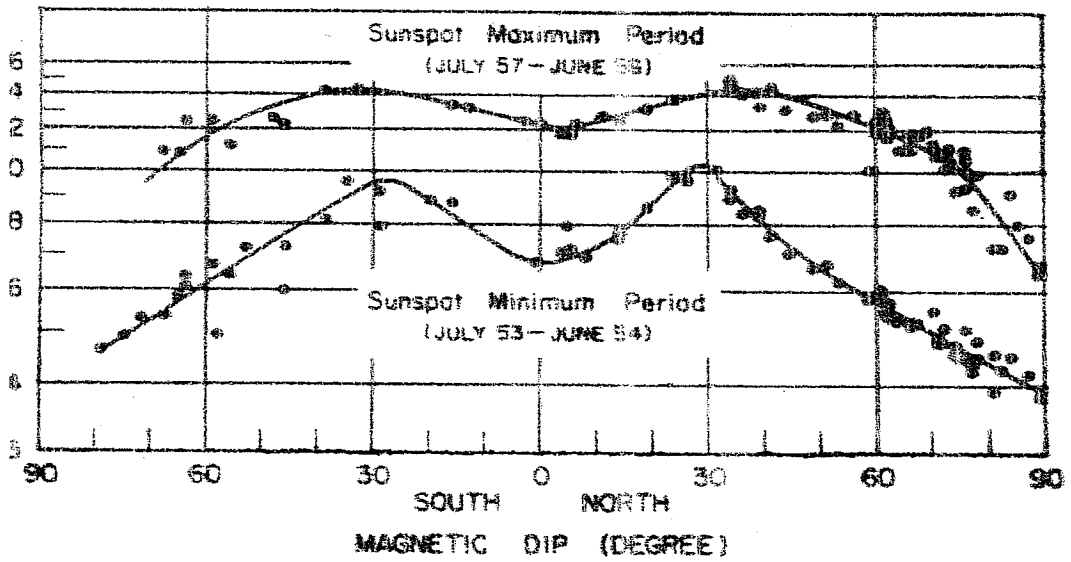

Fig.1.4 Equatorial anomaly in noon f_0F_2 for sunspot maximum and sunspot minimum period (after Rastogi 1966)

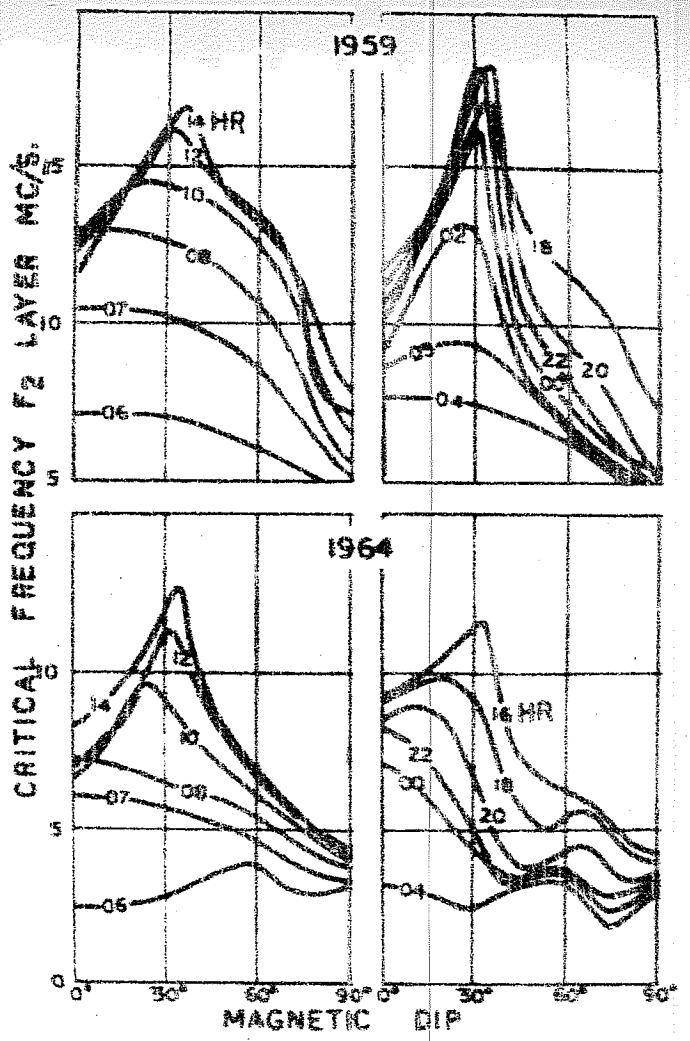

Fig.1.5 Diurnal development of equatorial anomaly during low (1964) and high (1959) sunspot years (after Rastogi 1966).

(b) The Daily Variation of h_mF_2:- Observations of h_mF_2, the height of the F_2 region peak electron density, are much fewer than those of N_{max} F_2 primarily because of the greater difficulty in reducing the ionosonde data to obtain it. Incoherent scatter radar yields the height directly but there are very few stations employing this technique.

During solar minimum years on quiet equinoctial days near the dip equator (African sector), Olatunji (1965) and Lyon (1965) reported that h_mF_2 lied between 300 km and 350 km from 1200 hr LT to 1800 hr LT. Farley (1966) using incoherent scatter radar found the same values of h_mF_2 in the American sector. All these investigations showed that during night h_mF_2 decreases slowly to around 275 km by 0500 hr LT.

A different daily variation of h_mF_2 is found during solar maximum years. In the African sector (Olatunji 1965) h_mF_2 is found to increase from 300 km at 0700 hr LT to 500 km by 1400 hr LT maintaining this altitude till sunset. After sunset, h_mF_2 rises rapidly attaining 600 km by 2100 hr LT. Similar post-sunset behaviour is also noticed in the American sector (Lyon and Thomas 1963).

In the Indian sector the noontime F-region heights are found to be around 500 km for high, 400 km for medium and 300 km for low sunspot years (Chandra et al. 1973, Rajaram and Rastogi 1977). A sudden rise in h_mF_2 after sunset is most pronounced in high sunspot, and is least in low sunspot years. The post-sunset

height rise of the F-region is a characteristic of the equa locations and is not observed at sub-tropical (say 18° dip latitude) or at mid-latitudes (say 30°N dip latitude) stations (Rastogi 1971). The Jicamarca incoherent backscatter radar has shown strong upward vertical plasma drifts in the F-region in high sunspot years soon after sunset (Woodman 1970) indicating the onset of a strong eastward electric field in the equatorial ionosphere.

(c) The Electron and the Ion Temperatures:- One of the consequences of the equatorial E x B uplift appears to manifest in the altitude profiles of the electron and ion temperatures. Normally electron temperature T_e, should gradually rise above neutral gas temperature T_g, in the region 70 km to about 400 km, and beyond it, it should become almost constant with altitude. The ion temperature T_i, would retain values near T_g till about 300 km, and beyond this swerve to values equalling T_e in the vicinity of 1000 km (Banks and Kockarts 1973). Thus the ratio T_e/T_i should decrease monotonically with height to approach unity near 1000 km. The observations of Farley et al. (1967) at the equatorial station Jicamarca indicate major deviations from the expected pattern. It is found that throughout the daytime hours, from 150-300 km, T_e is greater than T_i. The ratio T_e/T_i, commonly reaches a maximum value of 2 around 250 km, and it is unity below 150 km and above 300 km. During night at all altitudes, $T_e \sim T_i$. The explanation for the deviations from the expected behaviour seems to lie in the E x B upward drift which moves ion and electrons together. The thermal contact between

these components of plasma commences from 220 km onwards causing T_e to decrease; around 300 km, when the thermal contact is total, $T_e = T_i$.

1.1.4 The Geomagnetic Storm Effects on the Equatorial F-region

Over the years the scientific problems posed by geomagnetic storms and the accompanying ionospheric phenomena have proved very difficult. This applies particularly to the F-region effects, many possible causes of which have been proposed such as temperature increases (Appleton and Ingram 1935), changes in chemical composition (Seaton 1956), electromagnetic drifts (Maeda and Sato 1959) and neutral winds (Kohl and King 1967). None of these can be solely responsible for all the storm phenomena, though each may have a part to play (Rishbeth 1975).

(a) A Resume of the Storm Effects:- The F-region displays much day to day variability, so a "storm" is not always easy to define. Marked perturbations sometimes occur even in magnetically quiet times (e.g. Smith et al. 1968). However, some well-marked F-region phenomena do usually accompany severe magnetic storms (Rajaram et al. 1971, Somayajulu 1971, Kane 1973). The effect of magnetic storms on the critical frequency of the F_2 region (f_oF_2) at different latitudes has been studied by various workers. In general it is found that during disturbances f_oF_2 increases at low geomagnetic latitudes ($< 30°$ dip) and decreases at high geomagnetic

latitudes (>70° dip) in all seasons, while at mid-latitude (> 30° dip but <70° dip) stations, f_oF_2 shows a seasonal change over with an increase in winter and a decrease in summer and equinoxes. (Appleton et al. 1937, Berkner and Seaton 1940, Martyn 1953, Matsushita 1959, Maeda and Sato 1959).

Local time variation of changes in f_oF_2 at an equatorial station has been shown by Olatunji (1966) such that the f_oF_2 increases during daytime and decreases at night. Such a variation can be noticed in the results reported by Rajaram and Rastogi (1969) for summer, but different variations are observed for other seasons.

During storms the latitudinal trough in f_oF_2 - the Appleton anomaly - is poorly developed or completely absent (King et al. 1967, Rush et al. 1969, Rastogi et al. 1972). On occasions, however an enhancement of the anomaly has been found (Raghavarao and Sivaraman 1973). Lockwood and Nelms (1964) have shown that an equatorial ledge in topside electron density profile which corresponds to the formation of the equatorial anomaly tends to be lsss observable during high K_p periods.

A slight increase in h_mF_2 at the equatorial stations during storms has been shown by Matsushita (1962), while Olatunji (1965) and Rajaram and Rastogi (1968) have noted that disturbance variations in h_mF_2 at the equator are not significant.

(b) Mechanisms of the Storm Effects (Rishbeth 1975):- Atleast four processes are likely to make major contributions to the equatorial storm effects. First, the storm generated equatorward winds, though not necessarily symmetrical with respect to magnetic latitude, must tend to converge on the magnetic equator. Hence the field aligned drifts that they produce oppose the poleward diffusion of plasma along the field lines. Thus the formation of the crests of the equatorial anomaly is hindered (Burge et al. 1973). In fact calculations by Rush (1972) show that appropriately phased winds could have such an effect; they increase the mean lifetime of plasma by keeping it at a height where the loss coefficient is small, and retarding its diffusion to lower heights where it is large. As a consequence there must be a considerable increase in the total amount of plasma in the equatorial F-layer. Second, the convergence of the winds produces some plasma compression (which must operate at mid-latitudes too). If within a north-south distance (x) of 6000 km, say, the equatorward wind speed V decreases from 300 m/s to zero, the compression is :

$$N^{-1}\, dN/dt = -\, dV/dx = \tfrac{1}{2} \cdot 10^{-4} s^{-1} \qquad (1.7)$$

This is a significant fraction of the loss coefficient at the F-region peak (10^{-4}-$10^{-3} s^{-1}$, depending on circumstances). So there will be some effect on electron density N, though not on total electron content. Third, if the equatorward winds are strong enough, to reach the equatorial latitudes, the increased molecular/atomic ratio will tend to cause negative storm effects

just as it does elsewhere (Seaton 1956, Rishbeth 1962). Fourth, electromagnetic drifts are important at low latitudes and if they are altered during storms, the development of the equatorial trough will be affected. The E-W drift of the ionization irregularities near magnetic equator which are related to electric fields, are shown to be reduced on magnetically disturbed days (Rastogi et al. 1971) and even reversed on some of the magnetic storms (Chandra and Rastogi 1974). Abnormal vertical drifts, which must be due to electric fields, have been measured at Jicamarca during storms, and drift data for a great storm in March 1970 were used in a successful synthesis of the observed N(h,t) distributions (Woodman et al. 1972). This work confirms the importance of electric fields during storms though it did not consider the latitude variations of N which require further study.

1.1.5 Review of Total Electron Content (TEC) Studies at Low Latitudes

The earliest estimates of the total electron content (TEC) of the ionosphere were obtained by Browne et al. (1956) and Evans (1957) from the Faraday rotation of 120 MHz radio waves reflected from the moon. A big spurt of such measurements came with the launching of BE-B and BE-C satellites orbiting at heights of 1000-1400 km. Most of the data on equatorial and low latitude TEC has been obtained by low orbiting satellites (Shirke and Ramakrishnan 1966, Basu and Das Gupta 1968, Bandyopadhyay 1970, Tyagi and Mitra 1970, Rastogi et al. 1973, 75, Iyer et al. 1976,

using geostationary satellites (Garriot et al. 1965, Koster 1966, Hunter 1970, Yeboah-Amankwah and Koster 1972). Measurements using orbiting satellites are most suited to study the spatial variations of TEC, while geostationary satellites are superior in respect of continuous monitoring with high time resolution. TEC measurements using low as well as geostationary satellites have been extensively made at mid-latitudes (Titheridge 1966, 1972, 1973, Garriot et al. 1967, Smith 1968, Davis and da Rosa 1969, Mendillo et al. 1970), but comparatively very meagre data exist for low and tropical latitudes.

Latitudinal variation of TEC has been studied by Basu and Das Gupta (1968), Titheridge and Smith (1969), de Mendonca et al. (1969), Golton and Walker (1971) and Rastogi et al. (1973, 1975, 1977) in the equatorial and low latitudes using Faraday rotation of VHF signals from the satellites ATS-3 and ATS-C. The results from combined observations at Singapore (dip 18°S), Bangkok (13°N dip) and Hong Kong (30.5°N dip), all in the same longitude sector have indicated a distinct trough of TEC near the dip equator, and crests at $\pm$ 30° dip (Rufenach et al. 1968). Thus the above referred studies clearly indicate the existence of the equatorial anomaly in TEC similar to the one in f_0F_2, in its latitudinal variation. de Mendonca et al. (1969) have derived the contours of TEC in the southern hemisphere low latitudes which also indicate the presence of the equatorial anomaly in TEC.

Dunford (1967) obtained a positive correlation between E-region current system near the magnetic equator and the equatorial anomaly using topside sounder data. Mac Dougall (1969) and Rastogi and Rajaram (1971) using f_oF_2 values near the magnetic equator have given evidence that the equatorial anomaly shows high correlation with electrojet strength and poor correlation with Sq current strength. Rush and Richmond (1973) have obtained positive correlation between several parameters characterising the equatorial anomaly in f_oF_2 and the electrojet strength. As for the equatorial anomaly in TEC is concerned, geomagnetic control of this anomaly has been studied by Das Gupta and Basu (1971) and Iyer et al. (1976). Influence of solar flux and equatorial electrojet on the diurnal development of the equatorial anomaly in TEC was investigated by Walker and Ma (1972). Combining the orbiting satellite data for a few months one can also obtain a daily variation of TEC at a particular location. At a tropical latitude, i.e. Ahmedabad, close to the crest of the equatorial anomaly, daily variation of TEC and f_oF_2 have been found to be similar (Rastogi and Sharma 1971). However, there have been discrepancies in the daily variation of TEC in the equatorial region. Blumle (1962) reported absence of bite-out at Huancayo, whereas for the same station from later observations Bandyopadhyay (1970) inferred bite-out to be present. Observations at Ibadan, Thumba and Kodaikanal did not show any bite-out in TEC (Olatunji 1967, Rastogi et al. 1973, 1975, Iyer and Rastogi 1978). Rufenach et al. (1968) reported that f_oF_2 at Bangkok showed the presence of bite-out in its daily variation but no corresponding

One of the difficulties in deriving a conclusive result about the daily variation of TEC from measurements from the orbiting satellites has been that a single daily variation curve can be obtained only from data of at least a few months. The beacons aboard a geostationary satellite, therefore, are being used these days as it provides continuous observation over a long period of time. Thus a good time resolution is achieved.

1.2 Introduction to the Plasmasphere-Plasmapause

The region of space around the earth in which the earth's magnetic field is the dominant influence controlling the motions of charged particles is known as the magnetosphere. Basically the magnetosphere consists of two parts. There is an inner, corotating component called the plasmasphere, which belongs topologically to the region of influence of the ionosphere. The plasmasphere is surrounded by a region containing tenuous plasma, which is controlled by the convection electric field induced by the solar wind interaction with the earth's magnetic field (Axford and Hines 1961, Dungey 1961). The two regions are separated by a boundary situated in the equatorial plasma at a geocentric distance of 4 to 5 earth radii, known as the plasmapause (Carpenter 1963, Gringauz 1963). At the plasmapause the electron density drops sharply by a factor of 100 or so (for reviews see Carpenter and Park 1973, Chappell 1972, Gringauz and Bezrukikh 1977 and the references therein).

Thermal plasma in the plasmasphere originates in the ionosphere, where the photoionization of O produces copious amounts of electrons and O^+ ions. The resulting photoelectrons with energies of tens of electron volts can easily escape into the plasmasphere thereby increasing the energy density levels in that region. However, photoelectrons, unaccompanied by ions, do not result in net density increases in the plasmasphere because an equal number of cold electrons must flow downward in order to maintain charge neutrality. An increase in plasmaspheric number density requires upward fluxes of both electrons and ions. Ionospheric O^+ ions are too heavy to accompany the electrons to great heights. O^+ ions in the topside ionosphere first undergo a change exchange reaction;

$$O^+ + H \longrightarrow O + H^+ \qquad (1.8)$$

and the resultant H^+ ions diffuse upward to populate the plasmasphere. The change over from O^+ to H^+ ions occurs typically at 1000-2000 km, the so called "transition altitude".

There are two important mechanisms for loss of plasma from the plasmasphere. If plasma pressure in the underlying ionosphere decreases below an equilibrium level at night, or during magnetic storms, downward flow from the plasmasphere results. O^+ ions are produced by down coming protons through charge exchange with O (a reversal of the reaction cited in the foregoing paragraph) and help maintain the O^+ dominated F layer. The other loss mechanism involves large-scale convection electric fields, carrying tubes

of plasma into high latitude open field regions permitting the plasma to escape into the geomagnetic tail or interplanetary space. The second process has been widely accepted as an explanation of the large density jump at the plasmapause (Nishida 1966, Brice 1967, Kavangh et al. 1968). The plasmapause position may range from L = 2 during severe magnetic storms to L = 8 during very quiet times.

1.2.1 The Theory of Magnetospheric Convection

Magnetospheric plasma convection has been reviewed in detail by Axford (1969). A viscous-like interaction between plasma and magnetic field (Axford and Hines 1961) and magnetic-field-line merging (Dungey 1961) have been proposed as the mechanisms that produce magnetospheric convection. In general the convection model assumes the presence of a large scale electric field directed from dawn to dusk across the magnetosphere. Charged particles within the magnetosphere acquire an E x B directed drift owing to this electric field (E is the convection electric field and B is the earth's magnetic field). This drift is generally in a sunward direction in the magnetospheric equatorial plane. The motion of low-energy charged particles such as those in the plasmasphere can be significantly affected by this convection field, since their gradient and curvature drifts in the magnetic field are very small. The original convection models of the plasmapause explained the steep gradient in the plasma density profile as the boundary between magnetic flux tubes

of plasma that corotate with the earth, remaining always in a closed configuration and therefore holding their plasma, and those that have their motion dominated by the convection electric field (Nishida 1966, Brice 1967). The convection-dominated flux tubes are convected sunward to the magnetopause, where they lose their plasma. In the convection model, the precise shape and position of the plasmapause are determined in part by the magnitude of the dawn-dusk convection field in the magnetosphere and a change in this electric field is reflected in the changing dynamics of the plasmasphere.

Following the qualitative ideas of Axford and Hines, Nishida and Brice, Kavangh et al. (1968) made some more quantitative calculations of the drifts paths of particles in the magnetospheric convection field. These authors assumed different values for the strength of the convection electric field, and superimposed this field on the earth's corotation electric field in a model magnetic field due to Mead (1964). An example of the resulting drift path for zero energy particles is shown in Fig.1.6 (after Kavangh et al. 1968). The drift paths shown are also equipotentials since the drift of zero energy particles in the $E \times B$ direction is along equipotential surfaces. The last closed equipotential defines a "tear-drop" shaped plasmapause. A change in the magnitude of the convection field will not change the shape of the flow pattern, but only the size of the 'tear-drop' shape. For example, an increase in the convection field will decrease in the tear-drop region surrounding the closed flow paths.

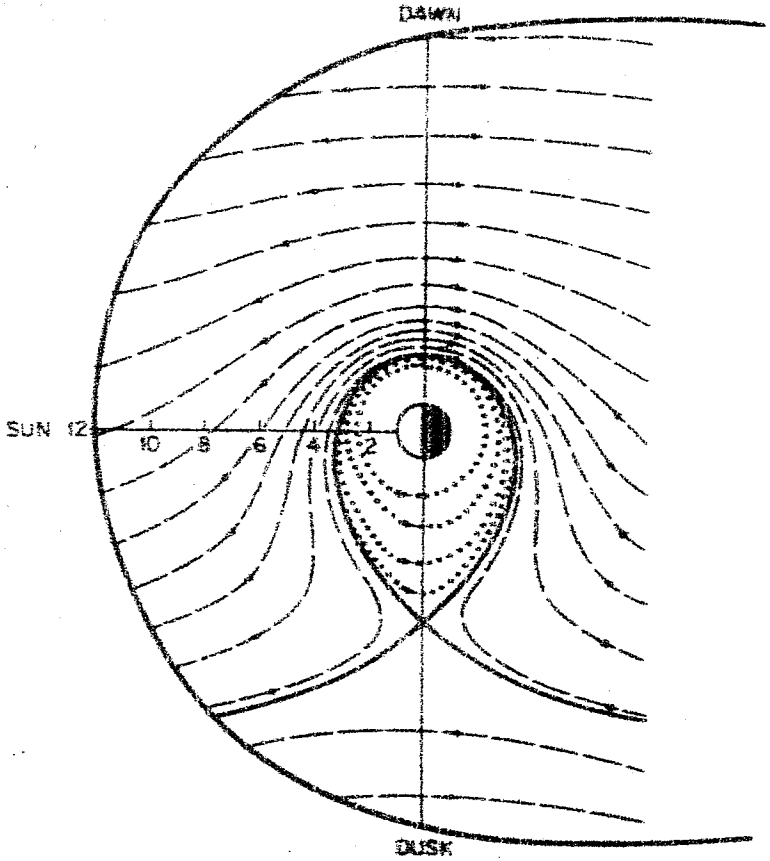

Fig.1.6 The calculated drift of zero energy particles in the equatorial plane. This 'tear-drop' model is derived from a superposition of the corotation and convection electric fields in a model magnetic field (after Kavangh et al. 1968).

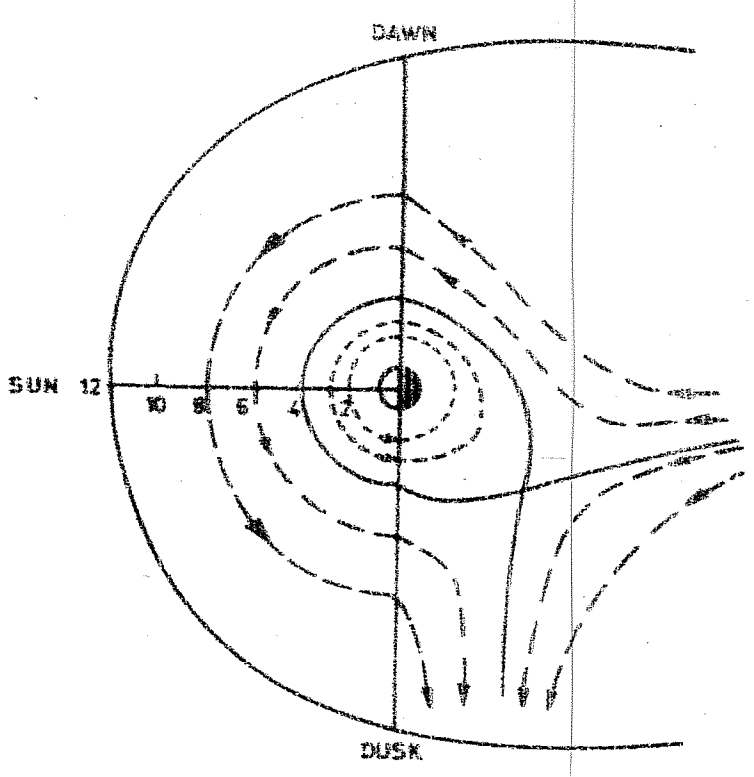

Fig.1.7 Equipotential contours resulting from superimposing the corotation electric field on a convection electric field which is completely shielded from the dayside (after Grebowsky 1971).

In the above analytical model, the solar wind induced electric field is supposed to have a uniform intensity directed from dawn to dusk across the magnetosphere. Wolf (1970) and Grebowsky (1971) pointed out that the concept of uniform convection electric field may be invalid on the dayside of the earth, due to the 'shorting out' of the magnetospheric electric fields by the highly conducting daytime ionosphere. Grebowsky (1971) proposed that the dayside electric field vanishes in the rest frame of the rotating ionosphere, and this results in the plasmapause configuration as depicted in Fig.1.7 (after Grebowsky 1971). The most marked difference from Fig.1.6 to Fig.1.7 is that the time of the extreme plasmapause bulge has changed from 1800 LT to 2100 LT. The comparison of the theoretical predictions with observations has been described in the following section.

1.2.2 A Resume of Previous Work on Plasmasphere-Plasmapause

Much work has been done about plasmasphere-plasmapause using in-situ satellite as well as whistler observations (Carpenter and Park 1973, Chappell 1972, Gringauz and Bezrukikh 1977). The highlights of these studies can be summarised as follows:-

(a) Results of In-situ Measurements:- Gringauz (1963) reported a marked decrease in the positive ion density at $\sim 4\ R_E$, using lunar rockets, launched in 1959. Also it was noted that plasmapause location L_{pp} (L is the McIlwain magnetic shell number) was inversely correlated with the maximum K_p index, the day before the measurements (Gringauz and Bezrukikh 1977).

Using Ogo 1 and 3 observations it was found that the plasmapause position was inversely related to the magnetic activity index A_p (Taylor et al. 1965, 1968). In particular L_{pp} was found to be well correlated with the maximum K_p index recorded during the 24 hour period before the observations. Using Ogo-3 observations in the middle of 1966, Taylor et al. (1970) investigated the dusk bulge region of the plasmapause. It was shown that the plasmapause was, at all local times, 1.5 to 2 L values farther from the earth than the average values derived from 1963 whistler observations. This could be due to the bias of the whistler observations to post main phase conditions when L_{pp} is reduced; alternatively Carpenter and Park (1973) suggest that Taylor et al. (1970) may have used the outermost plasmapause position in their studies.

Using Faraday cup observations aboard IMP2, Binasack (1967) showed that the plasmapause position was related to the K_p index at the time of the measurement by:

$$L_{pp} = 6.0 - 0.6 \quad K_p \qquad (1.9)$$

The satellite Ogo-5 provided the most extensive in-situ observations of the plasmapause. Using Ogo-5 observations, Chappell et al. (1970) have studied the influence of magnetic activity on the plasmapause position at 0200 $\pm$ 2 hours and 1000 $\pm$ 2 hours LT. For both periods L_{pp} decreases with increasing activity; for the former period, the lag of the

plasmapause behind the magnetic activity change is ~2 to 6 hours. With increased activity, the sharpness of the knee increases, the density inside and outside the knee remaining constant at $\sim 10^3$ cm^{-3} and ~ 1 cm^{-3} respectively. These points are illustrated by the four night-time profiles shown in Fig.1.8 (after Chappell et al. 1970). Chappell et al. (1971) deduced an average L-LT configuration of the plasmapause which was nearly symmetric about dusk. However, the Explorer 45 observations of the plasmapause showed a bulge located after dusk (Maynard and Grebowsky 1977) which is more in agreement with whistler observations (Carpenter 1966) than with Ogo-5 observations.

(b) Results of Whistler Measurements:-

(i) An abrupt decrease in the equatorial thermal plasma density with increasing geocentric distance was originally detected in 1963 by ground based whistler observations (Carpenter 1963) and by in-situ ion density measurements (Gringauz 1963).

(ii) The whistler observations have shown a dawn-dusk asymmetry in plasmapause equatorial radius (or L value) with a minimum typically between 0300 and 0900 LT and a maximum near 2000 LT (Carpenter 1966, 1967).

(iii) Also it is found that the plasmapause moves inward during periods of increasing magnetic disturbance. On the basis of data presented in Carpenter (1967), Carpenter and Park (1973)

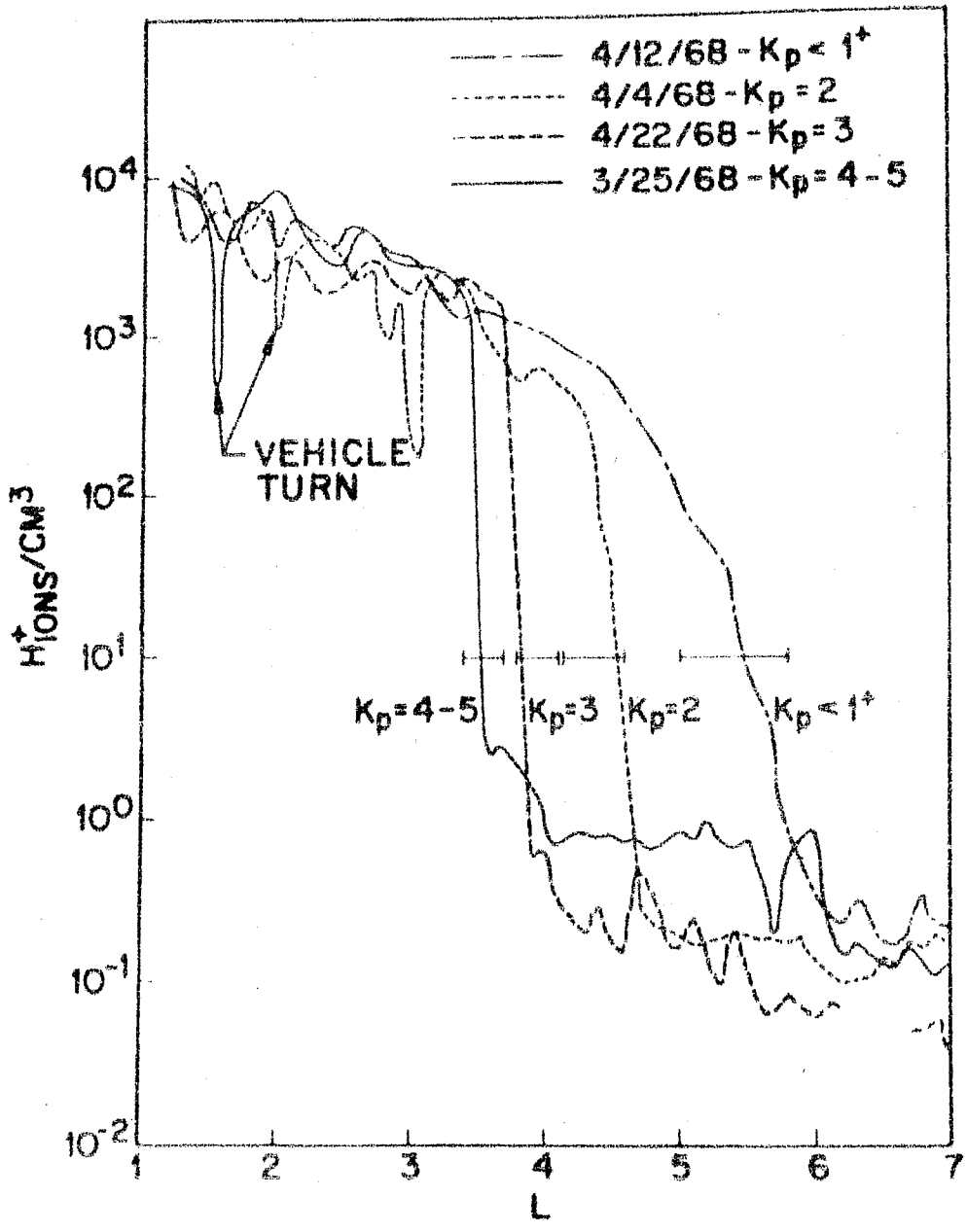

Fig.1.8 A composite graph showing the reaction of the plasmasphere in the nightside region to changes in the level of magnetic activity as measured by OGO-5. The plasmapause is found to steepen and move to lower L values with increasing activity (Chappell et al. 1970).

proposed a formula $L_{pp} = 5.7 - 0.47\ K_p$ which can be used as a crude predictor of plasmapause position in the midnight-dawn sector. K_p represents the maximum K_p value in the preceding 12 hours.

(iv) The whistler studies have also shown that most of the rapid displacements of the plasmapause occur in the midnight sector and that these changes are associated with magnetospheric substorms (Carpenter and Stone 1967, Carpenter 1970). More precisely the rapid inward displacements of the plasmapause observed during substorm events appear to be a part of the cross L motions of the plasma within the plasmasphere (Carpenter et al. 1972, Carpenter and Seely 1976).

(v) Whistler observations near L = 4 and under quiet-conditions showed a daytime upward flux of $\sim 3 \times 10^8$ el cm^{-2} s^{-1} and a night-time downward flux of $\sim 1.5 \times 10^8$ el cm^{-2} s^{-1} across the 1000 km level (Park 1970); this latter amount is considered sufficient to maintain the nocturnal ionosphere.

1.3 The Scope of the Present Investigations

As previously mentioned, orbiting satellites provide very good spatial resolution but the temporal resolution is seriously limited. The beacons aboard a geostationary satellite provide a continuous measurement of TEC at a particular location, hence with the combination of a number of stations using the same beacon, it is possible to have both temporal as well as spatial

resolution. The repositioning of ATS-6 at 35°E, in July 1975, provided such an opportunity when well coordinated measurements were carried out at a number of institutions in India. The Physical Research Laboratory, Ahmedabad undertook the scientific project on ATS-6 in collaboration with a number of institutions in India. The list of the collaborating institutions is as follows:-

(i) PRL, Ahmedabad
(ii) Punjabi University, Patiala
(iii) University of Rajasthan, Jaipur
(iv) University of Udaipur, Udaipur
(v) A.V. Parekh Technical Institute, Rajkot
(vi) Indian Institute of Geomagnetism, Bombay.

At all these stations, the measurements of Faraday rotation angle at 140 MHz were carried out during October 1975 - July 1976 using Titheridge (1966) type polarimeters. Also group delay measurements were made during May-August 1976 at Ahmedabad. In addition to above measurements, a joint radio beacon experiment was conducted by the NOAA Laboratories, Boulder and the Physical Research Laboratory, Ahmedabad at near equatorial station Ootacamund. The following measurements were carried out at Ootacamund:-

(i) Faraday rotation measurements on 40 and 140 MHz.

(ii) The group delay (or modulation phase) measurements on frequencies of 40.1, 41 and 141 MHz.

(iii) Amplitude measurements on frequencies 40, 140 and 360 MHz.

In the present study, the following measurements have been used:-

(i) Faraday rotation data at 140 MHz obtained at above mentioned institutions during the period October 1975 to July 1976.

(ii) Group delay measurements on 140 MHz carried out at Ahmedabad during May - August 1976.

(iii) Faraday rotation and the group delay measurements on 140 MHz made at Ootacamund during the period October 1975 to July 1976.

It is worthwhile to note that the ionosphere electron content measurements using a geostationary satellite were made for the first time, at a chain of stations at low latitudes (covering a latitude range of 2°N to 25°N dip lat). In addition plasmasphere electron content measurements were also made at Ahmedabad (sub. ion. dip lat 17.1°N) and Ootacamund (2.2°N). Such measurements at low latitudes were not available so far; hence the current investigations on the plasmasphere form a new contribution to the subject. The ionospheric and the geophysical data obtained from other places have also been utilised for interpretation, wherever necessary.

CHAPTER - II

METHODS OF ELECTRON CONTENT MEASUREMENTS

2.1 Introduction

Total electron content (TEC) is broadly defined as the number of free electrons in a column of unit cross section extending through the ionosphere and above. It can be measured by a number of techniques (Chiccac.ci 1972) out of which the group delay and the Faraday rotation techniques are of the present interest and are described in detail in the following sections.

2.2 Methods of Electron Content Measurements

2.2.1 The Group Delay Technique

In this technique the difference in transit times of two radio waves of different frequencies, across the medium is measured. The time difference or the group delay measured in this technique is equally sensitive to all the free electrons irrespective of their positions along the raypath, hence this technique gives the electron content upto the height of the satellite and the content is denoted as N_T. In the presence of the magnetic field, the ionosphere is a doubly refracting medium, and for such medium two modes of propagation, i.e. 'ordinary', and 'extraordinary' exist. The phase refracting indices for the two modes are given by the Appleton-Hartree

equation, which is given as (assuming negligible collision frequency):

$$\mu^2 = 1 - \frac{X\,(1-X)}{(1-X)^{-\frac{1}{2}}\,Y_T^{\,2} \pm \left(\frac{1}{4}\,Y_T^{\,4} + (1-X)^2\,Y_L^{\,2}\right)^{\frac{1}{2}}} \qquad (2.1)$$

where $X = \dfrac{N\,e^2}{4\,\pi^2\,\epsilon_o\,m\,f^2}$

$Y = \dfrac{f_H}{f}$

$Y_L = \dfrac{f_H \cos\theta}{f}$

$Y_T = \dfrac{f_H \sin\theta}{f}$

N is electron density

m is electron mass

f_H is gyrofrequency of an electron in the magnetic field

θ is the angle between the magnetic field and the wave normal.

The plus and minus sign refer to the ordinary and extra-ordinary modes respectively.

If the wave normal lies in the direction of the magnetic field ($\theta = 0$) then $Y_L = Y$ and $Y_T = 0$ and the equation (2.1) is considerably simplified. Even if θ is not zero, a good approximation of μ may be obtained by taking $Y_T = 0$; this is known as the "quasi-longitudinal" approximation, and it generally holds for high frequency waves in the ionosphere provided X is not close to 1, and θ is not close to 90°. The actual condition for its

validity is $\frac{1}{4} Y_T^4 << (1-X)^2 Y_L^2$. The refractive index is then given by:

$$\mu^2 = 1 - \frac{X}{1 \pm Y_L} \qquad (2.2)$$

For the high frequency case $X << 1$ and $Y_L << 1$. Under this approximation equation (2.2) reduces to:

$$\mu = 1 - \tfrac{1}{2} X (1 \pm Y_L) \qquad (2.3)$$

Hence the phase change produced by the medium is given by:

$$\phi = \frac{2\pi}{\lambda} \int_0^S (1 - \mu)\, ds$$

$$\text{or } \phi = \frac{2\pi}{\lambda} \tfrac{1}{2} \int_0^S \left(\frac{X}{1 \pm Y_L} \right) ds$$

$$\text{or } \phi = \frac{360\, k}{2c} \int_0^S \frac{N(S)}{f \pm f_L}\, ds \qquad (2.4)$$

where $k = 80.61$, $c = 2.998 \times 10^8$ m sec^{-1}.

The carrier frequencies of 140 and 360 MHz radiated from the satellite ATS-6 are modulated with 1 MHz and the modulation phase delay at 141 MHz, ϕ^R_{141} is derived according to the relation:

$$\phi^R_{141} = (\phi_{140} - \phi_{141}) - (\phi_{360} - \phi_{361}) \qquad (2.5)$$

where the 1st term on the right-hand side is affected by the ionosphere and the 2nd term is relatively less affected by the ionosphere. The purpose of taking the modulation phase delay at 360 MHz is to ensure the cancellation of any drift in the transmitted frequencies, which are coherent since they are

derived from a single frequency of 20.008 MHz. The modulation phase thus measured is used to compute the total columnar electron content N_T which is $\int_S^R N(s)\,ds$, according to the relation:

$$N_T = K_{141}\ \phi_{141}^R \qquad (2.6)$$

where $K_{141} = \dfrac{2c \times 10^{16}}{360\,k\left(\frac{1}{140+f_L} - \frac{1}{141+f_L} - \frac{1}{360+f_L} + \frac{1}{360+f_L}\right)}$

f_L being the average longitudinal component of the electron gyrofrequency.

$K_{141} = 4.82 \times 10^{14}$ taking $\bar{f}_L = 0.154$ MHz for Ootacamund to ATS-6 geometry corresponding to an altitude of 400 km.

The values of K_{141} are found to be very insensitive to the values of f_L (less than 0.5%) (Davies et al. 1979).

2.2.2 Faraday Rotation Technique

In traversing a magnetoionic medium like ionosphere a plane wave undergoes a rotation of its plane of polarization, the total angle of rotation depending approximately on the average field component in the direction of propagation and on the total number of free electrons in a column of unit cross-section along the ray path. The strong dependence of Faraday rotation on the earth's magnetic field makes it sensitive to the electrons encountered in the upper parts of the ray-path, hence this technique gives total electron content, N_F, upto certain height h_F, known as Faraday height. The value of h_F depends upon the satellite to the observer geometry.

The expression for the refractive index for the radio wave propagation, under QL (quasi longitudinal) and high frequency approximation simplifies to (2.3) which is as follows:

$$\mu = 1 - \tfrac{1}{2} X \pm \tfrac{1}{2} X Y_L$$

The two modes are (nearly) circularly polarised in opposite senses, and a plane polarised wave traversing the ionosphere can be regarded as the sum of "ordinary" and "extra-ordinary" components. Because the two components have different phase velocities, the plane of polarization continually rotates along the ray path of the wave. This phenomenon is known as "Faraday rotation".

Along a path element of ds, the "ordinary" and "extra-ordinary" waves undergo phase changes of:

$$d\phi_{o,x} = \frac{2\pi}{\lambda} \mu_{o,x} \, ds \qquad (2.7)$$

where λ is the free space wavelength. The plane of polarization of the resultant plane wave rotates through an angle $d\Omega = \tfrac{1}{2} (d\phi_o - d\phi_x)$ (2.8)

Using (2.3) we then have the Faraday rotation given by the relation:

$$\Omega = \frac{K}{f^2} \int_o^{hs} N(h) \; M(h) \; dh \qquad (2.9)$$

where M is the magnetic field factor, and is given by

$M = B \cos \theta \sec \chi$ in mks units,

B is the magnetic field of the earth in amp-turns/meter,

θ is the angle between the magnetic field and the direction of propagation of the satellite signal,

χ is the zenith angle of the satellite

f is the radio wave frequency in Hz,

N is the electron density in el.m^{-3},

K is a constant = 0.0297 and

h_s is the satellite height in meters.

The magnetic field factor is a much more slowly varying function of height than the electron density and hence can be taken out of the integration to obtain:

$$\Omega = \frac{K}{f^2} \bar{M} \int_0^{h_F} N(h)\, dh \qquad (2.10)$$

$$\Omega = \frac{K}{f^2} \bar{M} \; N_F \qquad (2.11)$$

where $N_F = \int_0^{h_F} N(h)\, dh$

and $\bar{M}$ is a weighted average of M over the height range of the ionosphere and it will be equal to the value of M at a particular height called the mean field height. The use of a mean magnetic field factor does not give the electron content upto the satellite height h_s, but gives the electron content N_F, upto certain height h_F, which is known as Faraday height, and its value depends upon the geometry of the observer to the satellite ray path. A detailed account of it has been given by Titheridge (1972), Almeida (1973), Davies et al. (1976) and Poletti-Liuzzi et al. (1977). The determination of the

corresponding h_F for Ootacamund to ATS-6 ray path has been described in the section 2.3. For all other low latitude stations, the mean field height has been taken to be 350 km with corresponding h_F equal to 2000 km (Titheridge 1972, Almeida 1973).

2.2.3 The Calibration Factors for Ω and ϕ

(a) The Calibration Angle for Ω (on 140 MHz):- In order to determine the absolute amount of Ω, the polarization of the transmitted wave at the satellite must be known. For an observer at any point on the earth's surface, the polar-aligned spin axis of a geostationary satellite will make an angle α with the observer's local vertical (Klobuchar 1966) where:

$$\alpha = (\cos \phi \sin h) \left[\sin (\cos^{-1} (\sin \phi \sin \delta + \cos \phi \cos \delta \cos h)\right]^{-1} \quad (2.12)$$

h being the equivalent celestial hour angle of the satellite

δ the equivalent declination of the satellite and ϕ the latitude of the observer

δ and h are determined using following relations:

$$\sin \delta = \cos Z \sin \phi + \sin Z \cos A \cos \phi \quad (2.13)$$

$$\cos \delta \sin h = - \sin Z \sin A \quad (2.14)$$

where Z is zenith distance of the satellite (=90 - elevation angle of the satellite)

A is azimuth of the satellite (north through east).

All these parameters for different stations to ATS-6 ray path are tabulated in table 2.1. The initial transmitted polarization

Table 2.1

Different parameters used for the calibration of Faraday rotation angle for ATS-6 to different stations ray-path

Station	ϕ °N	Z	A	δ	h	α
Ootacamund	11.4	49.5	257.7	-1.74	48.0	73.4
Bombay	19.1	48.1	247.5	-2.90	43.5	60.9
Rajkot	22.3	47.6	242.5	-3.40	41.0	55.3
Ahmedabad	23.0	49.7	243.3	-3.59	43.0	55.5
Udaipur	24.6	51.4	242.8	-3.73	44.2	54.1
Jaipur	27.0	54.5	242.5	-4.12	46.4	52.4
Patiala	30.3	56.8	240.3	-4.69	46.8	48.8

angle (β_T)at the satellite is +90° (Klobuchar 1975). If β_r is the angle recorded on the chart when the signal is vertical, then the Faraday rotation angle Ω_o corresponding to the zero of the chart is given by:

$$\Omega_o = \alpha + \beta_T - \beta_r + m\pi \qquad (2.15)$$

β_r was determined to be zero for the polarimeters used at Patiala, Udaipur, Ahmedabad, Rajkot and Bombay. The $m\pi$ ambiguity can easily be settled in the years of low solar activity. The nighttime value of TEC is of the order of 2×10^{16} el m^{-2} while one rotation of π is equivalent to 5.75 TEC units (1 TEC unit = 10^{16} el m^{-2}) for Patiala and increases to

about 10.3 TEC units for Bombay.

The NOAA receiver used at Ootacamund reads 93.5° when the transmitted signal at 140 MHz is vertical. Also the receiver has a scale from 0 to 360° while Ω has the range 0 to 180° hence

$$2\Omega_o = 93.5 - 2(\alpha + \beta_T)$$
$$\text{or } \Omega_o = 116.6° \simeq 117°$$

For the signal at 40 MHz, the corresponding angle Ω_o is equal to 7° since the receiver reads -19.8° or +340° for equal phase at receiver input.

(b) The Calibration Angle for ϕ (140/360 MHz, 1 MHz):-

For the equal phase at receiver input, the NOAA receiver reads -159.6° or approximately -160°. The transmitter phase difference on the satellite is -63° hence the total phase difference, in the absence of any ionosphere would be -160-63 = -223°.

Hence $\phi_c = \phi_R - 223°$ where ϕ_c is the corrected phase difference and ϕ_R is the phase as read from the chart or the tape.

2.3 Magnetic Field Factor Calibration for Ootacamund to ATS-6 Ray-path

A method of determining $\bar{M}$ has been described by Titheridge (1972). A slightly modified version of this technique has been used to determine $\bar{M}$ and h_F for Ootacamund to ATS-6 ray path. It is to be noted that Titheridge's analyses did not extent to stations with magnetic latitudes below 10° whereas Ootacamund is

a near equatorial station with magnetic dip latitude 3°.

From equations (2.9) and (2.11) it is found that :

$$\bar{M}\ N_F = \int_0^{h_s} N(h)\ M(h)\ dh \qquad (2.16)$$

The electron content upto certain height H is :

$$N_H = \int_0^{H} N(h)\ dh \qquad (2.17)$$

Hence

$$\frac{\bar{M}\ N_F}{N_H} = \frac{\int_0^{hs} N(h)\ M(h)\ dh}{\int_0^{H} N(h)\ dh} \qquad (2.18)$$

In Fig.2.1a,b the ratio $\bar{M}\ N_F/N_H$, as determined from the equation (2.18) is plotted against altitude H, for a variety of electron density profiles. If the various curves pass through a point of convergence, then that point gives the appropriate values of $\bar{M}$ and h_F for converting the Faraday rotation angle into electron content N_F, independent of the N(h) profiles within the range of profile shapes considered. Fig.2.1a has been constructed using electron density profiles obtained over Kodaikanal. The profiles for daytime and night-time hours are separately shown in Fig.2.2(a,b). These profiles have been obtained by combining simultaneous bottomside and the topside profiles. Bottomside profiles have been obtained by reducing the ionograms recorded at Kodaikanal, by Budden's matrix method whereas the topside profiles over Kodaikanal have been obtained by reducing the topside ionograms recorded at Ahmedabad. Out of different passes

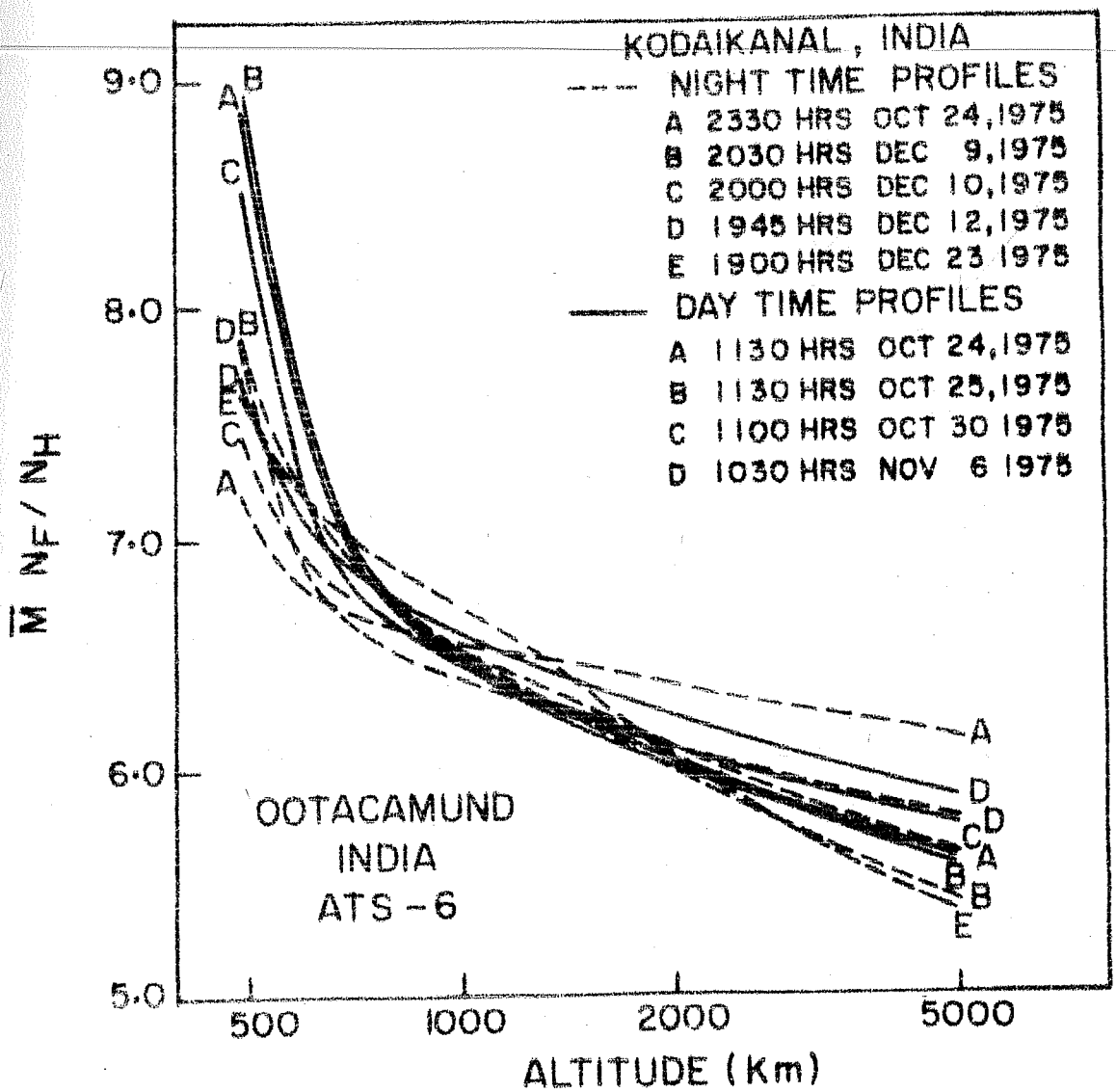

Fig.2.1a Ratio of $\int_{0}^{hs} N(h)\, M(h)\, dh$ to the content upto a height H versus height at Ootacamund using Kodaikanal N(h) profiles (Fig.2.2).

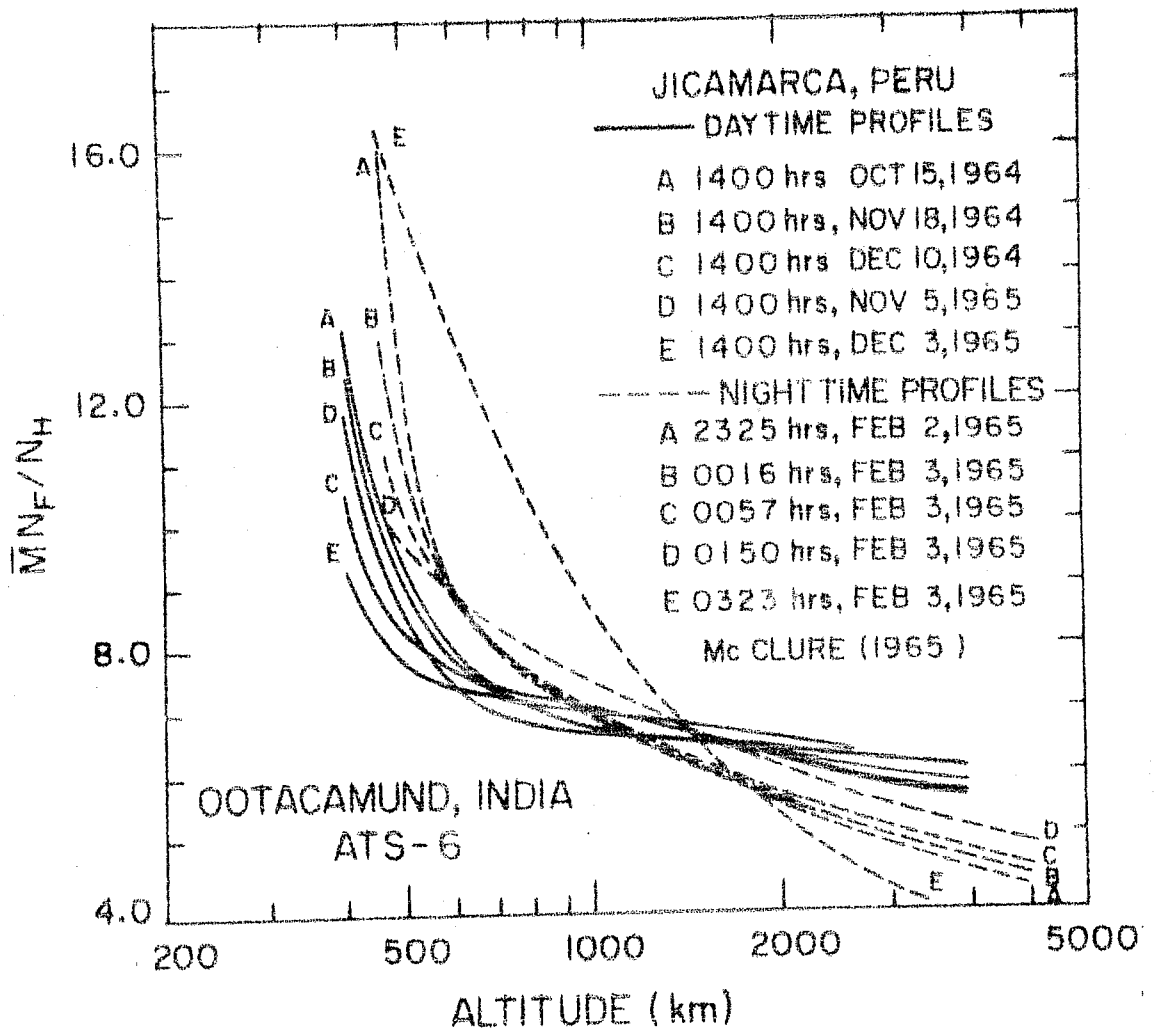

Fig.2.1b Similar to Fig.2.1a for Jicamarca profiles (Fig.2.3).

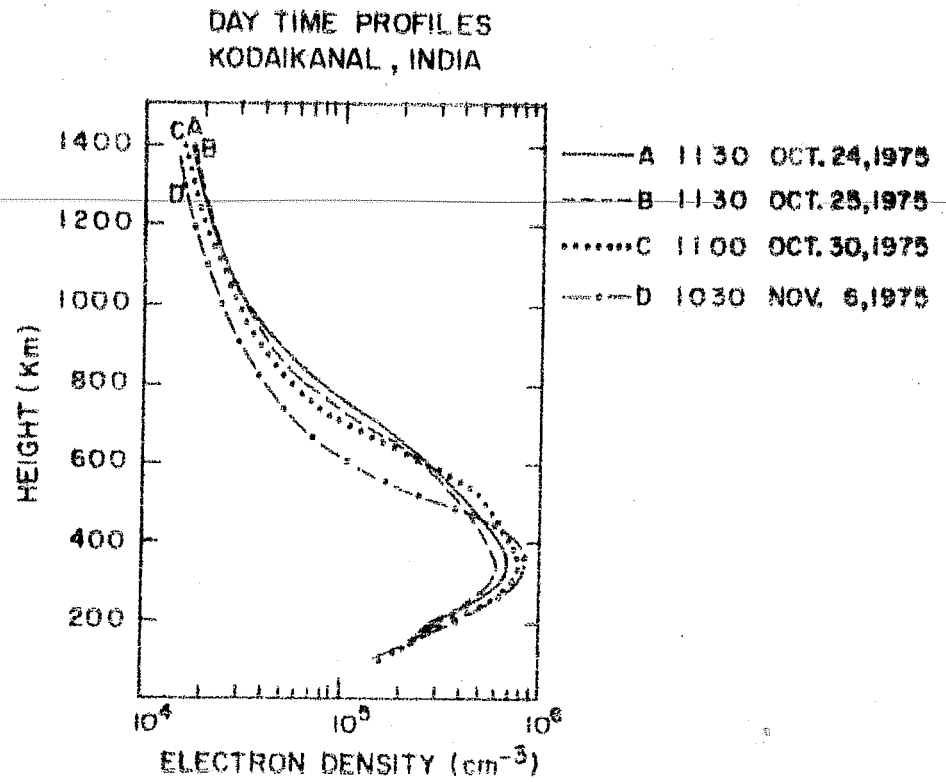

(a)

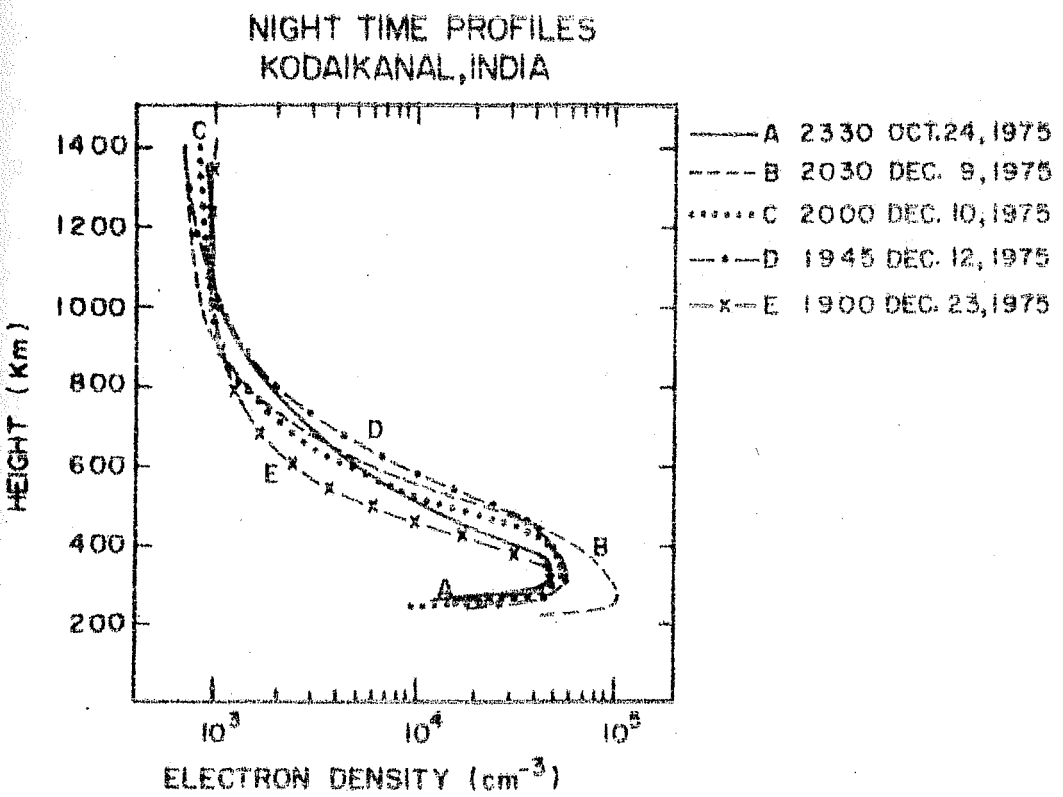

(b)

Fig.2.2 Electron density profiles over Kodaikanal for (a) daytime hours (b) night-time hours.

recorded at Ahmedabad, the ionograms over Kodaikanal were selected and reduced by "paraholic in log N method" (Jackson 1969). Fig.2.1b has been constructed from electron density profiles obtained at Jicamarca (Fig.2.3a, 2.3b) using incoherent backscatter radar (McClure 1965). The magnetic field model used has been described in a later section. From Fig.2.1a,b, it is noticed that if we pick $\bar{M}$ = 6.27 (which corresponds to an altitude of 400 km) and h_F =1500 km, then the value of N_F deduced from the Faraday rotation measurements would differ from the true $\int_0^{h_F} N(h)\, dh$ by about $\pm$ 5% among this group of electron density profiles. The Kodaikanal profiles have been used to obtain the integrated electron content upto an altitude of 3500 km which is the altitude of change over to quasi-traverse propagation for Ootacamund to ATS-6 raypath (Davies et al. 1979). The electron content so obtained has been compared with the electron content obtained by converting the measured value of Faraday rotation angle, into electron content using $\bar{M}$ = 6.267. The values have been tabulated in Table 2.2.

Table 2.2

Profiles	Calculated TEC	Observed TEC	ΔLong.
Daytime profiles			
A	27.5	29.9	7.3°
B	25.1	26.7	3.4°
C	30.3	32.0	0.6°
D	27.2	29.7	16.6°
Night-time profiles			
A	9.8	9.3	1.0°
B	22.9	22.6	2.3°
C	12.4	12.3	13.0°
D			

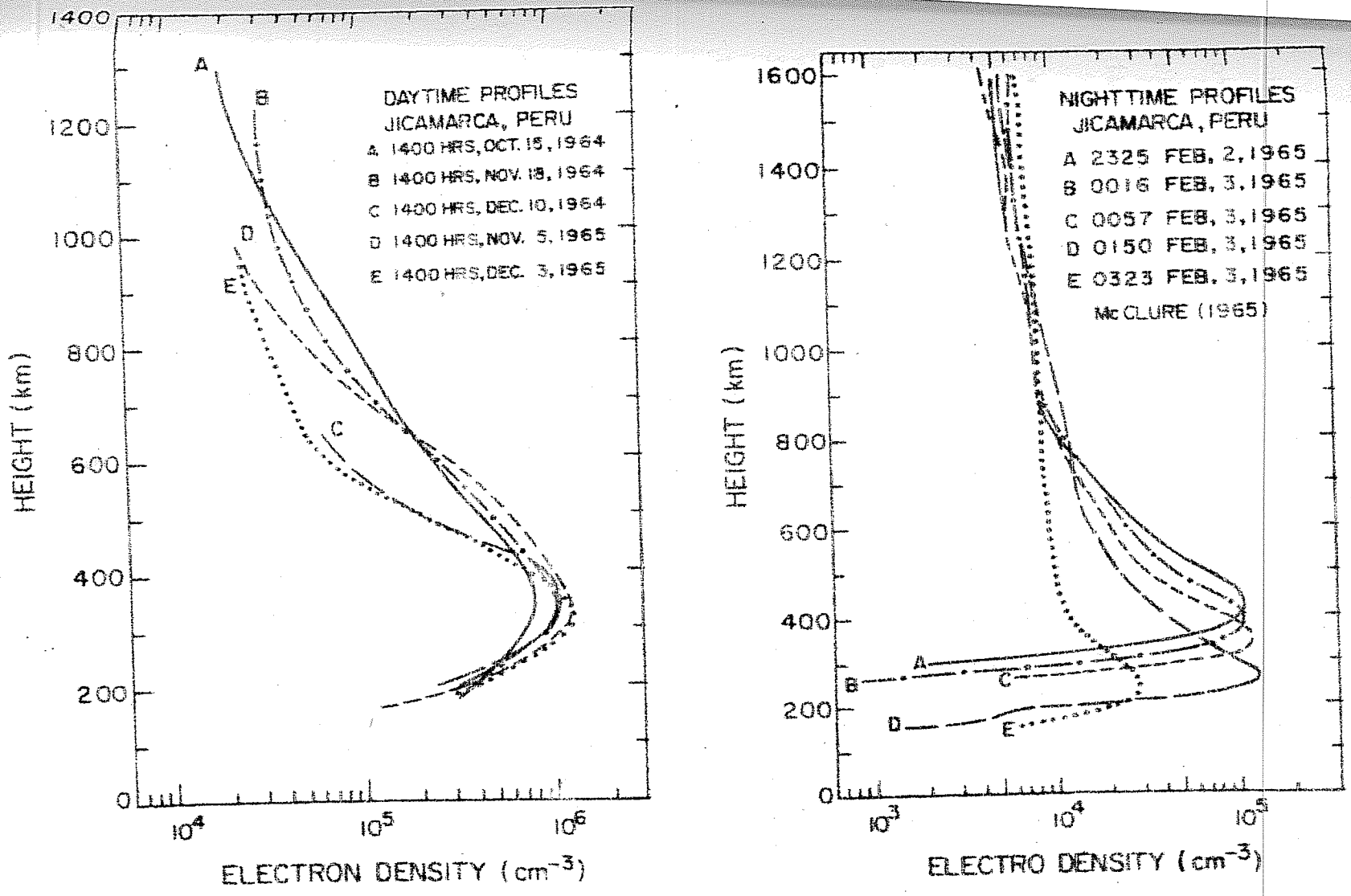

Fig.2.3 Electron density profiles over Jicamarca for (a) daytime hours and (b) night-time hours.

$\triangle$Long is the longitude difference between the topside pass and the Kodaikanal. It is noted that the calculated and the observed values are reasonably comparable. Some of the discrepancies may be attributed to the longitude difference between the observation points.

2.4 Computation of Elevation, Azimuth Range and Sub-Ionospheric Points

Let R be the radius of the earth and h_s be the height of the satellite. Also let us assume that ϕ_o is latitude and λ_o is longitude of the observer, whereas ϕ_s and λ_s are the corresponding quantities for the sub-satellite point. Then, referring to Fig.2.4, the range of the satellite R_s is given as:

$$R_s = R^2 + (R+h_s)^2 - 2R(R+h_s)\cos a)^{\frac{1}{2}} \qquad (2.19)$$

where $\cos a = \cos b \cos c + \sin b \sin c \cos A$

and $b = 90 - \phi_o$

$c = 90 - \phi_s$

and $A = \lambda_o - \lambda_s$

The elevation angle θ is expressed as:

$$\theta = \cos^{-1}\left(\frac{(R+h_s)}{R_s}\sin a\right) \qquad (2.20)$$

Therefore the zenith angle χ is given by:

$$\chi = 90 - \theta$$

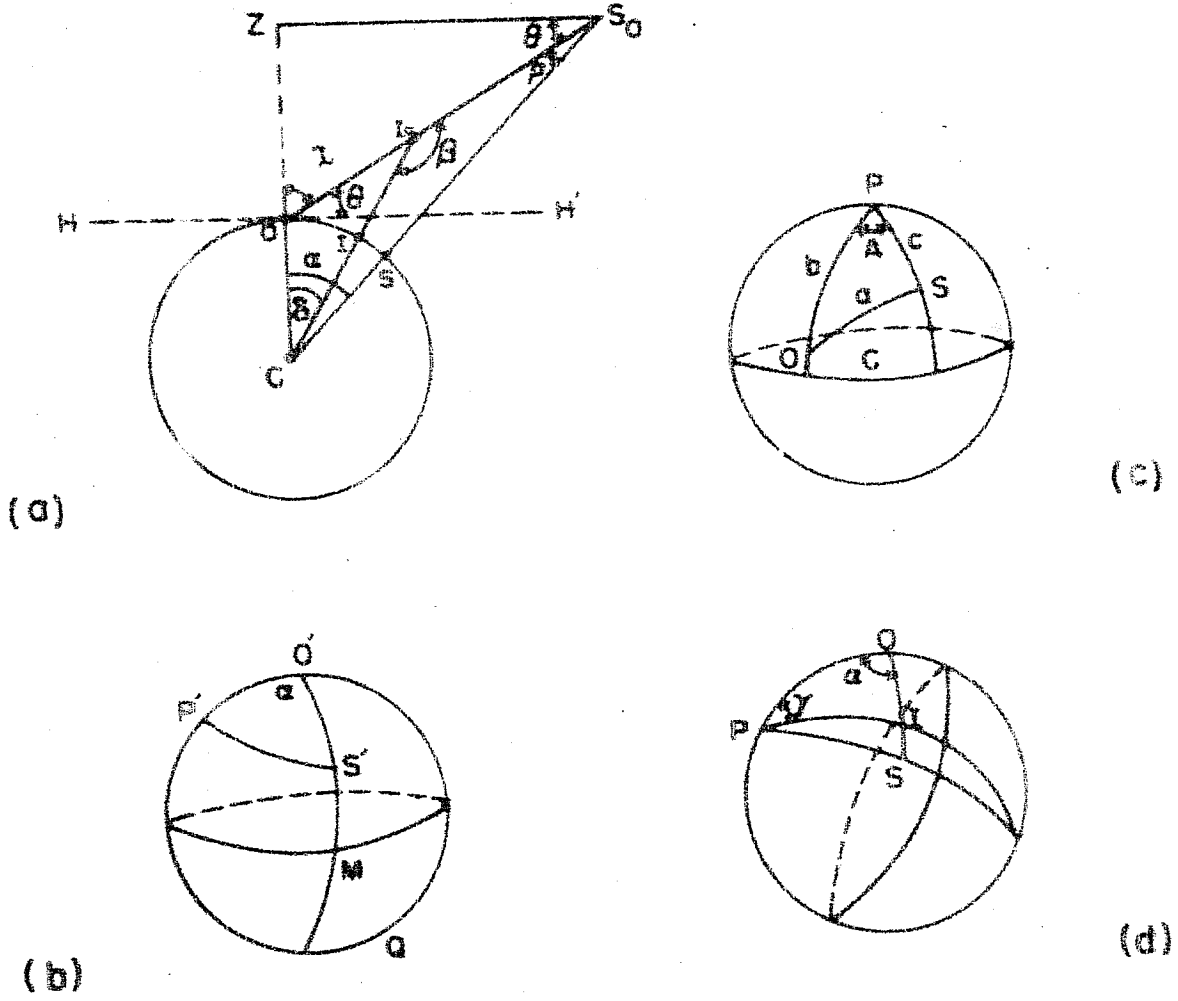

Fig.2.4 Geometry for the calculations of the elevation angle, the azimuth angle and the sub-ionospheric points.

The sub-ionospheric longitude (λ_i) and latitude (ϕ_i) are given as:

$$\lambda_i = \lambda_o - \tan^{-1}\left(\frac{\sin\delta \sin\alpha}{\cos\delta \sin\beta - \sin\delta \cos b \cos\alpha}\right) \quad (2.21a)$$

$$\text{and } \phi_i = 90 - \sin^{-1}\left(\frac{\sin\delta \sin\alpha}{\sin\gamma}\right) \quad (2.21b)$$

$$\text{where } \delta = \sin^{-1}\left[\left(\frac{R + h_s}{R + h_i}\right) \left(\frac{R \sin a}{R_s}\right)\right] - (90 + \theta)$$

$$\text{and } \alpha = 2 \sin^{-1} \left(\sin (s-b) \sin (s-a)/\sin b \sin a\right)^{\frac{1}{2}}$$

$$\text{where } s = \frac{a+b+c}{2}$$

and h_i is the ionospheric height, α as given above is the azimuth angle of the satellite.

In this way the elevation angle, azimuth angle, range and the sub-ionospheric points for the satellite can be calculated. All these parameters for different stations have been given in Tables 2.3(a,b).

Table 2.3a gives the coordinates of the stations and also the elevation, the azimuth and the range for the satellite APS-6. The elevation angle of the satellite as viewed from different locations in India will be different and will decrease as one progresses towards east. In Fig.2.5 is shown contour map of elevation angle and it is clear that in the west-coast of India, the angle is as high as 42° whereas in the eastern region it is as low as 20°. From a particular station when the satellite is being viewed the ionospheric latitudes and longitudes will be

Table 2.3a

Coordinates of ATS-6 stations in India and their look angles to the satellite

ation	Latitude °N	Longitude °E	Magnetic dip °N	Magnetic dip lat. °N	Elevation °above horizon	Azimuth °E of north	Range R_s (km)
umba	8.5	77.0	-0.6	-0.3	40.8	261.0	37931
tacamund	11.4	76.7	6.0	3.0	40.5	257.7	37952
ltair	17.7	83.3	19.9	10.3	32.1	255.1	38641
ona	18.6	74.0	22.6	11.8	41.0	248.0	37917
mbay	19.1	72.9	24.8	13.0	41.9	247.5	37851
pur	21.3	79.2	28.0	14.9	34.9	249.8	38400
jkot	22.3	70.7	33.0	18.0	42.4	242.4	37812
lcutta	22.4	88.2	32.0	17.4	26.0	254.3	39194
medabad	23.0	72.6	34.0	18.6	40.3	243.3	37968
aipur	24.6	73.7	36.6	20.4	38.6	242.8	38102
uhati	26.2	91.5	36.0	20.0	21.8	253.9	39594
ipur	26.9	75.8	39.2	22.2	35.5	242.5	38351
lhi	28.8	77.2	42.4	24.5	33.4	242.3	38527
tiala	30.4	76.4	45.0	26.6	33.3	240.4	38541

Table 2.3b

Coordinates of sub-ionospheric points for different stations to ATS-6 ray-paths and corresponding mean magnetic field factors

Station	Latitude °N	Longitude °E	Magnetic dip °N	Magnetic dip lat.°N	$\bar{M}$
Thumba	7.9	73.2	-1.4	-0.7	1.55
Cotacamund	10.6	72.9	4.4	2.2	6.27
Waltair	16.5	78.8	17.9	9.2	16.71
Poona	17.4	70.8	20.5	10.6	18.67
Bombay	17.8	69.8	22.5	11.7	19.51
Nagpur	19.8	75.1	25.6	13.5	22.85
Rajkot	20.8	67.7	30.6	16.5	24.69
Calcutta	20.8	82.5	29.8	16.0	24.69
Ahmedabad	21.5	69.4	31.6	17.1	25.77
Udaipur	22.9	70.2	34.1	18.7	28.15
Gauhati	24.2	84.6	33.8	18.5	31.07
Jaipur	25.1	71.9	36.8	20.5	31.74
Delhi	26.7	73.0	39.6	22.5	34.43
Patiala	28.2	72.1	42.3	24.5	36.72

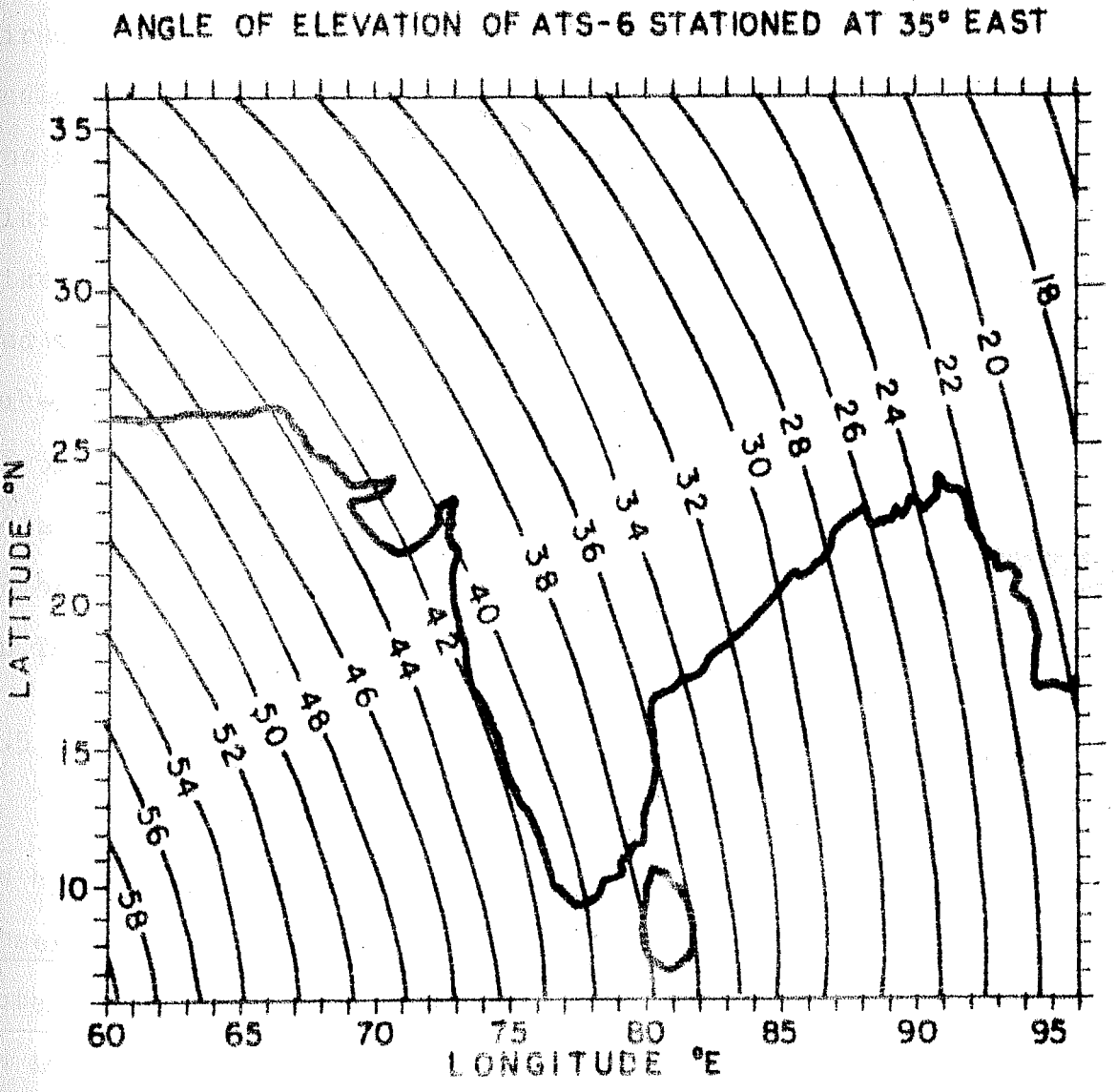

Fig.2.5 The contour map of elevation angle for the satellite ATS-6 positioned at 35°E.

different at different ionospheric heights. We have, therefore, computed these parameters at different ionospheric heights at intervals of 100 km. These results for 100, 200, 300, 400 and 500 km are shown in Fig.2.6, in which the arrows represent the directions to ATS-6 from each of the stations. The open circles indicate the sub-ionospheric points at every 100 km altitude. The separation between two open circles, for a western station like Ahmedabad will be less as compared to an eastern station like Gauhati. This is due to high elevation angle at Ahmedabad and the low elevation angle at Gauhati. The coordinates of the sub-ionospheric points (corresponding to a mean field height of 350 km for all the stations except the near equatorial station Ootacamund and Thumba for which the mean field heights are taken to be 400 km) for different stations to ATS-6 raypaths, are given in Table 2.3b.

2.5 Computations of Magnetic Field Factors

To evaluate the magnetic field at any point, the field has to be expressed in terms of a suitable model fitted from various observations. The spherical harmonic expansion of the magnetic potential of the earth, and the derivation of the field from it is followed here.

The magnetic field model used in the calculations of M is that of given by Jones and Melotte (1953). The magnetic vector potential in spherical harmonic coordinate system is given by:

$$V = R \sum_{n=1}^{\infty} \sum_{m=o}^{n} \left(\frac{R}{r}\right)^{n+1} H_n^m (\mu) \left(g_n^m \cos m \phi + h_n^m \sin m \phi\right) \qquad (2.22)$$

where $\mu = \cos\theta$

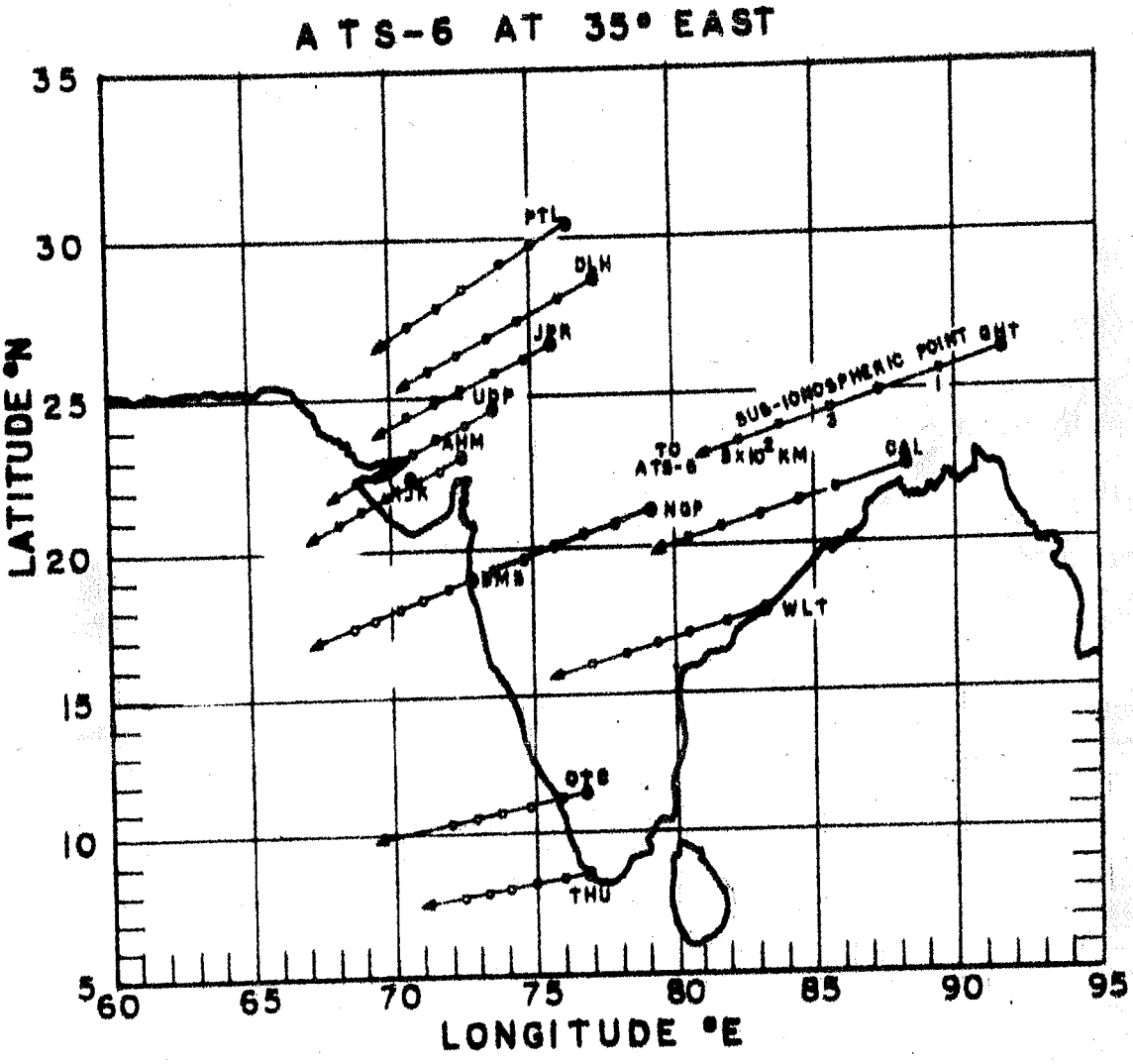

Fig.2.6 Some of the stations involved in ATS-6 project. The arrows point towards ATS-6 satellite and the open circles on the arrows indicate sub-ionospheric points at every 100 km altitude.

R is the radius of the earth

r is the distance of the point (from the centre of the earth) at which field is required.

θ is the geographic colatitude of this point

ϕ is the geographic longitude of the point

g_n^m and h_n^m are the Gaussian coefficients

$$\text{and } H_n^m(\mu) = \frac{2^n \lfloor n \lfloor n-m}{\lfloor 2n} (1-\mu^2)^{m/2} \frac{d^m}{d\mu^m} P_n(\mu) \quad (2.23)$$

The spherical harmonic expansion used 48 coefficients of Jensen and Cain (1962) which expands the magnetic potential upto the terms of 6th order and 6th degree. The legendre polynomials are taken from Morse and Feshbach (1953). The magnetic field factor M is given as:

$$M = B \cos\theta \sec\chi$$

M changes with height because of height dependence of B, cos θ and sec χ. The magnetic field factors have been calculated with altitude, for different stations to ATS-6 ray-paths and are shown in Fig.2.7. Near equator (like Thumba) M does not vary much with altitude whereas away from the equator (like Patiala), the variations of M with altitude are large. The mean magnetic field factors ($\bar{M}$) (corresponding to a mean field height of 400 km for Ootacamund and Thumba, and 350 km for all other stations) are given in Table 2.3b. These are the values which have been used in the present investigations to convert Faraday rotation angle into electron content N_F.

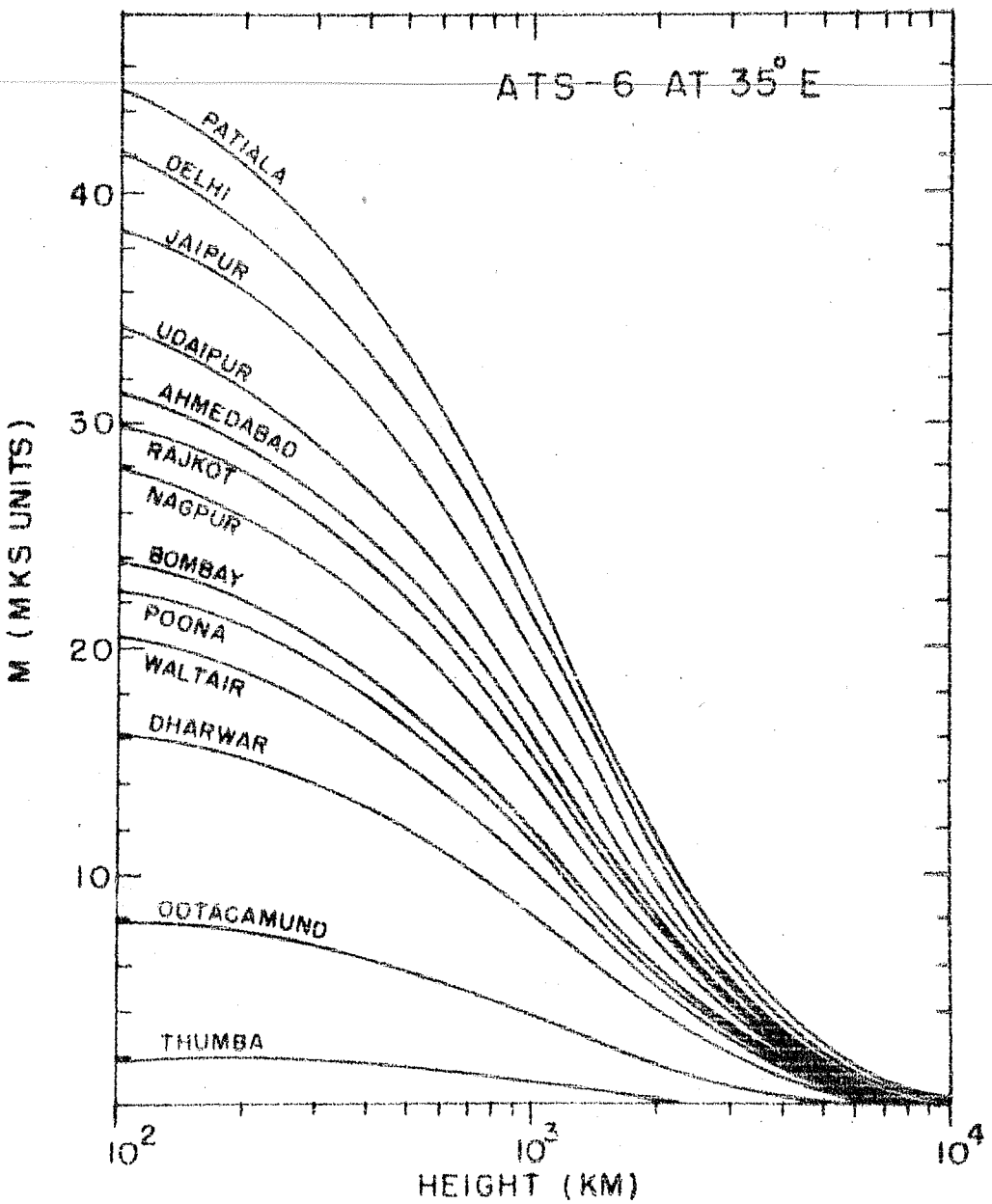

Fig.2.7 The variation of magnetic field factor (M) with altitude for different stations.

CHAPTER - III

MORPHOLOGY OF ELECTRON CONTENT MEASUREMENTS AT LOW LATITUDES

3.1 Introduction

The determination of Total electron content (TEC) in a vertical column of the ionosphere is of considerable importance for the study of the upper atmosphere as well as for planning the radio communication between an artificial satellite and a ground station. A big spurt of such measurements came with the launching of BE-B and BE-C satellites, orbiting at heights of 1000-1400 km. With proper coordination of two or more stations, one can cover a large portion of the ionosphere at one time. (Basu and Das Gupta 1967, Shirke and Ramakrishnan 1966, Olatunji 1967, Tyagi and Mitra 1970, Walker and Ma 1972, Rastogi et al. 1973). The data from these low orbiting satellites do not provide reliable estimate for diurnal variation of TEC and the transient phenomena like solar flare and sudden commencement effects cannot be studied with this method. The beacons aboard a geostationary satellite provide a continuous measurement of TEC at a particular location but do not give any idea of the spatial variation of TEC. With the coordination of a number of stations using the same beacons it is possible to have both temporal and spatial variation of TEC.

TEC measurements using low orbiting as well as geostationary satellites have been extensively made, however very meagre data exist for low and tropical latitudes. With the repositioning of

ATS-6 at 35°E longitude, a rare opportunity was provided to the scientists in different parts of India for continuously monitoring the beacon for a period of about one year. The details about the location of different institutions and other related parameters have been described in the Chapter-II. In sections 3.3 and 3.4 the results of electron content from Faraday rotation and Group delay measurements made at the equatorial station Ootacamund are described. A brief account of the results of FR measurements made at low latitudes in Indian zone, using orbiting and geostationary satellites has been given in the next section.

3.2 A Brief Account of TEC Measurements at Low Latitudes in Indian Zone

3.2.1 Using Orbiting Satellite Data

As a part of the Indian space research programme, a satellite study of the ionosphere by Faraday rotation technique was started at PRL, Ahmedabad when the beacon Explorer-B satellite of NASA went into orbit in the last quarter of 1964. The method of analysis and some of the preliminary results were reported by Shirke and Ramakrishnan (1966). Faraday rotation observations of signals from the Beacon satellites S_{66} (BE-B and BE-C) were made at Thumba during 1965-68 and the results were reported by Rastogi et al. (1973). The N_F value reached a minimum around 05 hr and a broad maximum between 14-18 hr, the diurnal ratio being more than 20. No definite conclusion was drawn regarding midday bite-out in N_F. Similar measurements made at Ahmedabad (34°N dip) during 1964-69 showed that the daily variation of N_F

and of maximum electron density N_{max}, for any season, are similar (Rastogi and Sharma 1971) viz. both show a minimum at 05 hr and a broad maximum around 14-16 hr. The diurnal ratio of N_F is found to be 15-20 for any of the seasons of low sunspot years. Rastogi et al. (1975) and Iyer and Rastogi (1978) made an extensive study of N_F at Kodaikanal, using Faraday rotation measurements from S_{66} satellites, for the period 1964-69. The diurnal variation of N_F shows the absence of noon bite-out. The diurnal ratios are found to be 16.7, 11.8 and 8.0 in equinoxes, winter and summer respectively of low sunspot years. A slight tendency of winter anomaly in N_F was noticed in high sunspot years but it was clearly noticed in the low sunspot years. Rastogi et al. (1977) studied the latitudinal variations of N_F in Indian zone, combining Faraday rotation measurements during 1964-69 from the orbiting satellite BE-B at Ahmedabad and Kodaikanal. A latitudinal coverage from 10°S to 26°N was obtained. The contour maps of N_F were obtained on a grid of latitude versus local time for the different seasons of low and high solar activity epochs. Equatorial anomaly in the latitudinal variation of N_F is clearly noticed. In equinoxes the anomaly peak is around 13-14 hr LT in both low and high solar activity periods. Latitudinal peak is formed at 15° and 20° respectively in high and low solar activity conditions. In winter, latitudinal peak is around 12° dip lat in both low and high solar activity periods. The diurnal peak is around 13 hr LT in low and 15-16 hr LT in high solar activity periods. In summer the peak is broad around 13°N dip latitude in low and high solar activity periods. It is formed around 13 hr
and

The results of Faraday rotation measurements made at Delhi during Oct. 1964 to June 1965, were reported by Tyagi and Somayajulu (1966). The diurnal maximum was noticed around 13-14 hr LT and the variations in N_F closely followed the f_0F_2 variations. The electron content was found to be independent of solar activity until the 10.7 cm solar flux exceeded 80 units. Similar measurements carried out at Haringhata (dip 32°N) near the crest of the equatorial anomaly were reported by Gupta and Basu (1973). The diurnal variation followed the expected pattern with predawn minimum and early afternoon maximum. The rate of decay in the afternoon was found to be slower than the rate of increase during morning hours.

3.2.2 Using Geostationary Satellite Data

Faraday measurements were made at Haringhata during Nov. - April 1972-73, using radio beacons from near geosynchronous satellite Intelsat 2F2 (Basu et al. 1974, Guhathakurta et al. 1978). The day to day variability and the magnetic activity effects on N_F and the slab-thickness were studied. The results of Faraday rotation measurements made during 1975-76 at Bombay (11.7°N, sub.ion. dip lat), Rajkot (16.5°N), Ahmedabad (17.1°N), Udaipur (18.7°N) and Patiala (24.5°N) using geostationary satellite ATS-6 have been reported recently (Singh et al. 1978). The main findings are as follows:- (i) The amplitude of diurnal peak is found to be higher at Rajkot, Ahmedabad and Udaipur as compared to that at Patiala or Bombay, indicating that the peak of Appleton anomaly in the latitudinal variation of N_F is close to the

latitude of Ahmedabad, (ii) The peak electron content shows a semiannual variation at all the stations with large values in equinoxes as compared to winter and summer, (iii) An important feature observed is that the daytime N_F at Bombay is more during winter than in summer (the feature is known as 'winter anomaly') whereas at other stations, either the summer and winter values are comparable (Ahmedabad and Rajkot) or the summer values are more than winter values (Udaipur and Patiala), (iv) The equatorial anomaly is prominent during 1000 hr to 1800 hr LT and the crest is located at about 14°N (dip lat.) in summer and equinoxes and at about 10°N in winter i.e. equatorward movement of the equatorial anomaly crest is noticed during winter, (v) The diurnal maximum of N_F occurs around the same time during summer and winter months. In equinoxes the diurnal peak occurs earlier than in winter and summer.

3.3 Electron Content Measurements at Ootacamund Using Faraday Rotation Technique (N_F)

3.3.1 Diurnal Variation

To examine the overall behaviour of N_F, the annual mean daily variation of N_F is studied and shown in Fig.3.1. This shows a predawn dip around 0500 hr LT and a flat maximum around 1400 hr LT with diurnal ratio (ratio of the maximum to minimum) around 11.5. There is no indication of the noon bite-out in N_F, so prominently observed in the daily variation of f_0F_2 at equatorial stations. Fig.3.2 shows mean daily variation of N_F during each of the seasons.

latitude of Ahmedabad, (ii) The peak electron content shows a semiannual variation at all the stations with large values in equinoxes as compared to winter and summer, (iii) An important feature observed is that the daytime N_F at Bombay is more during winter than in summer (the feature is known as 'winter anomaly') whereas at other stations, either the summer and winter values are comparable (Ahmedabad and Rajkot) or the summer values are more than winter values (Udaipur and Patiala), (iv) The equatorial anomaly is prominent during 1000 hr to 1800 hr LT and the crest is located at about 14°N (dip lat.) in summer and equinoxes and at about 10°N in winter i.e. equatorward movement of the equatorial anomaly crest is noticed during winter, (v) The diurnal maximum of N_F occurs around the same time during summer and winter months. In equinoxes the diurnal peak occurs earlier than in winter and summer.

3.3 Electron Content Measurements at Ootacamund Using Faraday Rotation Technique (N_F)

3.3.1 Diurnal Variation

To examine the overall behaviour of N_F, the annual mean daily variation of N_F is studied and shown in Fig.3.1. This shows a predawn dip around 0500 hr LT and a flat maximum around 1400 hr LT with diurnal ratio (ratio of the maximum to minimum) around 11.5. There is no indication of the noon bite-out in N_F, so prominently observed in the daily variation of f_oF_2 at equatorial stations. Fig.3.2 shows mean daily variation of N_F during each of the seasons.

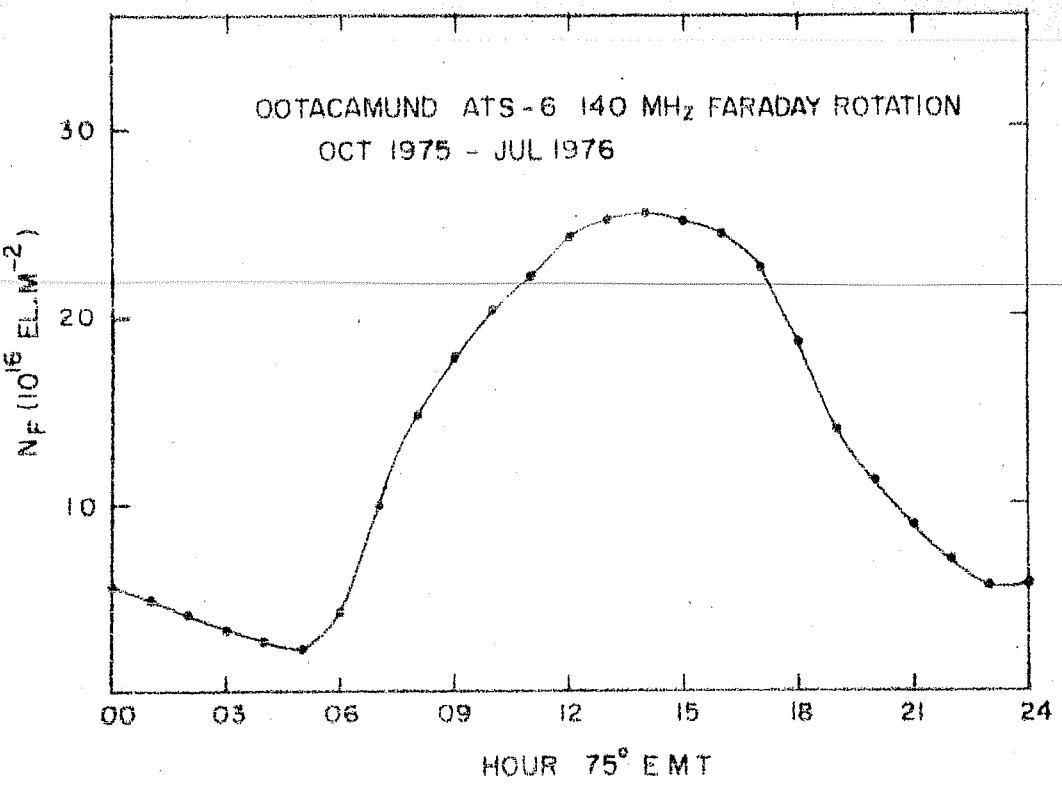

Fig.3.1 The annual mean daily variation of N_F.

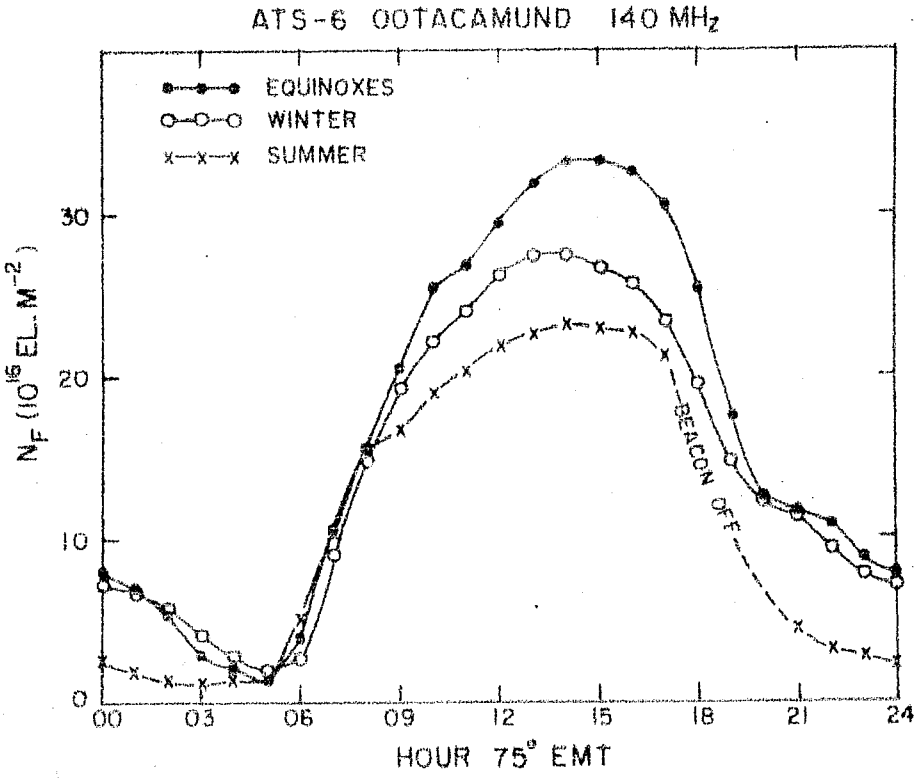

The equinoctial values during daytime hours are about 40% higher than the values for summer and about 20% higher than the winter values. The presence of 'winter anomaly' is noticed with daytime winter values higher than the summer values. During winter and equinoxes a steady decrease in N_F is observed between midnight and 0500 hr LT whereas in summer, the N_F remains more or less constant during this period. The diurnal peak for equinoxes and summer occurs around the same time (1400 hr LT) but in winter the diurnal peak occurs earlier by about an hour. The diurnal ratios for equinoxes, summer and winter are found to be around 28, 19 and 14 respectively. The diurnal ratio for other stations along with Ootacamund are given in Table 3.1. It is noted that diurnal ratios are the largest in equinoxes, the value being 25 ± 2 for all the stations. The locations near the crest of the equatorial anomaly have the lowest diurnal ratios in summer whereas Ootacamund and Patiala which are away from the crest have the lowest diurnal ratios in winter. In summer the maximum value of the diurnal ratio is found to be 19 at the equator, and 13 ± 1 at all other stations whereas in winter, the maximum value of about 16-17 is found to be near crest and the values decrease on either side of the crest, reaching as low as 8, at Patiala.

Table 3.1

Diurnal ratios for different seasons

Season	Ootacamund	Bombay	Ahmedabad	Udaipur	Patiala
Summer	19	13	14	13	12
Equinoxes	28	27	23	23	27

One significant feature which is noticed is the sharp decrease in the rate of increase of N_F around 0900 hr LT for summer and around 1000 hr LT for equinoxes (Fig.3.2). No such decrease is noticed for winter. These features are probably associated with the midday bite-out in f_oF_2 which is pronounced in equinoxes and summer but is weak in winter (Chandra and Rastogi 1971).

3.3.2 Seasonal Variation

The monthly mean hourly values for all the 10 months have been used to build a contour map on a grid of local time versus months (Fig.3.3). One notices a semi-annual trend in N_F with equinoctial maxima. This is suggested to be due to the observed excess of O/N_2 ratio during equinoctial months (Offerman 1974). Higher O/N_2 ratio not only yields excess production of ionization but also reduces the loss rate of ionization. An additional feature, one notices, is that the gradient in N_T is minimum in the immediate post-sunrise period. Also it is noticed that daytime N_F values for October are higher than the corresponding values for April. This feature described as anomalous semi-annual variation of N_F, has been discussed in Chapter V, section 5.3.

3.3.3 Latitudinal Variation

The mean annual contours of N_F on a latitude versus local time grid are shown in Fig.3.4. Presence of equatorial anomaly

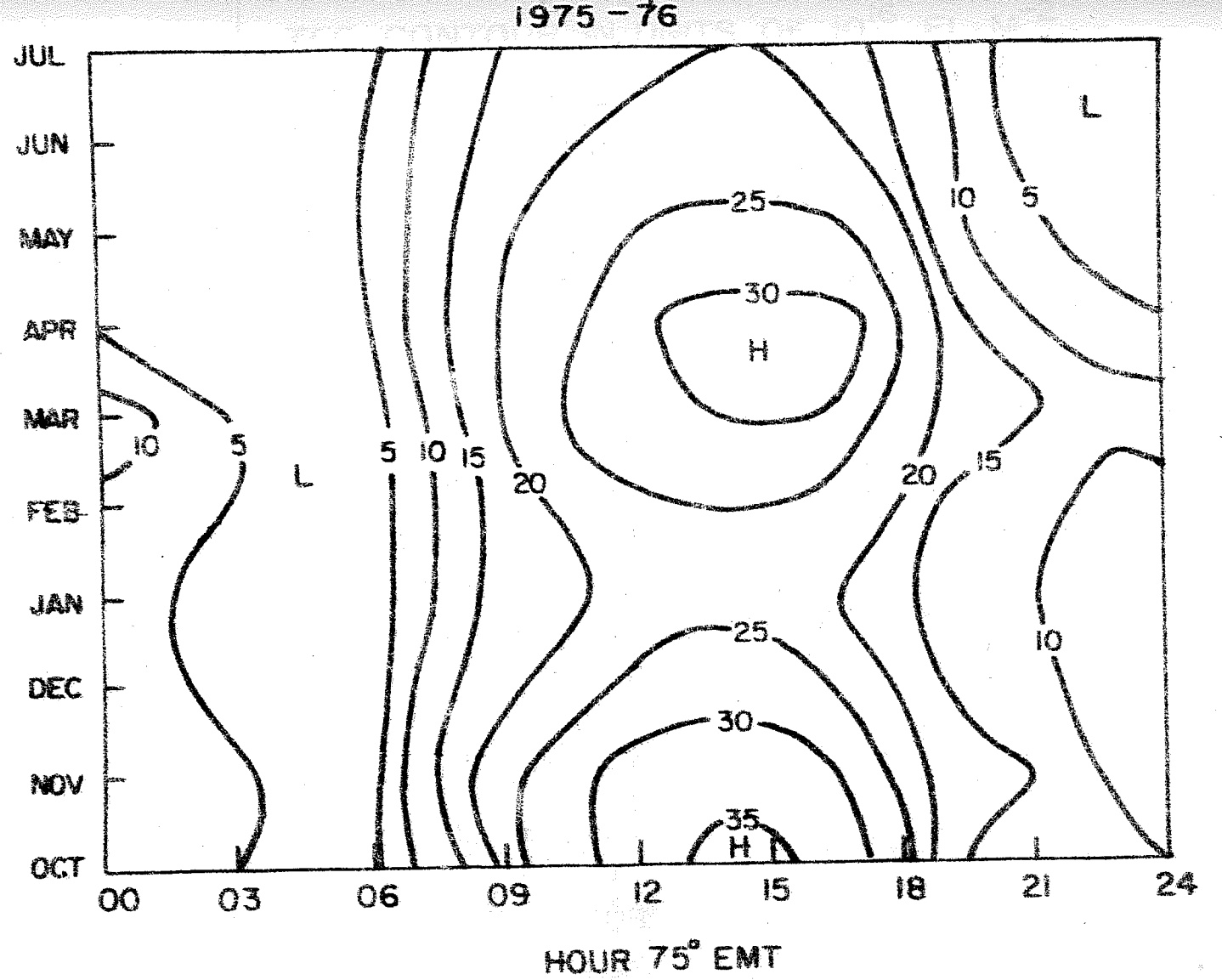

Fig.3.3 Contour map of N_F in units of 10^{16} el m^{-2} on a grid of local-time versus months.

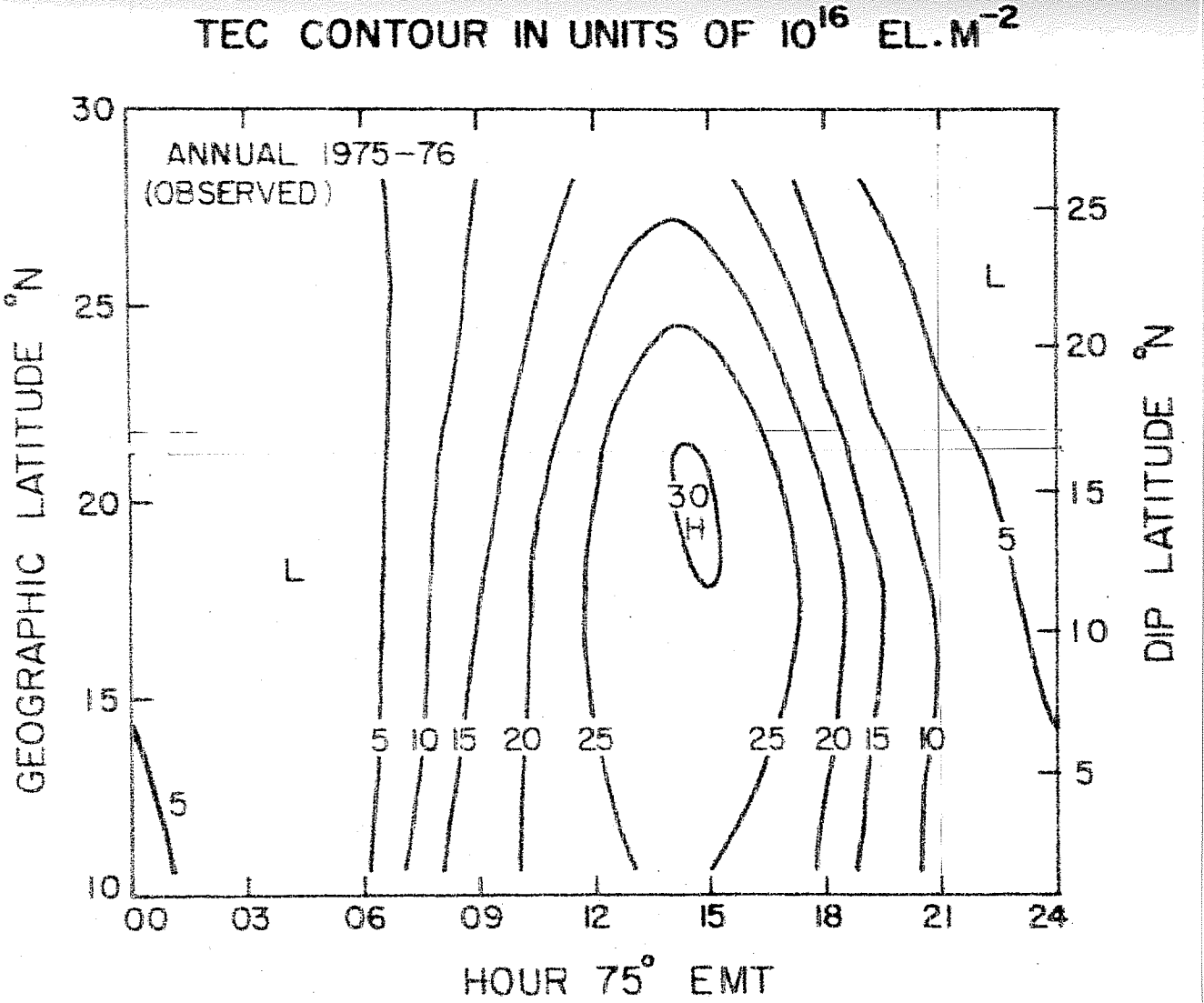

Fig.3.4 The mean annual contour of N_F on a grid of latitude versus local-time.

is clearly noticed with daytime contour lines being rounded off at latitudes going upto 25°N dip latitude. The crest is formed around 14°N dip lat and the crest to trough ratio is about 1.2 which is in agreement with theoretical estimations for a vertical drift of 4.1 m/s (Bramley and Peart 1965). For the sake of comparison with previous work and also for the purpose of model construction, the contours have been built up separately for each season and are shown in Fig.3.5(a,b,c). The crest of the equatorial anomaly is formed around 16°N, 15°N and 10°N dip latitudes for equinoxes, summer and winter respectively. The daytime N_F values for summer, winter and equinoxes are of the order of 25, 25 and 40 TEC units.

3.3.4 Day to Day Variation

To examine the day to day variability in N_F one base computer plots for three typical months (one each for each season) are shown in Fig.3.6 (a,b,c). Fig.3.6a shows one base plot for the month of January , a winter month. The daytime N_F values show the maximum variability and it is seen that N_F values for aan individual day may vary from its monthly mean by about 25-30%. Most of the days show the presence of secondary peak around 2100 hr LT. Fig.3.6b shows similar plot for the month of April, an equinoctial month. The general features are same except that presunrise values are quite low. Some of the days show exceptionally high values of N_F. These days are confirmed to be magnetic storm days. Most of the days show a decrease in the rate

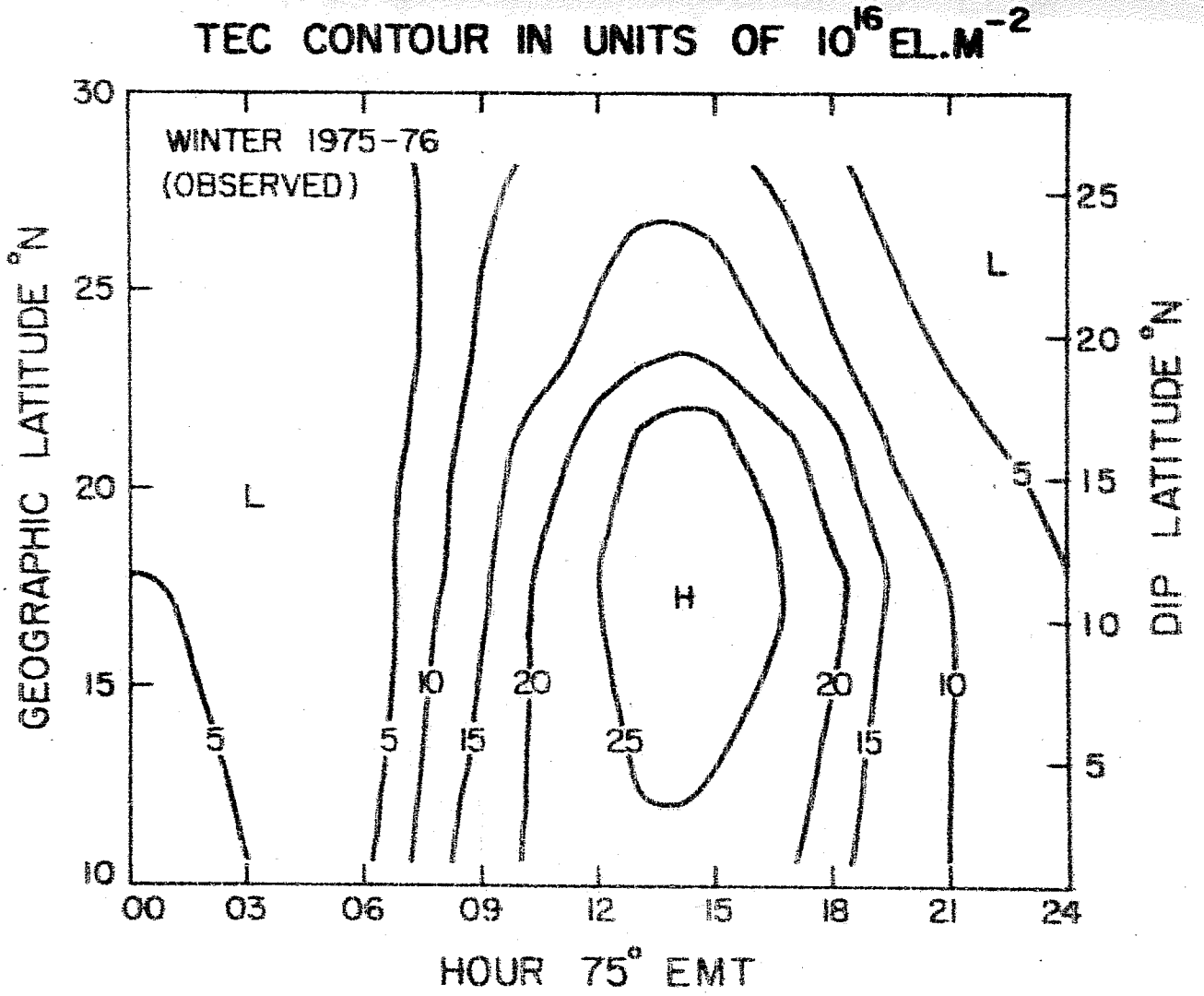

Fig.3.5a Seasonal TEC (N_F) contour for winter.

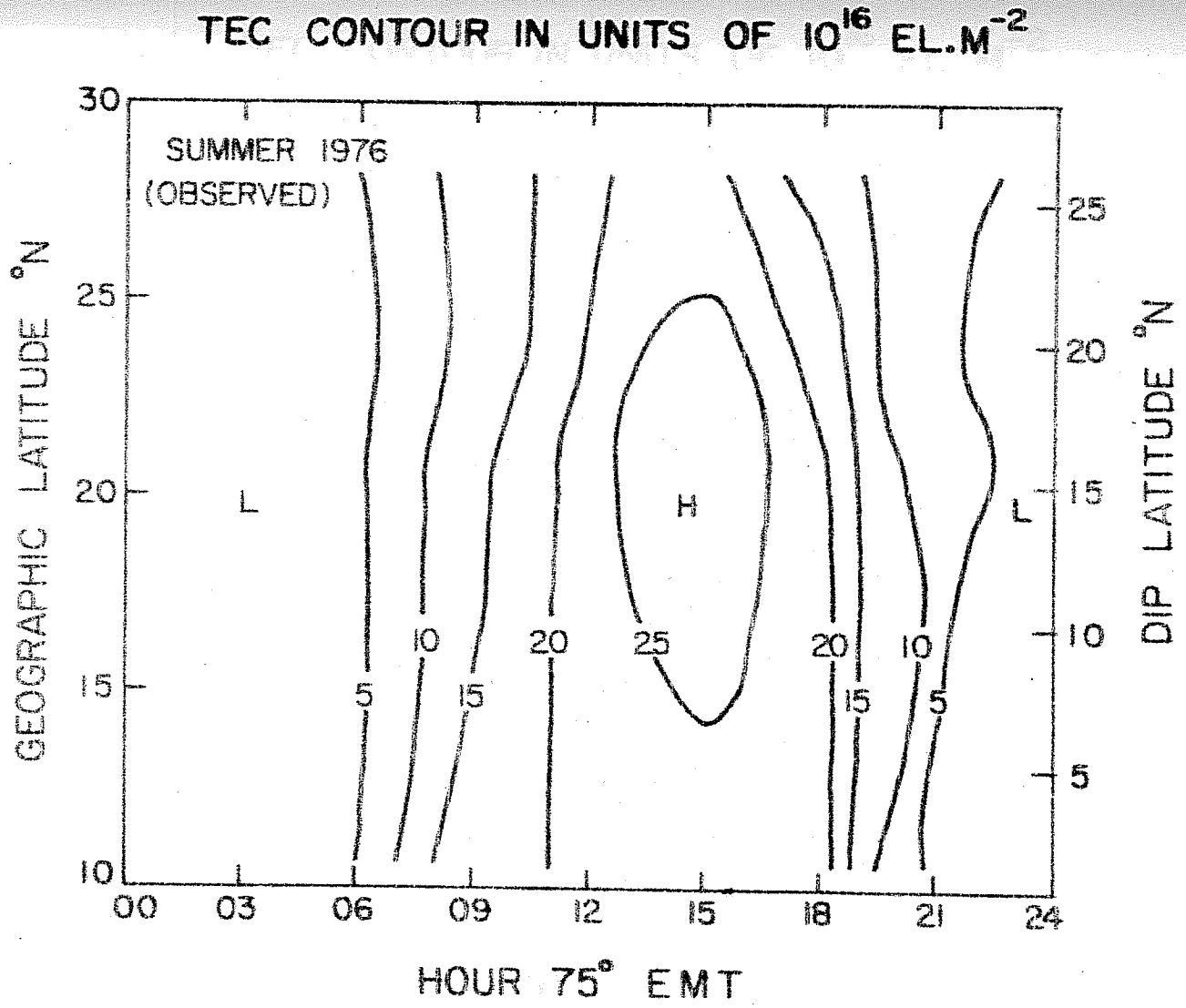

Fig.3.5b Seasonal TEC (N_F) contour for summer.

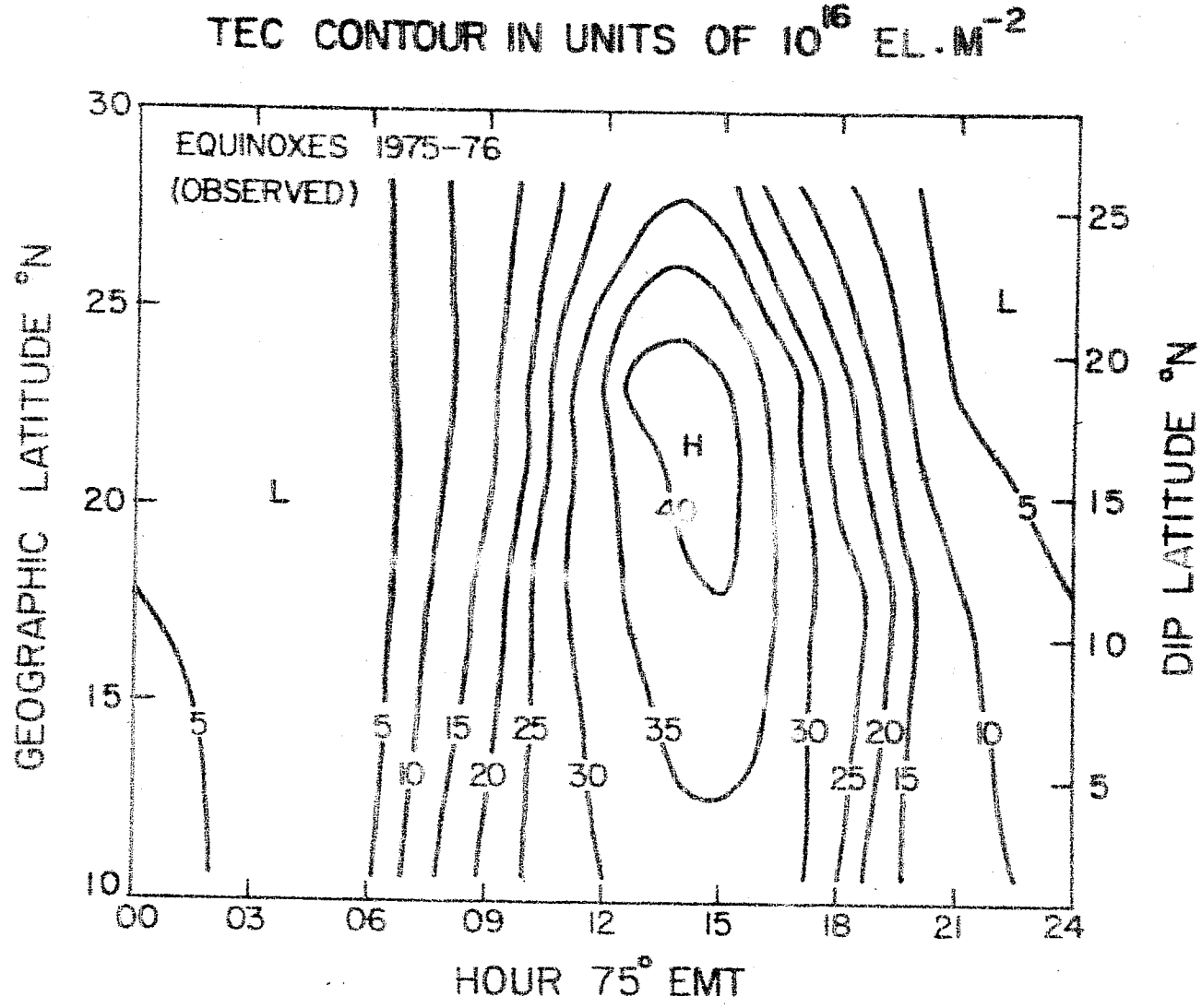

Fig.3.5c Seasonal TEC (N_F) contour for equinoxes.

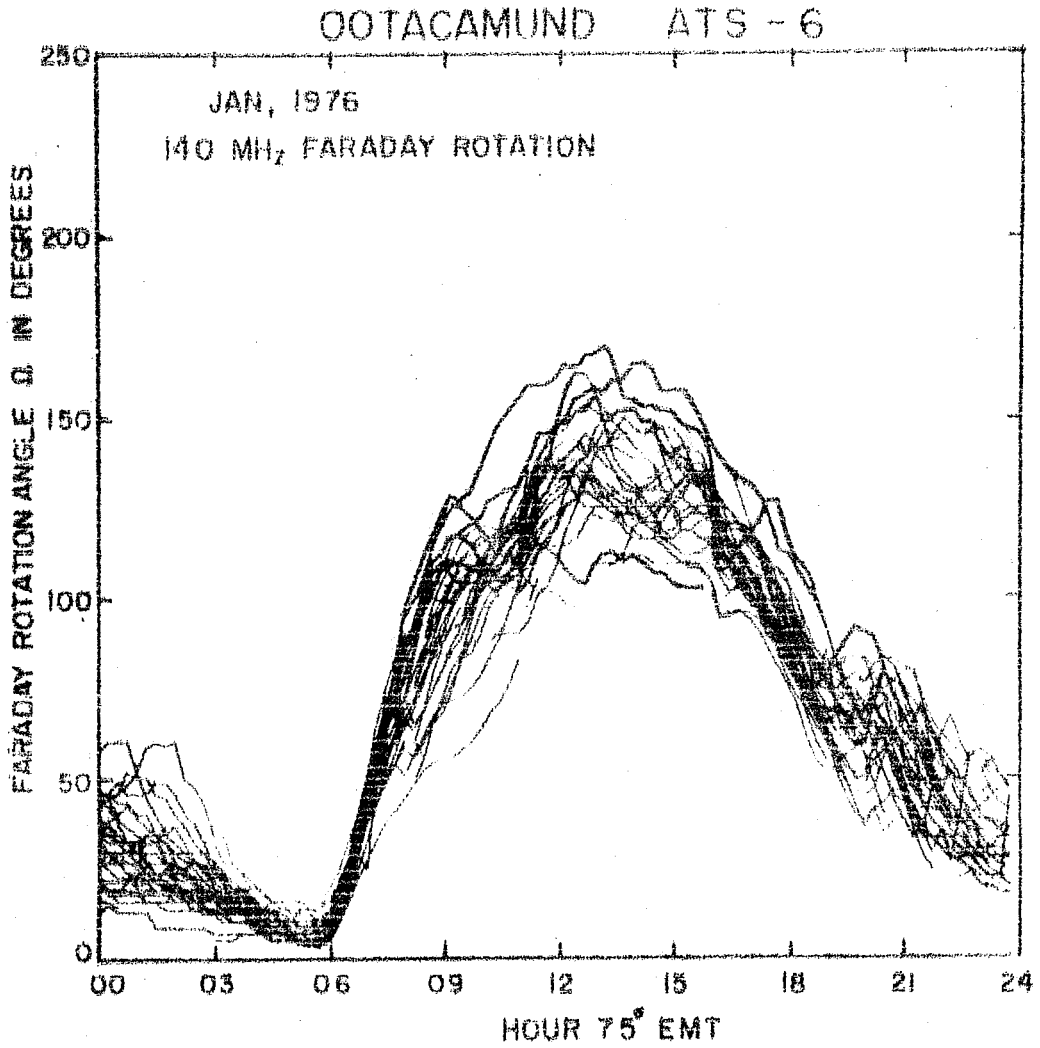

Fig.3.6a One base computer plots of Faraday rotation angle Ω, (which is a measure of N_T) for the month of January, a winter month.

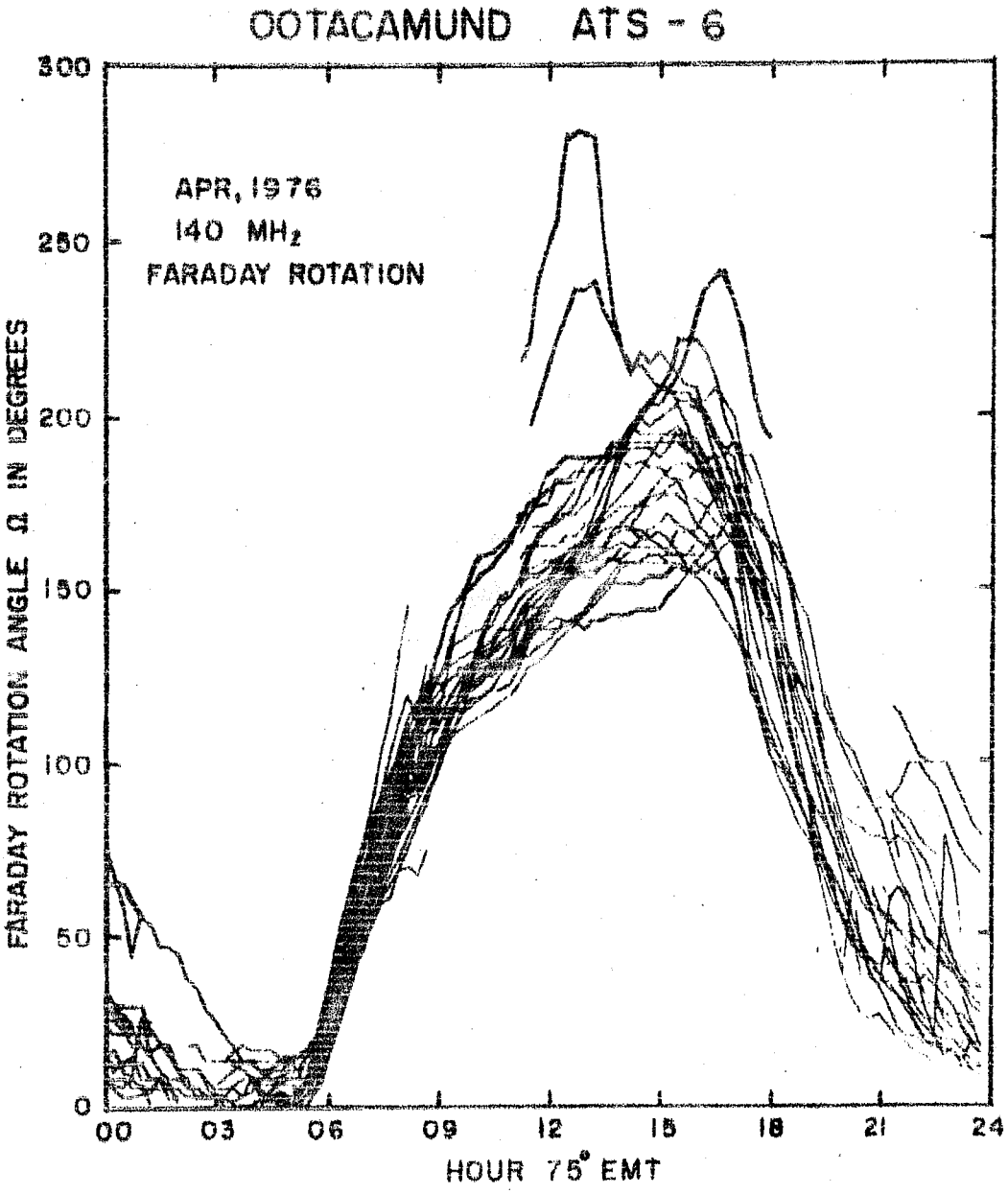

Fig.3.6b Similar to Fig.3.6a, for April., an equinoctial month.

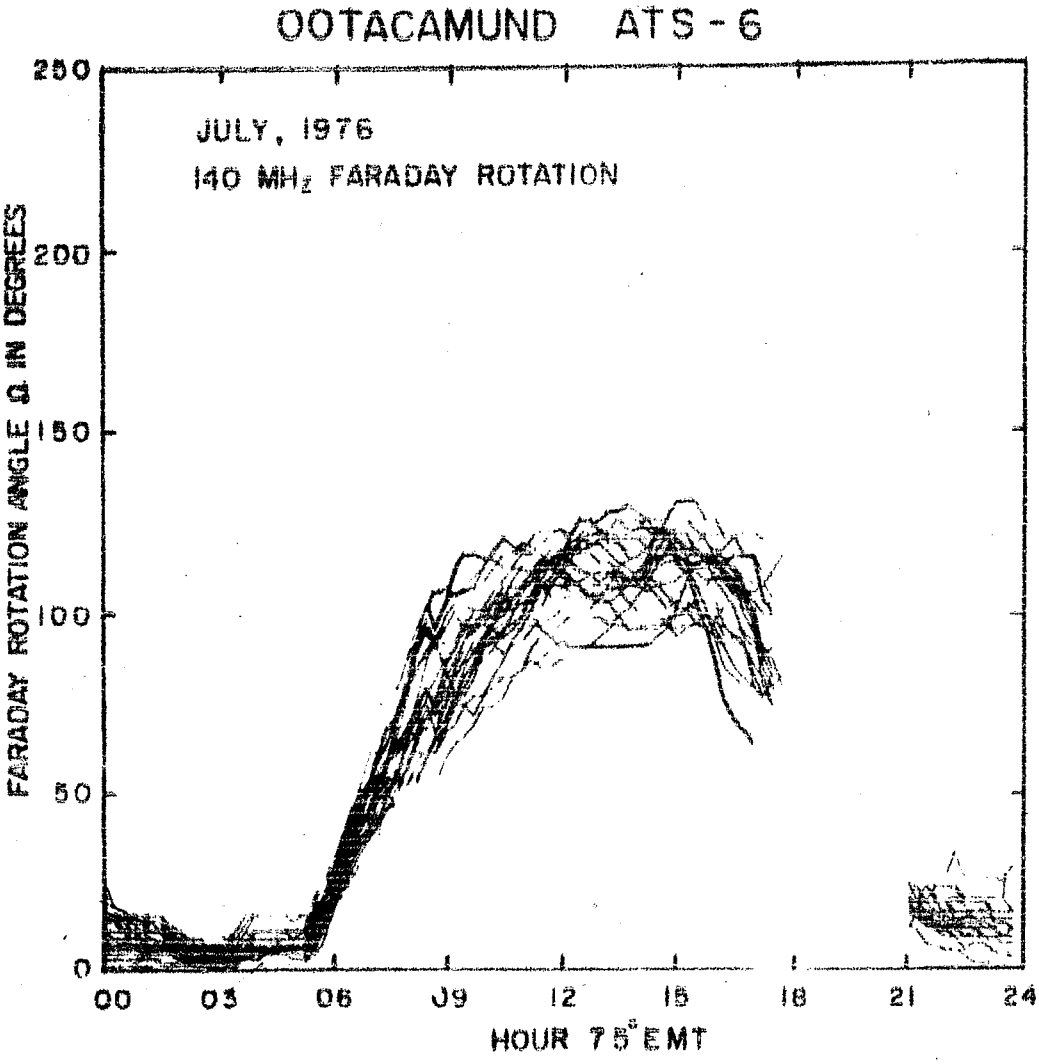

Fig.3.6c Similar to Fig.3.6a, for July, a summer month.

of increase of N_F around 1000 hr LT. Some of the days show even a dip around this time. Post-sunset peak around 2100 hr LT is also noticed on many days. Fig.3.6c shows the plot for the month of July, a summer month. The diurnal maxima are found to be flat. A dip around 0300 hr LT is also observed for most of the days. The presence of secondary peaks cannot be ascertained because of the beacon being off during 1800-2100 hr LT. The variability in TEC may be due to a number of factors, e.g. (i) changes in solar EUV flux, (ii) variations in electrojet strength, affecting the equatorial plasma transport, (iii) changes in neutral composition at F-region heights, (iv) different geomagnetic conditions which can give rise to changes in all the above mentioned three factors, in addition to changes in neutral wind patterns which may creat large dynamic upheavals in the upper atmosphere. The data under study are of the period October 1975 - July 1976 which is a low solar activity period and does not have much variations in 10.7 cm solar flux which is an indicator of changes in EUV flux. The 10.7 cm solar flux varied between 60-80 units, during this period and is not found to be correlated with TEC changes. The other factors have been considered in some of the later chapters.

3.4 Electron Content Measurements at Ootacamund Using Group Delay Technique (N_T)

As described in detail in Chapter II, the strong dependence of the Faraday rotation on the earth's magnetic field makes it

insensitive to the electrons encountered in the upper parts of the ray path whereas the group delay is equally sensitive to all the electrons irrespective of their position along the ray path, hence this technique gives the electron content upto the height of the satellite and the content is known as the group delay content (N_T). In this section the results of group delay measurements made for the first time near magnetic equator (Ootacamund) are described. These results have been compared with the results of Faraday rotation measurements made simultaneously at the same station.

3.4.1 Results and Discussions

The annual and the seasonal mean daily variations of N_T are shown in Figs.3.7 and 3.8. Fig.3.9 shows contour diagram for N_T, on a month versus local time grid. These three figures (i.e. Figs.3.7 to 3.9) are similar to corresponding figures (i.e. Figs. 3.1 to 3.3) for N_F. The gross features are similar to those observed in the results of Faraday rotation measurements. Some of the important points to be noted are as follows:-

(a) The diurnal ratios (N_T(max)/ N_T(min) for equinoxes, winter and summer are found to be around 6.5, 6.0 and 6.5 respectively. The corresponding diurnal ratios obtained from Faraday rotation measurements are 28.0, 14.0 and 19.0.

(b) A sharp decrease in the rate of increase of N_T around 1000 hr LT is clearly noticed for equinoxes and winter whereas this feature is not so pronounced for summer. It is to be noted that this feature was more prominent in summer than in winter

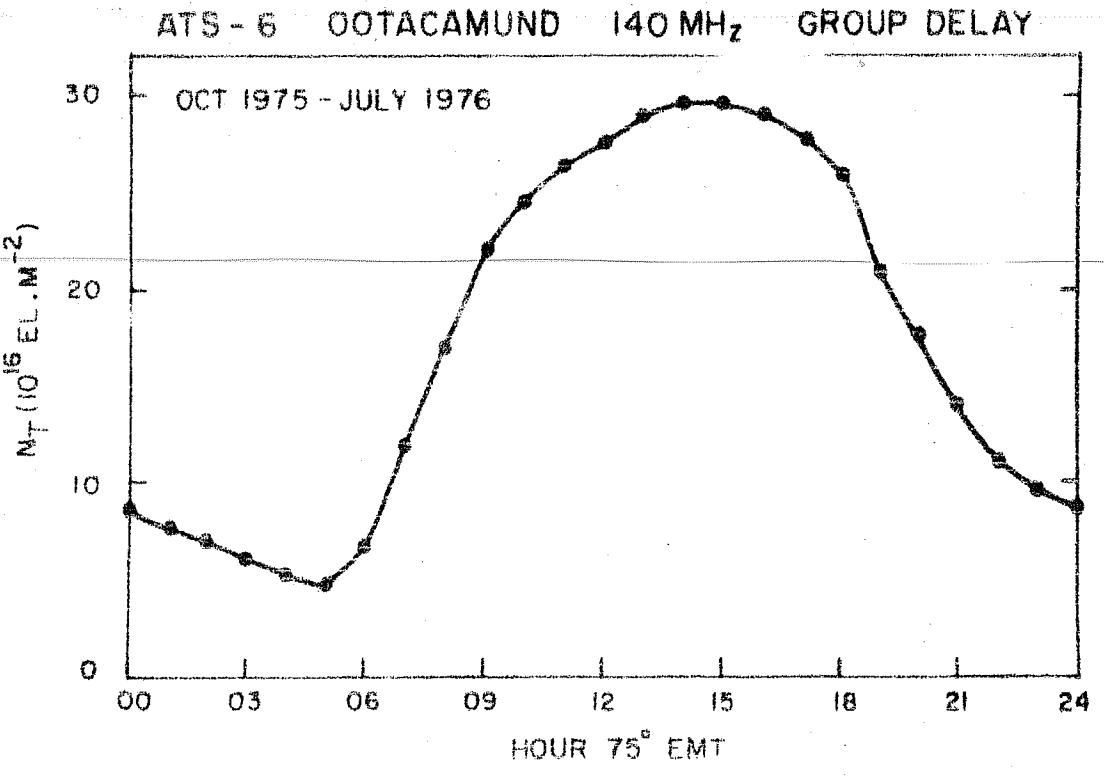

Fig.3.7 The annual mean daily variation of N_T.

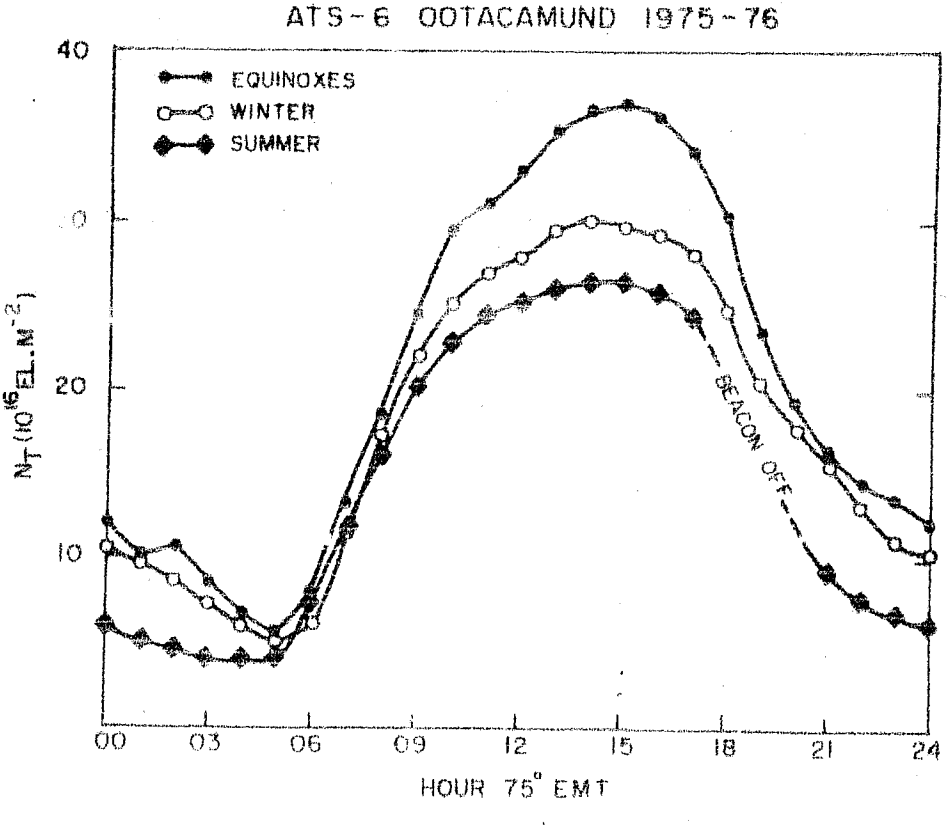

Fig.3.8 The mean daily variation of N_T for different

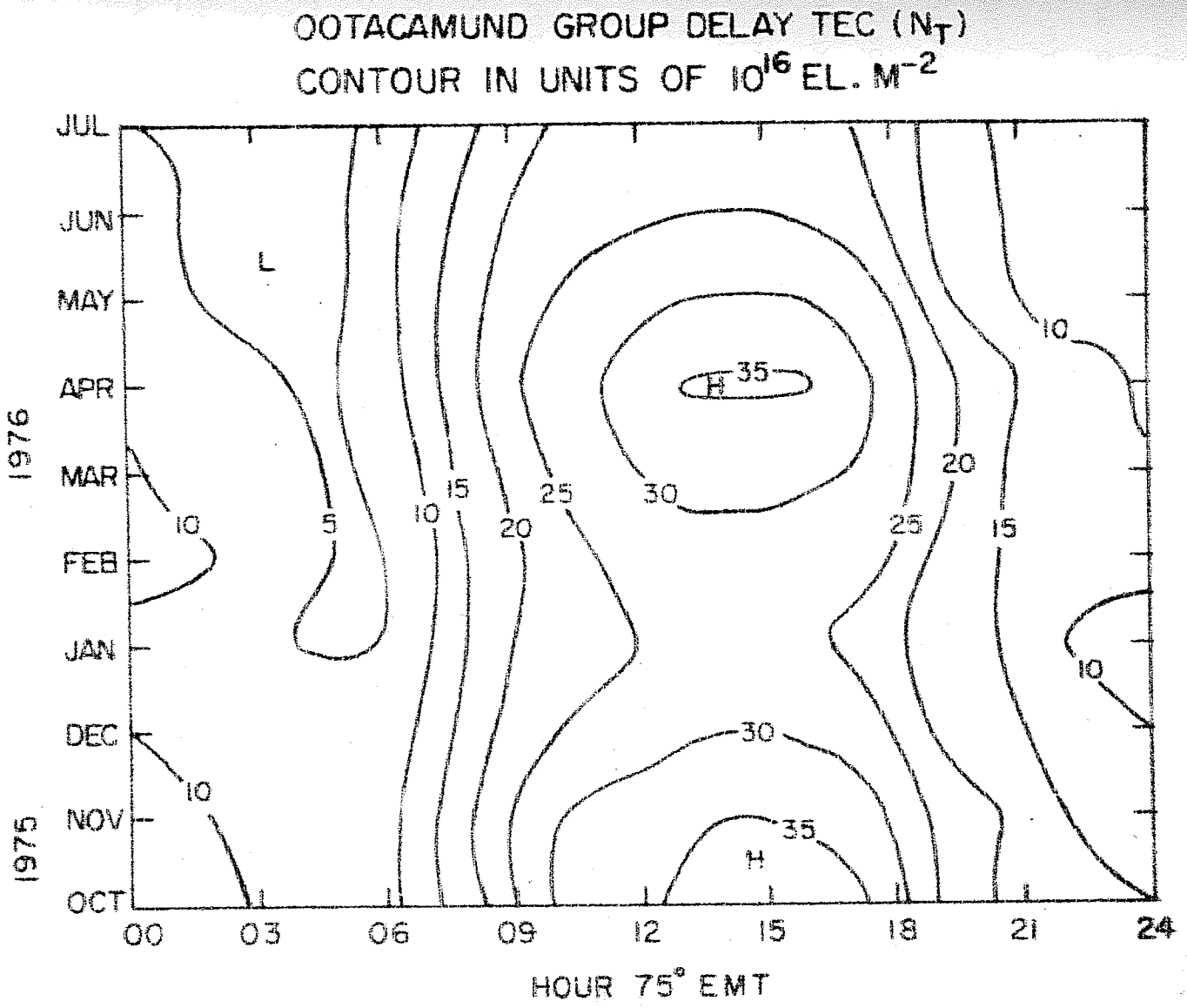

Fig.3.9 Contour map of N_T on a grid of local-time versus months.

The low diurnal ratio obtained for N_T, can be attributed to the fact that N_T, which also includes the contributions from above Faraday height h_F (which is around 1500 km for Ootacamund) is comparatively quite high during night-time than the electron content N_F obtained from Faraday rotation measurements, which does not include the contribution from the plasmasphere. The errors involved in determination of N_F and N_T have already been discussed in Chapter II and in light of conclusions arrived at there, an attempt of studying the only residual electron content (N_R) will be made in the next section.

3.5 Residual Electron Content (N_R) Derived from N_F and N_T

Simultaneous electron content measurements from Faraday rotation and group delay techniques using radio beacons aboard a geostationary satellite enables one to derive plasmaspheric electron content (Davies et al. 1976, 77). Results of plasmasphere content derived from such measurements at mid-latitudes have been reported recently by various authors (Davies et al. 1976, Kersley et al. 1978a,b, Kersley and Klobuchar 1978, Soicher 1975, 1976a,b, Poletti-Liuzzi et al. 1977, Webb and Lanzerotti 1977 and Degenhardt et al. 1977). Similar simultaneous measurements of Faraday rotation and group delay were made for the first time in the equatorial region (at Ootacamund) during the period Oct. 1975 - July 1976, when the ATS-6 was positioned at 35°E. As it is noted, the accuracies in determining N_F for Ootacamund to ATS-6 raypath are not sufficient enough to estimate the absolute values of

plasmasphere electron content, the difference between N_T and N_F is termed as residual electron content (N_R) which can be taken as a crude estimate of the plasmasphere electron content. In this section we describe and discuss the results of residual electron content (N_R) derived from these measurements at Ootacamund.

3.5.1 Quiet Time Variation of Residual Electron Content (N_R)

Electron content obtained from Faraday rotation technique denoted by N_F, is a measure of electron content along the ray-path upto a slant distance of about 2200 km (for Ootacamund to ATS-6 ray-path) whereas group delay content, denoted by N_T, gives the electron content along the complete ray-path, from the observer to the satellite. The values of N_F and N_T have not been converted into the equivalent vertical contents because of the different factors involved for the exact conversion. Slant residual electron content (N_R) is obtained by the simple relation:

$$N_R = N_{TS} - N_{FS} \qquad (3.1)$$

where N_{FS} and N_{TS} are the slant electron contents. Thus N_R gives the electron content between approximately 2200 km and the satellite along the slant ray-path.

Mean Daily Variations of N_{FS}, N_{TS}, N_R and N_R/N_{TS}

The annual, the seasonal and the monthly mean daily variation of N_{FS}, N_{TS} and N_R as well as of the ratio N_R/N_{TS}, which is a crude estimate of the relative abundance of the plasmasphere with

reference to total electron content N_{TS}, are shown in Figs. 3.10 to 3.12 respectively. The main features are listed below:-

(1) The mean daily variations of N_{FS} and N_{TS} are similar in nature viz. both are having flat maximum around 1400-1600 hr LT (75°EMT) and the predawn minimum around 0400-0500 hr LT.

(2) On the average, mean daily values of N_R are found to be around 6×10^{16} el m^{-2} (Fig.3.10) but in equinoxes N_R is found to be little higher than the N_R values for winter and summer (Fig.3.11).

(3) The mean daily variation of N_R shows "peak" around 1900-2000 hr LT which is observed in annual, seasonal, as well as in the monthly mean curves. For summer months, data are not available between 1800 to 2100 hr LT as beacon was off but there is an indication of a maximum around post-sunset hours.

(4) There is a dip around 07-08 hr LT, followed by a flat maximum around 1000 hr LT in N_R (Fig.3.10). In the summer months, this secondary maximum is noticed to be flattened and in equinoxes one additional maximum is observed in the post-midnight hours (Fig.3.11). For the months of December, February and April, this feature is very pronounced whereas in other months it is less pronounced.

(5) For pre-midnight hours N_R is around 60% of N_{TS} in winter and summer and around 50% of N_{TS} in equinoxes (Fig.3.11). For post-midnight hours N_R is around 70-80% of N_{TS} and during daytime it is about 15% of N_{TS}. It is interesting to note that during predawn hours, N_R is found even larger than the ionospheric electron content (N_{FS}).

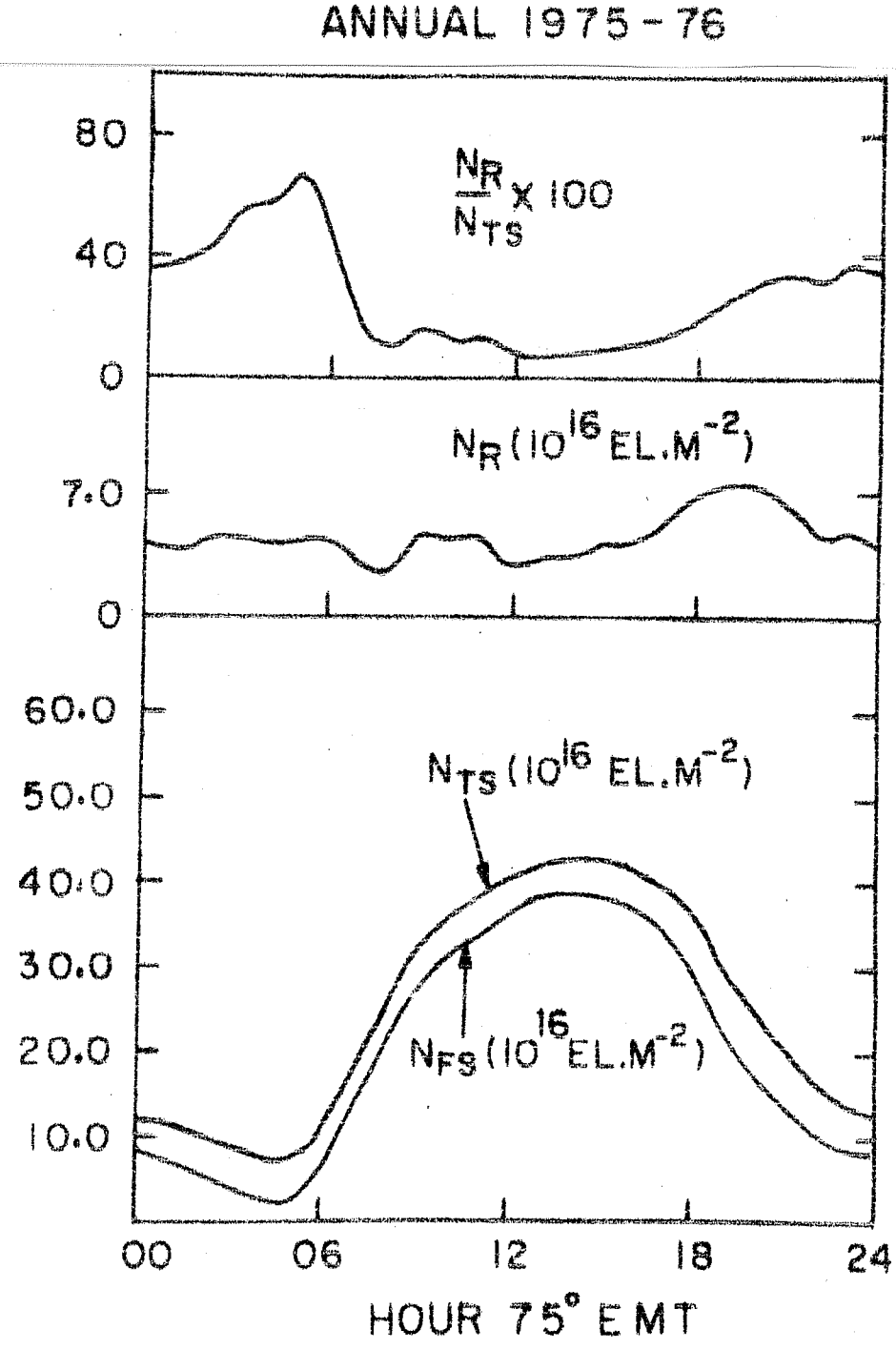

Fig.3.10 The annual mean daily variation of N_{FS}, N_{TS}, N_R and N_R/N_{TS}.

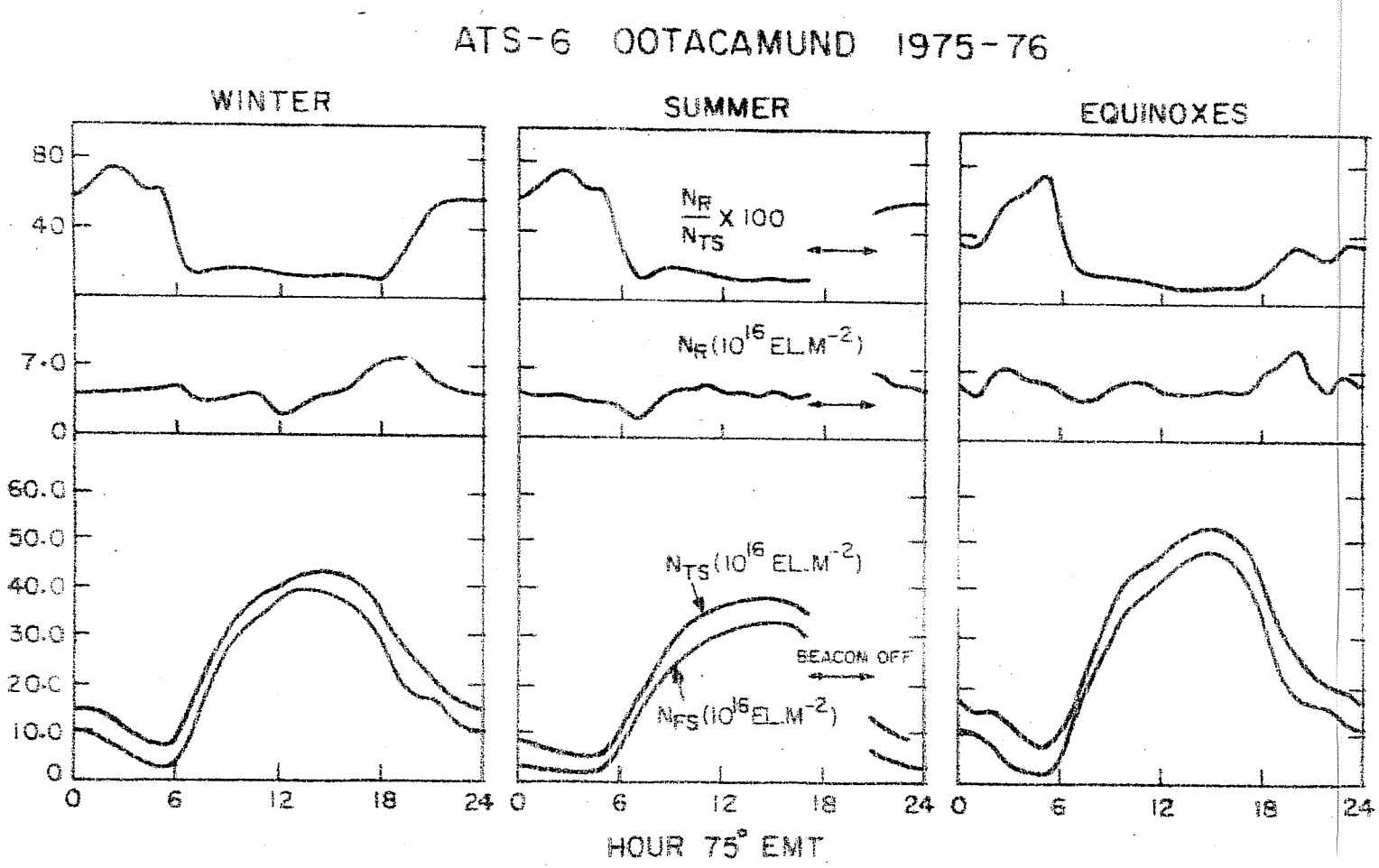

Fig.3.11 Mean daily variations of N_{FS}, N_{TS}, N_R and N_R/N_{TS} for different seasons.

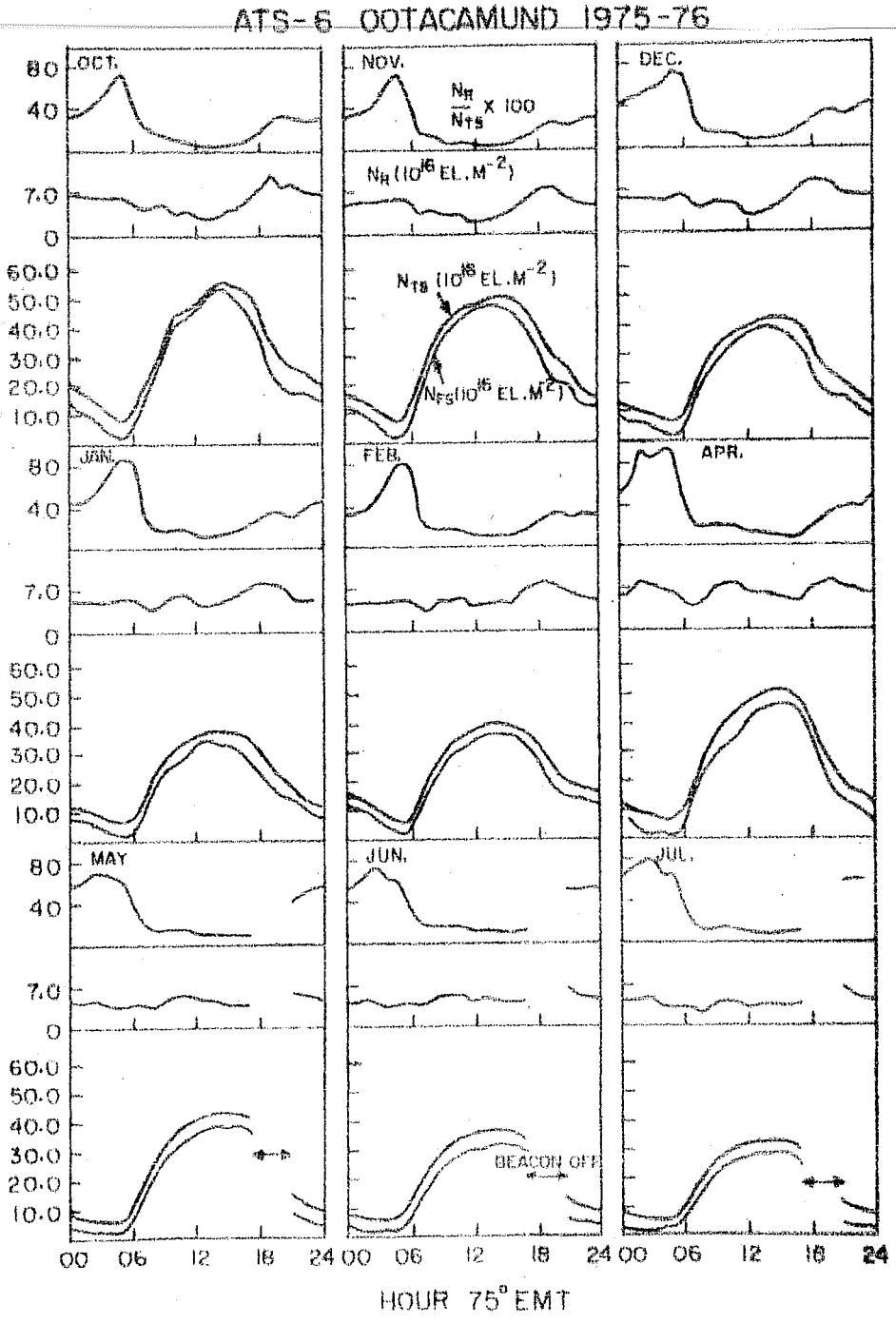

Fig.3.12 Mean daily variations of N_{FS}, N_{TS}, N_R and N_R/N_{TS} for different months.

3.5.2 Discussions

It is worthwhile to summarise some of the important features of Ootacamund to ATS-6 geometry as this will help in interpreting the present results.

(1) Ootacamund is at longitude 76.6°E whereas ATS-6 was positioned at 35°E, hence the ray-path is towards west. As a consequence sunrise at the ionospheric termination points, corresponding to geomagnetic field lines which intersect the ray-path from ATS-6 to Ootacamund is later than the sunrise at the station. The time difference extends upto about two and a half hours. For L shell corresponding to an altitude of about 5000 km, the time difference is about 1.5 hour (L is magnetic shell number, McIlwain 1961).

(2) In the case of the ATS-6 to Ootacamund geometry, the field line intersecting the ray-path at 2200 km, has an L value of 1.25. Hence the lowest magnetic shell contributing to the residual content has the L value 1.25. For mid-latitude stations like Aberystwyth and Hamilton, the corresponding values are found to be 1.72 and 2.27 respectively (Kersley and Klobuchar 197 Hence it is noticed that the residual content as observed for ATS-6 to Ootacamund geometry is contributed by low magnetic shells with higher densities hence one expects N_R as observed from Ootacamund to be higher compared to N_P observed from mid-latitude stations. The annual mean daily values of N_P for Hamilton and Aberystwyth, alongwith N_R for Ootacamund are

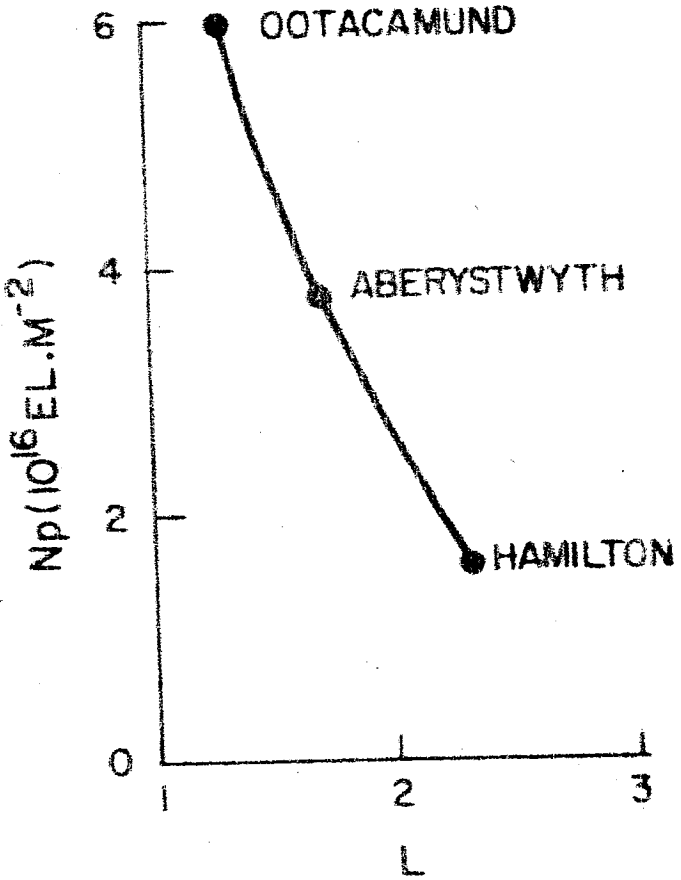

Fig.3.13 The annual mean daily values of N_R (N_p for Hamilton and Aberystwyth) plotted against L - the lowest magnetic shell contributing to the residual content.

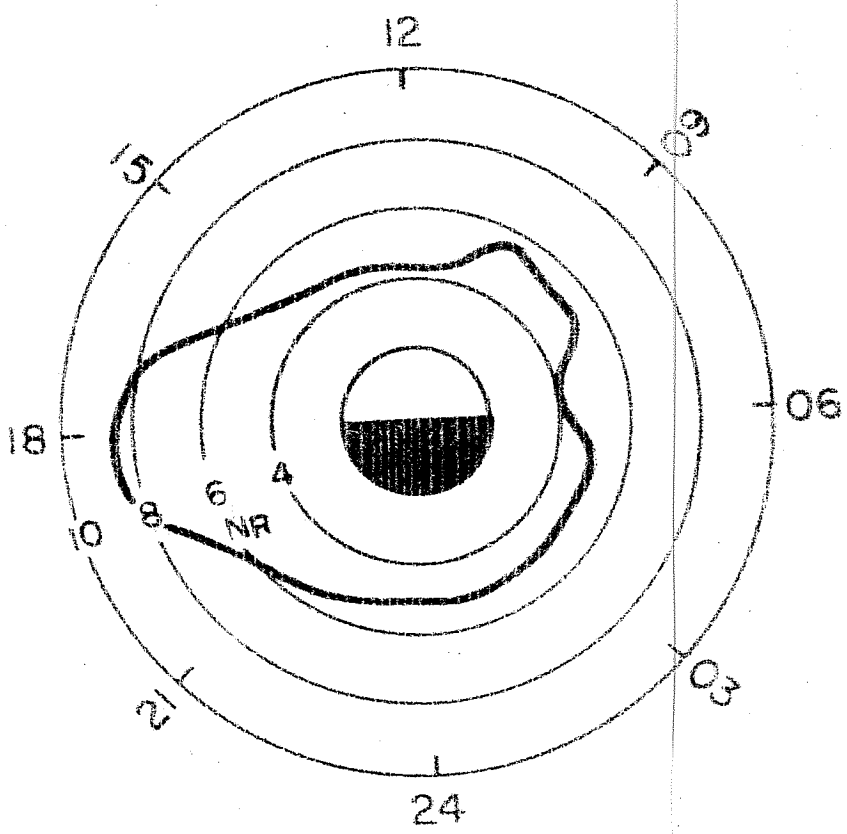

Fig.3.14 The polar plot of the annual mean daily variation of N_R at Ootacamund.

increases almost linearly with decrease in L. The figure can be used to make a rough estimate of N_R, for a given satellite to observer geometry.

A maximum around 1800 hr LT (taking into consideration the local time difference between the station and the sub-plasmasphere point at 5000 km) observed in the mean daily variation of N_R can be the consequence of two possible factors. Firstly the ionosphere to plasmasphere flow of the ionization may give rise to diurnal density variation so as to produce a maximum in N_R around dusk hours. Kersley and Klobuchar (1978) interpreted the diurnal patterns of N_p at Hamilton and Aberystwyth, in terms of geometry of the ray-paths and the ionosphere to plasmasphere flow of the thermal plasma. It is to be noted that equatorial plasma densities for magnetic shells having $L > 3$, do not show a clear diurnal patterns because of large day to day variations due to storm and sub-storm effects (Park et al. 1978). The magnetic shells with $L \lesssim 3$, show a diurnal pattern with post-midnight minimum and midday maximum (Chen et al. 1976, Park et al. 1978). But N_R at Octacamund shows a maximum around dusk, hence it is rather difficult to understand the diurnal patterns of N_R in terms of topside changes of electron density.

Second possibility which seem to be more probable is the L-LT configuration of the plasmapause location which shows a bulge around 1800 hr LT (Chappell 1972). The larger extent of the plasmasphere around dusk hours can give rise to larger values of N_R

around these hours, though the rate of increase of N_R with L, depends on the density distribution assumed and the L values under consideration (Webb and Lanzerotti 1977). If the plasma density varies as $1/L^4$, N_R shows almost negligible dependence on the plasmapause position. But Webb and Lanzerotti (1977) have shown that there is evidence that power law distributions over the entire range i.e. 1/L to $1/L^4$ can occur; and for density variations as 1/L or $1/L^2$, N_R depends significantly on the plasmapause position.

To have a visual comparison of the L-LT configuration of the plasmapause and the daily variation of N_R, the annual mean daily variation of N_R given by Fig.3.10, has been replotted in Fig.3.14. One notices a striking similarity between the daily variation of N_R and of plasmapause position L, as given by Chappell (1972).

3.6 Plasmasphere Electron Content (N_P) Obtained at Ahmedabad

The near equatorial plasmasphere electron content N_P, has been measured from Ahmedabad (Mag. dip lat.17.1°N) during June and July 1976, near the equatorial anomaly peak, by taking the difference between the electron contents N_T and N_F obtained from the group delay and Faraday rotation measurements respectively, from the radio beacons on the geostationary satellite ATS-6.

As mentioned earlier, in section 3.5, the plasmasphere electron content derived from such measurements at mid-latitude have recently been reported by many authors (for references, see section 3.5) but similar simultaneous measurements of Faraday rotation and the group delay were carried out for the first time in the equatorial region.

3.6.1 Results and Discussions

The mean daily variations of N_F, N_T and N_P for the months of June and July 1976, are given in Figs.3.15 and 3.16 respectively. The variation in N_F and N_T go hand in hand, with predawn minimum around 0500 LT and daytime maximum around 1500 LT. The mean daily variation of N_P shows some interesting features which are as follows:-

(1) N_P increases steadily from sunrise to midnight and decays afterwards to a near sunrise minimum. The value of N_P varies between 1 to 4 TEC units.

(2) The post-midnight decay in N_P is accompanied by nearly constant low values of local ionosphere electron content N_F, indicating that, in the absence of electric fields, the plasmasphere content flows, not into the local equatorial ionosphere, but down the field lines to the mid-latitudes.

(3) There is a slight but definite indication of a small secondary peak in N_P around 0600 LT.

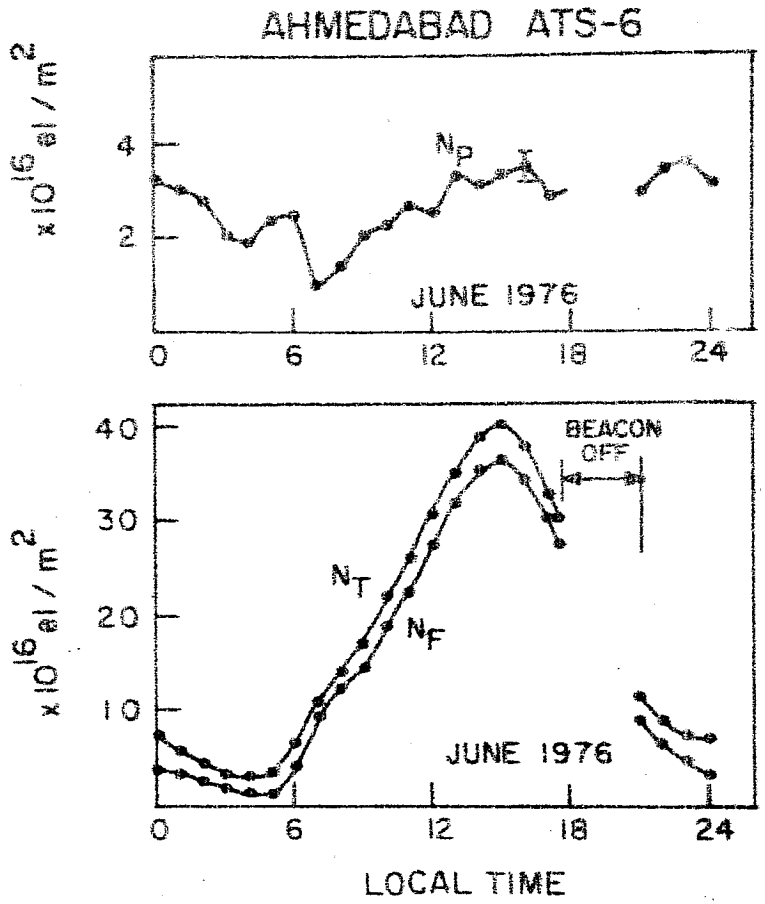

Fig.3.15 The mean daily variation of N_T, N_F and N_P at Ahmedabad for the month of June, 1976.

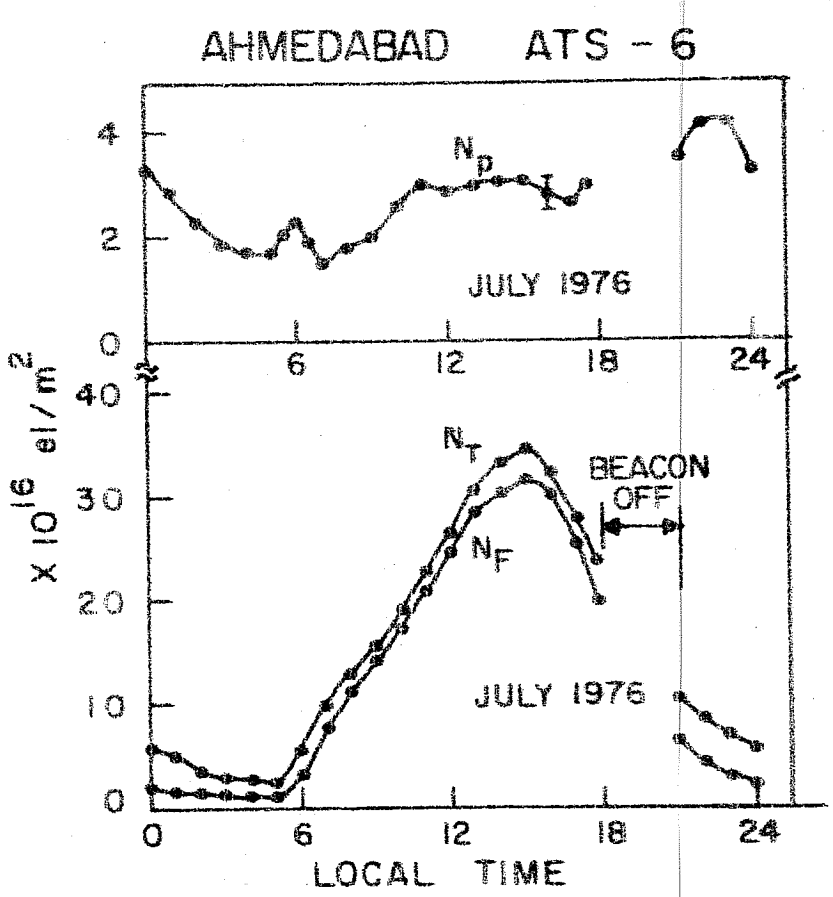

Fig.3.16 Similar to Fig.3.15 for July, 1976.

(4) During daytime hours N_P is found to be around 10 to 15% of N_T whereas during night-time hours it is found to be 30-50% of N_T.

The day to day structure of N_P specially during night hours shows interesting behaviour as depicted in Fig.3.17. One distinct feature is that the plasmasphere content is higher than the ionosphere content. In the first example of July 13, 1976, both N_F and N_P decrease during post-midnight hours. In the second example (July 25, 1976) the N_F remains steady whereas a sharp decrease in N_P is clearly noticed. This emptying of plasmasphere should be felt as an ionospheric content increase at a station north of Ahmedabad or else it would show up as an increase of plasmasphere content south of Ahmedabad since the ionization diffuses along the field lines. However, the data to confirm this are not at hand. In the third case (July 26, 1976) neither the plasmasphere nor the ionosphere content shows any appreciable charge.

To ascertain the form of electron density distribution in the plasmasphere, the model calculations can be carried out, by fixing the upper and the lower limit on N_P. The electron density at any height L (in terms of mag. shell number) is given by:

$$n(L) = n_o L^{-m} \qquad (3.2)$$

where m is varied between 1 and 4, n_o is the electron density

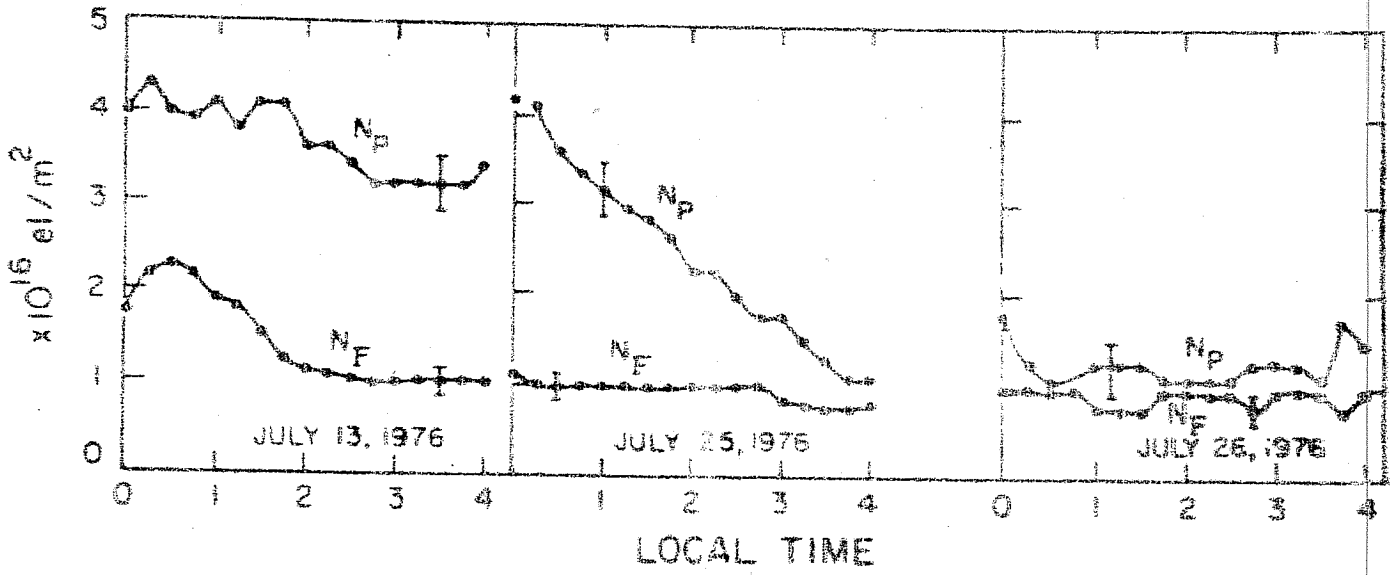

Fig.3.17 Three different cases of plasmasphere and ionosphere electron content variations during post-midnight hours.

at 2000 km which is taken to 10^4 el.cm^{-3} (N_F includes electron contribution upto 2000 km).

The plasmasphere contents for different density distributions are obtained by integrating n(h) upto plasmapause, i.e.

$$N_P = \int_0^{L_{pp}} n(h) \, dL \qquad (3.3)$$

where L_{pp} is the plasmapause location.

The results are shown in Fig.3.18. For slow density variations i.e. low values of m, the N_P attains very high values whereas N_P is found to be varying between 1 to 4 TEC units at Ahmedabad. Hence the model calculations indicate that the electron density in the plasmasphere varies most likely as L^{-n} where n is between 2 and 4.

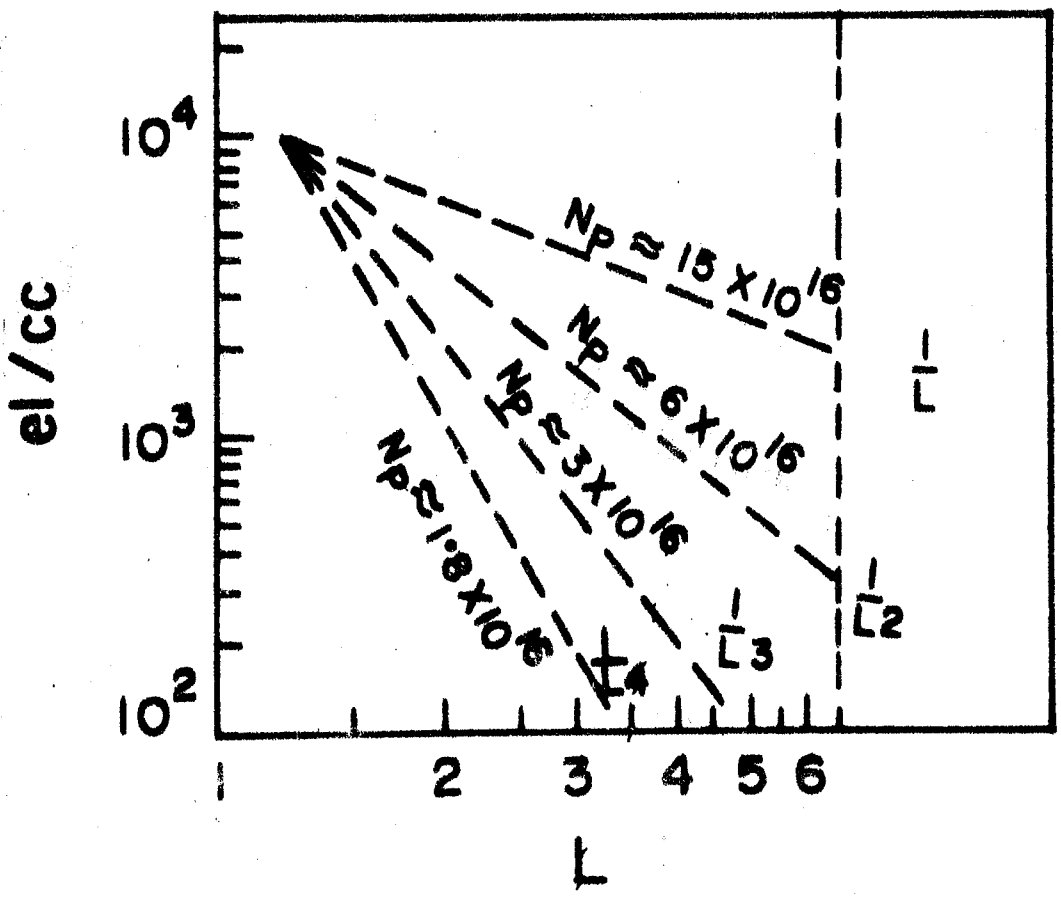

Fig.3.18 Equatorial plasmaspheric electron content to ATS-6 for various $1/L^n$ values assuming N_e (1000 km)= 10^4 el.cm^{-3}.

CHAPTER - IV

ELECTRON CONTENT STUDIES IN CONJUNCTION WITH BOTTOMSIDE IONOGRAM DATA

4.1 Introduction

The equatorial ionosphere is known to have a number of distinct features:

(a) There is a pronounced noon-time bite-out in the diurnal variation of electron density at equator.

(b) There is an anomaly in the latitudinal variation of electron density over the equator, gradually increasing to form peaks in the northern and southern sub-tropics.

These aspects of the F-region geomagnetic anomaly first recognised by Appleton (1946) and Bailey (1948), have been the subject of considerable investigations (Rastogi 1959a,b,c, Lyon and Thomas 1963, Sharma and Mewens 1976). The physical mechanisms responsible for the equatorial anomaly were first outlined by Mitra (1946) and Martyn (1947) and these were put to test through the theoretical models of various workers (Hanson and Moffett 1966, Bramley and Peart 1965, Bramley and Young 1968, Anderson 1973a).

With the advent of radio beacon on board satellites, Faraday rotation measurements, which give ionospheric total electron content (N_T), are being widely used for ionospheric studies.

It is to be noted that orbiting satellites provide good spatial resolution but the temporal resolution is seriously limited. For getting a single diurnal curve, averaging over about three months' data is required and which in consequence makes the temporal behaviour of TEC and other related parameters uncertain, because of the mixing of temporal, seasonal and spatial variation. The repositioning of ATS-6 at 35°E (in July 1975) provided an opportunity to make a detailed study of the equatorial ionosphere. In the present chapter, results of these studies are described and also discussed critically.

4.2 Comparison of the Daily Variations of Equatorial N_F and N_m

In this section mean daily variations of N_F at Ootacamund are compared with the mean daily variation of F_2 region peak electron density (N_m) obtained from the ionograms at a neighbouring station Kodaikanal (77.5°E, 10.0°N). The ATS-6 signals received at Ootacamund cross the 400 km level of the ionosphere at 72.9°E and 10.6°N. Thus it is expected that the electron density variation at Kodaikanal would be representative of the variation at ionospheric cross-over point. The value of N_m and the height of the peak electron density (h_m) have been calculated from the ionograms using Budden's matrix method for the true height analysis.

4.2.1 Results

In Fig.4.1 are shown the mean daily variations of N_F at Ootacamund and N_m at Kodaikanal for the period October 20 to November 5, 1975, for which simultaneous observations were available. Both these data are plotted at an interval of 15 min., the error bars of some representative points are also indicated in the diagram. As expected, N_m shows very distinct bite-out at noon with maximum magnitude of 10.2×10^{11} electrons/m^3 at 0915 LT in the morning and another maximum of 11.3×10^{11} electrons/m^3 at 1630 LT in the afternoon. The minimum value of N_m is 7.2×10^{11} electrons/m^3 at 1145 LT. The standard error of these points is about 0.5×10^{11} electrons/m^3, and therefore midday minimum is statistically highly significant. The curve for N_F does show different rates of increase but no minimum around midday hours is noticed. Thus the continuous data of N_F derived from geostationary satellite confirm the earlier observations of low orbiting satellite S_{66} (Rastogi et al., 1975).

In Fig.4.2 are shown the daily variations of N_F at Ootacamund as well as N_m and h_m at Kodaikanal for three individual days. On all these three days, N_m showed strong bite-out around noon corresponding to a maximum of h_m around those hours. The curves for N_F to some extent suggest a weak bite-out, but not enough to produce a minimum, especially the one for 25 October 1975.

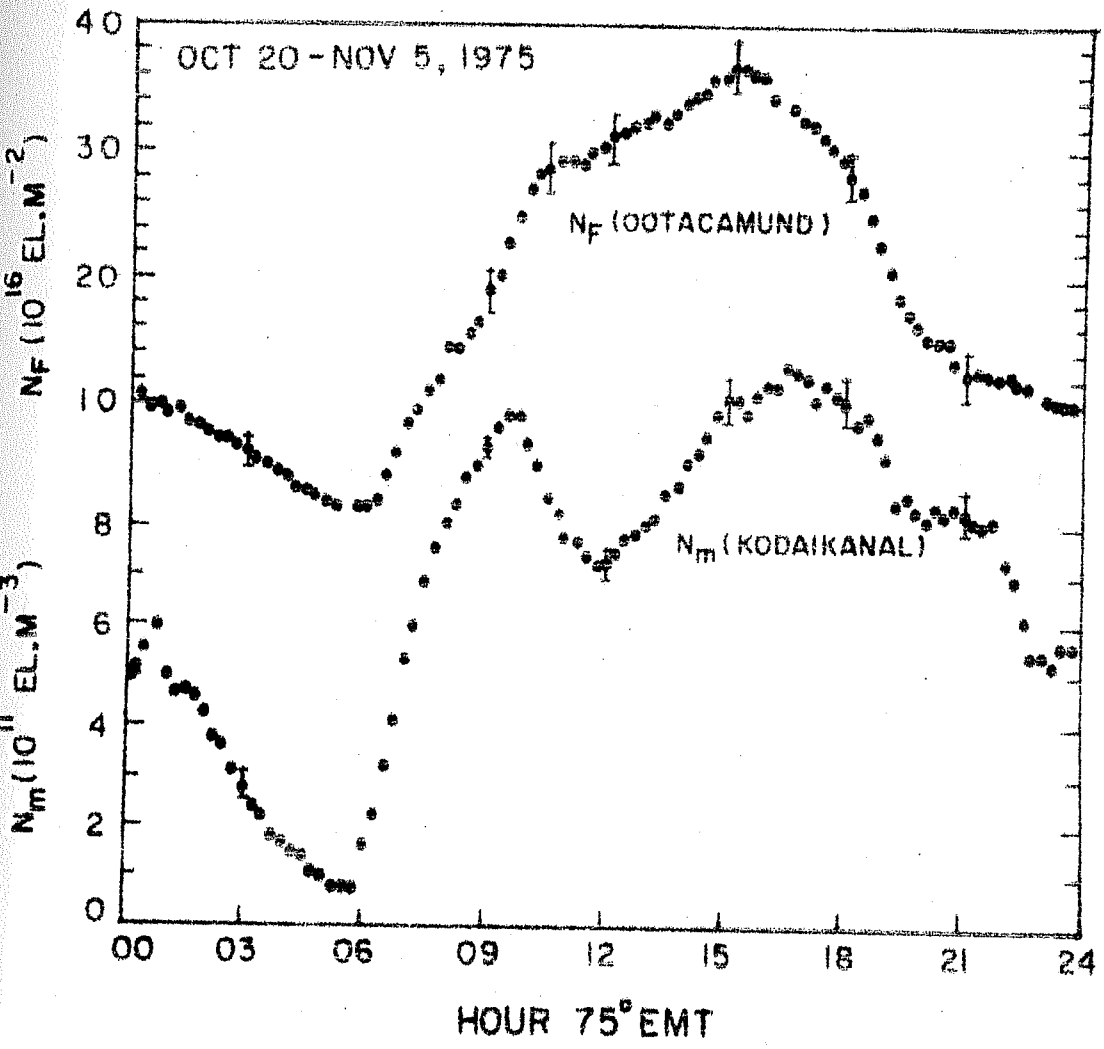

Fig.4.1 Mean daily variation of the Faraday content N_F at Ootacamund and of peak F_2 region electron density N_m, at Kodaikanal for the period Oct. 20 - Nov. 5, 1975.

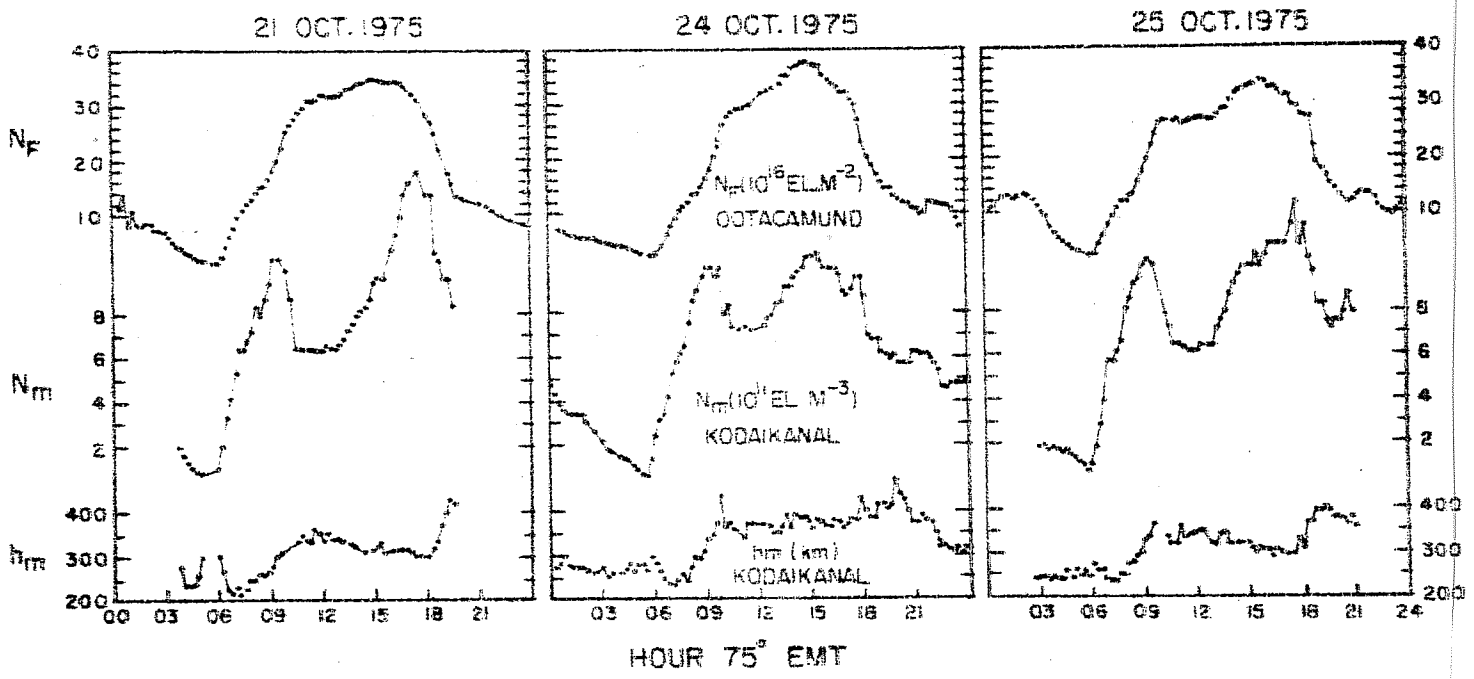

Fig.4.2 The daily variations of N_F, N_m and h_m for three individual days.

To understand further the distribution of electron density with height, the ionograms of a particular day (25 October 1975) were subjected to true height analysis and the electron contents were integrated upto the level of peak electron density (electron content below peak N_b). Knowing N_F, the amount of electron content above the peak (N_a) is calculated according to the equation $N_a + N_b = N_F$. Temporal variations of these parameters for October 25, 1975 are shown in Fig.4.3. It is seen that the electron content below the peak (N_b) is very low in the night-time, starts rising at sunrise till about 0915 hr, remains fairly constant till 1800 hr in the evening and slowly drops down to the night level. Electron content above the peak N_a, steadily decreases in the night-time upto sunrise, starts increasing from 0600 to 0730 hr, remains fairly constant till 0930 hr and later increases steadily reaching a peak about 1600 hr. It is interesting to note that N_a/N_b is less than one between 0800 and 1000 hrs and is more than 2.5 in the evening hours. This accumulation of extra ionization above the peak rather than below the peak suggests another effect of Fountain effect through the electric field in the electrojet region.

4.2.2 Discussion

The close chain of ionospheric stations operating at low latitudes in India had shown that the two peaks in the daily variation of N_m, systematically change with increasing latitude, suggesting an intimate relation between the diurnal anomaly at

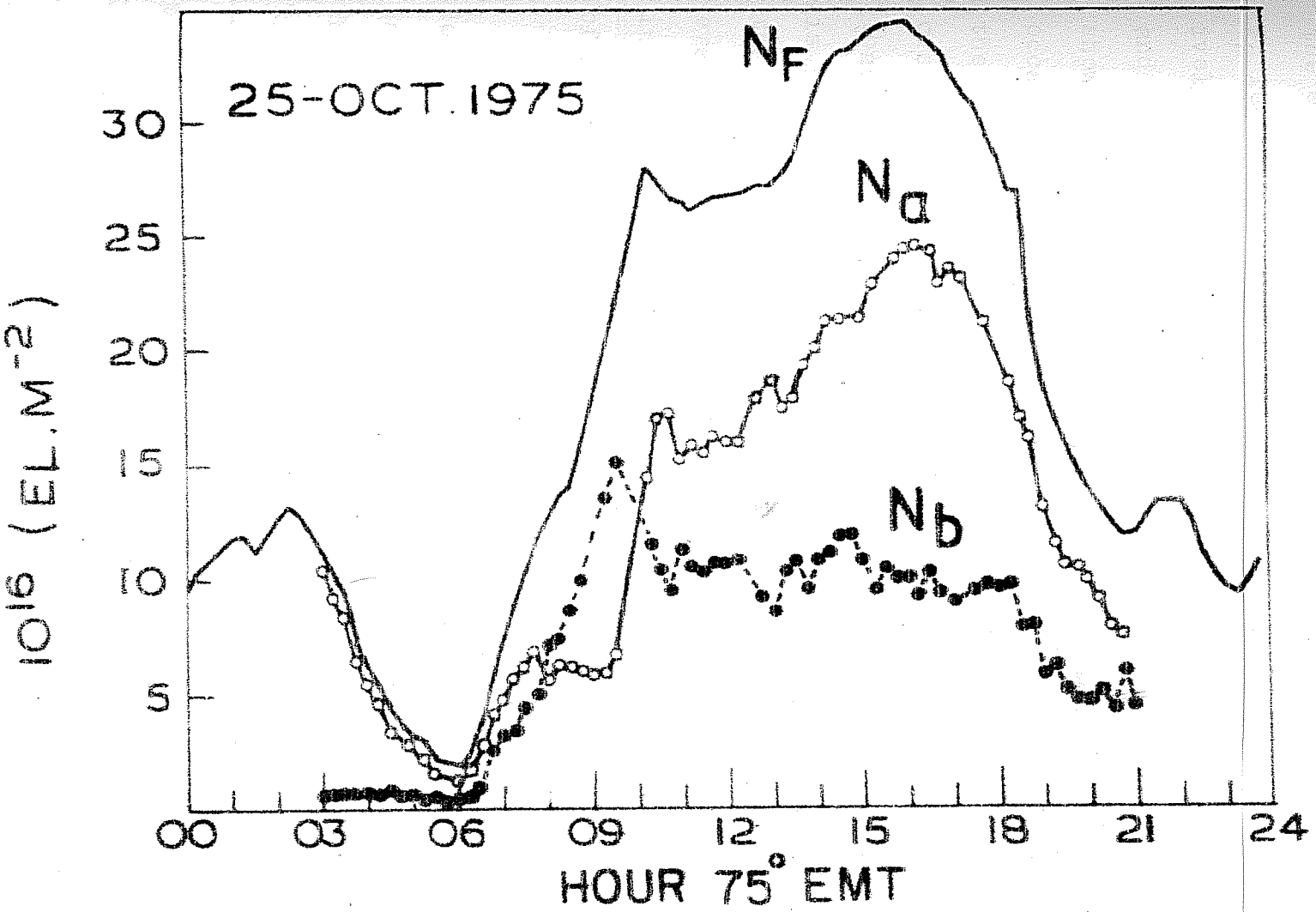

Fig.4.3 The daily variation of electron content N_F, topside content N_a, and bottomside content N_b, on 25th October 1975 (Ootacamund).

the equator and the latitudinal anomaly around noon, in the F_2 region (Rastogi 1959a). These features have been very effectively explained in terms of so called Fountain effect (Moffett and Hanson 1965, Bramley and Peart 1965). Chandra et al. (1973) showed that the bottomside electron content at Thumba on some occasions did not show a midday bite-out which was present in the daily variation of N_m. King et al. (1967) using simultaneous bottomside and topside ionograms taken at Singapore, showed that the ratio of topside to bottomside electron content (N_a/N_b) is less than one around noon and increased to more than 1.5 in the afternoon hours; this increase of the ratio from noon to evening hours is suggested by them to be due to fast increase in topside electron content, which is compatible with the idea of Fountain effect.

Croom et al. (1959) had shown that the latitudinal anomaly does not exist below 200 km. Chandra et al. (1973) showed that the daily variation of electron density at constant heights over Thumba showed the midday bite-out only at heights above 200 kms. King et al. (1964) showed that the equatorial anomaly disappears above the heights of about 900 kms. These features suggest that the Fountain effect is effective only between 200 and 900 kms at low latitudes. Hanson and Moffett (1966) have computed the electron flux at different latitudes and altitudes due to electrodynamic force associated with the Fountain effect. Their results clearly indicate that this flux at a particular low latitude is

most effective between altitudes 400 and 600 kms. Thus the present results are consistent because while integrating the electron density over a large height upto the top of the F-region, one would dilute the consequences of the Fountain, which are localised in altitude.

4.3 Equatorial N_F Compared with the N_F at the Crest of the Equatorial Anomaly

It is observed that the equatorial N_F does not show the noon bite-out corresponding to that observed in the daily variation of N_m but the presence of equatorial anomaly is clearly noticed in the latitudinal variation of N_F. In this section we compare the mean daily variation of N_F at equator (Ootacamund) with N_F near the crest of the equatorial anomaly (Ahmedabad).

4.3.1 Results and Discussions

In Fig.4.4 are shown the mean daily variations of N_F at Ootacamund and at Ahmedabad for the period Oct. 20 to Nov. 5, 1975. The points have been plotted at an interval of 15 min. The error bars on some of the representative points are also indicated in the curve for Ootacamund. The lower two curves in the same figure show the rate of change of N_F with time, calculated for Ahmedabad as well as for Ootacamund at an interval of 15 min. Some of the important features to be noted are as follows:-

(i) Night-time (1900-0400 hr LT) as well as daytime (0600-1200 hr LT) N_F values for Ootacamund are higher than the corres-

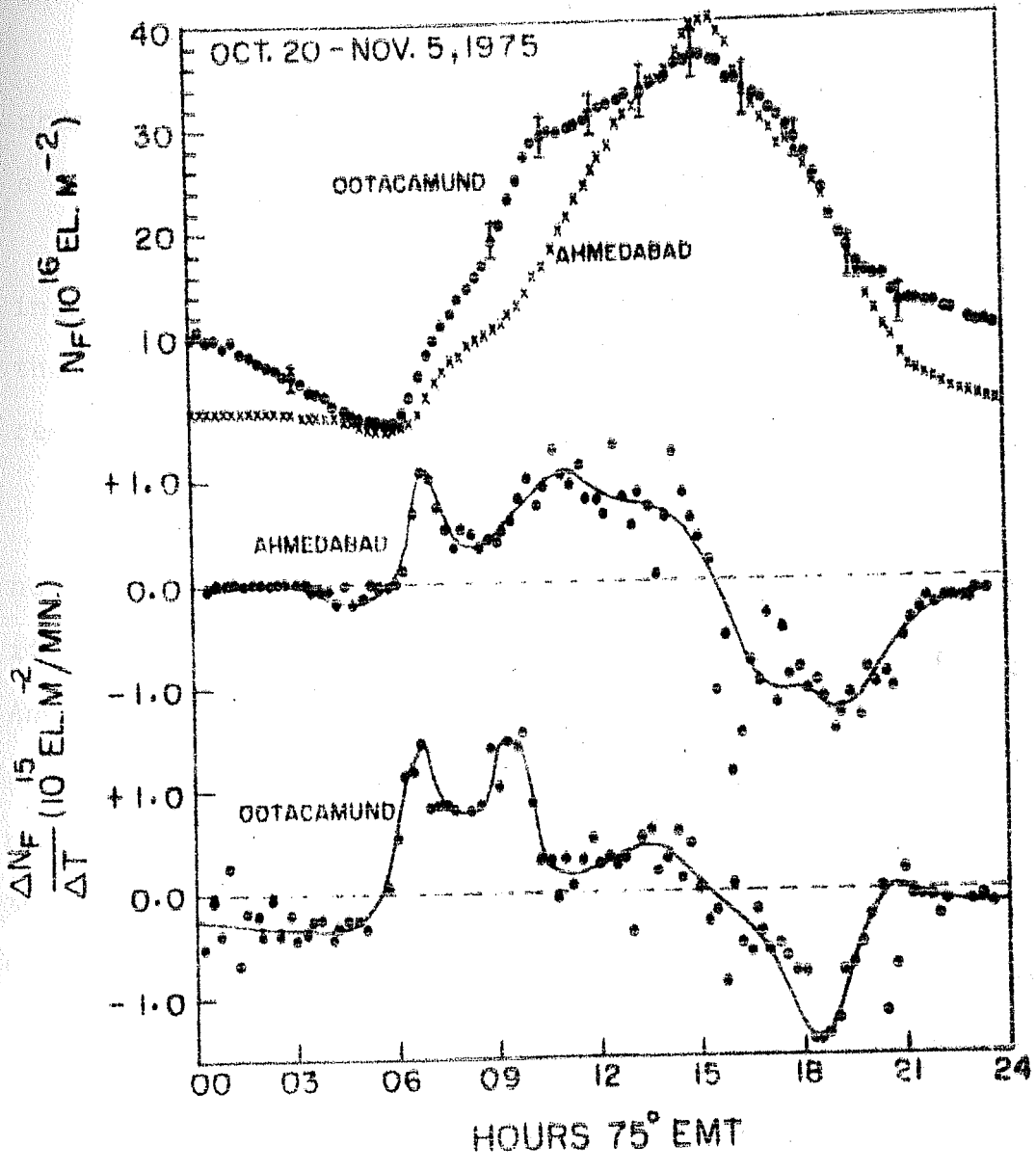

Fig.4.4 Mean daily variation of N_F at Ootacamund compared with N_F at Ahmedabad. The lower two curves give the rate of change of N_F at the two stations.

(ii) During 1400-1600 hr LT, N_F values at Ahmedabad are higher than the Ootacamund N_F values showing the presence of equatorial anomaly.

(iii) The mean daily variation of N_F at Ahmedabad shows a sharp peak around 1500 hr LT, whereas for Ootacamund, one notices a flat maximum during afternoon hours.

(iv) One clearly notices a sharp decrease in the rate of increase of N_F at Ootacamund, at around 1000 hr LT which is thought to be a manifestation of the Fountain effect which is responsible for the noontime bite-out in N_m.

Examining the curves showing the rate of change of N_F, one notices sharp dips around 0800 hr LT for both the stations. Also it is noticed that during daytime (1000-1600 hr LT) N_F at Ahmedabad increases with a rate of about 0.9×10^{15} el/m^2/min whereas during the same period, N_F at Ootacamund increases very nominally. The increase of N_F during daytime at Ahmedabad, shows the dumping of the ionization because of the Fountain effect, but corresponding to it, the decrease in N_F at the equatorial station Ootacamund, is not that marked. It is to be noted that the Fountain effect is most effective between the altitudes 400 and 600 km (Hanson and Moffett 1966), whereas N_F contains the electron content upto altitude of approximately 1500-2000 km (Davies et al. 1979; Titheridge 1972). Also it is found that the equatorial F-region becomes thick during noon-time (Huang 1974).

Hence, keeping in view, above two factors, it is suggested that the effect of the noon bite-out, which is present very prominently in f_oF_2 gets diluted in N_F.

Around sunset one gets an enhanced rate of decrease of N_F, the peak rate of decrease, being sharper for Ootacamund. During post-midnight hours, N_F at Ootacamund decreases from 10 to 2 TEC units whereas at Ahmedabad, N_F remains more or less constant at a low value equal to 2 TEC units.

4.4 Slab-thickness Studies of the Equatorial Ionosphere

The ratio of TEC (N_F or N_T) and the F_2 region peak electron density (N_m) is known as slab-thickness (τ) which is a measure of the thickness of the ionosphere, if it were of uniform electron density N_m. The slab-thickness τ, is related to the shape of ionization distribution, the smaller the value of τ, the more skewed is the ionization profile. For an α- Chapman type distribution of ionization Wright (1960) has shown that:

$\tau = 4.13H$ where H is the scale height of the ionization constituent (atomic oxygen).

For the present study of slab-thickness (τ), the ionosonde data from Kodaikanal (77.5°E, 10.0°N) which is very close to sub-ionospheric point (72.9°E, 10.6°E) for Ootacamund to ATS-6 ray-path have been used.

4.4.1 Results

The mean daily variations of N_F, N_m and τ_F (= N_F/N_m) for different months are shown in Fig.4.5a. The daily pattern of τ_F is characterised by two maxima, one around pre-sunrise hours and the second around noon hours. The peak value of τ_F around noon is found to be around 400 kms. For summer months one observes a rise in pre-midnight hours, but no firm conclusion can be drawn regarding the presence or the absence of pre-sunrise peak because N_m data during night is discontinuous due to spread-F condition. Fig.4.5b shows the mean daily variation of N_F, N_m and τ_F on international quiet and disturbed days, grouped for different seasons. One does not find much of the variation in τ_F during disturbed and quiet periods indicating the preservation of the shape of the ionization distribution during disturbed periods. As expected the daytime values of N_F and N_m for disturbed days are more compared to quiet day values. The slab-thickness studies were also done using total electron content N_T obtained from the group delay technique. The results are shown in Fig.4.6a,b. The general features are the same as obtained using N_F data. The pre-sunrise peak in the slab-thickness obtained using N_T, is found to be much larger than the daytime maximum whereas in the case of slab-thickness obtained using N_F, the pre-sunrise peak is only as large as the daytime maximum or even smaller than the daytime maximum.

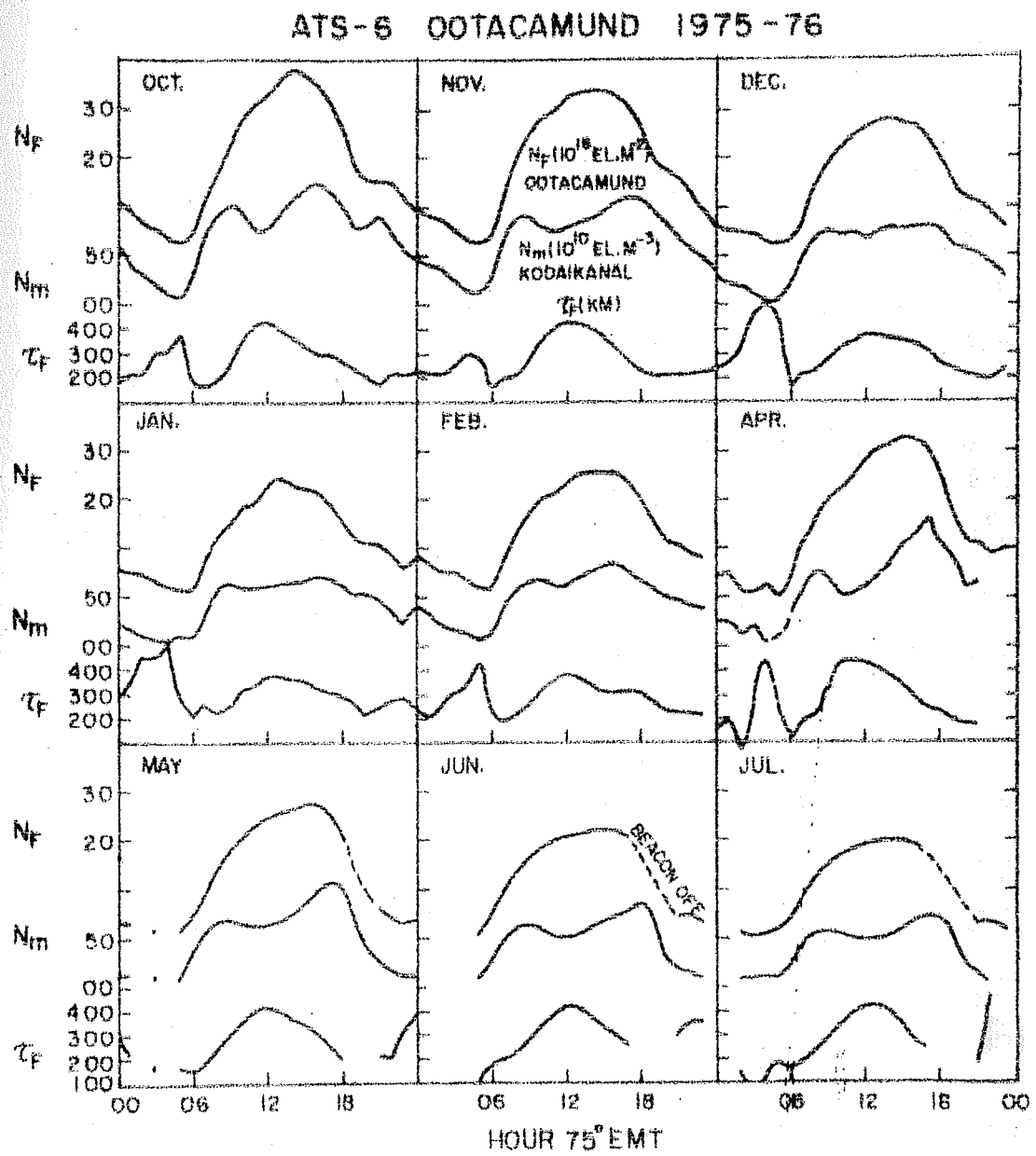

Fig.4.5a Mean daily variation of N_F, N_m and slab-thickness for different months.

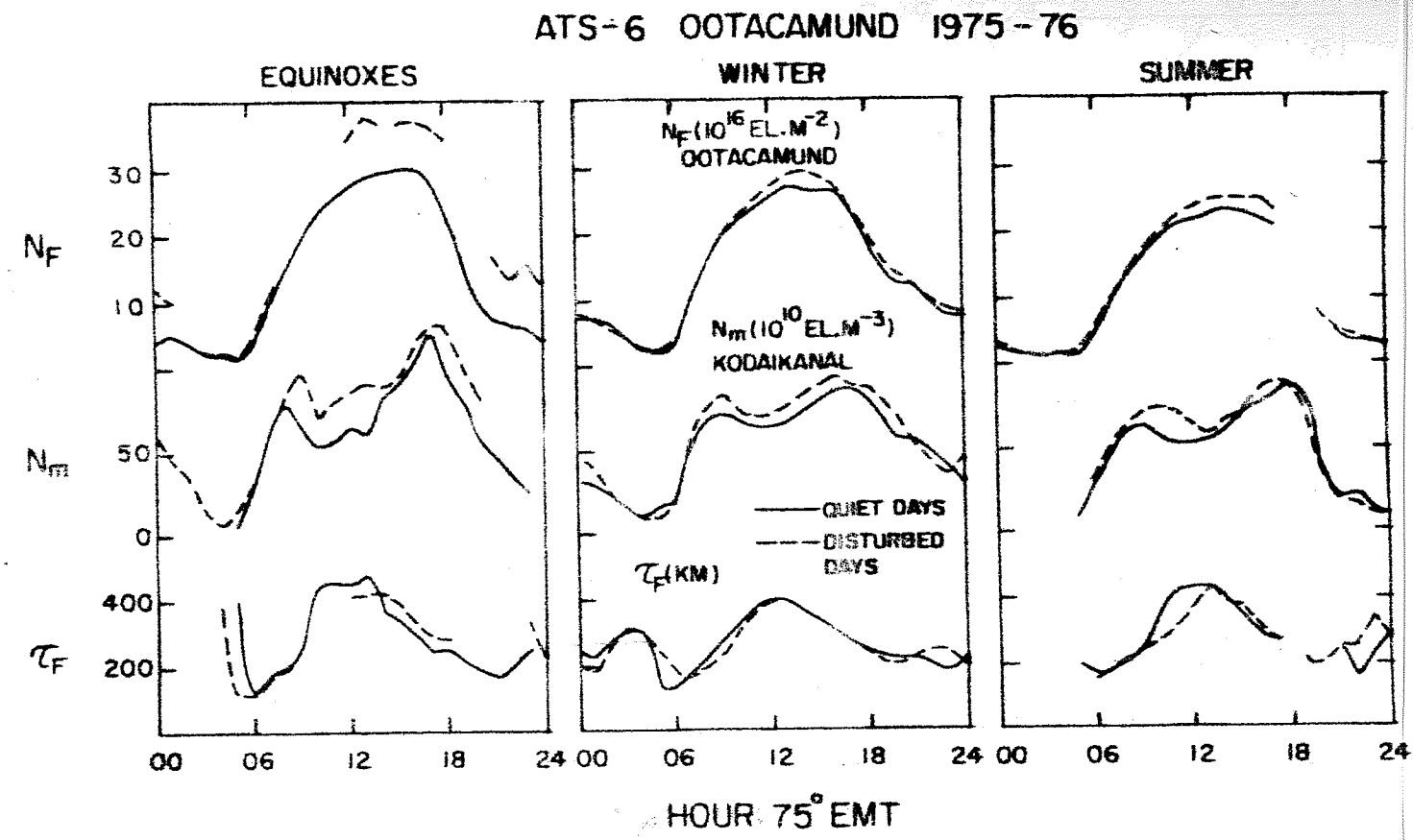

Fig.4.5b Mean daily variations of N_F, N_m and τ_F on international quiet and disturbed days grouped for different seasons.

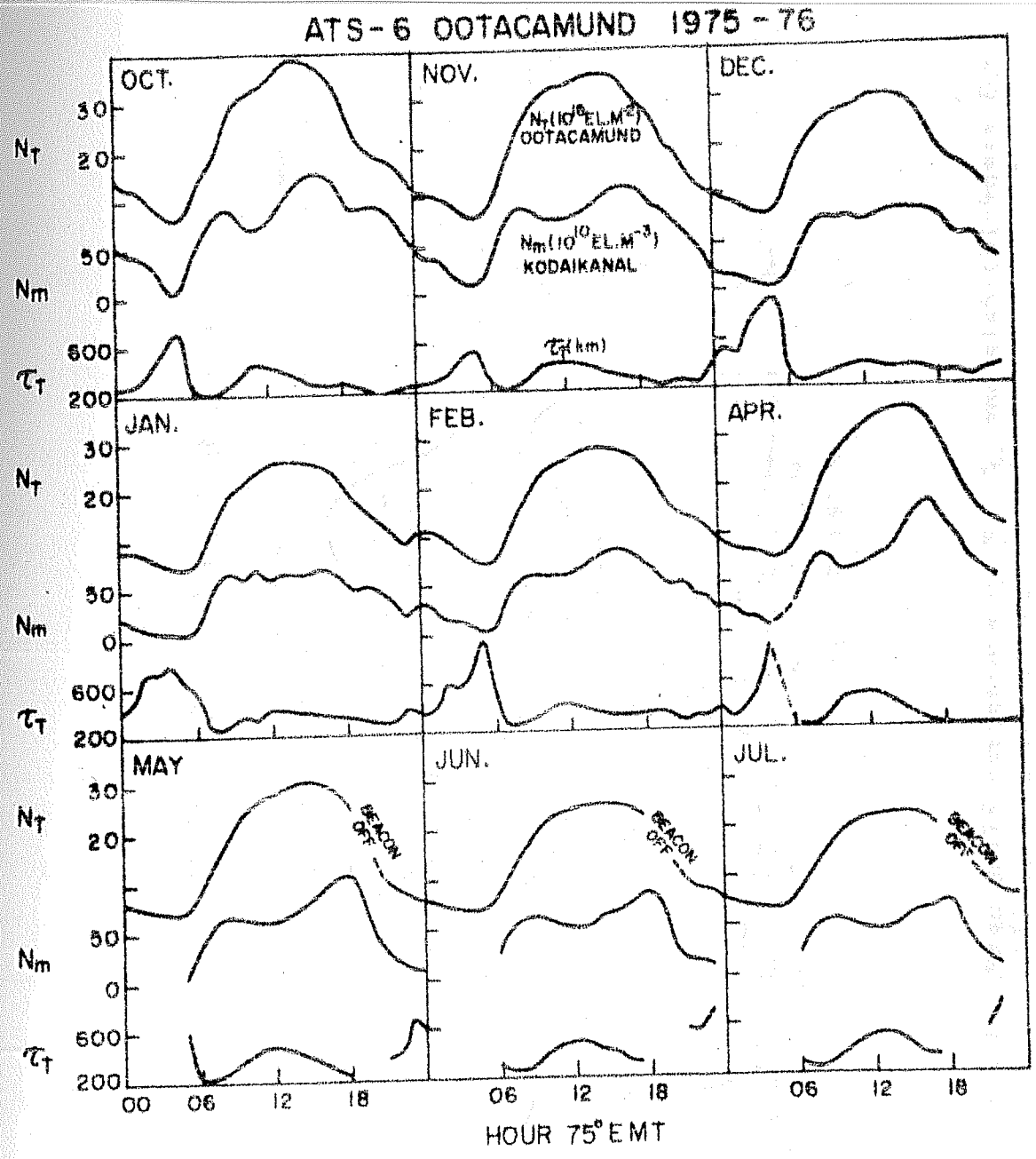

Fig.4.6a The mean daily variations of N_T, N_m, and τ_T for different months.

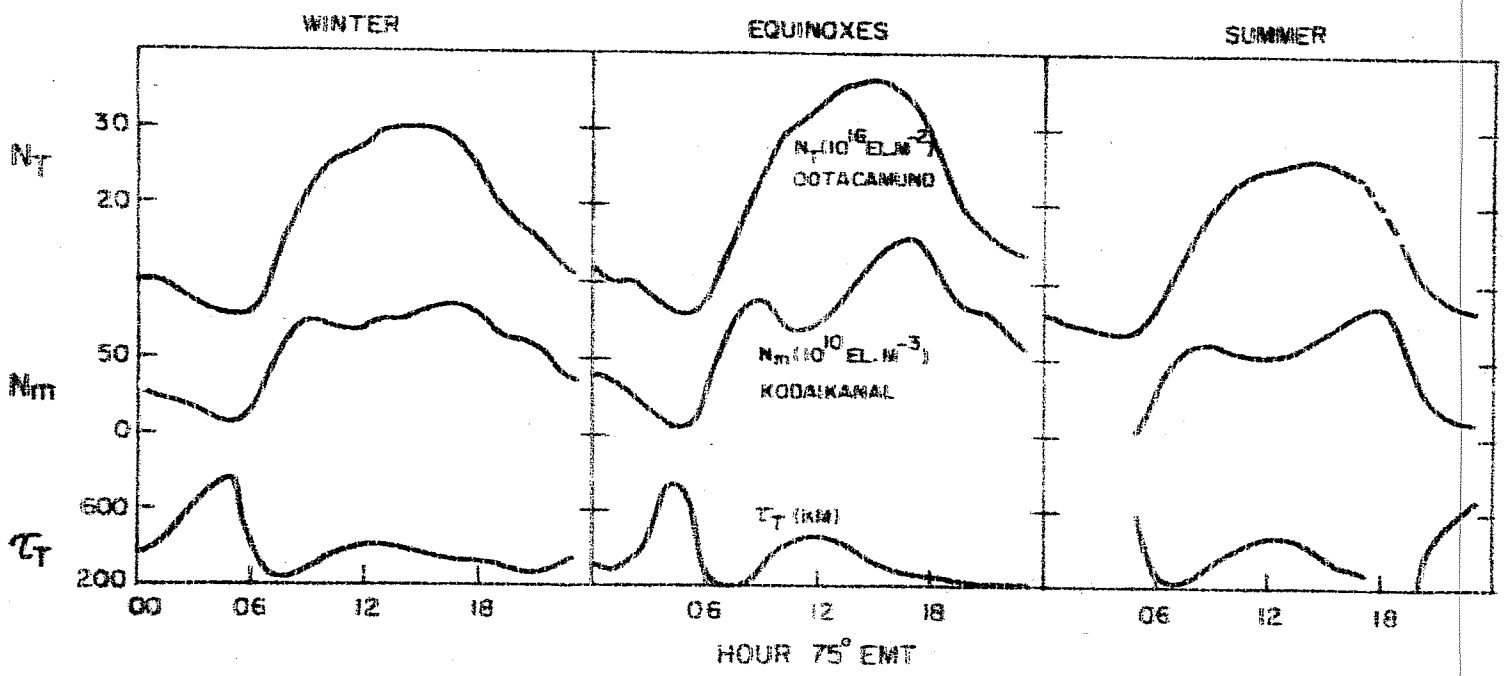

Fig.4.6b Mean daily variations of N_T, N_m and slab-thickness for different seasons.

4.4.2 Discussions

The interesting feature to be noted in the diurnal variation of τ is the occurrence of large morning peak followed by very sharp decrease. Similar feature has earlier been reported by various workers (Yuen and Roelofs 1967, Walker and Ting 1972, Titheridge 1973) using data from geostationary satellite. Klobuchar and Allen (1970) have reported rather abnormal diurnal variation in winter with night-time values greater than daytime values. Iyer and Rastogi (1978), Skinner (1966), Rufenach et al. (1968) and Bandyopadhyay (1970) also observed the presence of the morning peak in the diurnal variation of τ at equatorial stations; the data used being from orbiting satellites. Various theories have been advanced to explain this feature. Titheridge (1973) had discussed the dependence of τ on different ionospheric parameters and concluded that τ is primarily a measure of the neutral temperature and not plasma temperature. Yeh and Flaherty (1966) have studied the dependence of τ on T_e/T_i ratio. Furman and Prasad (1973) have shown that τ is neither a measure of neutral temp. nor of T_e/T_i ratio; but the departure of τ from the Chapman value decided by 4.13H is a measure of the departure from the diffusive equilibrium at topside. Coming to the theories for pre-sunrise peaks, Bandyopadhyay (1970) suggested it to be due to conjugate photo-electrons from summer pole heating the winter pole ionosphere. Skinner (1966) attributed it to early sunrise above the layer peak. In the present geometry of

the ATS-6 to Ootacamund path, the sunrise along the entire ray-path occurs in a very short-time and since the production is very small above 500 km, its role in producing the predawn peak in is probably small. Garriot et al. (1965) proposed the presence of significant H_e^+ and H^+ above the F layer peak which could account for the predawn peak in τ . This also explains the fact that larger values of the peak are obtained for τ_T which is derived from N_T than τ_F which is derived from N_F. A significant contribution to N_T comes from the electrons associated with H^+ and H_e^+ ions whereas similar contribution to N_F is smaller in extent. A more detailed discussion is given in the next section using top and bottomside electron content data.

4.5 Comparative Studies of the Daily Variation of Different Ionospheric Parameters

Here we shall compare the total electron content (N_T) data from the group delay measurements with the electron density versus height derived from the Kodaikanal ionogram, available for every 15 min. interval. The daily variations of N_T and the bottomside ionosphere parameters are discussed for an average period of sixteen days as well as for a quiet, a disturbed and a counter-electrojet day.

The ionograms at Kodaikanal were reduced using the Budden's matrix method and the following parameters were derived (i) the peak electron density, N_m, (ii) the electron content below the peak, N_b, (iii) the height of the peak F-region electron density h_m

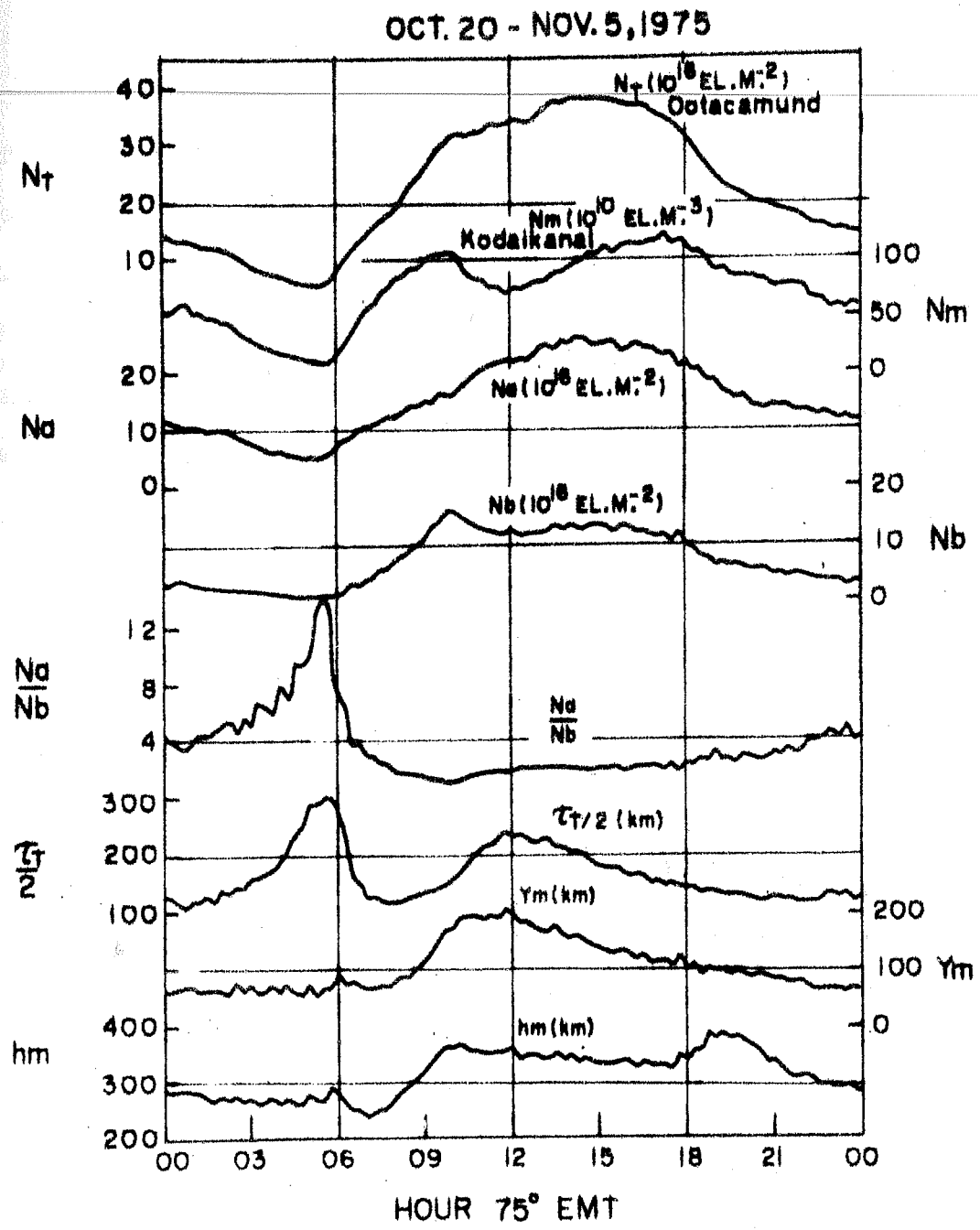

Fig.4.7 Mean daily variation of N_T at Ootacamund compared with N_m, N_a, N_b, N_a/N_b, τ_T, y_m and h_m for the period Oct. 20-Nov. 5, 1975.

The daily variation of N_T differs significantly from that of N_m during the midday hours; no midday bite-out is seen in N_T. The value of N_T starts increasing from the sunrise till the afternoon reaching a rather flat maximum around 1500 LT and continues to decrease thereafter to its minimum value near sunrise. Separating N_T into the components below (N_b) and above (N_a) the F-region peak, one finds that the N_b shows the maximum value at about the time of the forenoon peak of N_m, later it remains at a rather constant and high value during the rest of the daytime hours; starts decreasing slowly after sunset to its minimum value around sunrise and no increase is seen corresponding to the evening peak of N_m. The value of N_a, on the otherhand, starts increasing after sunrise reaches an afternoon peak around 1500 LT and decreases thereafter to its sunrise minimum value. The daily variation of the topside electron content does not show any characteristics peculiar to the low-latitude ionosphere.

The ratio of topside to the bottomside electron content (N_a/N_b) remains constant at a value around 2 during 1100-1800 LT, starts increasing after sunset but a sharp and abnormally large peak of value exceeding 15 is seen around 0500 LT. The slab-thickness $\tau_T = N_T/N_m$ shows a midday peak similar to that of y_m but a pre-sunrise peak is seen in τ_T similar to that of N_a/N_b while y_m does not have similar pre-sunrise peak. In order to test whether the average daily variation of the parameters discussed above, differs significantly on individual days, we discuss the daily variation on a geomagnetically quiet, a geomagnetically disturbed, and a counter electrojet day.

Fig.4.8a, shows the daily variations of the various parameters on Oct. 25, 1975, a geomagnetically quiet day (A_p=4) with a strong equatorial electrojet (ΔH = 85 gamma). The daily variation of N_m shows a strong midday bite-out around 1100 LT. The daily maximum of y_m and h_m occurs about at the same time as that of H suggesting strong equatorial electrojet effects on the bottomside ionosphere. The bottomside electron content N_b is maximum around 1000 LT but the topside electron content N_a, has the largest value in the afternoon hours. The ratio N_a/N_b is fairly constant for the most of the daytime hours with a very sharp peak around 0500 hr LT. The N_T does not show a midday bite-out but there is a decrease in the rate of temporal increase of N_T around midday hours.

Fig.4.8b shows the daily variations of the various parameters on 3rd Nov. 1975, a geomagnetically disturbed day (A_p=65). On the disturbed day, all the parameters show a comparatively significant fluctuations superimposed on the smooth daily variation. The daily variation of N_m is highly distorted, the afternoon peak is delayed to post-sunset hours (at 1900 LT). The N_T shows a depression around 1100 LT but it is doubtful if this is a significant feature of the storm effect. The daily variation of N_b maximises slightly before noon and N_a is maximum during afternoon hours. The h_m does not have any post-sunset peak so prominent during the quiet days. The slab-thickness and the ratio N_a/N_b shows a number of peaks in the morning hours associated with the depressions of N_m or of N_b.

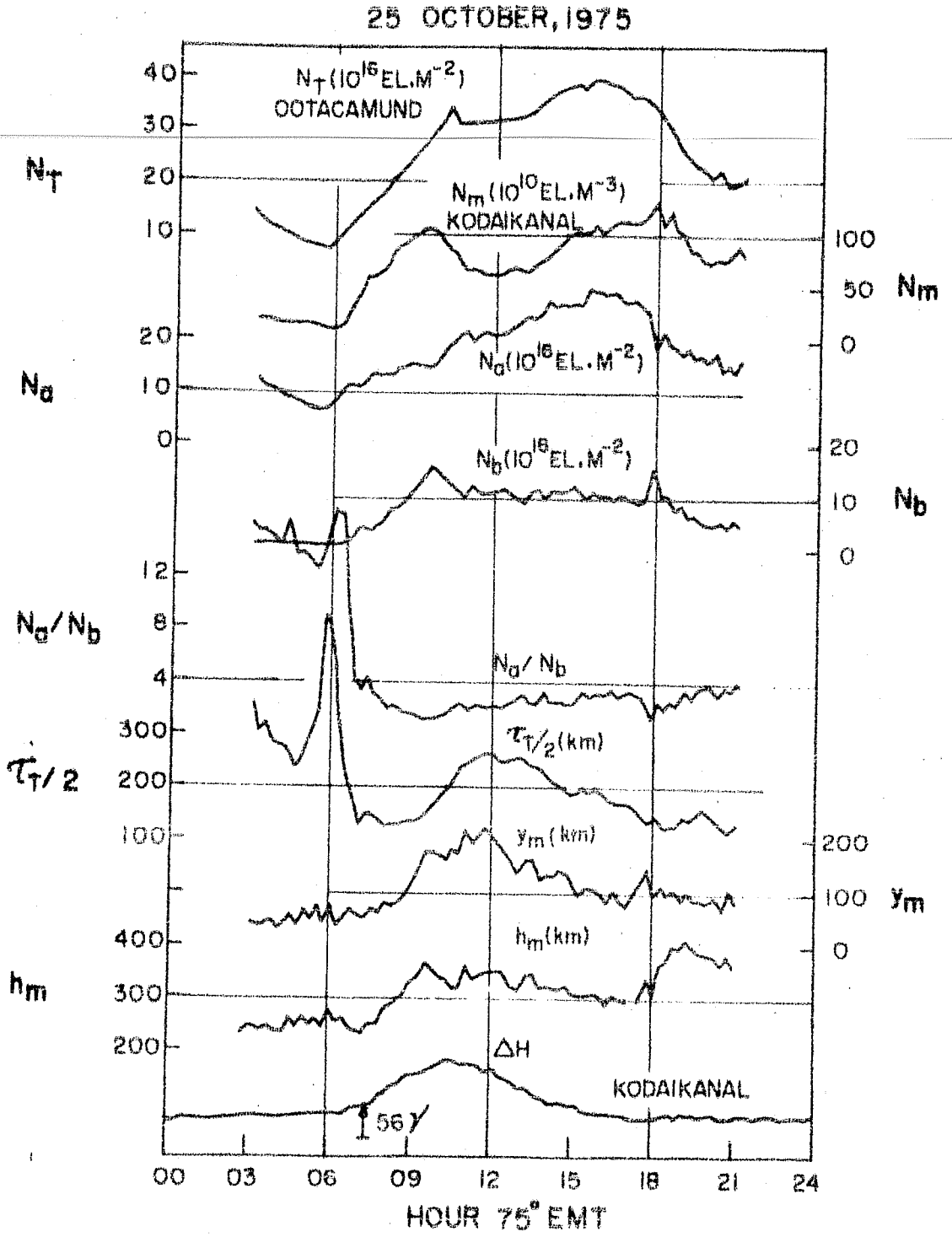

Fig.4.8a Daily variations of different ionospheric parameters and the horizontal component of geomagnetic field at Kodaikanal on a strong electrojet day (25th October, 1975).

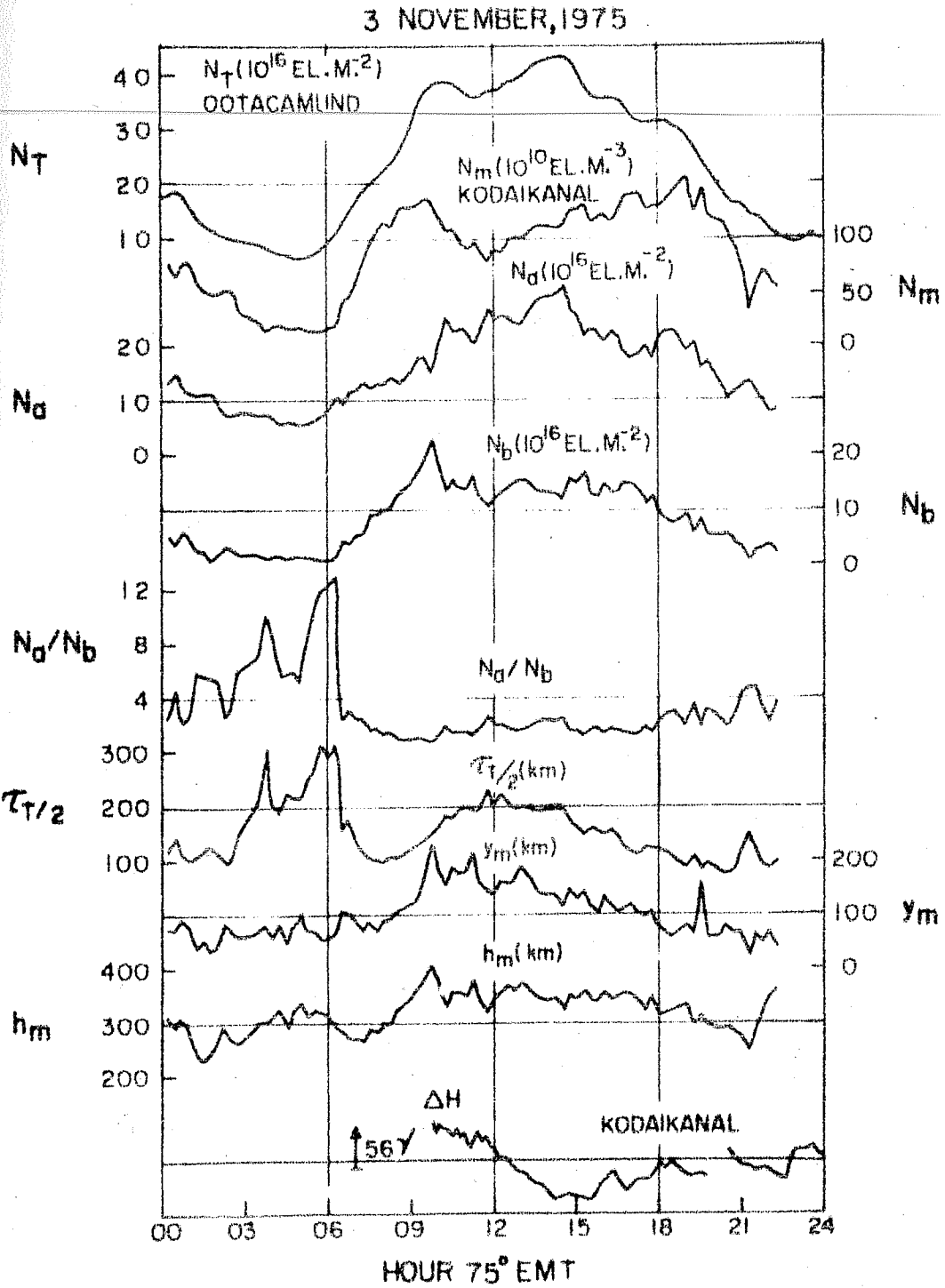

Fig.4.8b Daily variations of different ionospheric parameters and the horizontal component of geomagnetic field at Kodaikanal on a magnetically disturbed day (3rd November, 1975).

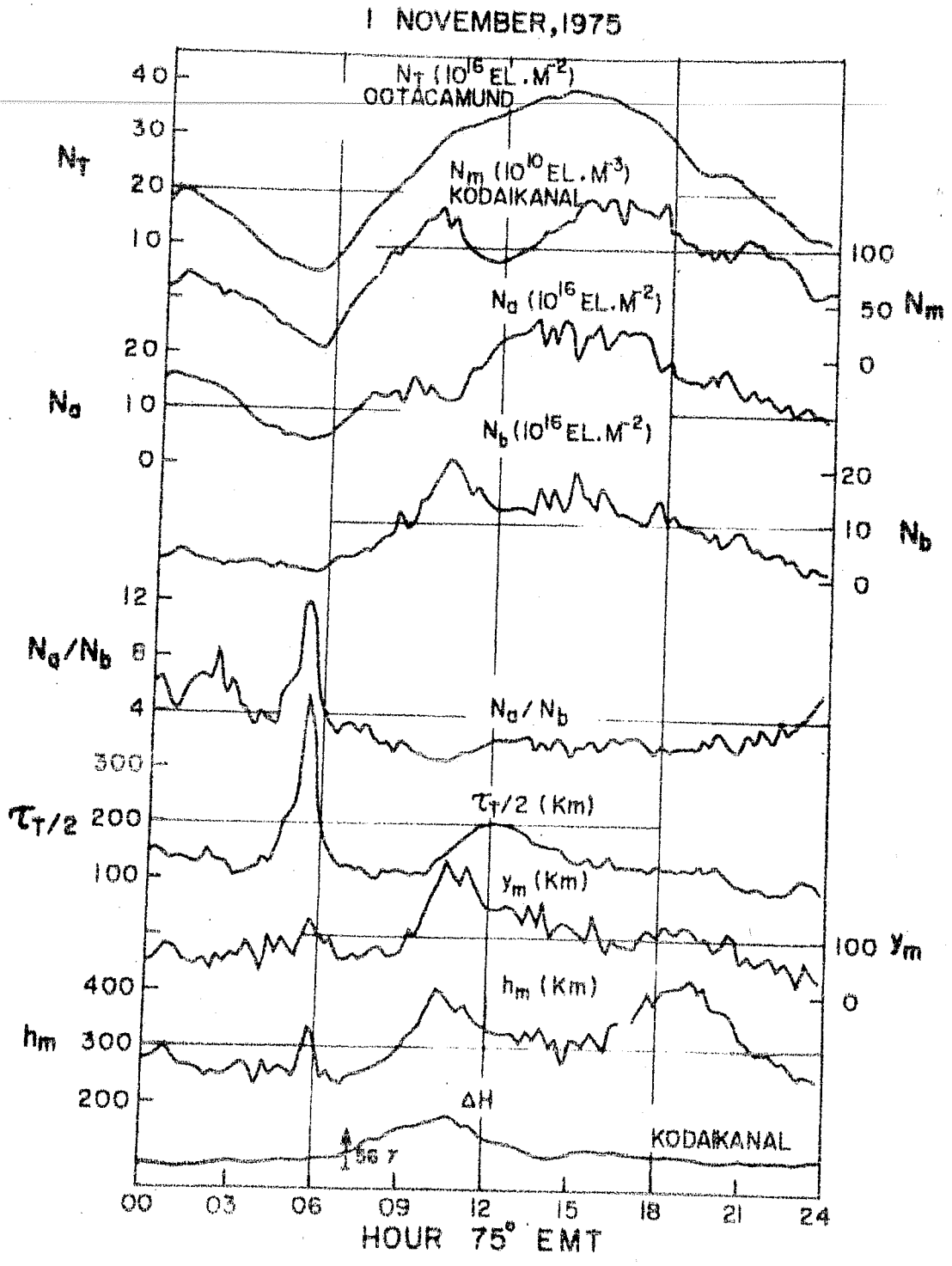

Fig.4.8c Daily variations of different ionospheric parameters and the horizontal component of geomagnetic field at Kodaikanal on a counter electrojet day (1st November, 1975).

Fig.4.8c shows the daily variations of all the parameters on 1st Nov. 1975, which is a quiet day with A_p=7, but a small counter-electrojet occurred in the afternoon hours. The most of the features are similar to that obtained for quiet days except that a significant dip in h_m variation is observed around 1500 LT.

To examine the seasonal effects in these parameters, the hourly ionograms of the international quiet days of each month are reduced to get N_m, N_b, h_m and y_m. Combining these data with N_T data of the corresponding days, τ_T, N_a, N_a/N_b are obtained. The data is grouped seasonally and the mean daily variation of each parameter, for each season is obtained. The results are shown in Fig.4.9. The gross features are similar in all the three seasons. τ_T does not show the midday peak in winter and is probably connected with the near absence of bite-out in N_m.

4.5.2 Discussions

The absence of a midday bite-out in N_T corresponding to the bite-out in N_m on individual days suggests, in the first instant, that the midday decrease of N_m due to so called equatorial Fountain generated by the special configuration of the electric fields at low latitudes, is confined to a narrow region around the F_2 peak. During the period from sunrise to about 0900-1000 LT, the values of N_m, N_T, and N_b increase, thereafter each of the parameters have different temporal variations: the N_T continues to increase till the evening hours; N_b continues to decrease and N_m shows the midday bite-out followed by the afternoon peak.

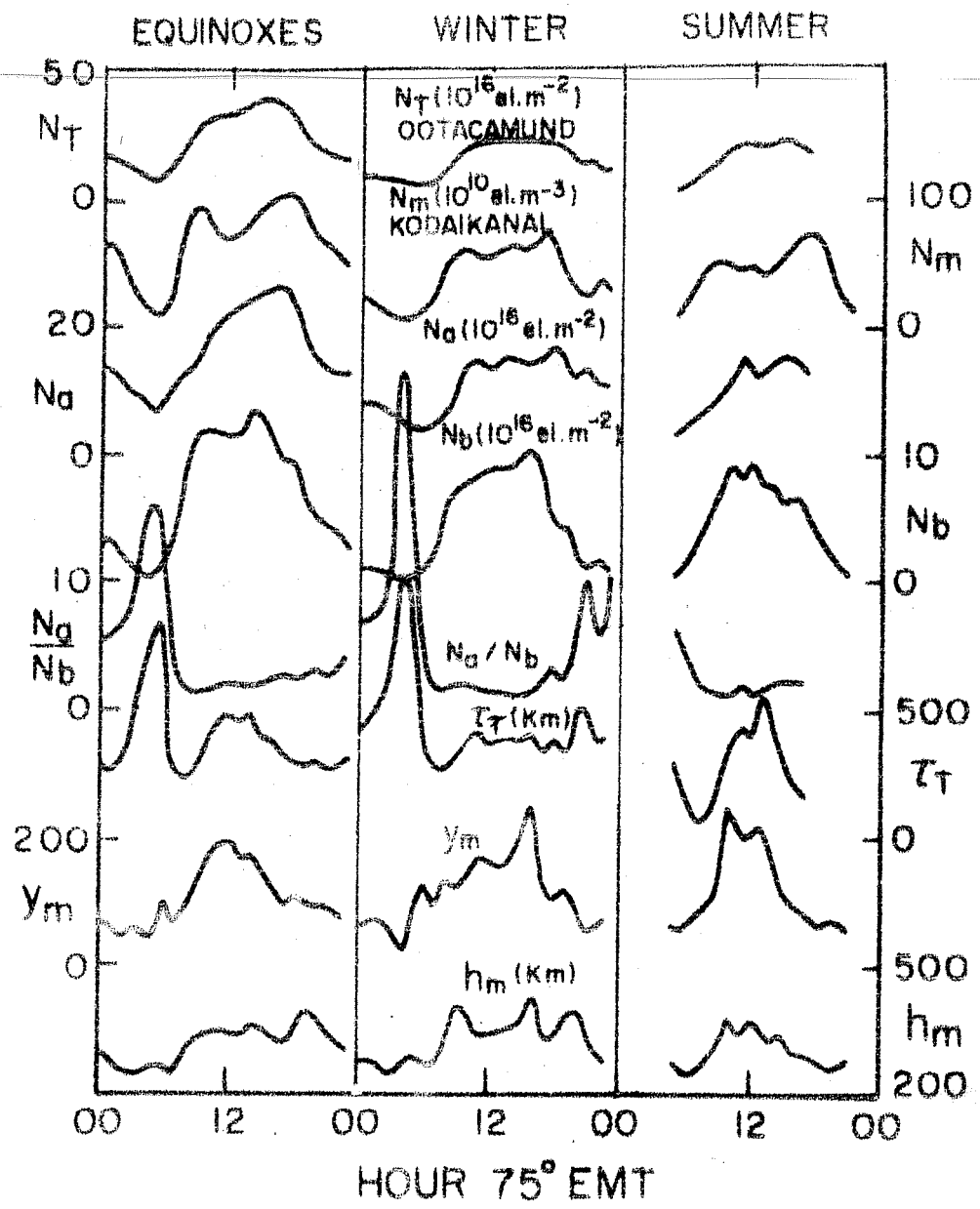

Fig.4.9 Mean daily variation of N_T at Ootacamund compared with N_m, N_a, N_b, N_a/N_b, τ_T, y_m and h_m for different seasons.

Thus it seems that the equatorial electrojet effects on the bottomside of the ionosphere become important only after about 0900 LT.

The daytime values of N_a/N_b are in good agreement with the value calculated for a Chapman layer (Wright 1960). This suggests that inspite of large electrodynamic uplifting of the F-region near the dip equator during the daytime hours the general shape of the F_2 region (including the topside) does not depart considerably from that of the Chapman layer.

It is only during the pre-sunrise hours, when the ratio of N_a to N_b shows abnormally large values. Skinner (1966) explained the presunrise peak in N_T/N_m in terms of earlier ionization in the topside ionosphere prior to ground sunrise. Rastogi et al. (1973) showed that the abnormal values of N_a/N_b was as due to the rapid decrease in the height of the F-region and thereby rapid erosion of N_{max} whereas N_e-h profile above 700 km remained fairly constant with time. This pre-sunrise peak in N_a/N_b is similar to the deep minimum in the shape factor, F, discussed by Davies et al. (1979). In the present geometry of the ATS-6 to Ootacamund path, the sunrise along the entire path occurs in a very short-time and since the production is very small above about 500 km, its role in producing the N_a/N_b peak is probably small.

CHAPTER - V

INFLUENCE OF ELECTROJET ON THE LOW LATITUDE IONOSPHERE

5.1 Introduction

Two unique features of the equatorial ionosphere are the equatorial F_2 region anomaly and the equatorial electrojet. Both are controlled by the dynamo electric fields set-up in this region; so an interrelationship between the two phenomenon is expected. Dunford (1967) obtained a positive correlation between E-region current system near the magnetic equator and the equatorial anomaly using topside sounder. Mac Dougall (1969) and Rastogi and Rajaram (1971) using f_oF_2 values near the magnetic equator have given evidence that the equatorial anomaly shows high correlation with electrojet strength. Rush and Richmond (1973) have obtained positive correlation between several parameters of the equatorial anomaly in f_oF_2 and the electrojet strength. As for the equatorial anomaly in TEC is concerned, geomagnetic control of this anomaly has been studied by Das Gupta and Basu (1971). Influence of solar flux and the electrojet on the diurnal development of the equatorial anomaly in TEC has been investigated by Walker and Ma (1972). A better latitudinal coverage of the anomaly region from dip equator to beyond the anomaly peak was obtained by Iyer et al. (1976) by combining orbiting satellite data from two stations, one near equator and another one near the crest. The beacons aboard a geostationary satellite not only provide a continuous measurement

of TEC but even a good spatial resolution can be obtained by combining data from a number of stations using the same beacon. The availability of ATS-6 data provided such an unique opportunity to study the electrojet control of the low latitude ionosphere. The details about the stations are given in chapter II. The study has been carried out using electron content (N_F) and the F_2 region peak electron density (N_m) data from the chain of the stations. Mainly three aspects of the electrojet effects have been investigated in the present study. Firstly the role of electrojet in the equatorial anomaly under different geomagnetic conditions has been discussed. Secondly, the anomalous semiannual behaviour of TEC has been examined in light of semiannual variation of the electrojet strength. Lastly, the day to day variability in TEC and N_m in conjunction with electrojet strength has been discussed.

5.2 Electrojet Effects on the Latitudinal Distribution of TEC (N_F)

Latitudinal variation of TEC has been discussed by various workers (Basu and Das Gupta 1968, Titheridge and Smith 1969, de Mendonca et al. 1969, Golton and Walker 1971, Rastogi et al. 1973, 75, 77, Iyer et al. 1976) using TEC data from orbiting satellites. These studies clearly indicate the existence of an equatorial anomaly in TEC, in its latitudinal variation, similar to one in F_2 region critical frequency. In the present section we describe the results of latitudinal variations of TEC under different

geomagnetic conditions namely (a) a normal electrojet day, (b) a geomagnetic disturbed day and (c) a counter-electrojet day.

5.2.1 Results

The latitudinal profiles of N_F on four typical days namely: (i) a normal electrojet day, 18th May 1976, A_p=3, (ii) a geomagnetically disturbed day, 3rd May 1976, A_p=94, (iii) a strong counter-electrojet day, 12th May 1976, A_p=7, and (iv) a weak counter-electrojet day, 14th May 1976, A_p=4 are shown in Fig.5.1a, b,c,d. For all the four days the horizontal component of the earth's magnetic field (H) for an equatorial station Kodaikanal, dip 3.4°N, are also shown in the same figures. The magnetic field during daytime is a representative indication of the electrojet strength. In addition N_F plots against latitude are shown for different local times of the day, to examine the diurnal development of the equatorial anomaly. It is noticed that on the normal electrojet day, the anomaly is well developed (Fig.5.1a) whereas on the disturbed day, the anomaly is not at all present (Fig.5.1b). On both the counter-electrojet days, the well developed anomaly is present till 1400 hr LT and then the crest moves towards equator and at about 1730 hr, the crest has moved south of Rajkot (Fig.5.1c,d) whereas on a normal electrojet day, the crest is over Udaipur even at 1730 hr LT (Fig.5.1a).

5.2.2 Discussions

On a normal electrojet day the magnetic field shows flat night-time minimum (Fig.5.1a). After sunrise the electron density

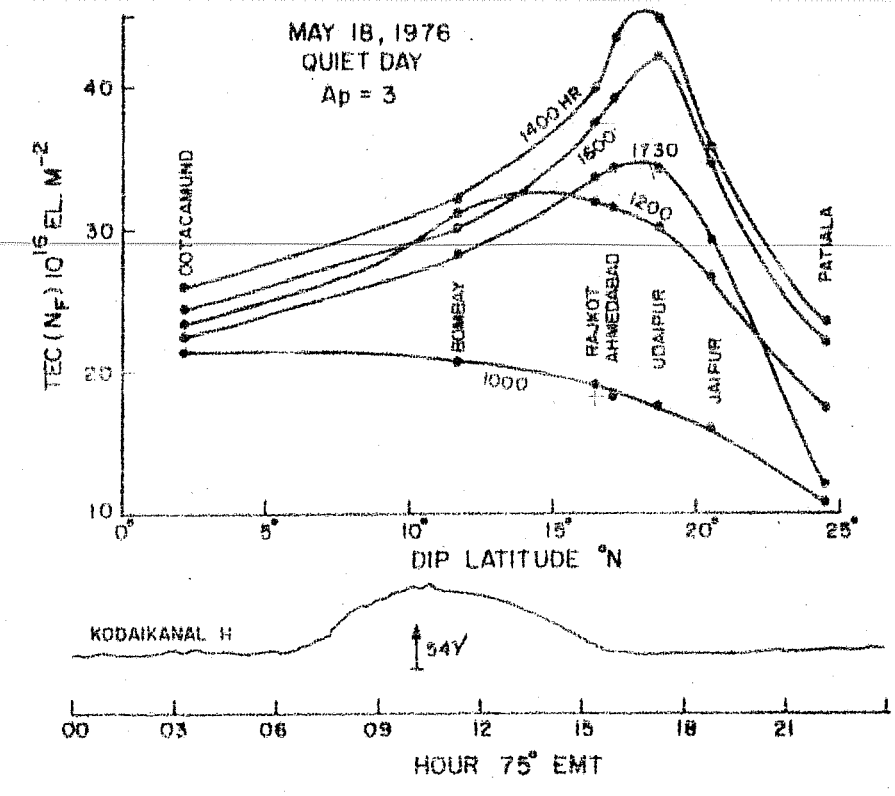

(a)

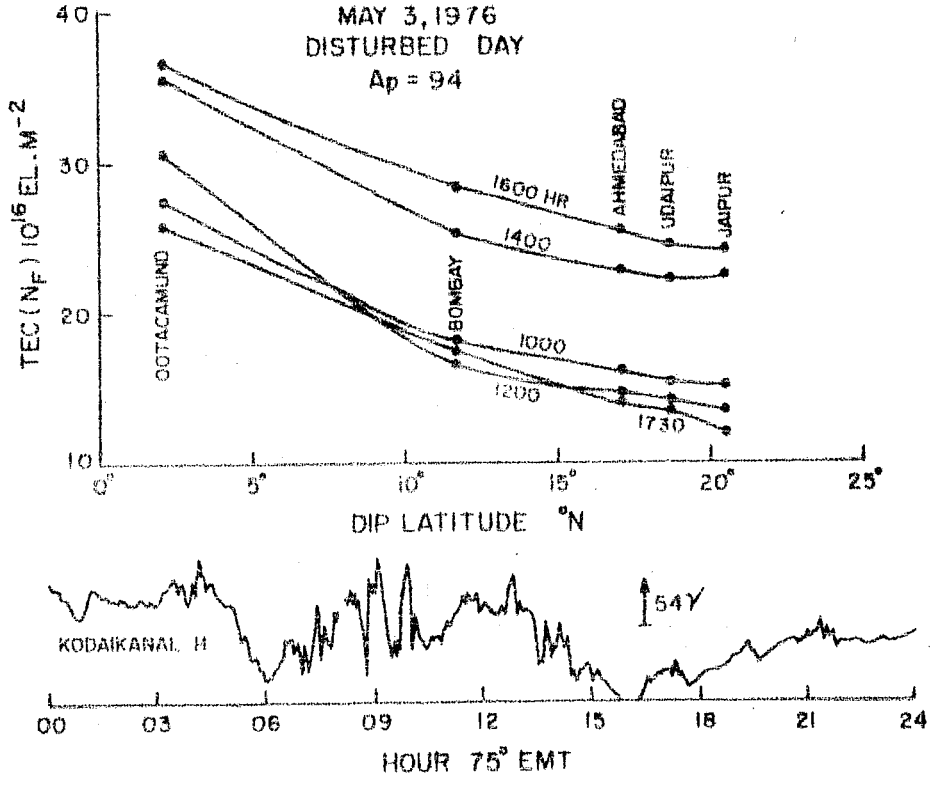

(b)

Fig. 5.1 (a,b) Diurnal development of equatorial anomaly on (a) a normal electrojet day and (b) a geomagnetically

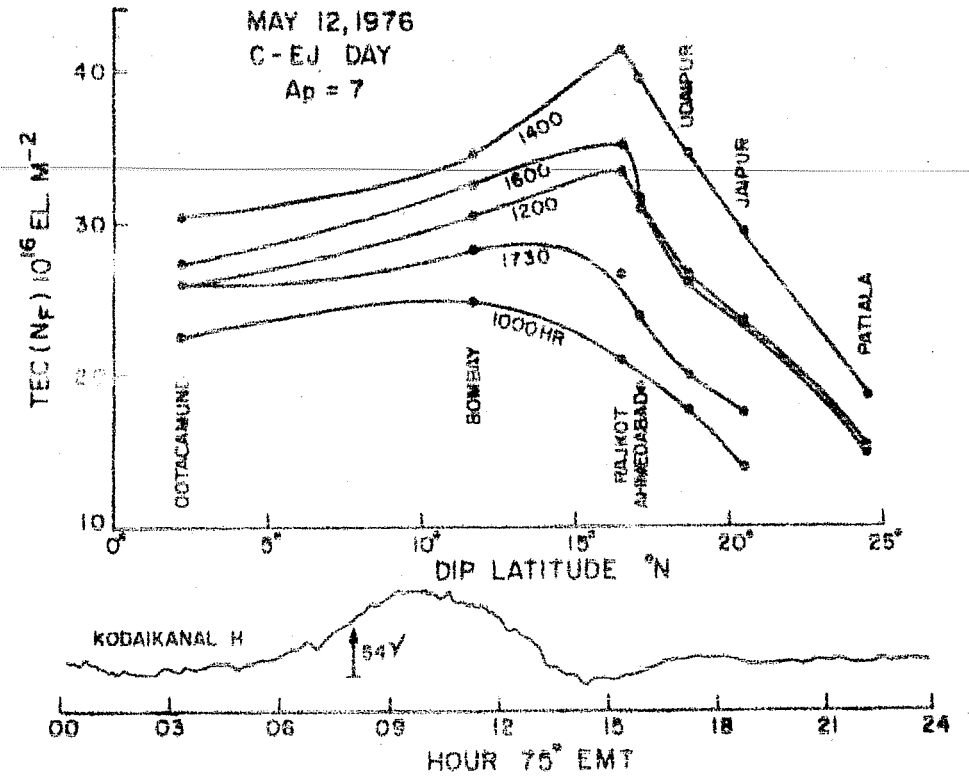

(c)

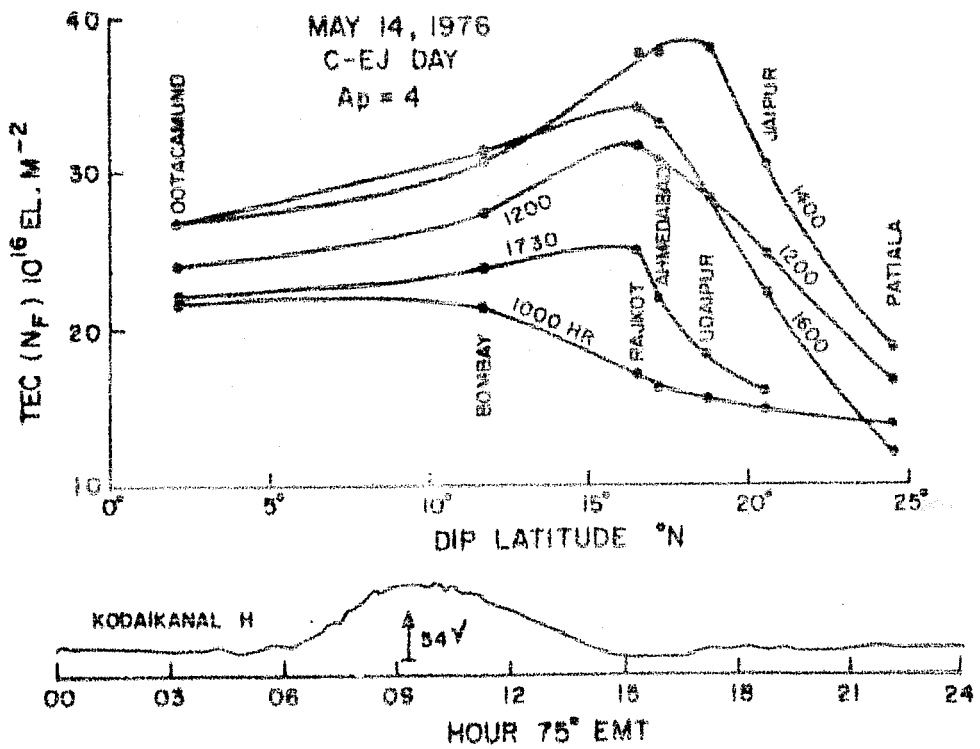

(d)

Fig.5.1 (c,d) Diurnal development of equatorial anomaly on (c) a strong counter electrojet day and (d) a weak counter electrojet day.

in the E-region increases and the H field shows a steady increase until around 1100 hr LT, after which it starts decreasing. Such behaviour of the magnetic field is due to currents associated with the eastward electric field (E) during daytime. Owing to this electric field and the north-south magnetic field at the equator, E x B drifts are produced and the electrons are lifted to higher altitudes. The lifting of electrons takes place upto a few scale heights above the F_2 region peak, beyond which they diffuse along the lines of force and are deposited in the latitude regions of about 15° to 20° dip latitude. This process takes approximately 2 hours (Iyer et al.1976) and any effects in electric fields at E region heights at the equator are seen at latitudes 15° to 20° after an approximate two-hour delay. At 1000 hr, the latitudinal profile of N_F is showing a normal behaviour with high equatorial values (Fig.5.1a). As time progresses, at 1200 hr, the anomaly starts developing with maximum N_F at Udaipur. By 1400 hr, more electrons have flowed along field lines to Udaipur and the anomaly is well developed. The latitudinal profile at 1600 hr shows that the anomaly is now in its declining phase but crest still remaining over Udaipur till 1730 hr.

The data for a highly geomagnetically disturbed day, 3 May 1976, are shown in Fig.5.1b. On this day the electrojet is weak as estimated from Trivandrum minus Alibag H data and the transfer of ionization from the equator to higher latitudes does not take place to any noticeable extent, and hence one does not notice any anomaly in the latitudinal variation of N_F.

On the counter-electrojet day the H component of the geomagnetic field shows a depression at about 1340 hr. The latitudinal profiles of N_F for different hours of 12th and 14th May, show a small latitudinal anomaly at 1200 hr reaching a maximum at 1400 hr, at Rajkot. But by 1600 hr and later at 1730 hr, the anomaly becomes less prominent with the crest moving considerably towards equator. The reversal of the electric field causes downward drift motion at the equator and consequently the movement of ionization to the crest region is suppressed. The daily plots of N_F at Ahmedabad and Ootacamund on 3rd, 12th and 18th May 1976, are shown separately in Fig.5.1c. In the afternoon hours of the quiet day, the Ahmedabad values are much higher than the Ootacamund values, indicating the presence of equatorial anomaly during these hours. On the disturbed day, Ootacamund day-time values are higher than Ahmedabad values, indicating the absence of equatorial anomaly on this day. On the counter-electrojet day, the presence of a poorly developed equatorial anomaly is indicated, and the anomaly vanishes around 1800 hr LT whereas at the same hour on quiet day, the anomaly is still well developed.

5.3 Electrojet and the Anomalous Semiannual Variation of N_F

Peak electron density of F_2 layer is known to reveal a significant semiannual variation. The phase of this variation agrees with the semiannual variation in atmospheric density (Yonezawa 1971). Also the electron content shows a semiannual variation. The magnitude of this variation in TEC is dependent

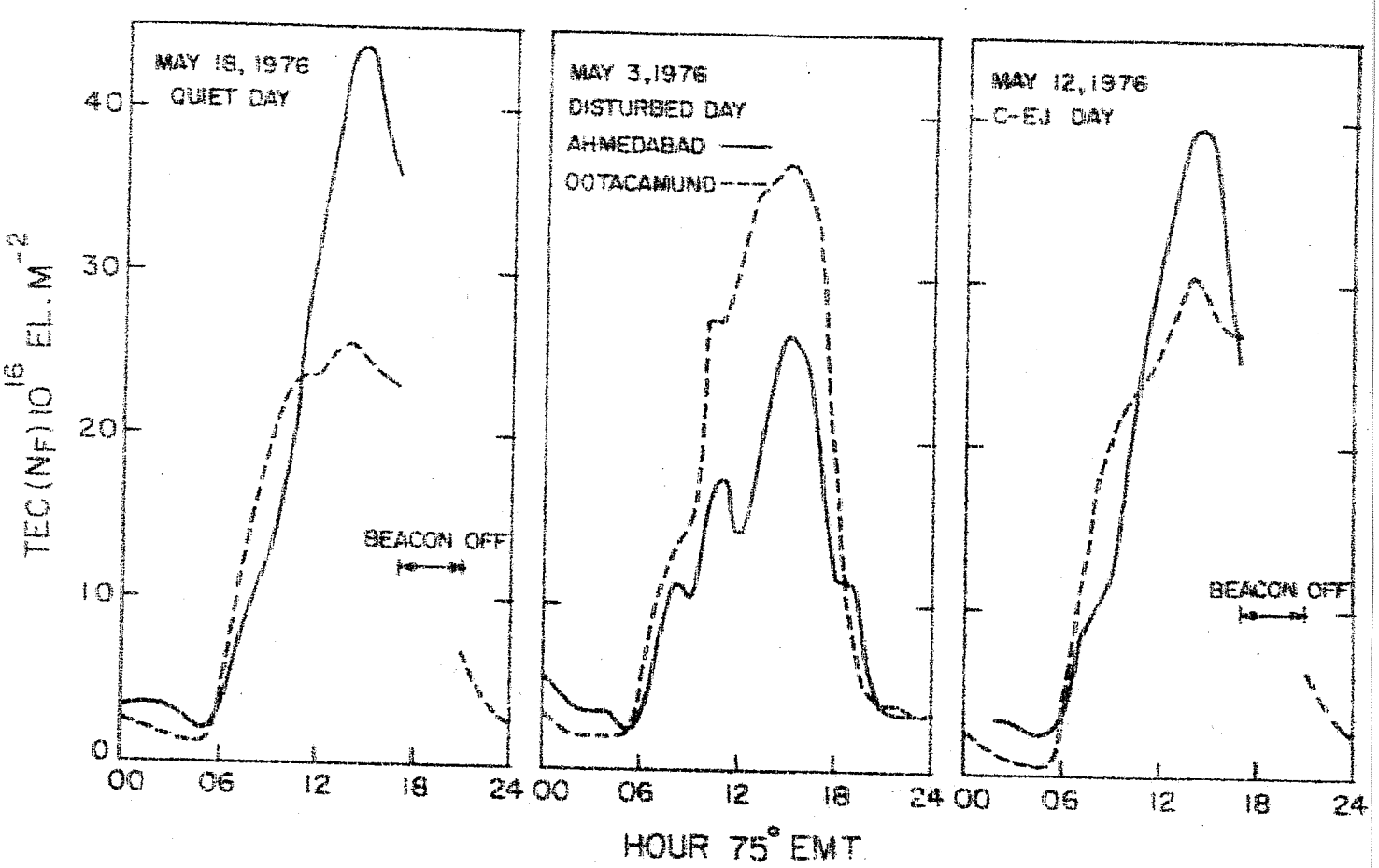

Fig.5.1e Daily plots of N_F at Ahmedabad and Ootacamund on three typical days.

on solar activity, particularly in the northern hemisphere (Titheridge 1973, Galdon and Alberca 1970, da Rosa et al. 1973). There, however, appears to be an anomaly in the semiannual variation with a larger peak in March-April equinox than in the Sept. - Oct. equinox (da Rosa et al. 1973, Titheridge 1973). Essex (1977) studied the equinoctial variations in the ionospheric TEC (N_F) at a number of stations in northern and southern hemisphere. It was found that the semiannual variation of N_F shows an anomaly with a larger peak in the March-April equinox than in Sept. - Oct. equinox in high sunspot year (1971-73) and the anomaly almost disappears in 1973-74. All the stations, used in that study are outside the equatorial anomaly region. The present study, using a chain of stations at low latitudes provides an opportunity to look into the phenomenon taking place in the equatorial anomaly region.

5.3.1 Results

The daytime maximum value in the monthly mean daily variation of N_F for each month are plotted in Fig.5.2 for each station. The values show a semiannual behaviour, with maximum in equinoxes. It is seen that for Patiala, the April value of 37×10^{16} el m^{-2} is much higher than the Oct. value of 21×10^{16} el m^{-2}. For Udaipur and Ahmedabad, the same trend continues but the difference has decreased significantly whereas for Bombay and Ootacamund the trend has reversed viz. the Oct. peak N_F value is higher than the April peak N_F value. It is also to be noted

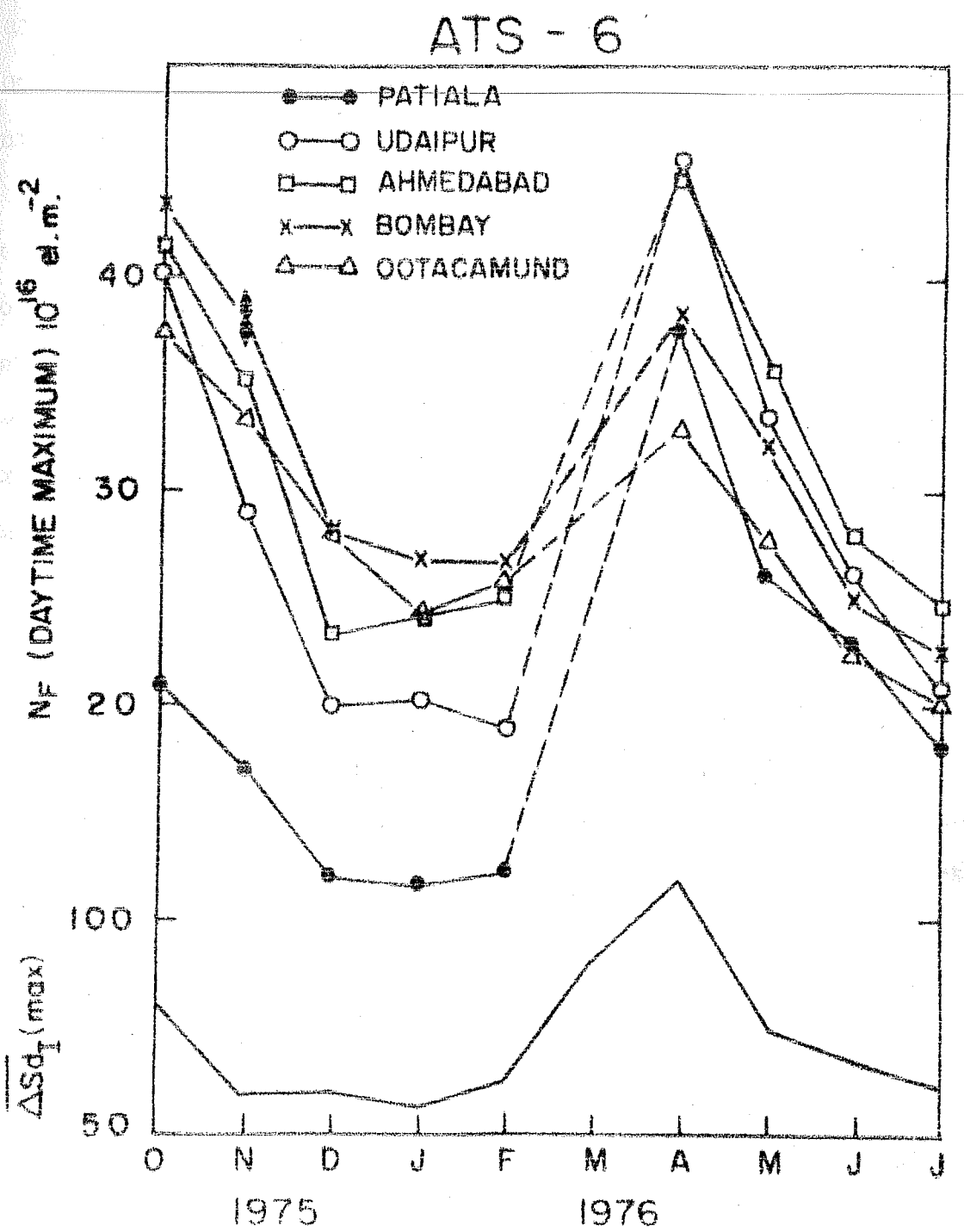

Fig.5.2 Month to month variation of the peak daytime N_F, at the chain of stations in India during ATS-6 Phase II. The bottom curve shows the mean monthly electrojet strength for the corresponding months.

that during the months Oct. to Feb., the crest of the equatorial anomaly extends equatorward to Bombay only, whereas for summer months (May - June- July) the crest is formed at Ahmedabad, and in the month of April, the crest extends poleward to Udaipur. The difference between the April value and the Oct. value is plotted against. mag. dip latitudes in Fig.5.3. It is noticed that the difference decreases linearly with decrease in latitude to $\sim 10^{\circ}$N. It then remains almost constant for both the stations (Bombay and Ootacamund) which are well within the equatorial anomaly region.

5.3.2 Discussions

To understand the role of electrojet in above mentioned features, the mean maximum electrojet strength $\Delta\overline{Sd_I}$ (max) (Kane 1973) for different months have been calculated (the lower part of Fig.5.2). The electrojet strength ΔSd_I is defined as $\Delta Sd_I = \Delta H$ (Equator) $- \Delta H$ (θ) + Sq (θ) where ΔH (equator) and ΔH (θ) are the value of H field at equator and at a low latitude station outside electrojet respectively. The maximum value of ΔSd_I in its diurnal variation (ΔSd_I(max)) on a day is taken as the electrojet strength for that day. The magnetic H field data recorded at Alibag (outside electrojet) and Trivandrum (equator) have been used in these calculations. Monthly mean values of H field at the two stations were used in a similar fashion in deriving $\Delta\overline{Sd_I}$(max) values for different months. A semiannual behaviour with a maximum at the equinoxes is apparent, in the

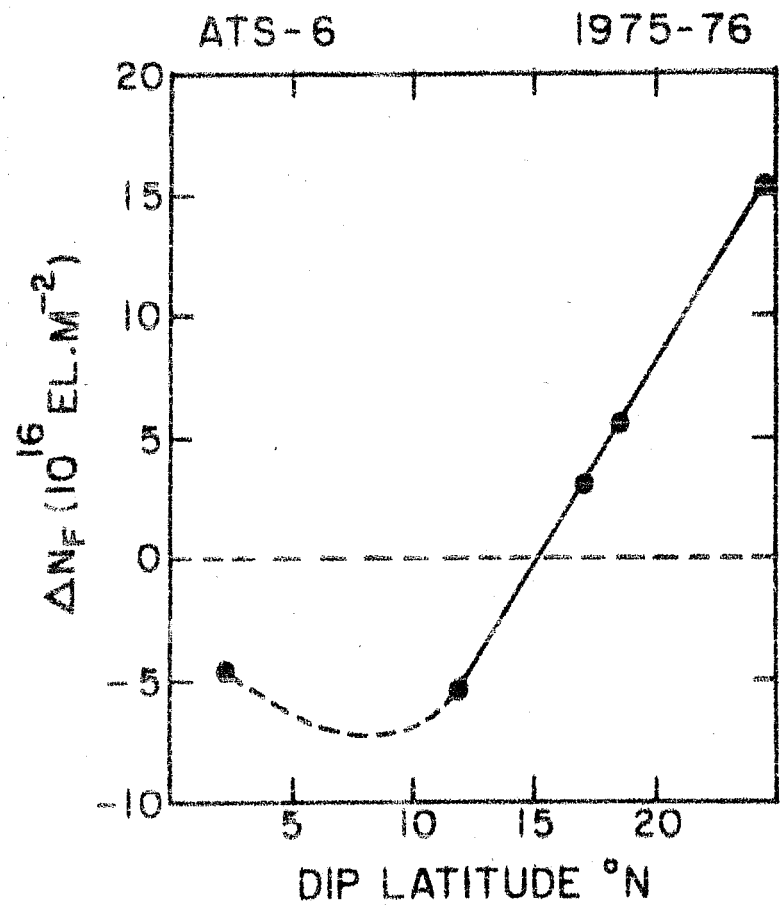

Fig.5.3 Latitudinal variation of the difference of April peak to October peak in $N_F(\Delta N_F)$ obtained from Fig.5.2.

electrojet strength also. It is noticed that electrojet is much stronger in April than in October, though both April and October are equinoctial months. The much stronger electrojet in April causes the equatorial anomaly crest to go much further away from the equator and as is seen from Fig.5.2, the crest is formed over Udaipur whereas in the month of Oct., when the electrojet strength is smaller than of April, the crest is formed over Bombay. The equatorial electrojet controls the low latitude ionosphere through "Fountain effect", i.e. the ionization at equator is moved up by the E x B drift and then it diffuses along the magnetic lines of force to the tropical latitudes. A stronger electrojet means a stronger "Fountain effect", which in turn gives larger anomaly crests extending further poleward. Thus the electrojet seems to be a probable agency for the trend reversal for the stations well within the equatorial anomaly region. It is also seen that electrojet is a little stronger in summer, than in winter. This again seems to explain the fact qualitatively that in the winter months, the equatorial anomaly crest extends to Bombay only whereas in the summer months, the crest extends to Ahmedabad. To examine how the day to day variations in N_F at the equatorial station Ootacamund responds to the electrojet strength $\Delta\overline{Sd}_I$, the N_F at Ootacamund at 1200 hr LT for each day during April and October are plotted against the corresponding electrojet strength (Fig.5.4). An overall negative correlation of 0.74 is found. For individual months, the negative correlation of 0.60 for October and of 0.56

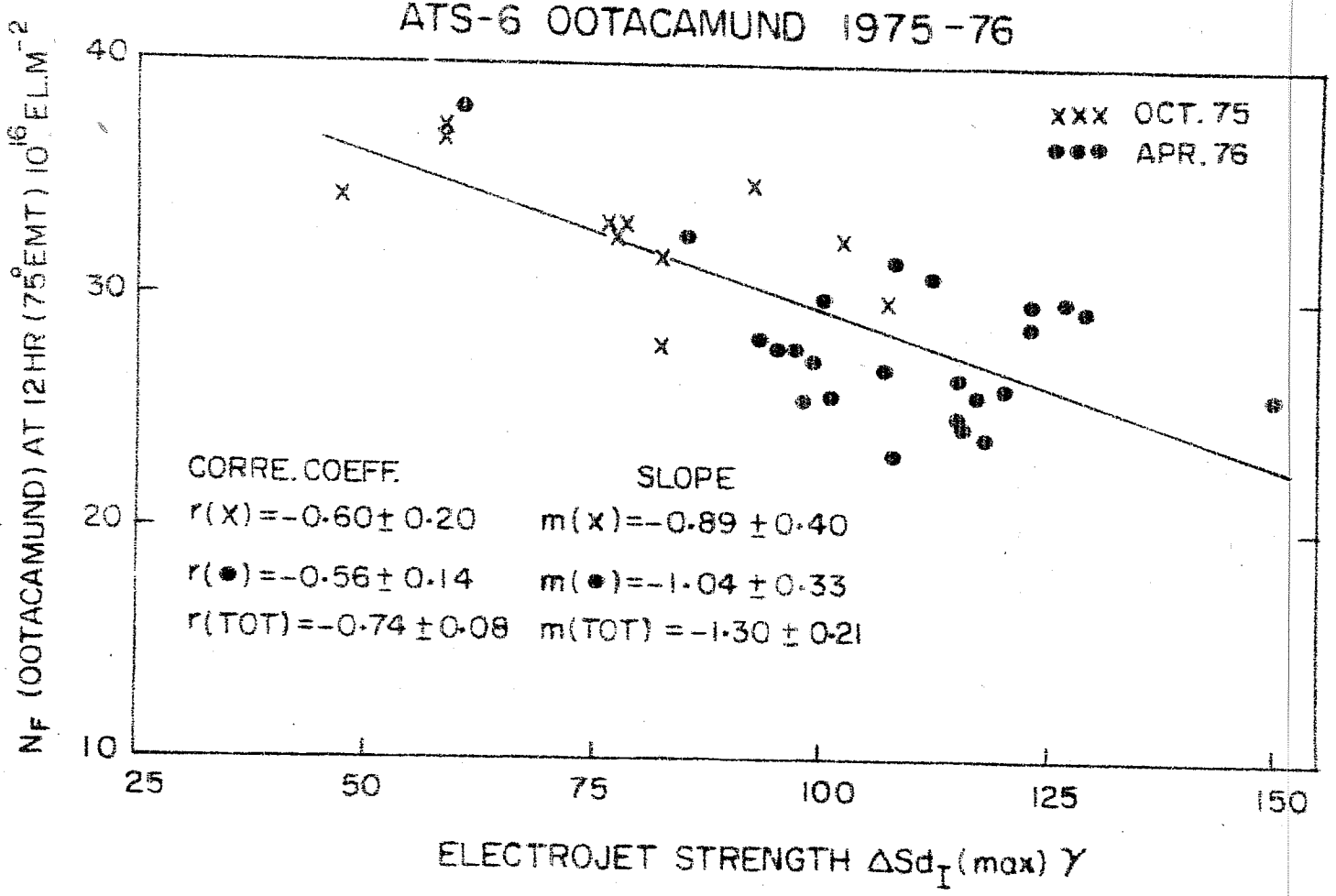

Fig.5.4 Dependence of midday N_F at Ootacamund on the electrojet strength, obtained from data for the months of October 1975 and April 1976.

for April are found. The daytime N_F near the crest of the equatorial anomaly shows positive correlation with the electrojet strength. The correlation coefficients for individual months as well as for the two months combined are given in Table 5.1. It is interesting to note that Bombay behaves as an equatorial station during April with N_F showing a negative correlation with electrojet strength. A more detailed account of it is presented in the next section.

Table 5.1

Station	Correlation coefficients of daytime (1200) TEC with electrojet strength		
	October	April	October - April combined
Ootacamund	-0.60	-0.56	-0.74
Bombay	0.84	-0.33	0.05
Ahmedabad	0.86	0.48	0.82
Udaipur	0.86	0.80	0.84
Patiala	0.68	0.82	0.90

5.4 The Correlative Studies of the Electrojet Strength and the Ionospheric Parameters N_F and N_m

One of the most common features of the ionosphere is its day to day variability. To study the day to day variability of TEC extended over the twenty-four hours, one needs to have continuous data, obtained from geostationary satellites.

In the beginning, the geostationary satellites were available only at preferred longitudes. As such the study of the day to day variability has been confined to these longitudes and at middle latitudes. Many authors (Yuen and Roelofs 1966, Titheridge 1966, and Kane 1975) have observed that variability could be correlated to magnetic activity, solar flux, or effect of neutral winds at these latitudes.

Equatorial and low latitude ionosphere is characterised by equatorial anomaly both in f_oF_2 and TEC, which is a manifestation of the equatorial Fountain, generated by the electric field configuration at low latitudes. The day to day variability in the equatorial electrojet strength will affect the movement of ionization from the equator and which in consequence results in day to day variability in TEC and f_oF_2 observed at these regions.

In this section the results of the correlative studies made between electrojet strength and the ionospheric parameters N_F and N_m (F_2 region peak electron density) at different hours and for different locations, have been described. Such studies are being made for the first time to understand the electrojet control on day to day variability of the low latitude ionosphere. An attempt has also been made to discuss the results critically.

5.4.1 Results

The electrojet strength as given by the index ΔSd_I (Kane 1973) for all the days, during the period October 1975 to July 1976, have been calculated using the horizontal component of the earth's magnetic field (H) recorded at Alibag and Trivandrum. The maximum value of ΔSd_I i.e. $\Delta Sd_I(max)$ has been taken as a measure of electrojet strength on that particular day. On most of the days maximum in ΔSd_I occurs around 11 hr LT (75° EMT). The correlation coefficients between $\Delta Sd_I(max)$ and N_F values for all the stations at different hours (0800-1800 hr LT) have been calculated for different seasons and are shown in Fig.5.5a. The error bars on correlation coefficients are shown for different hours. One notices that N_F at Ootacamund shows a negative correlation with electrojet strength in equinoxes; the correlation coefficient being around -0.6 around midday. In winter a slight negative correlation is noticed whereas for summer months, no correlation is observed. For Bombay one notices a positive correlation between 1000 to 1600 hr LT in winter and summer, whereas in equinoxes a positive correlation is observed, only in the prenoon hours and a negative correlation is observed in the afternoon hours. This is quite interesting in the sense that Bombay whose sub-ionospheric dip lat. is as high as 11.7°N, behaves as an equatorial station in the afternoon hours, under equinoctial conditions. In equinoxes, the maximum negative correlation at Ootacamund and the maximum positive correlation at Bombay is

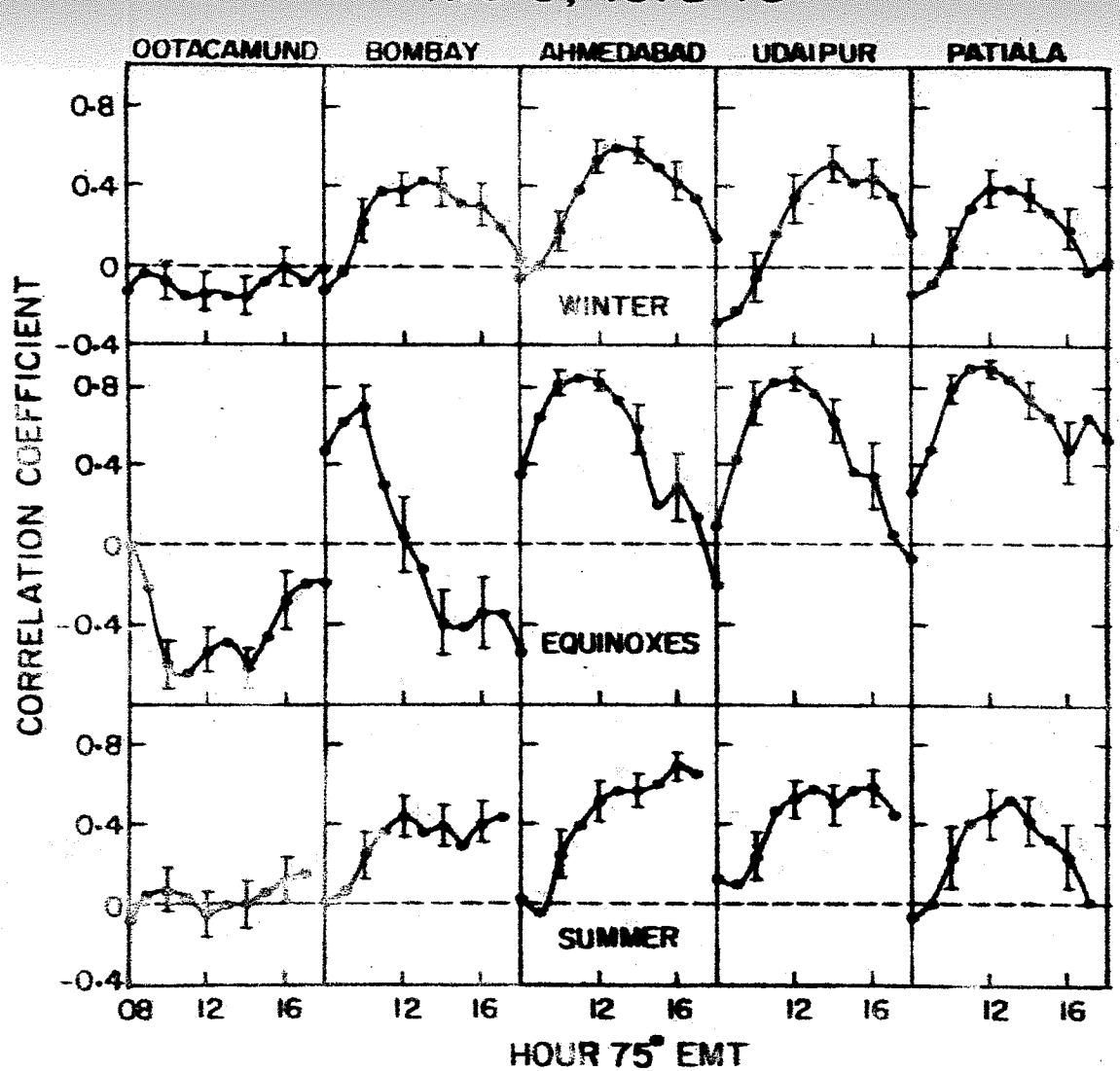

Fig.5.5a The correlation coefficients between electrojet strength and N_F values for all the stations at different hours (0800-1800 hr LT) for different seasons.

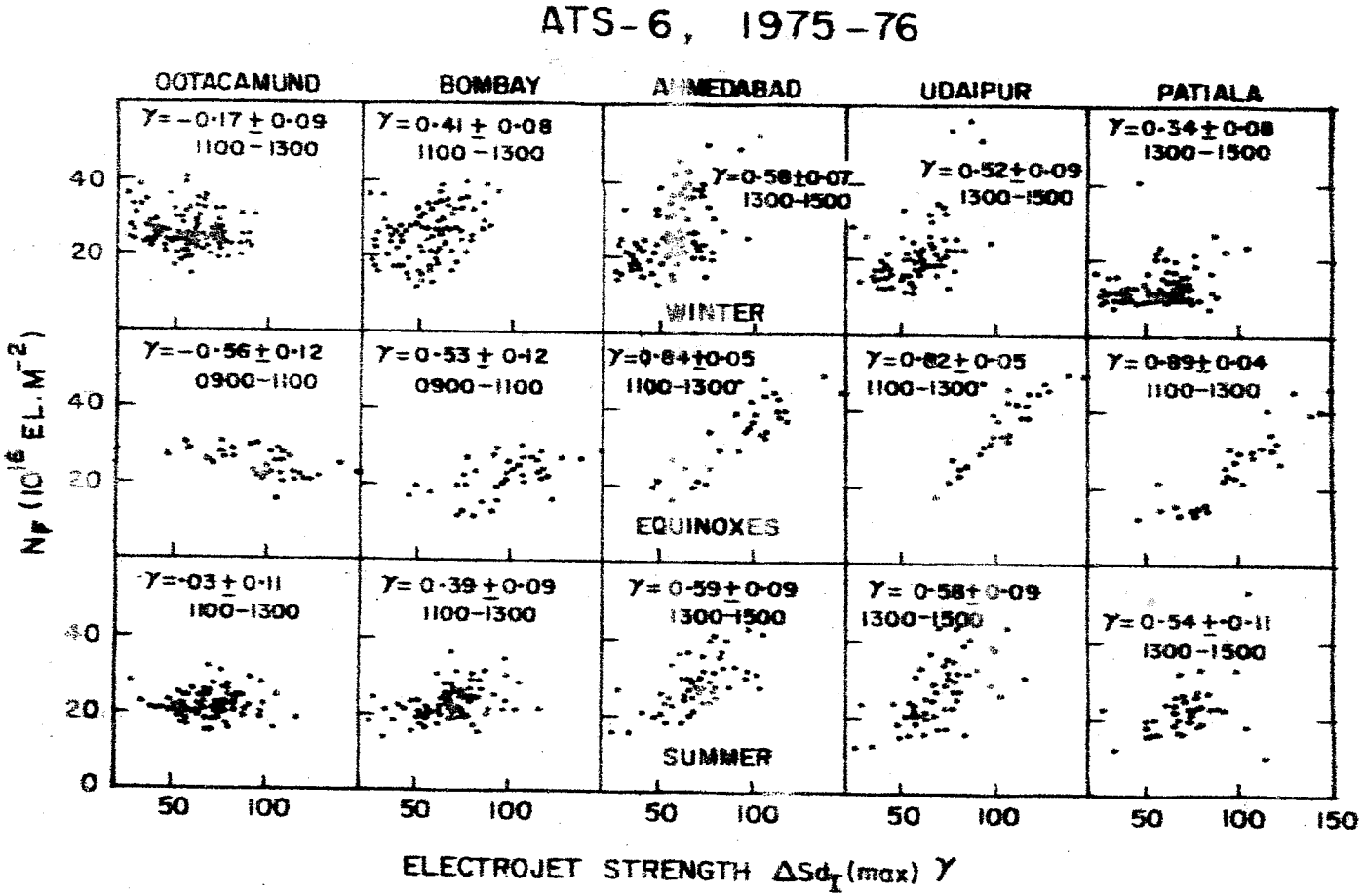

Fig.5.5b Mean N_F, plotted against electrojet strength for different seasons for all the stations.

found to be around 0900-1100 hr LT whereas in winter and summer, the corresponding time can be taken as 1100-1300 hr LT. For Ahmedabad, Udaipur and Patiala, one notices positive correlations ranging between 0.4 to 0.6 for winter and summer months and 0.8 to 0.9 for equinoctial months. For winter and summer months, the maximum correlation is found to occur around 1300-1500 hr LT whereas for equinoxes the maximum correlation is found to occur two hours earlier, i.e. around 1100-1300 hr LT. The interesting point to be noted here is a strong electrojet control on N_F at Patiala whose sub-ionospheric dip lat. is about 25°N. In Fig. 5.5b mean N_F have been plotted against electrojet strength, for different seasons for all the five stations. The correlation coefficients and the hours over which the mean of TEC values is taken, have been shown in each block. These are the hours, for which mean N_F shows the maximum positive correlation (all stations except Ootacamund) and the maximum negative correlation (for Ootacamund). For all the stations, except Ootacamund, the maximum electrojet influence is noted to be earlier by about two hours in equinoxes, than in winter or summer. One notices that the maximum correlation at Ahmedabad, Udaipur and Patiala is delayed by about two hours as compared to the time of the maximum correlation at Bombay. Similar analysis is done for N_m data from Kodaikanal, Ahmedabad and Delhi and the results are shown in Fig.5.6a and 5.6b. Winter data is not available for Delhi. For Kodaikanal, which is an equatorial station, one notices (Fig.5.6a) that N_m shows a negative correlation with electrojet

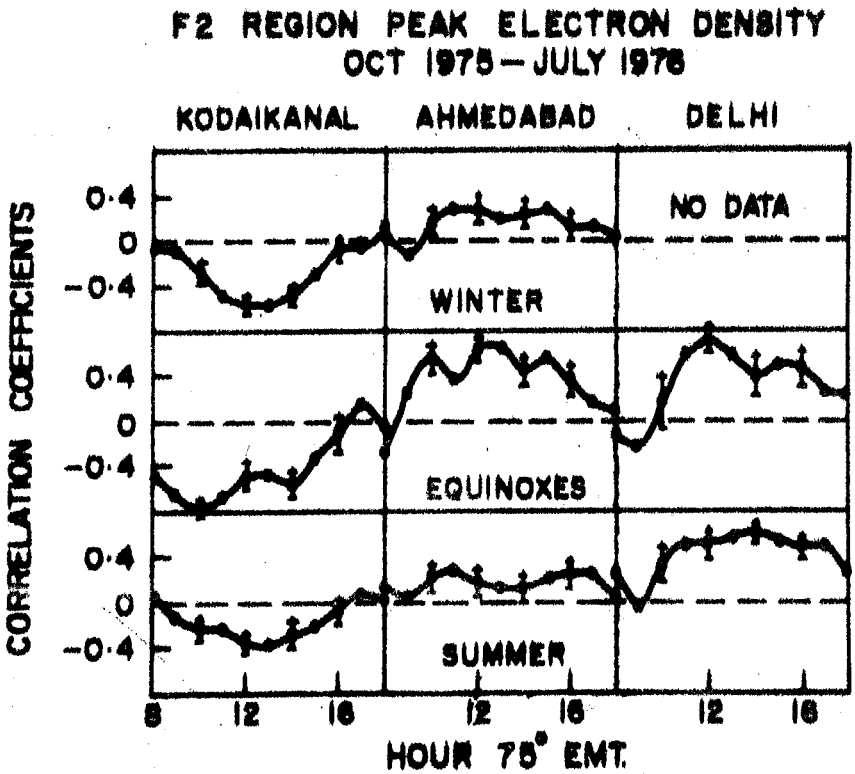

Fig.5.6a The correlation coefficients between electrojet strength and N_m values for all the stations at different hours (0800-1800 hr LT) for different seasons.

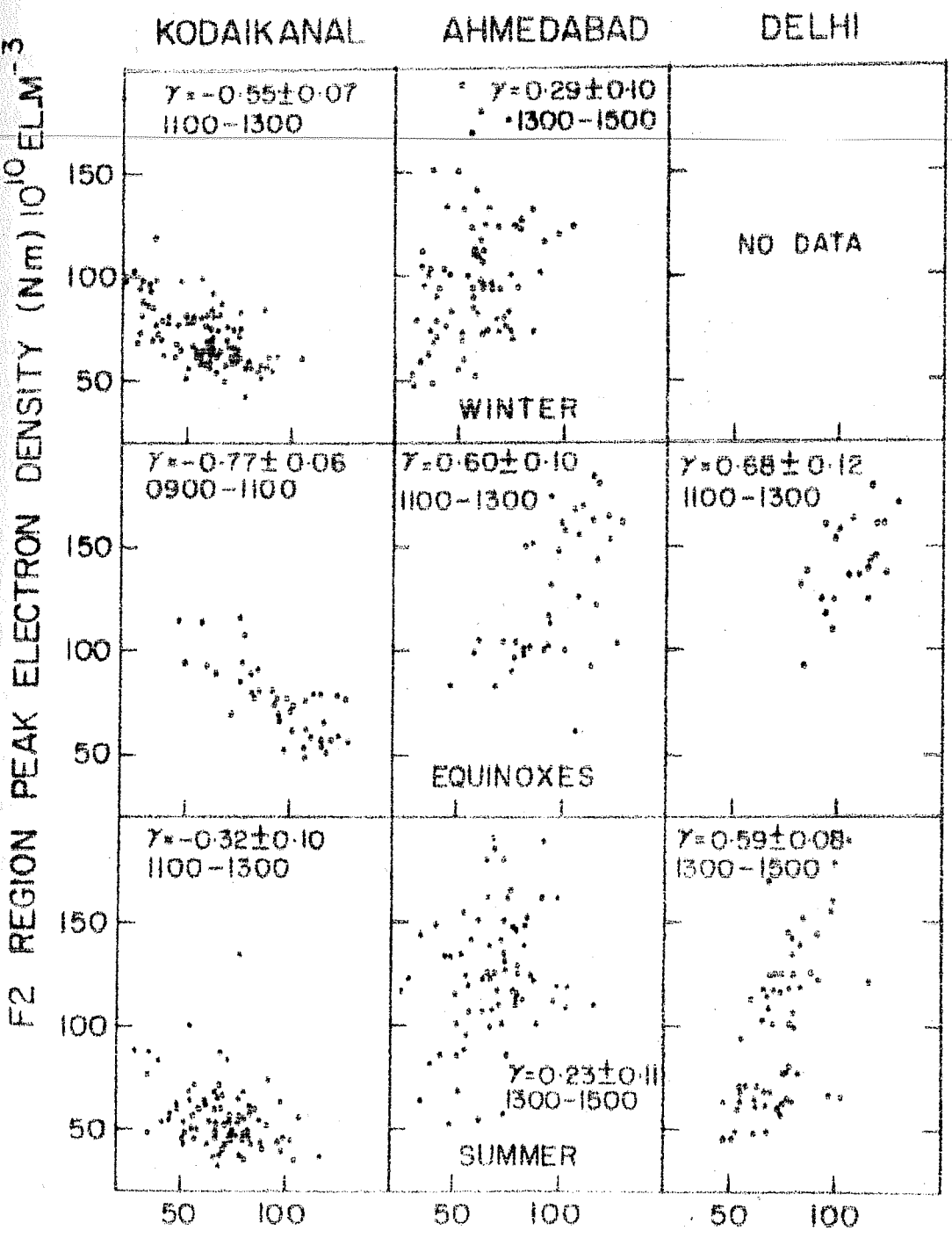

Fig.5.6b Mean N_m, plotted against electrojet strength for different seasons for all the three stations.

strength with correlation coefficients being maximum in equinoxes. The negative correlation is higher in winter than in summer. In equinoxes the maximum negative correlation is around 0900-1100 hr LT whereas for winter and summer, it is around 1100-1300 hr LT. For Ahmedabad and Delhi, one finds positive correlations, with maximum correlation around 1100-1300 hr LT in equinoxes and around 1300-1500 hr LT in winter and summer. One can compare these results with the results obtained for N_F and notice that N_F and N_m in general show a similar trend as regards electrojet effect is concerned. At Kodaikanal N_m shows much pronounced negative correlation in winter and summer whereas TEC at Ootacamund shows a slight negative correlation in winter and no correlation in summer. Also TEC at Ahmedabad shows much more pronounced positive correlation than N_m at the same station. Fig.5.6b for N_m is similar to Fig.5.5b for N_F. The correlation coefficients and the hours over which the mean of N_m values is taken, are shown in each block.

5.4.2 Discussions

Before going into the discussion and the interpretation part of the results, it would be worthwhile to summarise the results. The main highlights of the results are as follows:

(i) Electrojet effects on N_F and N_m are much more pronounced in equinoxes than in winter and summer.

(ii) There is a time delay of maximum correlation between equinox and solstices and is found to be of the order of 2 hrs.

(iii) Ootacamund N_F in winter and summer does not seem to be correlated with electrojet strength whereas at all other stations N_F shows a good positive correlation with electrojet strength. Kodaikanal N_m does show a negative correlation with electrojet strength in all the three seasons.

(iv) Electrojet effect is also found at latitudes beyond the anomaly crest, e.g. N_F at Patiala (24.5°N sub-ion. dip lat.) and N_m at Delhi (22.5°N dip lat.) show strong positive correlation with electrojet strength whereas the crest is formed around 14°N dip lat.

(v) When the electrojet is sufficiently strong, even stations at low latitudes like Bombay, behave as equatorial stations i.e. N_F shows a negative correlation with electrojet strength.

Electrojet effects being most pronounced in equinoxes is consistent with the feature that electrojet is found to be the strongest in equinoxes (Chapman and Rajarao 1965). The ionospheric drift measurements at Thumba (Chandra and Rastogi 1969) and at Ibadan (Morriss 1967) show similar equinoctial maxima in the daytime westward drift velocity. Further the time when the daytime velocity is maximum has been shown to occur earliest in equinoxes (Morriss 1967). Thus the electro-dynamical effects are expected to occur earlier in equinoxes than in other seasons. In the present study the time delay of maximum correlation between equinox and solstices is found to be around two hours.

In winter and summer one observes negative correlation between Kodaikanal N_m and electrojet strength, but does not find any appreciable anti-correlation between Ootacamund N_F and the electrojet strength. This gives rise to two possibilities. Firstly, the electrojet which is weak in summer and winter may be playing an important role only in redistributing the ionization, but the subsequent diffusion of the ionization is inhibited. But it is not easily understandable that if this is so then why N_F and N_m at non-equatorial stations show a positive correlation with electrojet strength. The other possibility which has recently been explored by Rajaram (1977) is the possibility that ionosphere to plasmasphere ionization flow may play an important role in compensating the ionization loss because of the Fountain effect. In equinoxes, the electrojet which is sufficiently strong, overcomes this compensating agency, and consequently one observes a negative correlation between Ootacamund TEC and the electrojet strength. A confirmation of this possibility requires further numerical computations so as to determine the extent to which it can be effective.

Observing the electrojet effect at latitudes beyond the latitude of crest formation is in confirmation with theory. Fig.2 of Hanson and Moffett (1966) clearly shows that magnetic latitudes as high as 25° are also influenced by Fountain effect.

CHAPTER - VI

LUNAR TIDAL OSCILLATIONS IN THE LOW LATITUDE IONOSPHERE

6.1 Introduction

Besides producing oceanic tides, the moon's gravitational force affects many geophysical properties like atmospheric pressure and temperature, winds, geomagnetic field and ionospheric heights and densities. The lunar tidal effects in these parameters are, in general, very small and are marked by large solar variations and other irregular variations. Their determination, therefore, requires large amount of continuous data and special methods of analysis. Before describing the methods of analysis in detail, a discussion of various parameters regarding the motion of the moon around the earth would be useful and hence is presented below.

6.2 Lunar Parameters

In such studies it is considered that the moon revolves round the earth with a uniform angular speed i.e. all the data reduction are made with reference to the mean moon. Mean lunar time (τ) is defined, by analogy with mean solar time (t) in terms of the hour angle of the moon from its lower transit. At the lower transit of the mean moon τ = 0 hr or 0° while at the upper transit of the moon τ = 12 hr or 180°. The moon's sidereal period of rotation around the earth is $27^{d}7^{h}43^{m}$, so that

the time interval between two successive lower transits of the moon i.e. the length of the one lunar day is $24^h\ 50.47^m$ in solar time or 1.03505 solar days or 24 lunar hours.

The mean moon revolves round the earth, relative to the sun-earth line, once in 29.5306 solar days, a period called a lunation, lunar month or synodic month. The moon's phases repeat after a lunation and depend upon the angle ν, between the meridian half planes containing the sun and the moon, which is reckoned positive when the moon is to the east of the sun. The angle ν is called lunar age, and can be expressed as 0 to 24 lunar hour or 0 to 360°, from one new moon to the next in course of a lunation. From one solar day to the next, the lunar age increases by 0.81272 hr.

The solar time t, lunar time τ, and lunar age ν, are related by the equation:

$$t = \tau + \nu \qquad (6.1)$$

where t, τ and ν may be expressed in hours or in degrees. The geophysical lunar almanac by Bartels and Fanselau (1938) gives complete tables for the mean moon (referred to Greenwich mean moon) for the years 1850-1975. They have given the values for $24 - \nu = \mu$, instead of lunar age ν; μ is known as lunar phase and was used in some of the earlier works. Sugiura and Fanselau (1966) have published tables of ν (for Greenwich mean moon) for the years 1850 to 2050.

6.3 Methods of Analysis

For computing lunar tides in a geophysical quantity, three main methods are generally used. They are as follows:-

6.3.1 Fixed age 'ν' method of computing lunar daily variations at fixed phases of the moon (L_ν)

6.3.2 Method for computing whole lunation average lunar daily variation (L)

6.3.3 Fixed solar hour 't' method of computing lunar monthly variations (M) at fixed solar hours.

The fixed age method, was earlier used by Brown (Chapman and Bartels 1940) and in its modern form, is due to Chapman and Miller (1940). Its practical application to a series of geophysical data was described by Tschu (1949) with a latter correction by Chapman (1952). The method in its simplest form, has been described by Malin and Chapman (1970). This method gives lunar daily variations of the parameter with periods related to one lunar day ($24^h\ 51^m$, $12^h\ 25^m$, $6^h\ 12^m$ etc) at fixed lunar age. The advantage of the method is that dependence of lunar tides on lunar age i.e. Chapman's phase law can be studied.

The second method determines lunar daily variations averaged over the whole lunation. This method is described by Chapman and Bartels (1940) and is the most widely used one. Because of purely lunar nature of the variations, obtained by using this

method, it is very suitable for studying the correlation between lunar ionospheric and geomagnetic variations while any study of luni-solar effects (i.e. dependence of lunar tides on solar time) is not possible with this method. The third method is due to Van'der stok (Chapman and Bartels 1940). For a fixed solar hour, lunar monthly variations with respect to lunar age ν, with periods related to a lunar month (29.53 days, 14.76 days etc.) are computed. The main advantage of the method is that it enables detailed study of luni-solar effects of the tide.

In the present study lunar tidal oscillations in different parameters are computed by using all the three methods. The procedure of computing lunar tides according to different methods, is described below.

6.3.1 Lunar Daily Variations at Fixed Lunar Age ν (L_ν)

Firstly the data on magnetically disturbed days ($A_p > 40$) are excluded to remove the irregular disturbance effects. The monthly mean value of the element at each hour is calculated and these are taken to represent average solar daily variation, S, during the month. In order to remove the S variation, the monthly mean value of the element for each hour is subtracted from all the values at that hour during the month. This is done for all the months for which data is utilised. This leaves a series of hourly deviations for each day which are free from solar variations but contain lunar variations. At this stage

the data are divided into three seasons, viz. winter (November, December, January and February), summer (May, June, July, and August) and equinoxes (September, October, March and April).

Now, for each day of a particular season, a series of hourly deviations are available, let us denote the deviations for day j by $a_i(j)$, where i is an integer ranging from 0 to 23 (i.e. i denotes solar hour). The days with same ν value are collected together and average hourly sequence for these days are obtained for each ν (ν ranges from 0 to 23 lunar hr). Mathematically, if total number of days with same ν value for the hour i be denoted by $N_i(\nu)$, then the following 24 sequences are obtained, one for each value of ν:

$$b_i(\nu) = \frac{1}{N_i(\nu)} \sum_{j=1}^{N_i(\nu)} a_i(j) \qquad (6.2)$$

For further analysis, the sequences $b_i(\nu)$ for three consecutive values, centred at 00, 03, 06, 09, 12, 15, 18 and 21 l hour, are grouped and average hourly deviations are calculated. This gives eight sequences $C_i(\nu)$ of hourly values centred at the above mentioned ν values. The above sequences represent lunar daily variation at fixed lunar ages (ν = 00, 03, 06, 09, 12, 15, 18 and 21 lunar hr) in terms of solar hour. It is necessary to represent these variations in terms of lunar time rather than solar time. To do this, first the value corresponding to lunar time τ = 00 is fixed using the relation $t = \tau + \nu$ (equation 6.1). For example, for C (ν = 00) sequences, the value at t = 00 hr corresponds to

value at τ = 00 hr and for C (ν = 03) sequences, the value at t = 03 hr gives the value corresponding to τ = 00 hr. This value at τ = 00 hr is taken as the starting value of the sequences in terms of lunar time. The values at other lunar hours are obtained from the corresponding values in terms of solar hour by using the following arithmetical formula given by Egedal (1956):

$$L(\tau + 1) = S(t) + \tau * 0.035 \, (S(t+1) - S(t)) \qquad (6.3)$$

where τ is lunar hour (00 to 23)

and t is the corresponding solar hour using equation (6.1) i.e. $t = \tau + \nu$.

The resulting sequences in terms of lunar time τ, representing daily variations at fixed lunar ages, are harmonically analysed for four harmonics. The amplitude and phase angle of first four harmonics of lunar daily variation at a fixed age ν (L_ν) is represented by the following equation known as the Chapman's phase law (Chapman 1919):

$$L_\nu = \sum_{n=1}^{4} C_n \sin (n\tau + (n-2)\nu + \alpha_n) \qquad (6.4)$$

or $$L_\nu = \sum_{n=1}^{4} C_n \sin (n\tau + \phi_n) \qquad (6.5)$$

Such that the phase angle

$$\phi_n = (n-2)\nu + \alpha_n \qquad (6.6)$$

where α_n is independent of lunar age and is called phase constant. According to this expression the second harmonic i.e. L_2 has the phase independent of the lunar age ν. The phase of the

first harmonic ϕ_1, decreases by 2 π during a complete lunation while those of third and fourth harmonic i.e. ϕ_3 and ϕ_4 increase by 2 π and 4 π respectively.

The most important component of the lunar daily variation has a period half of a lunar day and is expressible as:

$$L_{\nu 2} = C_2 \sin (2\tau + \phi_2) \qquad (6.7)$$

Besides $L_{\nu 2}$, which is purely lunar daily variation, L_ν has a part $(L_\nu - L_{\nu 2})$, which is dependent on both lunar and solar time and is called luni-solar component. When the original data is in GMT, a proper longitude correction is applied to the phase angle ϕ_n since the lunar tide depends on local lunar time at the station.

6.3.2 Whole Lunation Average Lunar Daily Variation (L)

To derive L variation, the above eight sequences of L_ν variations are averaged. The resulting sequence represents a lunar daily variation averaged over a lunation and is analysed harmonically for four harmonics according to the equation:

$$L = \sum_{n=1}^{4} C_n \sin (n\tau + \phi_n) \qquad (6.8)$$

where C_n and ϕ_n denote the amplitude and the phase angle respectively of the nth component.

6.3.3 Lunar Monthly (M) Variations at Fixed Solar Hours

The procedure for M variation is the same as in the first method till the seasonal grouping is done. In each season a series

of hourly deviations $a_i(j)$ for the jth day is obtained. Now the analysis is done for a fixed solar hour (i.e. i = constant). For a particular solar hour, the deviations of all the days are grouped according to lunar age 00, 01,.....21, 22 and 23 hr, and average value of all the deviations for a particular lunar age is obtained. Thus a sequence of deviations in terms of lunar age is obtained for a particular solar hour. This process is repeated for each solar hour resulting in 24 sequences, one for each solar hour. These sequences represent the lunar monthly (M) variations at different solar hours. Each sequence is then harmonically analysed for two harmonics according to the equation:

$$M = \sum_{n=1}^{2} r_n \sin (n\nu + \rho_n) \qquad (6.9)$$

where r_n and ρ_n are the amplitude and phase angle respectively, of the nth component. Since the value of 'ν' assigned to a day is referred to Greenwich nooon, the following corrections in the phases ρ_n are necessary:

(i) Local time correction

(ii) Longitude corrections.

The lunar age ν_t at local solar time t at any station is related to the lunar age ν_o at Greenwich noon through the following relation:

$$\nu_t = \nu_o + 0.0339 ((t-12) + \lambda) \qquad (6.10)$$

where λ= longitude of the station expressed in hours and is measured positive east of Greenwich.

The so corrected phase angle (ρ_n) can also be expressed in terms of lunar time using equation (6.1).

6.4 Probable Errors and Their Significance

Probable errors in the amplitudes and the phases of the lunar variations are calculated following Rastogi (1962). The estimation of probable errors, in the present study, is done at an earlier stage of analysis rather than calculating them from the harmonic components of the L variation. Here, the probable error calculations are made along with the calculations of average hourly sequence $b_i(\nu)$ for each ν value, from the sequence $a_i(j)$. For a fixed angle ν, the value $b_i(\nu)$ corresponding to the ith hour is the mean of $N_i(\nu)$ values of deviations $a_i(j)$. The variance of this mean, denoted by $\sigma_i^2(\nu)$ is calculated as:

$$\sigma_i^2(\nu) = \frac{1}{N_i(\nu)} \sum_{j=1}^{N_i(\nu)} a_i^2(j) - b_i^2(\nu) \qquad (6.11)$$

The weighted mean variance, $\sigma^2(\nu)$, for all hours i = 00 to 23, is then calculated for a fixed age ν as:

$$\sigma^2(\nu) = \sum_{i=0}^{23} N_i(\nu) \; \sigma_i^2(\nu) \; / \; \sum_{i=0}^{23} N_i(\nu) \qquad (6.12)$$

The probable error, P.E., in the amplitude (ΔA_p) of lunar daily variation at a fixed ν value is then calculated as (Rastogi 1962):

$$\Delta A_p = C^* \sigma(\nu) \qquad (6.13)$$

where C = 0.195 for 1st harmonic
= 0.275 for 2nd harmonic
= 0.338 for 3rd harmonic
= 0.390 for 4th harmonic.

The corresponding probable error in phase ($\Delta\phi_p$) is obtained as follows:

$$\Delta\phi_p = \frac{\Delta A_p}{A} \qquad (6.14)$$

The probable error for the amplitude and the phase of whole lunation average lunar daily variation is obtained by first taking the weighted mean of $\sigma^{-2}(\nu)$ for ν = 00 to 23 hr and then using equations (6.13) and (6.14).

By a similar procedure for a fixed solar hour t, probable errors in the amplitude and the phase of lunar monthly variations were also obtained. The magnitude of the probable error determines the significance of the harmonic coefficients of lunar variations of a geophysical quantity.

6.5 A Brief Summary of the Previous Work on Lunar Tidal Effects in the F-region of the Equatorial Ionosphere

Lunar tidal oscillations in the equatorial ionosphere were first computed by Martyn (1947) utilising the data of height and critical frequency of F_1 and F_2 layers at Huancayo. Burkard (1951) found that the lunar tide calculated from daytime f_oF_2 at Huancayo was about four times larger than the amplitude calculated from all day values and that the night-time f_oF_2 at Huancayo did not show any significant lunar tidal variation. Later, Brown (1956) computed lunar tides in critical frequency (f_oF_2),

height of maximum ionization (h_{max}), semithickness (y_m) and minimum virtual height ($h'F_2$) of the F_2 layer at another equatorial station, Ibadan. Rastogi (1961, 62) showed that the amplitude of the lunar tide in f_oF_2 at low latitudes is enhanced within few degrees from the magnetic equator and suggested close association between the equatorial ionospheric tides and electrojet currents.

Bartels and Johnston (1940) had computed lunar tides in the solar daily range of H at Huancayo for individual months and had shown that the amplitude of lunar semi-monthly oscillation shows remarkable seasonal variation with the maximum value of about 24 gamma during January and the minimum value of about 5 gamma during June. The lunar age for the maximum positive deviation varied from 4.5 lunar hour in December to 0.5 lunar hour in June. Rastogi (1963a) computed lunar tides in midday f_oF_2 at Huancayo during individual months and showed that the amplitude of lunar semi-monthly oscillation is maximum in January and minimum in June; the lunar age of maximum positive deviation varied from 9.5 l. hr. in Dec. to 6.5 l. hr in June. It was thus shown that the lunar tides in the range of H and f_oF_2 show a remarkable similarity following similar seasonal variations of the amplitude, maintaining almost anti-phase relationship. Similar close relationship between lunar tides in the range of H and midday f_oF_2 at low latitude stations were shown in their longitudinal, latitudinal and solar cycle variations (Rastogi 1964, 65a).

Rangaswamy (1963) showed that the phase of lunar tides in noon f_oF_2 at low latitude has very large seasonal variation, which was suggested as the cause of the decrease of the amplitude of annual average lunar tides.

Rao and Rao (1966) computed lunar tides in f_oF_2 (10-14 hr) at Waltair (dip 20°N) and found the phase to be of equatorial type in D- and J-months and of tropical type in equinoxes. They attributed the smallness of the lunar-tide at low latitude stations due to large seasonal variations in the phase at these stations. However, Sharma and Rastogi (1969), analysing f_oF_2 data from stations Hyderabad (dip 19°N), Bunia (dip 20°S) and Dakar (dip 20°N) and examining the earlier results covering dip latitudes 16° to 25° found inconsistency in the phase of the lunar variations on seasonal basis. They attributed this to the large probable errors in determination of the phase of lunar tides and cautioned against drawing any conclusion about the seasonal shift, in the absence of good statistics. Ahmed and Rao (1967) computed lunar tides at Singapore (dip 16°S) and at Baguio (dip 19°N) to study the seasonal shift in the region of phase reversal and did not find any appreciable phase change with season at these stations. Rastogi and Alurkar (1966) computed lunar monthly tides in f_oF_2 for each hour of the day at Huancayo for the low sunspot year. Detailed lunar daily as well as lunar monthly tides had been computed in f_oF_2 and H at Huancayo for the low as well as high sunspot periods (Rastogi 1968a,b). It was found that the lunar-daily variations in f_oF_2 and H are almost opposite

in phase to each other. Rastogi (1969) computed lunar tides in f_oF_2 and h'F at Huancayo to explain the variations of peak ionization density in the F_2 region. Sharma and Rastogi (1970) computed the lunar daily and lunar monthly tides in H as well as in various parameters (like N_{max}, h_{max}, y_m etc.) defining the structure of the F_2 layer at Huancayo. It was noted that the lunar tidal variations in h_{max} follow the variations in H but the lunar tides in N_{max} are opposite in phase to that of h_{max} with a delay of about 1-2 hours. The lunar tides in semi-thickness (y_m) were found to be similar in phase to that in h_{max}.

Some theoretical work has also been done in explaining the lunar tidal effects. Dunford and Lawden (1969) solved the equilibrium electron continuity equation with a vertical drift at the equator and showed that the many of the observed features can be explained satisfactorily. Anderson et al. (1973b) showed that the numerical solutions of the time dependent electron continuity equation with a lunar electric field included give amplitudes and phases of the lunar oscillations in f_oF_2, consistent with observational results.

The most of the studies regarding lunar tidal variations have been made using ionospheric parameters deduced from the bottomside soundings. With the advent of geostationary satellites it has been possible to extend such studies to the topside of the ionosphere. Rao and Stubenrauch (1967) reported for the first time

the tidal variations in the electron content and the slab-thickness of the ionosphere using about three months data. Bernhardt et al. (1976) estimated the lunar perturbations in electron content obtained at Stanford, and interpreted the results in terms of dynamo electrostatic fields. Huang (1978, 79) computed the lunar daily variations in TEC at Lunping which is near the crest of the equatorial anomaly.

With the availability of ATS-6 electron content data from a chain of stations, it has been possible to compute the lunar tidal variations in TEC and the related parameters in the complete equatorial anomaly region. The present chapter describes the lunar-daily (L) and lunar-monthly (M) variations in N_F, N_T, N_m and τ for the equatorial stations Ootacamund/Kodaikanal and in N_F for all other low latitude stations.

6.6 Results of the Present Investigations

6.6.1 Lunar Monthly Variations (M)

(a) The Annual Average Lunar Monthly Variations in TEC (N_F and N_T), N_m and τ, near Magnetic Equator:-

TEC data obtained from the Faraday rotation (N_F) and the group delay measurements made at Ootacamund during October 1975 - July 1976, have been used to compute the lunar monthly oscillations in TEC, at fixed solar hours. The results are shown in Fig.6.1a. The original data points along with the built-up curves

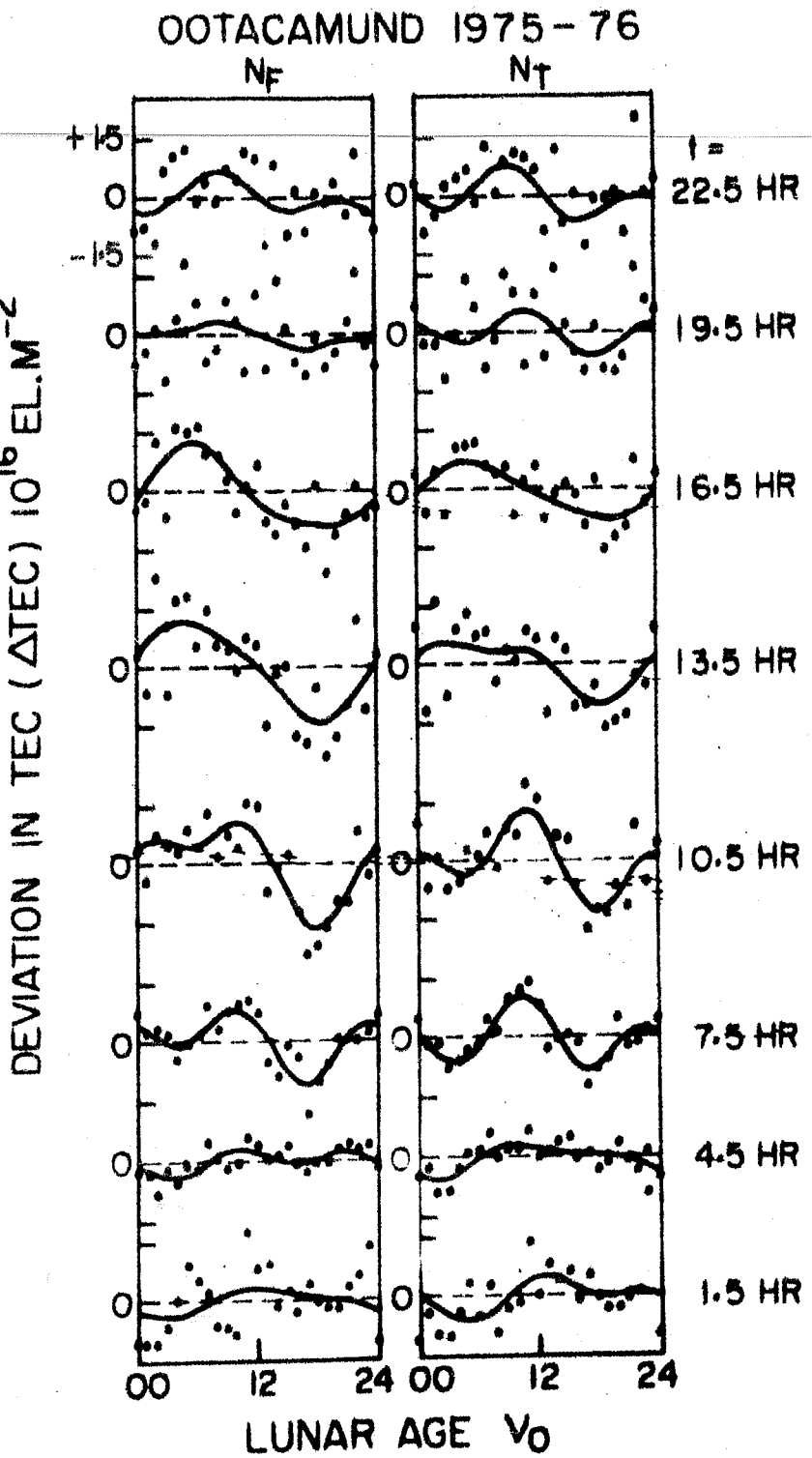

Fig.6.1a The annual average lunar monthly oscillations in TEC (N_F and N_T) for different daytime solar hours at Ootacamund. The original data points along with the built-up curves have been plotted.

obtained from the first two harmonics M_1 and M_2, have been plotted. The variations in N_F and N_T are found to be strikingly similar. It is noted that the amplitudes of the oscillations are comparatively small ($\lesssim$ 0.5 TEC unit) during night-time hours (2000-0500 hr LT) and are large ($\sim$ 1 TEC unit) during daytime hours. Similar analysis was done for N_m obtained from f_oF_2 data for Kodaikanal, which nearly lies under sub-ionospheric point for Ootacamund to ATS-6 ray-path. The analysis was done only for the data of the daytime hours since the data for the night-time hours were not sufficient enough for such analysis. The results are shown in Fig.6.1b. Using TEC and N_m data, the slab-thickness (τ = TEC/N_m) of the ionosphere can be determined. Fig.6.1c shows the lunar monthly oscillations in τ_F (= N_F/N_m) and τ_T (=N_T/N_m) for different daytime solar hours.

The following important features are noted in these figures (Fig.6.1a,b,c):-

(i) The significant lunar tidal effects are observed in N_F and N_T at about 7.5, 10.5, 19.5 and 22.5 hrs LT. The effects are a little more prominent in N_T (Fig.6.1a).

(ii) A slight indication of the presence of lunar semimonthly oscillations in N_m is noticed at 10.5 hr LT (Fig.6.1b).

(iii) The lunar semi-monthly oscillations are observed much more prominently in τ_F and τ_T for almost all the daytime solar hours (Fig.6.1c).

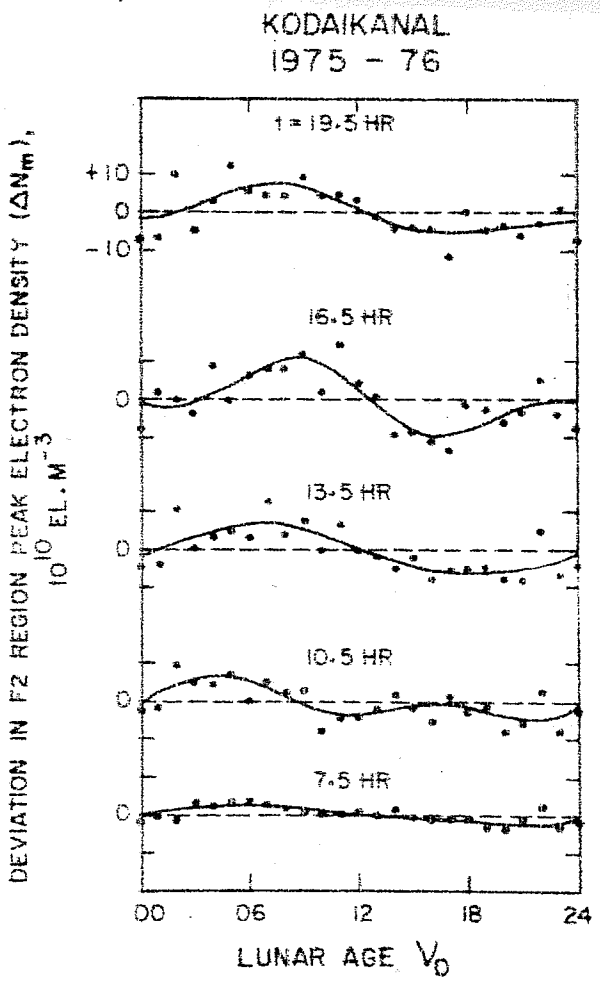

Fig.6.1b The annual average lunar monthly oscillations in N_m at Kodaikanal.

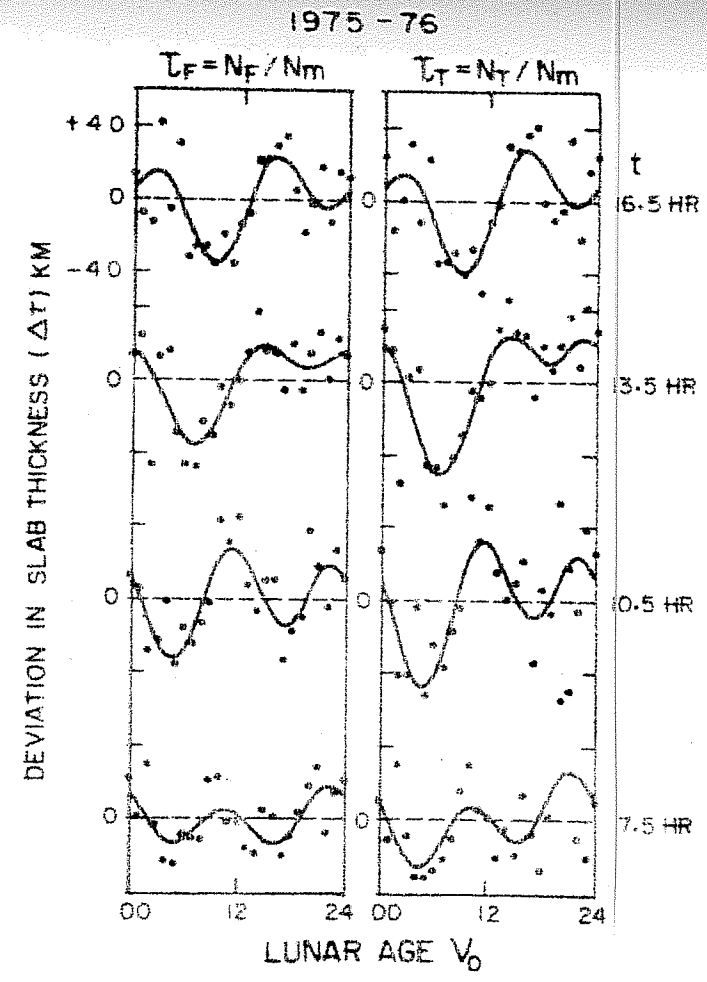

Fig.6.1c The annual average lunar monthly oscillations in slab-thickness.

The amplitude (r_2) of the semi-monthly (M_2) tide and the phase (τ_2) of maximum positive deviation in lunar time at different solar hours for all the parameters are presented in Table 6.1. The mean probable errors (PEs) have also been given in the table; however it is to be noted that PE is different at different hours and the values which are less than the PE at that hour, have been bracketed. The amplitude of the M_2 tide (r_2) maximises at 10.5 hr LT for all the parameters and the lunar time of maximum positive deviation for M_2 tide is 10.6 and 10.8 l.hr for N_F and N_T respectively whereas for τ_F and τ_T, it is delayed by 0.6 hr i.e. 11.2 and 11.4 l. hrs respectively. The corresponding time for N_m is 5.9 l hr, hence there is a phase shift of 5.3 (or 159°) and 5.7 (or 165°) l. hr respectively from the corresponding phases for τ_F and τ_T. For all other solar hours also, this phase difference is found to be around 6.0 l. hr hence it is noted that the M_2 lunar tides in N_m are very nearly in phase opposition to that of τ_F and τ_T.

(b) The Average Lunar Monthly Variations in N_F for Different Stations:-

TEC data obtained at different stations have been used to determine the annual average lunar monthly oscillations at different latitudes ranging from the magnetic equator to the latitude as high as 24.5°N dip latitude. The results are shown in Fig.6.2a. Only built-up curves have been plotted. The important points to be noted are enumerated below:-

Table 6.1

The amplitude (r_2) and lunar tide (τ_2) of max. positive deviation of lunar semi-monthly oscillations in N_F, N_T, N_m, τ_F and τ_T at Ootacamund-Kodaikanal averaged over the period October 1975 - July 1976

	$N_F(10^{16}$ el.$m^{-2})$		$N_T(10^{16}$ el.$m^{-2})$		$N_m(10^{10}$ el.$m^{-3})$		τ_F(km)		τ_T(km)	
	r_2	τ_2l.hr	r_2	τ_2l.hr	r_2	τ_2l.hr	r_2	τ_2l.hr	r_2	τ_2l.hr
	(0.11)	3.9	(0.27)	2.1						
	0.22	6.8	0.19	7.8						
	0.58	8.8	0.64	8.8	(0.74)	3.0	12.3	8.8	17.4	9.4
	0.58	10.6	0.71	10.8	3.03	5.9	22.8	11.2	27.2	11.4
	(0.18)	11.8	(0.30)	0.3	(0.74)	5.2	13.8	11.9	19.0	0.4
	(0.22)	10.6	(0.15)	0.2	4.45	6.6	18.7	0.7	20.7	0.8
	(0.09)	9.3	(0.37)	7.6	(1.65)	10.7				
	(0.28)	1.7	(0.39)	0.0						
.E.	0.42		0.38		2.1		12.3		12.6	

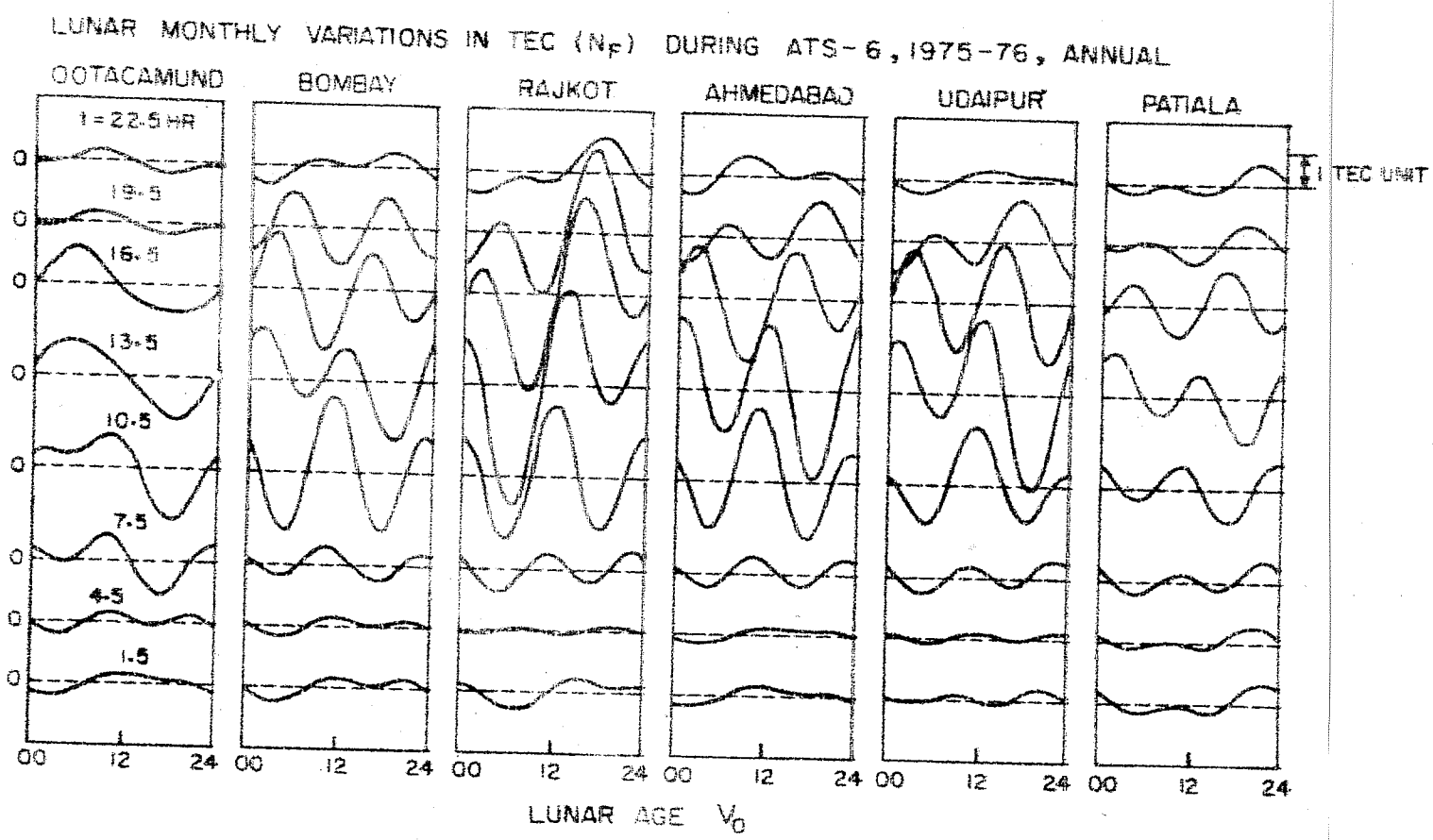

Fig.6.2a The annual average lunar monthly oscillations in TEC (N_F) at different stations.

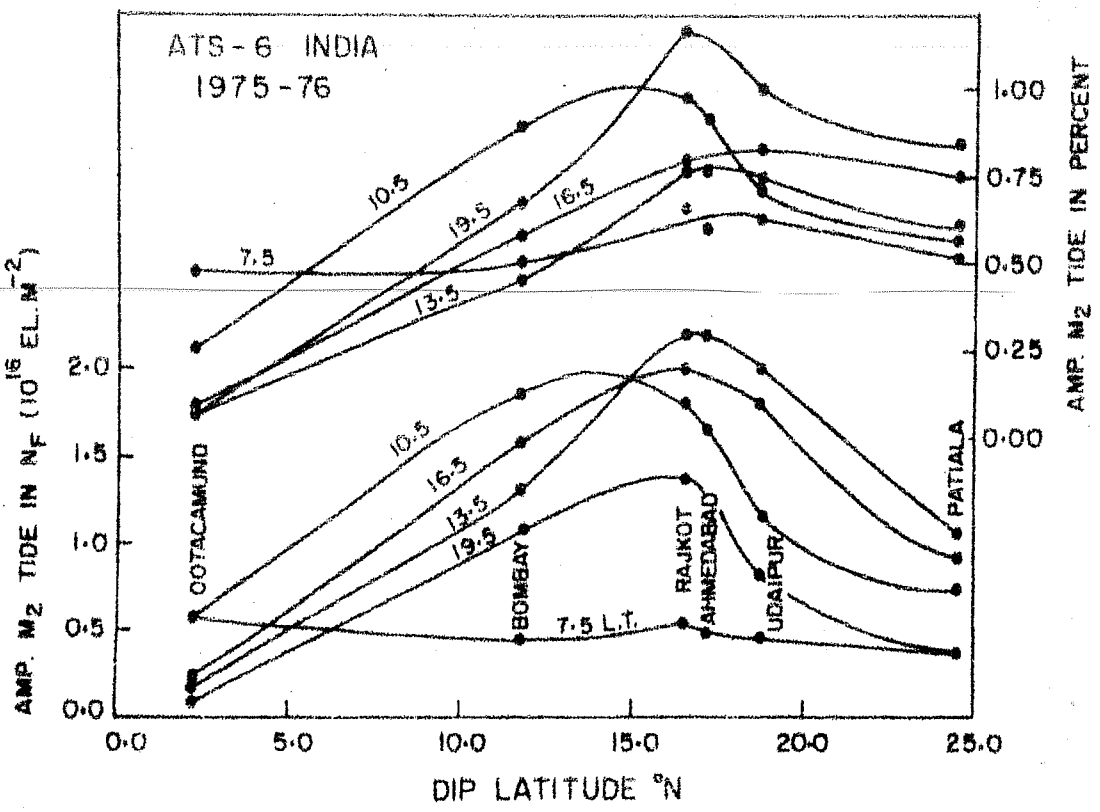

Fig.6.2b The amplitude of the annual average lunar semi-monthly oscillation in TEC, as a function of dip latitude for different daytime solar hours.

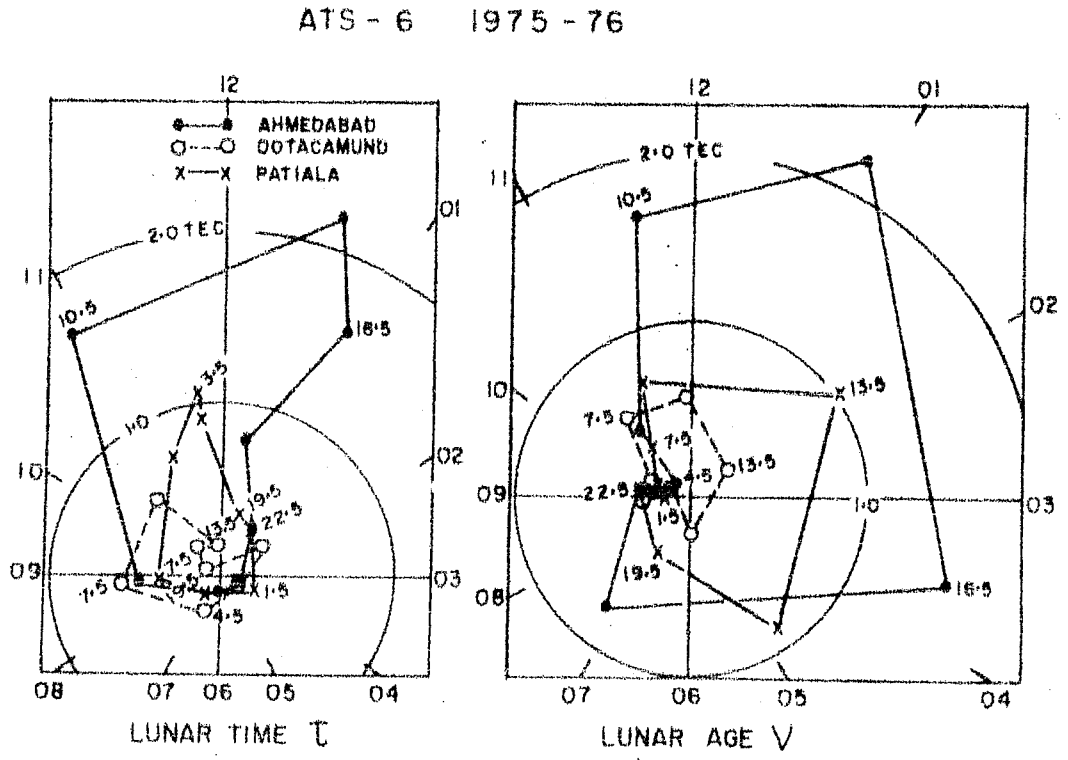

(i) The amplitudes of the lunar oscillations are in general found to be larger in daytime than in night-time.

(ii) A visual comparison between data for the equatorial station Ootacamund and other stations shows that the lunar oscillations at non-equatorial stations viz. Bombay, Rajkot, Ahmedabad, Udaipur and Patiala are predominantly semi-monthly in nature whereas it is not that prominent for Ootacamund.

The amplitude (r_2) of the M_2 tide and the phase (τ_2) of maximum positive deviation in lunar time at different solar hours for all the stations are presented in Table 6.2a. The amplitude is found to be maximising around 10.5 hr LT for Ootacamund and Bombay and about 13.5 hr LT for all the other stations. The phase of max. positive deviation is found to be around 10.5 l.hr for 10.5 hr LT grouping and about 12 l. hr for 13.5 hr LT grouping. The maximum amplitude is noticed near the crest (Rajkot, Ahmedabad and Udaipur) with amplitude decreasing on either side of the crest. This is depicted in Fig.6.2b for different daytime solar hours. The lower set of the curves show the latitudinal variations in the absolute amplitude of M_2 tides whereas the upper set of curves have been obtained by determining the percentage change due to the tide. Both the absolute deviation and the percentage change in TEC show a maximum near the crest region, except for the curves corresponding to 7.5 hr grouping which do not show much of the latitudinal variations. The latitude corresponding to the max. amplitude or the max.

Table 6.2a

The amplitude (r_2) and lunar time (τ_2) of max. positive deviation of lunar semi-monthly oscillations in N_F (10^{10} el.m^{-2}) for different stations (Annual)

	Ootacamund		Bombay		Rajkot		Ahmedabad		Udaipur		Patiala	
	r_2	τ_2l.hr	r_2	τ_2l.hr	r_2	τ_2l.hr	r_2	τ_2l.hr	r_2	τ_2l.hr	r_2	τ_2l.hr
)	(0.11)	3.9	(0.18)	3.1	(0.21)	11.8	(0.11)	4.2	(0.17)	4.6	0.20	3.9
5	0.22	6.8	(0.17)	6.5	(0.09)	9.0	(0.09)	6.2	(0.11)	5.0	(0.15)	7.5
5	0.58	8.8	0.44	8.5	0.56	8.5	0.48	8.8	0.45	8.6	0.37	8.8
5	0.58	10.6	1.85	10.9	1.81	10.2	1.65	10.9	1.16	10.5	0.74	11.3
5	(0.18)	11.8	1.30	11.9	2.20	0.1	2.19	0.6	2.00	0.2	1.06	11.7
5	(0.22)	10.6	1.56	0.2	1.99	0.6	1.58	0.9	1.81	0.9	0.92	11.7
5	(0.09)	9.3	1.08	1.1	1.37	1.8	0.80	0.3	0.83	1.5	0.36	0.4
5	(0.28)	1.7	(0.29)	1.9	0.42	3.3	(0.30)	1.3	(0.15)	10.9	0.30	1.3
m	P.E. 0.42		0.54		0.58		0.62		0.59		0.37	

percentage change is about 16° N dip latitude for the solar hour groupings 13.5, 16.5 and 19.5 whereas it is about 14°N dip lat for 10.5 hr grouping. TEC changes at Ootacamund are of the order of 0.5 TEC unit in terms of absolute deviations and are less than 0.5% in terms of percentage. At all other stations the absolute deviations are of the order of 1-2 TEC units whereas in terms of percentage, they are about 0.5 to 1.0%. The lunar semi-monthly coefficients for TEC at Ootacamund, Ahmedabad and Patiala are plotted in Fig.6.2c on the harmonic dials of both lunar time and of lunar age ν (Table 6.2a). It is noted that on the lunar age dial the points for different hours of the day move around the origin giving rise to small value of the vector average from all hours whereas on the lunar time dial, the points for various hours of the day lie within a comparatively narrow sector. Thus it may be suggested that the lunar semi-monthly oscillation in TEC is rather controlled by lunar time than by lunar age.

The average lunar monthly oscillations for winter and summer are shown separately in Fig.6.3a and 6.3b respectively. The data are not sufficient enough for similar analysis for equinoxes. Similarly the data for Rajkot for both summer and winter and also the data for Patiala for summer are not sufficient enough to be included in the diagram. The features, in general are similar to **what** are noticed from the annual average picture. The semi-monthly nature at Ootacamund is clear

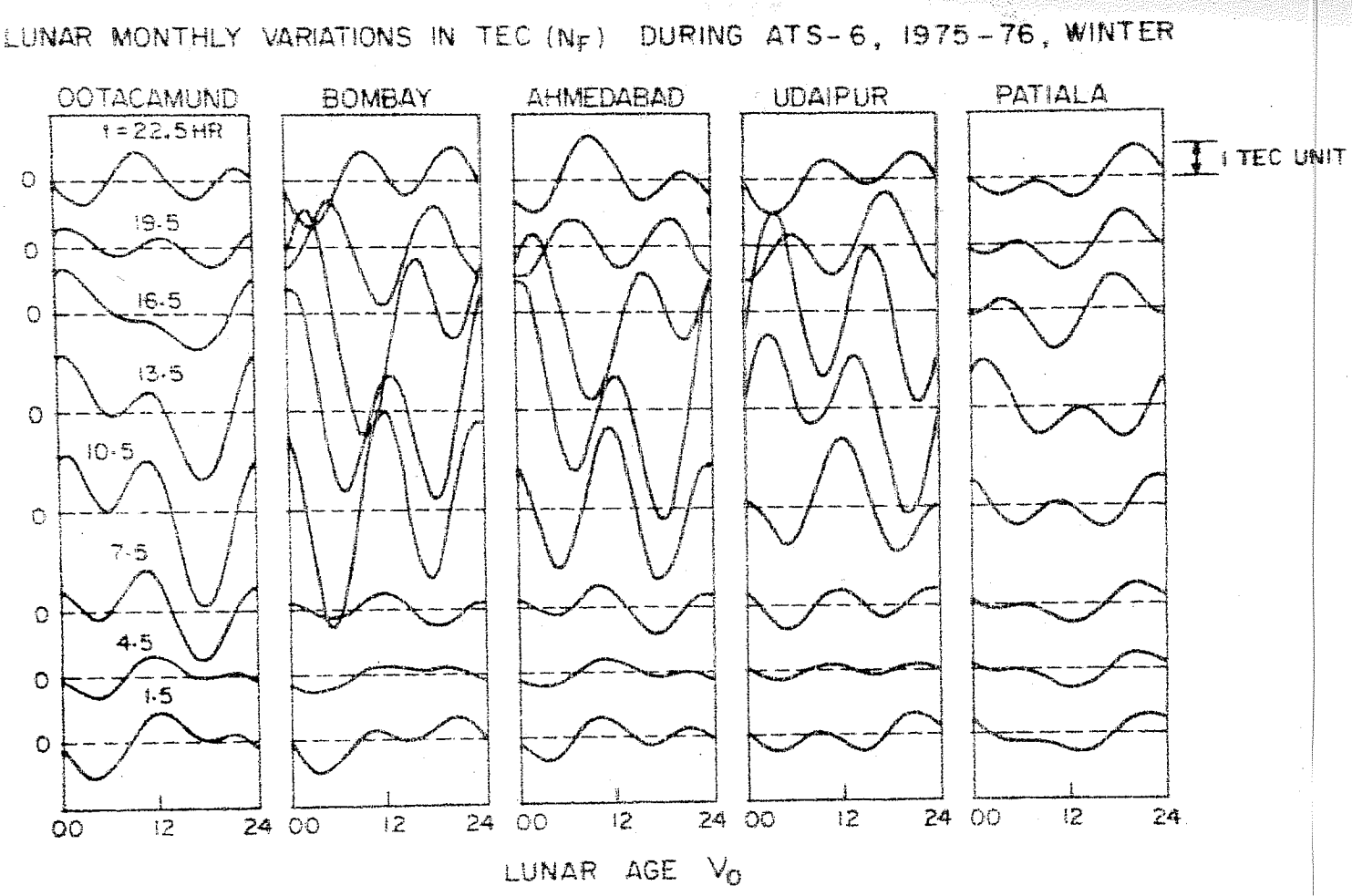

Fig.6.3a The average lunar monthly oscillations in N_F at different stations for winter.

LUNAR MONTHLY VARIATIONS IN TEC (N_F)
DURING ATS-6, 1975-76, SUMMER

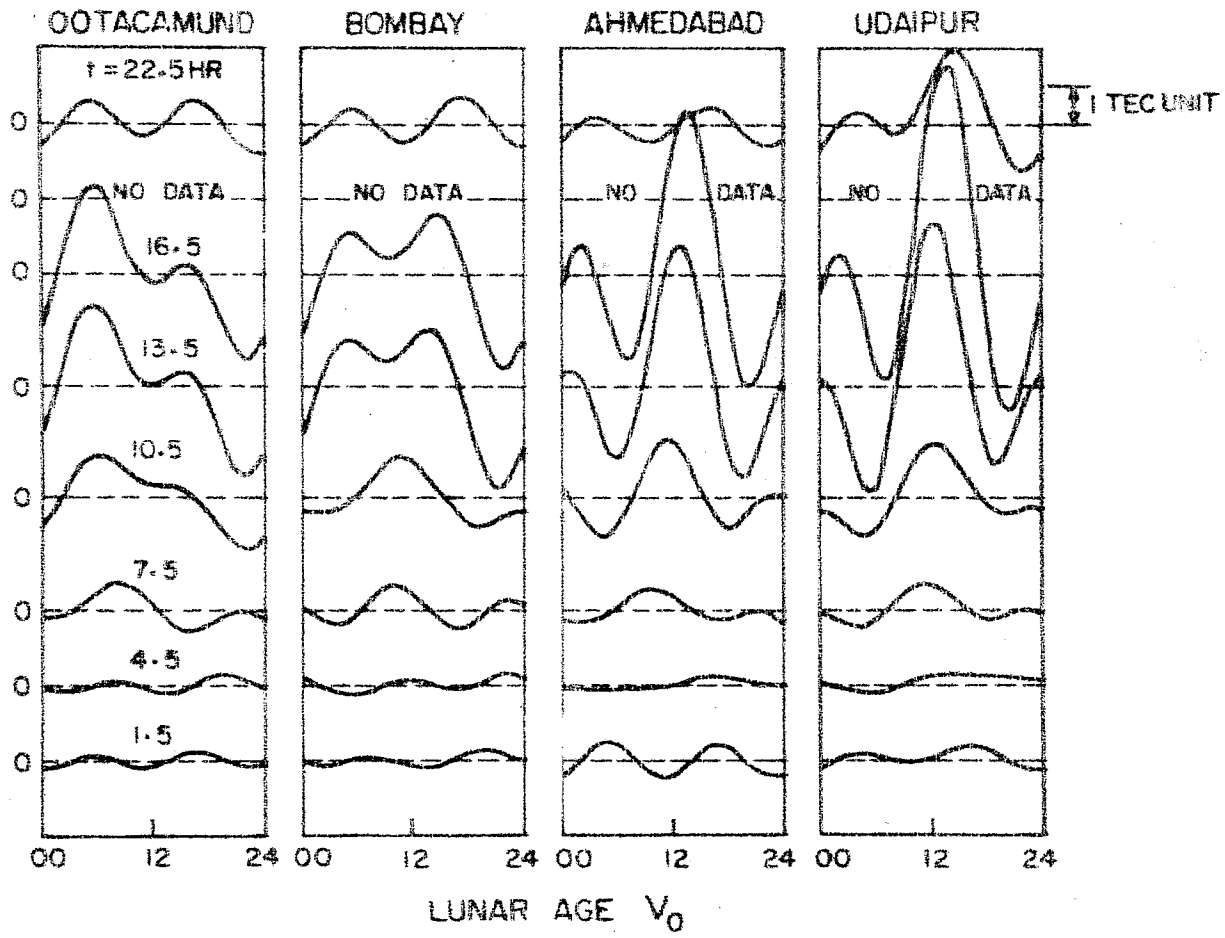

Fig.6.3b The average lunar monthly oscillations in N_F at different stations for summer.

in an individual season whereas it is not that clear in the annual average picture. The lunar oscillations at Bombay are in general found to be similar to that obtained at other stations near the crest but in summer the variations at Bombay are more similar to that observed at Ootacamund. The amplitude (r_2) of the M_2 tide and the phase (τ_2) of maximum positive deviation in lunar time at different solar hours for all the stations, for winter and summer are presented in Tables 6.2b and 6.2c respectively. The max. amplitude of M_2 tide in winter is observed at 10.5 hr LT grouping for Ootacamund and Bombay, 13.5 hr LT grouping for Ahmedabad and Patiala, and 16.5 hr LT grouping for Udaipur. For summer months, the max. amplitude of M_2 tide is observed at 16.5 hr LT grouping for all the stations considered. The amplitude of the tide in both the seasons is found to be larger at the crest, as compared to that on either side of the crest.

6.6.2 Lunar Daily Variations (L)

(a) The Annual Average Lunar Daily (L) Variations in TEC (N_F and N_T), N_m and τ, near Magnetic Equator:-

The mean lunar daily variations in terms of TEC are derived separately for the days with different lunar ages i.e. ν = 00 to 23. For further analysis, the days at intervals of three lunar age hours have been grouped together to get average lunar daily variation values for days with lunar age 00, 03, 06, 09, 12, 15, 18 and 21. The mean of the lunar daily variation on lunar ages 8, 9,

Table 6.2b

The amplitude (r_2) and lunar time (τ_2) of max. positive deviation of lunar semi-monthly oscillations in $N_F(10^{16}$ el.$m^{-2})$ for different stations (winter)

L.T.	Ootacamund		Bombay		Ahmedabad		Udaipur		Patiala	
	r_2	τ_2l.hr	r_2	τ_2l.hr	r_2	τ_2l.hr	r_2	τ_2l.hr	r_2	τ_2l.hr
1.5	0.45	2.4	0.45	4.1	0.46	3.6	0.40	4.2	0.21	4.3
4.5	0.33	5.6	(0.13)	7.2	0.20	6.3	0.19	6.3	0.23	9.0
7.5	0.86	8.1	0.36	7.5	0.50	8.7	0.52	7.9	(0.27)	11.4
10.5	1.43	10.2	2.86	10.6	1.99	10.8	1.14	9.9	0.56	11.3
13.5	1.02	0.8	2.49	0.3	2.54	0.4	1.97	10.8	0.76	11.3
16.5	0.44	3.3	2.31	0.7	1.77	0.9	2.48	0.0	0.66	10.8
19.5	0.41	5.4	1.28	0.8	0.82	11.7	0.98	0.9	0.51	0.2
22.5	0.64	11.4	0.95	0.5	0.78	0.5	0.64	11.9	0.46	1.5
Mean P.E.	0.43		0.58		0.63		0.53		0.28	

Table 6.2c

The amplitude (r_2) and lunar time (τ_2) of max. positive deviation of lunar semi-monthly oscillations in N_F(10^{16} el.m^{-2}) for different stations (summer)

L.T.	Ootacamund		Bombay		Ahmedabad		Udaipur	
	r_2	τ_2l.hr	r_2	τ_2l.hr	r_2	τ_2l.hr	r_2	τ_2l.hr
1.5	0.19	7.4	(0.12)	6.3	0.47	8.6	0.21	9.2
4.5	0.19	8.6	0.19	5.4	(0.03)	0.0	(0.06)	3.8
7.5	0.32	10.5	0.42	9.0	0.26	9.7	0.34	8.1
10.5	0.46	5.5	(0.37)	10.8	0.83	10.9	0.57	10.2
13.5	1.10	8.3	1.02	9.6	2.06	0.0	2.31	0.5
16.5	1.12	10.9	1.08	0.2	2.55	1.9	3.09	1.9
19.5	-	-	-	-	-	-	-	-
22.5	0.57	4.3	0.54	4.3	0.41	5.7	0.88	6.4
Mean P.E.	0.36		0.44		0.71		0.65	

10 is represented as the lunar daily variation for lunar age, 09 and similarly for other lunar ages. The whole year (Oct. 1975 - July 1976) average lunar variations (in N_F and N_T) at Ootacamund for each of the eight lunar age groups are shown in Fig.6.4a. The variations during the daytime hours are shown by full lines; those during the night by dotted lines.

The whole lunation curves obtained by averaging the eight individual curves, are also presented in the same figure. It is to be noted that only the built up curves, and not the original data points, have been shown in this figure and in the subsequent figures described in this section. The built-up curves have been obtained by using the first four harmonics of the lunar daily variations at a fixed lunar age.

To test the Chapman's phase law (equation 6.6), the phase of each harmonic as a function of lunar age are shown separately for N_F and N_T in Fig.6.4b. The phase of L_2 oscillations i.e. $\emptyset_2$ is fairly constant of the lunar age. Similarly the phase of L_1 oscillation i.e. $\emptyset_1$, is found to decrease by 360° in the course of one lunation. The phases of L_3 and L_4 oscillation i.e. $\emptyset_3$ and $\emptyset_4$ are found to increase by 360° and 720° respectively during one complete lunation. The mean values of amplitude $\overline{C}_n$, averaged over eight values for different lunar age groups for each of the four harmonics are also given in the Fig.6.4b. The amplitude decreases with increase in the order of the harmonic.

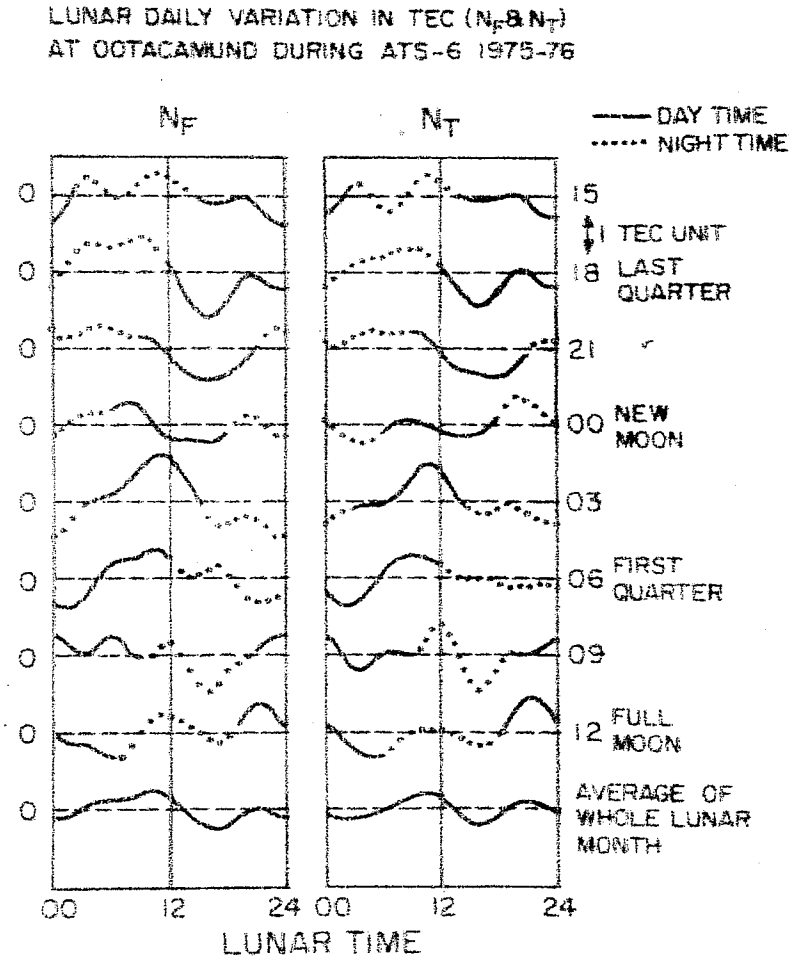

Fig.6.4a The annual average lunar daily oscillations in TEC (N_F and N_T) for different lunar ages at Ootacamund. Only built up curves have been plotted.

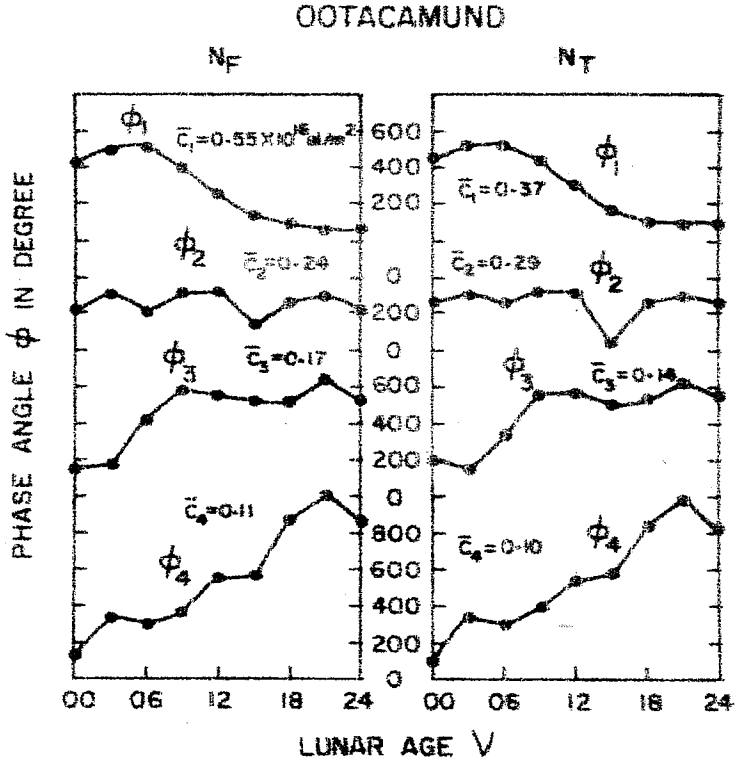

Fig.6.4b The variation with lunar age of the phases of the different harmonics of the annual average lunar daily variations of TEC at Ootacamund for eight ages of the moon.

Combining TEC data with N_m data (obtained from f_oF_2 for Kodaikanal), the slab-thickness ($\tau_{F,T} = \frac{N_{F,T}}{N_m}$) of the ionosphere can be obtained. The lunar daily variations (for whole lunation) in TEC, N_m and τ are shown separately in Fig.6.5. The data being not sufficient enough the lunar daily variations for individual lunar ages are not shown in the figure.

The following important features are noted in these figures (Figs.6.4a, 6.4b, 6.5):-

(i) The variations in N_F and N_T are strikingly similar.

(ii) The lunar variations in N_F and N_T at Ootacamund, during day and night are found to be of the same order ($\sim$1 TEC unit).

(iii) Chapman's phase law is found to be valid for the lunar oscillations in TEC at Ootacamund.

(iv) The lunar oscillations are found to be of the order of 5×10^{10} el m^{-3} in N_m and 50 km in $\tau_{F,T}$.

The whole lunation, lunar daily variation curves of N_F, N_T, N_m, and $\tau_{F,T}$ have been harmonically analysed for the first four harmonics. The amplitudes and the phases of the harmonics are tabulated in Table 6.3. The amplitudes of L_3 and L_4 oscillations are small for TEC but it is not so in case of N_m and $\tau_{F,T}$. The amplitude of L_2 oscillation, which is purely a lunar variation, has a maximum at 9.5 hr for N_F and 9.8 hr for N_T, 5.2 hr for N_m, 12.5 hr for τ_F and 11.5 hr for τ_T.

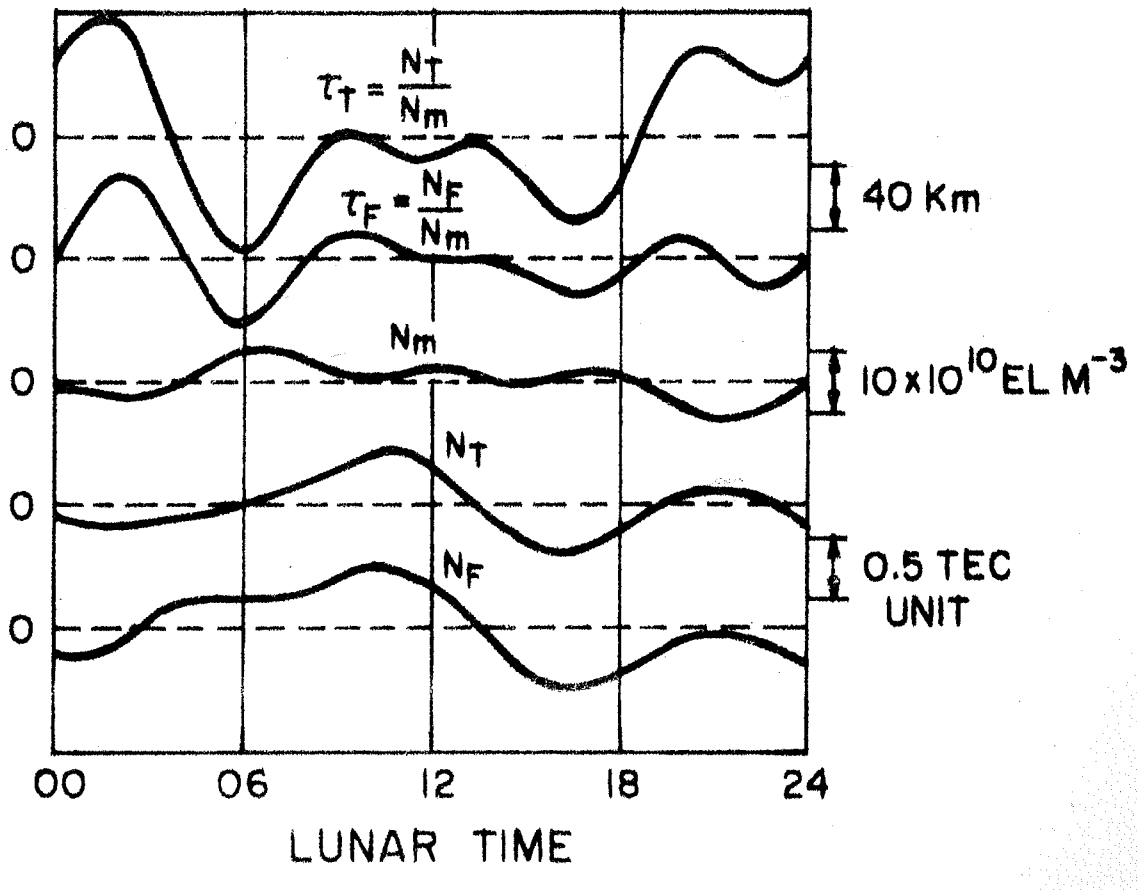

Fig.6.5 The whole lunation, annual average lunar daily variations in TEC (N_F and N_m) at Ootacamund, N_m at Kodaikanal and τ_F, and τ_T.

Table 6.3

The coefficients of whole lunation annual average lunar daily oscillations in N_F, N_T, N_m, τ_F and τ_T.

	C_1	ϕ_1 in deg.	ϕ_1 l.hr	C_2	ϕ_2 in deg.	ϕ_2 l.hr.	C_3	ϕ_3 in deg.	ϕ_3 l.hr.	C_4	ϕ_4 in deg.	ϕ_4 l.hr
Ouagamund												
$N_F(10^{16}$ el.$m^{-2})$	0.34	113	7.5	0.18	285	9.5	0.14	172	3.8	0.02	241	4.0
$N_T(10^{16}$ el.$m^{-2})$	0.15	132	8.8	0.25	295	9.8	0.10	166	3.7	0.01	1	0.0
Kodaikanal												
$N_m(10^{10}$ el.$m^{-3})$	1.63	138	9.2	0.67	155	5.2	0.50	346	7.7	0.85	1	0.0
Slab-thickness												
τ_F(km)	4.2	22	1.5	7.0	14	0.5	10.2	109	2.4	8.8	139	2.3
τ_T(km)	20.1	346	23.0	17.9	345	11.5	9.0	121	2.7	11.8	132	2.2

(b) The Average Lunar Daily Variations in N_F at Different Stations:-

The whole lunation lunar daily variations in TEC (N_F) for different seasons and annual, for different stations are shown in Fig.6.6a. For comparison purpose, the variations in N_T at Ootacamund have been included in the same figure. These curves have been harmonically analysed and the amplitudes and the phases of the first four harmonics are given in Table 6.4. In general the amplitudes of L_1, L_3 and L_4 oscillations are found to be less prominent than the amplitude of L_2 oscillation in the annual average variations. But it is not so observed in an individual season. The amplitude of the semi-diurnal (L_2) oscillations is noticed to be maximising near the crest of the equatorial anomaly and decreasing on either side of the crest. Fig.6.6b gives the latitudinal profile of the amplitude of L_2 tide for different seasons as well as for annual. The amplitude seems to be maximising around 14-15°N dip latitude for winter and annual but the corresponding latitude for summer and equinoxes is around 19°N. The amplitude in winter is found to be more than that in summer and equinoxes for all the stations except Patiala, where the amplitude in summer is found to be little higher than that in winter.

The whole year (Oct. 1975 - July 1976) annual average lunar daily variations (built-up curves using first four harmonics) in TEC (N_F) for different stations for each of the eight lunar age

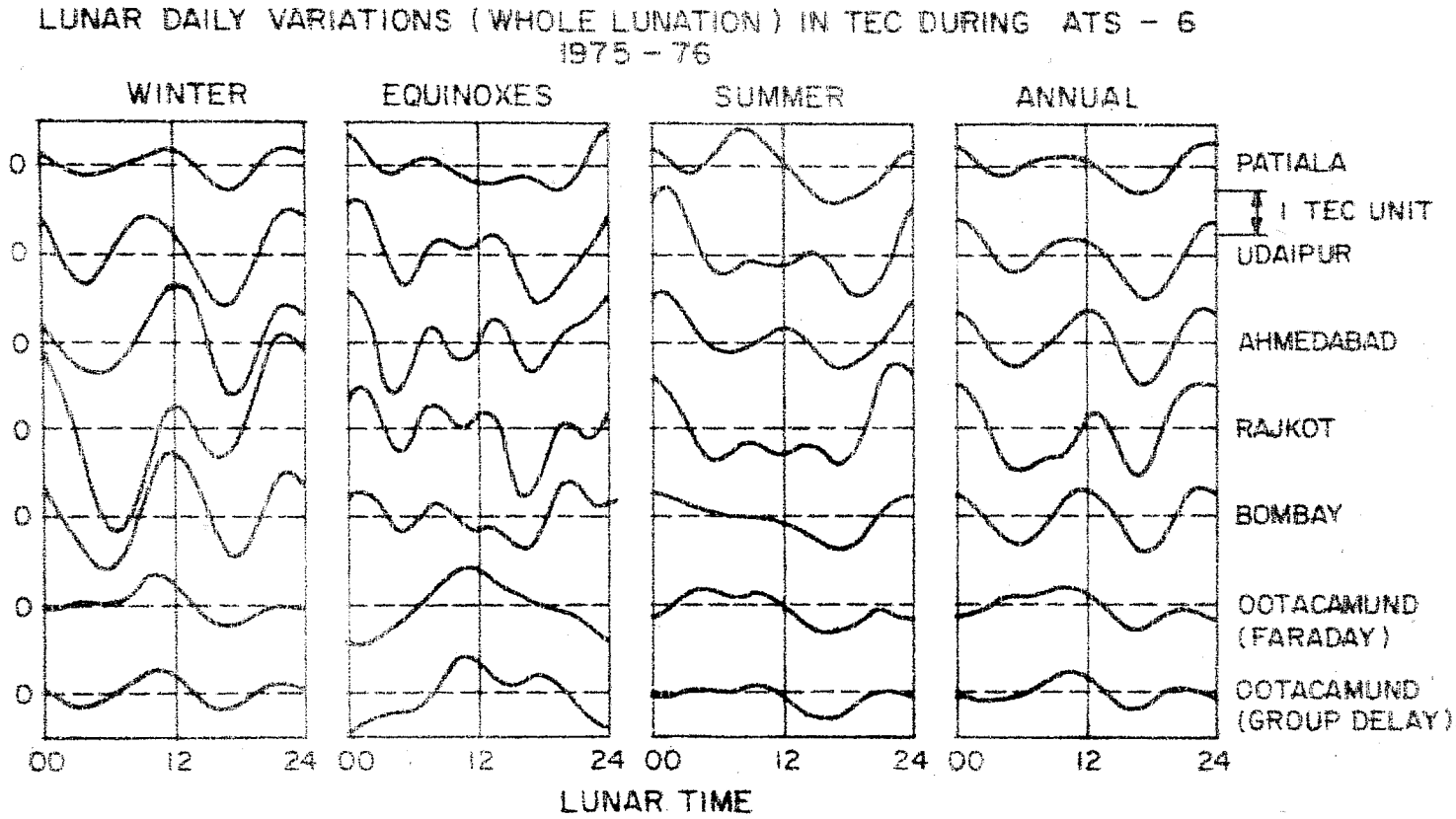

Fig.6.6a The whole lunation annual and the seasonal average lunar daily variations in TEC at different stations.

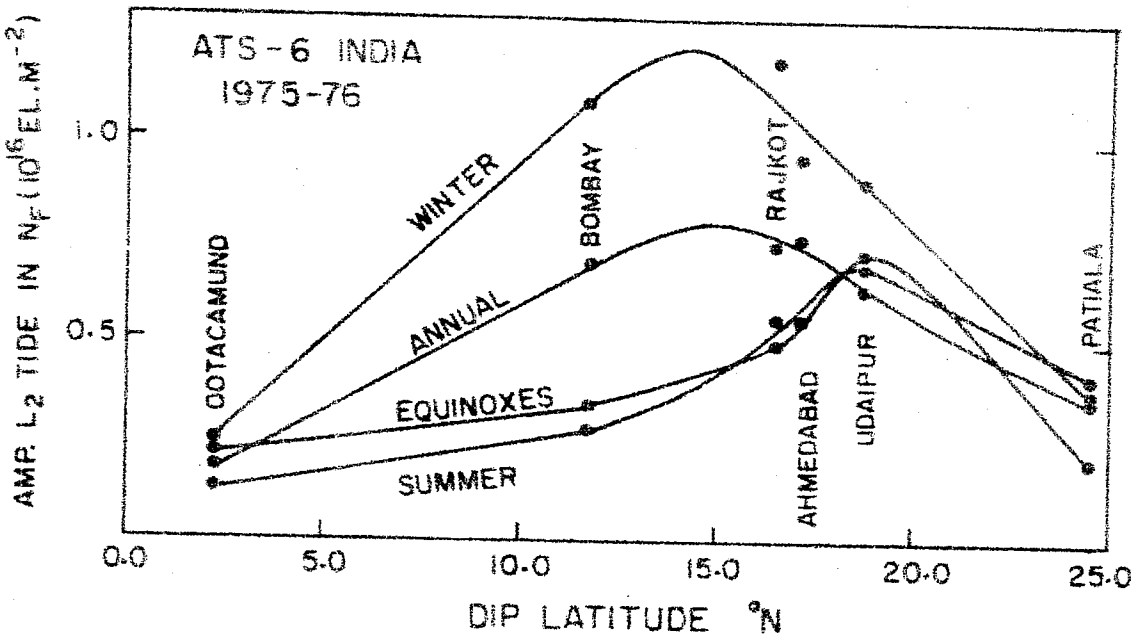

Fig.6.6b The amplitude of the lunar semi-diurnal variations in TEC, as a function of dip latitude for different seasons and annual.

Table 6.4

The coefficients of whole lunation average lunar daily oscillation in $N_F(10^{16}$ el.$m^{-2})$ for different stations.

	C_1	ϕ_1 in deg.	ϕ_1 l.hr	C_2	ϕ_2 in deg.	ϕ_2 l.hr	C_3	ϕ_3 in deg.	ϕ_3 l.hr	C_4	ϕ_4 in deg.	ϕ_4 l.hr
Annual												
Nacamund	0.34	113	7.5	0.18	285	9.5	0.14	172	3.8	0.02	241	4.0
Bay	0.03	336	22.4	0.70	341	11.4	0.11	214	4.8	0.09	150	2.5
Cot	0.60	334	22.3	0.74	347	11.6	0.17	217	4.8	0.23	90	1.5
Ahmedabad	0.07	50	3.3	0.76	347	11.6	0.17	247	5.5	0.08	110	1.8
Kanpur	0.35	58	3.9	0.64	346	11.5	0.11	349	7.8	0.07	109	1.8
Kodaikanal	0.22	60	4.0	0.37	324	10.8	0.11	299	6.6	0.04	36	0.6
Winter												
Nacamund	0.32	120	8.0	0.25	317	10.6	0.11	154	3.4	0.05	271	4.5
Bay	0.35	221	14.7	1.09	346	11.5	0.16	219	4.9	0.07	210	3.5
Cot	1.37	313	20.9	1.20	346	11.5	0.31	183	4.1	0.07	243	4.1
Ahmedabad	0.27	191	12.7	0.96	343	11.4	0.37	244	5.4	0.07	198	4.4
Kanpur	0.32	66	4.4	0.90	317	10.6	0.13	316	7.0	0.05	89	2.0
Kodaikanal	0.08	56	3.7	0.38	327	10.9	0.15	310	6.9	0.04	67	1.1
Equinoxes												
Nacamund	0.74	184	12.3	0.22	273	9.1	0.06	182	4.0	0.06	252	4.2
Bay	0.37	7	0.5	0.34	284	9.5	0.11	121	2.7	0.32	110	1.8
Cot	0.44	67	4.5	0.49	328	10.9	0.13	140	3.1	0.53	85	1.4
Ahmedabad	0.32	325	21.7	0.56	340	11.3	0.33	333	7.4	0.42	82	1.4
Kanpur	0.36	62	4.1	0.72	9	0.3	0.22	14	0.3	0.27	114	1.9
Kodaikanal	0.35	32	2.1	0.21	350	11.7	0.29	352	7.8	0.11	347	5.8
Summer												
Nacamund	0.42	89	5.9	0.13	265	8.8	0.15	175	3.9	0.05	230	3.8
Bay	0.46	49	3.3	0.28	340	11.3	0.07	275	6.1	0.03	133	2.2
Cot	0.85	350	23.3	0.56	332	11.1	0.16	305	6.8	0.17	172	2.9
Ahmedabad	0.40	35	2.3	0.55	18	0.6	0.05	36	0.8	0.08	84	1.4
Kanpur	0.57	36	2.4	0.69	39	1.3	0.29	37	0.8	0.10	153	2.6
Kodaikanal	0.58	95	6.3	0.42	304	10.1	0.16	359	8.0	0.07	32	0.5

groups are shown in Fig.6.7a. The variations during the daytime hours are shown by full lines and those during night by dotted lines. The whole lunation curves obtained by averaging the eight individual curves are also plotted in the same figure and correspond to the annual curves of Fig.6.6a. Due to insufficient data, similar analysis for an individual season has not been undertaken. It is noted that the amplitudes of the lunar oscillations are larger during daytime hours as compared to that in night-time hours for all the stations except Ootacamund, where not much of difference in amplitude between day to night is observed. To test the validity of Chapman's phase law (equation 6.6) at different latitudes, the phase of each harmonic as a function of lunar age are shown separately for Ootacamund (near equator), Ahmedabad (near crest) and Patiala (beyond crest) in Fig.6.7b. The mean values of amplitude $\overline{C_n}$ averaged over eight different lunar age groups for each of the four harmonics are also given in the figure, for all the three stations. It is noted that the phase of L_2 oscillation i.e. ϕ_2 is fairly constant of the lunar age. Also the phase of L_1 oscillation i.e. ϕ_1 decreases by 360° in the course of one lunation. The phases of L_3 and L_4 oscillations i.e. ϕ_3 and ϕ_4 are found to be increased by 360° and 720° respectively during the one complete lunation. Hence it is noted that the Chapman's phase law is fairly well obeyed at low latitudes. Also it is noted that the value of mean amplitude decreases with increase in the order of harmonic, as expected by the Chapman's law.

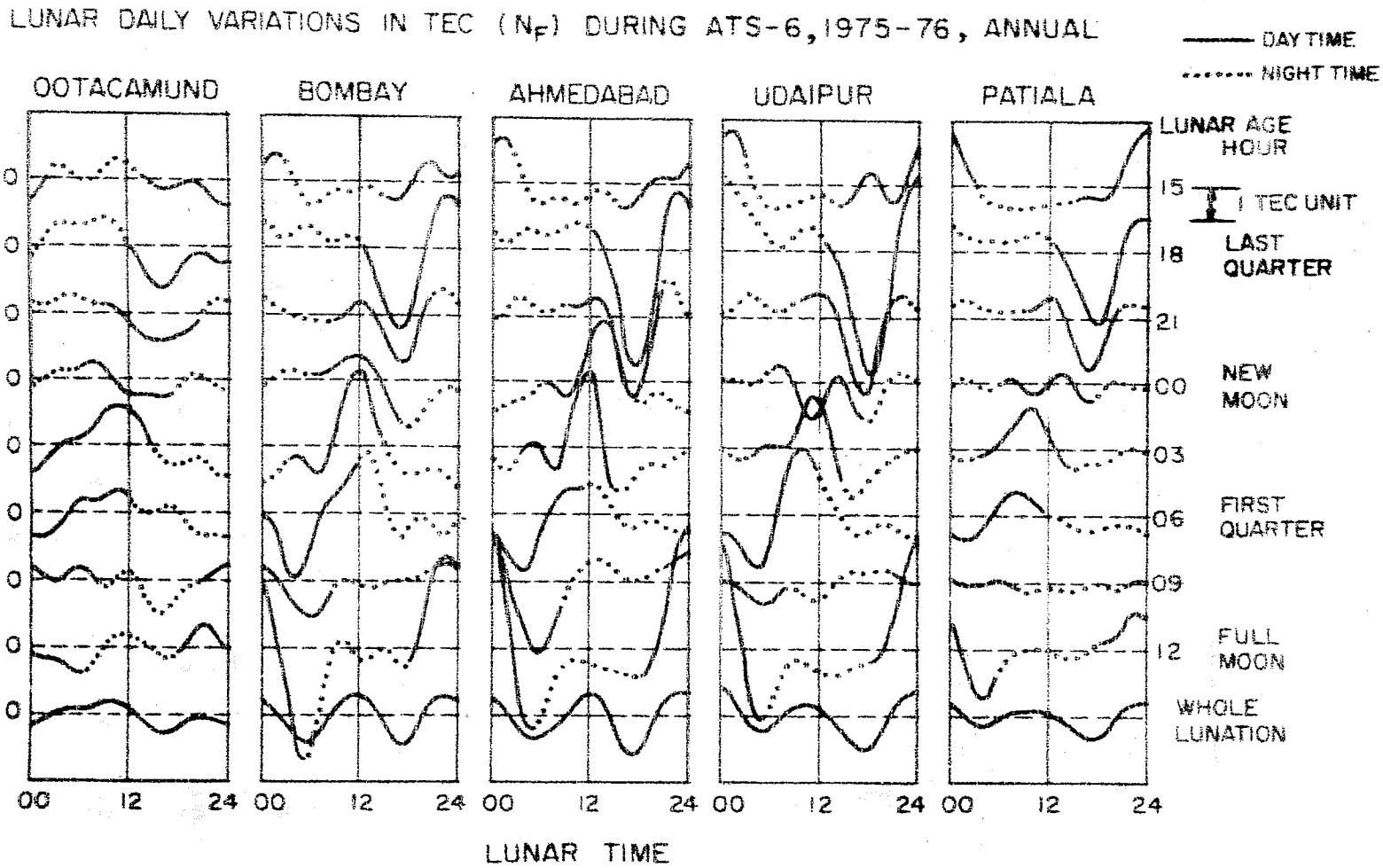

Fig.6.7a The annual average lunar daily variations in TEC (N_F) at different stations for different lunar ages as well as averaged over the whole lunation.

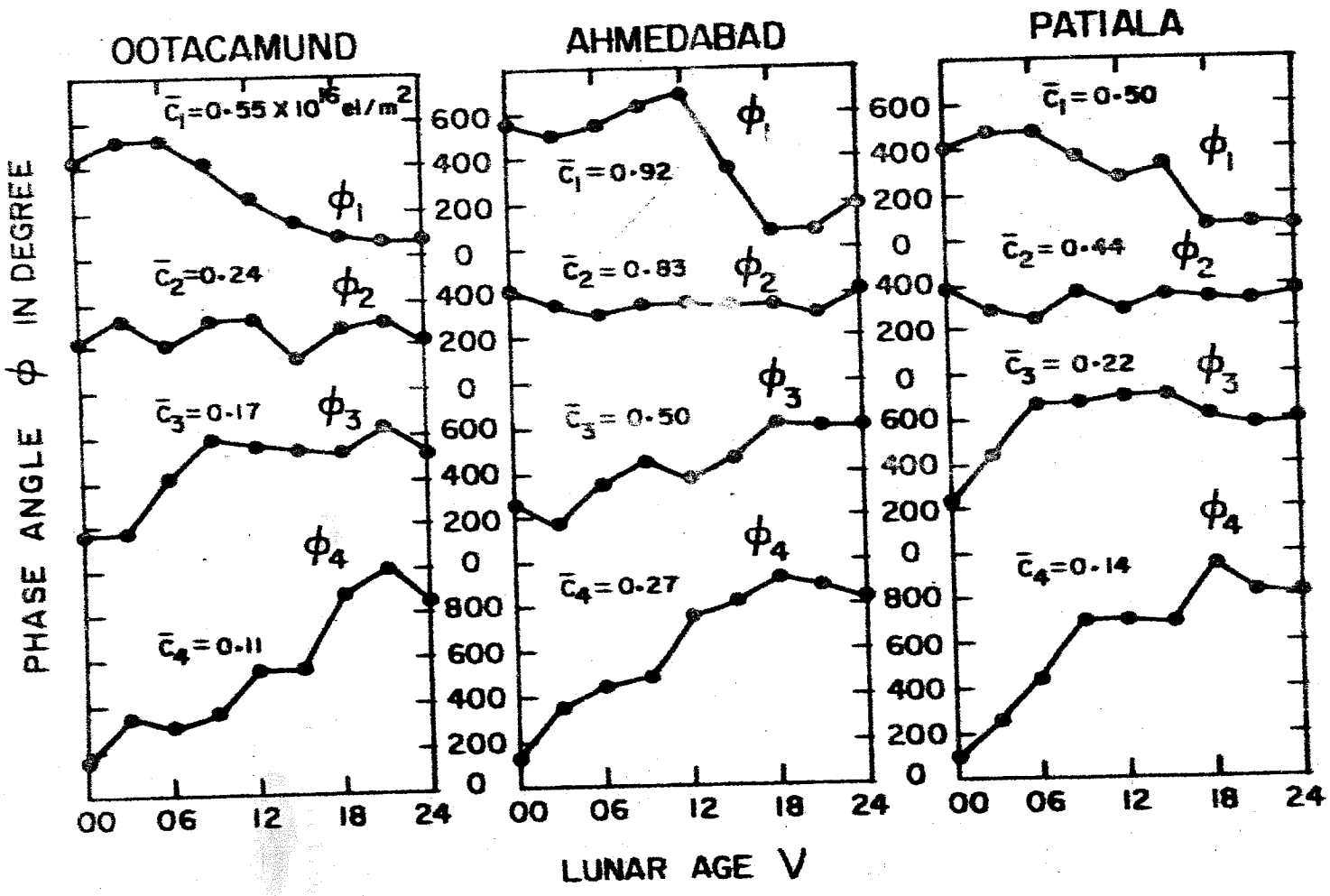

Fig.6.7b The phase angles for different harmonics of the annual average lunar daily variation of N_F at Ootacamund, Ahmedabad and Patiala, as a function of lunar age.

6.6.3 Discussions

The possible explanation of the lunar semi-diurnal variation, L_2, in F_2 layer was suggested as due to additional "Fountain effect", caused by the lunar semi-diurnal (L_2) variation of the electric field at the equatorial region (Martyn 1947). Matsushita and Maeda (1965) showed that the maximum L_2 variation of H at the equator occurs at about 9 l. hr. Trivedi and Rastogi (1969) computed the lunar tidal oscillations in H at an equatorial station Kodaikanal for low as well as high sunspot years and showed that the phase of the maximum positive L_2 deviation in H, is about 8.8 l. hr. In the present investigations it is noted that the amplitude of the L_2 oscillation in TEC maximises at about 9.5 l.hr for the equatorial station Ootacamund and at about 11.5 l. hr for the stations situated near the crest of the equatorial anomaly. The time required for the ionization to diffuse along the magnetic field lines from the equator to the crest zone of the equatorial anomaly is estimated to be about two hours (Duncan 1960, Iyer et al. 1976); hence the present results are in agreement with the interpretation of L_2 oscillation in F_2 region, given in terms of enhanced "Fountain effect" caused by the L_2 oscillations of the electric field in the equatorial region. Similar conclusion was also arrived at by Huang (1978) by studying the lunar daily variations of TEC at a station (Lunping) close to the crest zone of the equatorial anomaly. The average lunar daily variations in TEC at Lunping for different lunar ages are given in their Fig.3.

They show an excellent resemblance with the corresponding variations for the stations, near the crest (Bombay, Ahmedabad, Udaipur) given in Fig.6.7a of the present study.

The geomagnetic control in lunar semi-diurnal (L_2) tide in the noon value of f_oF_2 was first demonstrated by MacNish and Gautier (1949); the maximum positive displacement was found to be around 04 l. hr at equatorial stations, while at stations at geomagnetic latitude greater than 20°, the phase was shifted almost by 180°. Rastogi (1961) showed that the tide in midday value of f_oF_2 is controlled by the dip latitude and not by dipole latitude; the reversal in phase takes place at about 10° dip lat. The tidal amplitude was found to have very sharp maximum over the magnetic equator and two broad maxima at about 20° dip lat. with a minima around 5° dip lat. In the present study, the dip latitude coverage is from 2.2°N to about 24.5°N. The latitudinal variations of the phase of the L_2 oscillation in N_F does not show any phase reversal except that the phase at Ootacamund (9.5 l. hr) differs from the phase at the stations near the crest (11.5 l. hr) by about two hours (Table 6.4). It is interesting to be noted that the phase of the L_2 oscillations in N_m at Kodaikanal(1.7°N dip lat) does show a phase 5.2 l. hr (Table 6.3) which is close to the expected value of 04 l. hr. Hence the present results indicate that L_2 oscillation in equatorial N_m is in almost phase opposition to that in TEC at the crest region, whereas the phase of the L_2 oscillation in equatorial TEC is lagging behind the corresponding

phase in N_F at the crest region by about two hours. Rao and Stubenrauch (1967) and Huang (1978) found that the lunar daily variations in N_F and f_oF_2 are similar; none of these two studies are for an equatorial station. For equatorial station, the variations in N_F and N_m are not found to be similar as shown by Fig.6.5. The phase of the L_2 oscillation in TEC at Octacamund is ahead by about 4 hr, as compared to that in N_m (Table 6.3). Rastogi (1963b) studied the lunar tidal effects in f_oF_2 obtained at a number of Indian stations and it was noted that phase of maximum amplitude of L_2 variations at Ahmedabad and Bombay is around 12 l. hr which agrees well with the corresponding phase observed in the present study using TEC data at these stations.

CHAPTER - VII

STORM TIME TEC AT LOW LATITUDES

7.1 Introduction

The relationship between geomagnetic storms and F-region ionospheric storms has been a field of much investigations since the earliest work of Appleton and Ingram (1935), Harang (1937) and Appleton et al. (1937). Martyn (1953) found that at all latitudes, an ionospheric storm begins simultaneously or within an hour after the sudden commencement of the magnetic storm, and the initial effect on the F-region depends on the local time of sudden commencement. Morphological studies of F-region storms indicate that during geomagnetic storms, N_m, the maximum ionization density of F layer, exhibits strong latitudinal and seasonal dependence (Matsushita 1959, Rajaram and Rastogi 1969, 1971). In recent years, renewed efforts for an understanding of the ionospheric response to geomagnetic activity have been made by utilizing data on total electron content of the ionosphere in addition to the maximum ionization density of F-region. Usually, the studies on the behaviour of TEC during geomagnetic storms have been carried out for some particular storms (Klobuchar et al. 1971, Low and Roelofs 1973) or certain special aspects of the problem have been studied such as the effect of geomagnetic activity on the latitude distribution of TEC in the equatorial anomaly region (Basu and Das Gupta 1968) or the association of TEC

enhancements to large negative excursions in the horizontal component of local geomagnetic field, H (Nelson and Cogger 1971). Mendillo (1971) carried out a comprehensive statistical study of the variation of TEC, during geomagnetic storms at Hamilton, a mid-latitude station, and observed that the percentage deviation of TEC from its median value is positive in the early phase of storms but becomes negative during the following phase. From a similar statistical study carried out at Hawaii (21°N geomag.) Huang et al. (1974) concluded that at low mid-latitudes the response of TEC to magnetic activity depends on the seasons.

From theoretical standpoint, it has been shown that neutral air winds (Kohl and King 1967, Rishbeth 1972, Evans 1973) and/or electric fields (Evans 1970, Papagiannis et al. 1971, Mendillo 1973) at ionospheric heights can cause the observed increases of ionospheric parameters. On the other hand, changes in neutral air composition can account for the observed decreases (Seaton 1956, Duncan 1969, King 1971, Chandra and Herman 1969, Obayashi 1972). Relative assessment of these stormtime perturbations has been made on a theoretical basis by several workers (Jones and Rishbeth 1971, Jones 1971, 73, Rajaram et al. 1971). Recently Davies (1974a,b) has developed a model for the global morphology of the depletion phase of ionization during geomagnetic storms by considering a heat source located at magnetic noon on the dayside auroral oval (Feldstein 1969). Davies and Ruster (1976) have made the theoretical investigations on the effects

produced by thermospheric winds, composition changes and magnetospheric electric fields on the ionospheric F-layer during disturbed conditions.

The data for low and equatorial latitudes have been rather meagre, specially in the Indian zone. With the availability of present ATS-6 data from a chain of stations namely Ootacamund (3.0°N dip lat), Bombay (13.0°N), Ahmedabad (18.6°N), Udaipur (20.4°N) and Patiala (26.6°N), it is possible to undertake a study of storm time effects on TEC at low latitudes. Some results of such studies obtained from the data for the last four locations have already been reported by Jain et al. (1978a,b). Patiala is located to the north of the well-known latitudinal F-region electron density anomaly, while Udaipur and Ahmedabad are near the crest of the anomaly and Bombay is to its south. Jain et al. (1978a,b) reported that all the locations show large increases in TEC in the evening or night following the geomagnetic storm onset and the effects often last for more than three days. The increase in TEC was noticed more commonly during forenoon hour of day-1 (day-0 is the MPO day) and almost throughout on day-2. Negative phase was also noticed on afternoon of day-1 and also on day-3. Both positive and negative phases were found to be largest at Ahmedabad and Udaipur, less at Bombay and least at Patiala. The storm time changes were in general agreement with the changes in the Fountain effect which are depicted by the changes in equatorial f_0F_2 and equatorial electrojet. Some abnormal changes in TEC

which could not be explained on the basis of Fountain effect were suggested to be due to the effects of equatorial neutral winds from higher latitudes during the geomagnetically disturbed period. Since then, the data for Faraday rotation and also Group delay for the near equatorial location Ootacamund have been processed. The storm time effects in TEC observed at Ootacamund (near equator) by both Faraday rotation (N_F) and the group delay (N_T) methods simultaneously and a critical study of the storm time behaviour of TEC from equator to about 25° dip lat. for a few selected storms is described in this chapter.

7.2 Storm Time Studies of TEC at Different Stations

7.2.1 Results

There were several geomagnetic storms in November 1975; the two of them are shown in Fig.7.1. The first curve in the upper half of the figure shows the plot of D_{st} for the period Nov.21-24. The first day Nov.21 is not completely quiet (D_{st} had negative values about -30 gamma) but the big storm has started on Nov.22 at about 1200 LT. The next two plots are for TEC observed at Ootacamund by Faraday rotation method (N_F) and Group delay method (N_T). What is plotted is ΔN_F and ΔN_T i.e. deviation of N_F and N_T from their respective monthly mean daily variation pattern. The resemblance between the two is very remarkable with large changes, positive as well as negative indicated by both. The lower half of Fig.7.1 shows similar plots for another storm which occurred

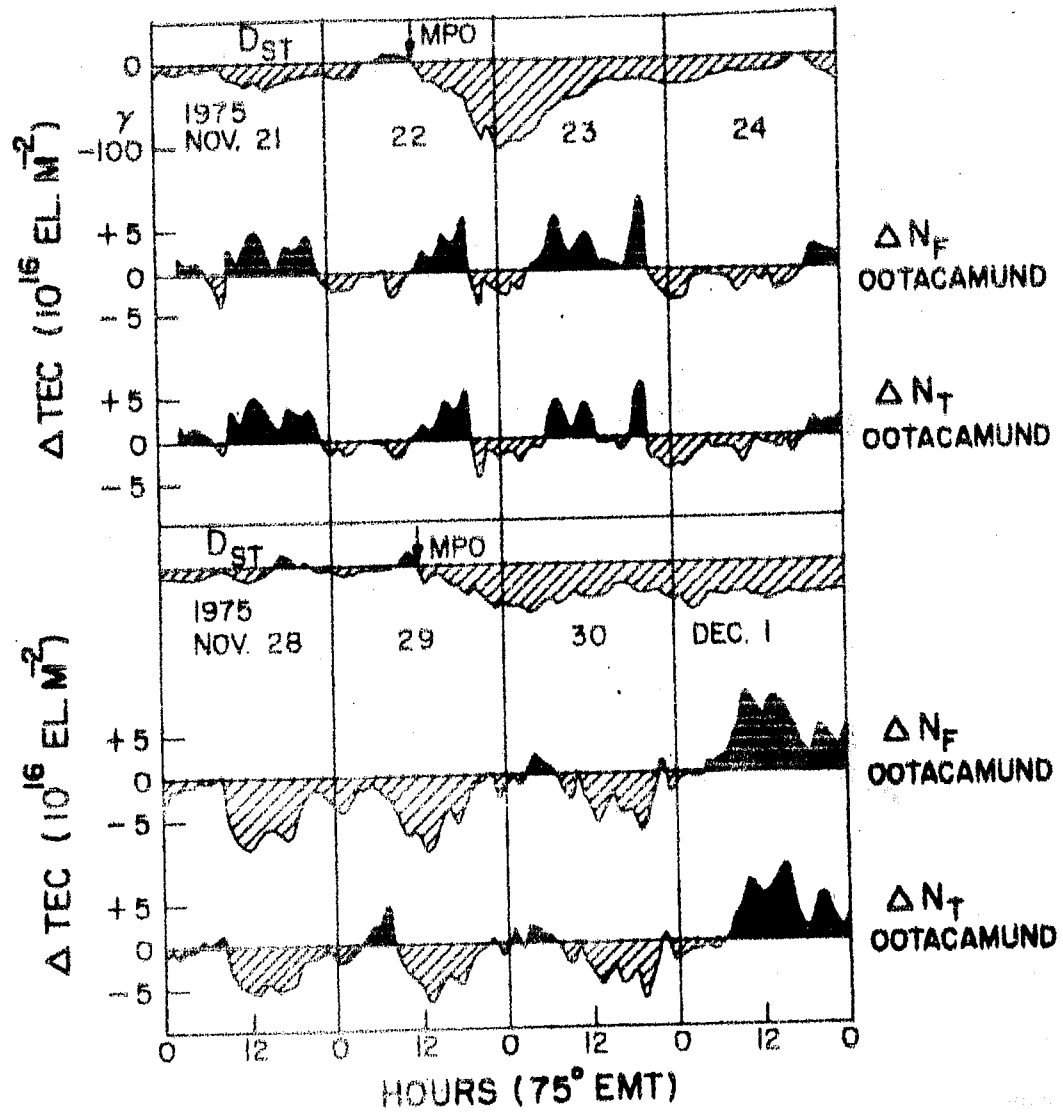

Fig.7.1 Plot of hourly values of geomagnetic D_{st} and the variations from monthly average curves for the TEC measured at Ootacamund, by the Faraday rotation method (ΔN_F) and by the group delay method (ΔN_T) for the storms Nov.21-24, 1975 (upper half) and of Nov.28-Dec.1, 1975 (lower half). Positive deviations are shown black and negative deviations are shown hatched.

a few days later (Nov.28 - Dec.1, main phase onset on Nov.29 at about 1200 LT i.e. same as for the earlier storm). The two storms have almost the same main phase onset time (1200 LT) and the D_{st} magnitudes are exceeding 50 gamma in both. But the TEC patterns are completely different in the two cases. In the Nov.22 storm, ΔTEC is highly positive on all the days from noon to dusk whereas during night hours, ΔTEC is negative on all the nights. The daytime increases are not high all through but seem to be made up of positive oscillations of a few hours duration at a time. In contrast, the Nov.29 storm shows highly negative ΔTEC on the storm days and even before and a highly positive ΔTEC on the third day. Comparison with variations of ΔTEC at other higher latitudes is undertaken later on; but the important point to be noted here is that in the same season (northern winter) for two storms within a few days of each other and having a noontime MPO for both, the ΔTEC patterns at equator are radically different, showing a highly positive phase in one storm and a highly negative phase in another. There is also a large difference in the post-storm period of these two storms. On the 3rd storm day, the first storm shows negligible ΔTEC but the latter storm shows a very large positive phase. Of course in the latter case, the D_{st} had not yet recovered to normal and there might be a second storm in progress; but the D_{st} values are only about -40 gamma, while the positive ΔTEC is very large, larger than even the positive ΔTEC of the earlier geomagnetic storm which had a D_{st} as large as -100 gamma.

In the storm of Nov.29 (lower half of Fig.7.1), there is a dissimilarity of Δ TEC obtained by the two methods in the morning hour. The ΔN_T shows a positive phase while ΔN_F shows a negative phase. A comparison with ΔN_{max} as obtained from f_oF_2 at the equatorial station of Kodaikanal shows that the N_{max} changes are more similar to the N_F changes. Thus, the increase shown by ΔN_T is probably of plasmaspheric origin. The actual plots of ΔN_{max} are shown in later diagrams (Figs.7.5 and 7.6) where these storms are reconsidered. A comparison of the TEC changes at various latitudes for a few selected storms, including the above two storms is given below:-

Storm of Nov.1-4, 1975 (Fig.7.2):- The MPC as shown by D_{st} in the top curve is on Nov.2 at about 1600 LT. Data for Bombay and Udaipur are missing. On Nov.1, D_{st} is not fully quiet. There is probably a recovery of a previous storm. ΔTEC at Patiala is almost zero but ΔTEC at Ahmedabad is highly negative and that at Ootacamund positive on the afternoon of Nov.1. ΔN_{max} at Kodaikanal is similar to ΔTEC at Ootacamund in the afternoon. However, in the morning hours, ΔN_{max} is abnormally large and coincides with a counter-electrojet as indicated by the equatorial electrojet strength ΔSd_I shown in the bottom curve of Fig.7.2 and obtained as a difference between the geomagnetic H values at the equatorial station Trivandrum and the non-equatorial but low latitude station Alibag (Bombay) (Kane 1973). The normal expected pattern is that whenever the equatorial electrojet is

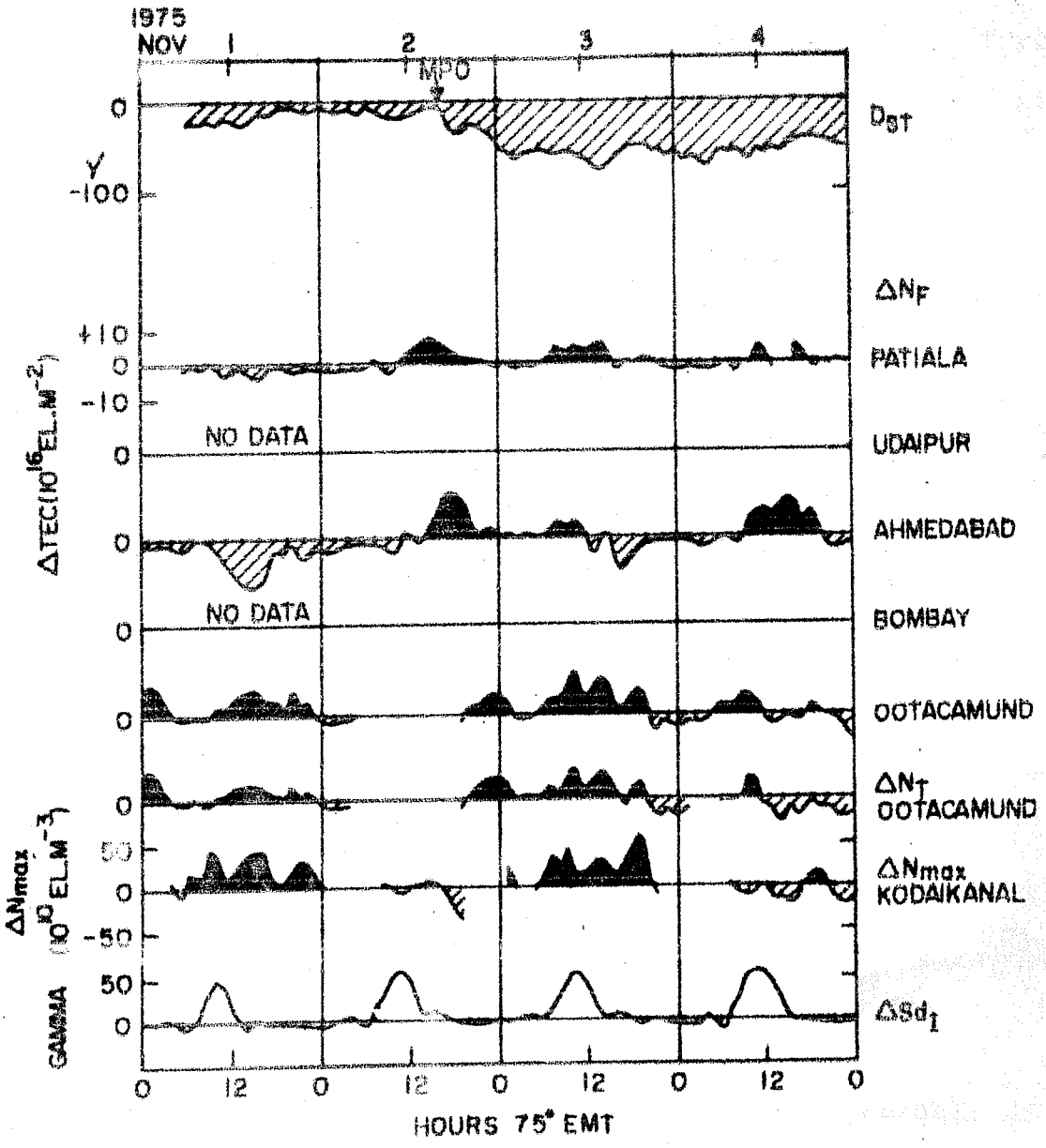

Fig.7.2 Plot of geomagnetic D_{st}, deviations of TEC from the monthly median for different stations, N_{max} deviations for Kodaikanal and the equatorial electrojet strength Sd_I at Trivandrum for the storm period Nov.1 to 4, 1975.

strong, the equatorial noon-time bite-out in f_oF_2 (and hence in N_{max}) is prominent (though this may not be reflected in equatorial TEC), and the latitudinal anomaly is strong i.e. f_oF_2 and TEC at the crest of the anomaly (in Ahmedabad-Udaipur region) should show positive changes. Contrarily, whenever the equatorial electrojet is weak or reversed (counter-electrojet) the equatorial f_oF_2 noon-time bite-out is restored giving positive ΔN_{max} (which may or may not reflect in equatorial TEC) and the latitudinal anomaly reduces giving negative Δ TEC (near Ahmedabad). On Nov.1, the equatorial electrojet shows a strong suppression and distortion and ΔN_{max} as well as ΔTEC at equator shows positive changes and ΔTEC at Ahmedabad is negative. Thus, the changes are consistent with a large scale inhibition of the Fountain effect from equator to low-latitudes; but this inhibition occurred before the storm of Nov.2 and hence must be attributed not to any geomagnetic storm effect but to the day to day variability of the equatorial electrojet strength and low and mid-latitude ionospheric content on quiet days (McDougall 1969, Kane 1972).

On the storm day Nov.2, 1975 and later, the N_{max} as well as TEC at equator show positive phases. Surprisingly, ΔTEC changes at Ahmedabad are positive on Nov.2 and Nov.4 but on Nov.3 these are slightly positive in the pre-noon hour and negative in the afternoon. The electrojet patterns as indicated by ΔSd_I are similar on all the three days. The storm time changes at Ahmedabad tally neither with the equatorial changes nor with the northern

location Patiala. A check of the data showed no error.

Storm of Nov.8-11, 1975 (Fig.7.3):- The D_{st} storm has an MPO at about 12 noon on Nov.9. Most of the TEC data are missing for Nov.9 and a part of Nov.10. The most spectacular feature is a very large positive $\triangle$ TEC in the afternoon of Nov.11, highly accentuated near the crest of the anomaly. The main D_{st} storm has recovered considerably by Nov.10 end but a new small storm seems to have started on early Nov.11 and has a maximum D_{st} change of -50 gamma. Thus the large TEC increase seem to be associated with this very weak geomagnetic storm. Data for Ootacamund TEC are missing for Nov.11. But N_{max} does not show any abnormal behaviour on Nov.11 afternoon. Instead, it shows a large positive effect between dusk and midnight. The equatorial electrojet is stronger than for all the three previous days.

Storm of Nov.16-19, 1975 (Fig.7.4):- This is a large storm (-100 gamma) with MPO at about 1700 LT on November 17. Nov.16 was not completely quiet and D_{st} changes of -20 gamma occurred. But very large positive TEC changes are noticed in the afternoon at the crest but none at equator. In contrast $\triangle N_{max}$ at equator is negative and the equatorial electrojet is strong. Thus a strong Fountain effect giving an equatorial N_{max} bite-out and a piling up at the crest is indicated. During the main storm, TEC data are not continuous; but only a positive phase is indicated. On Nov.18, the equatorial electrojet is abnormally weak and N_{max} is abnormally

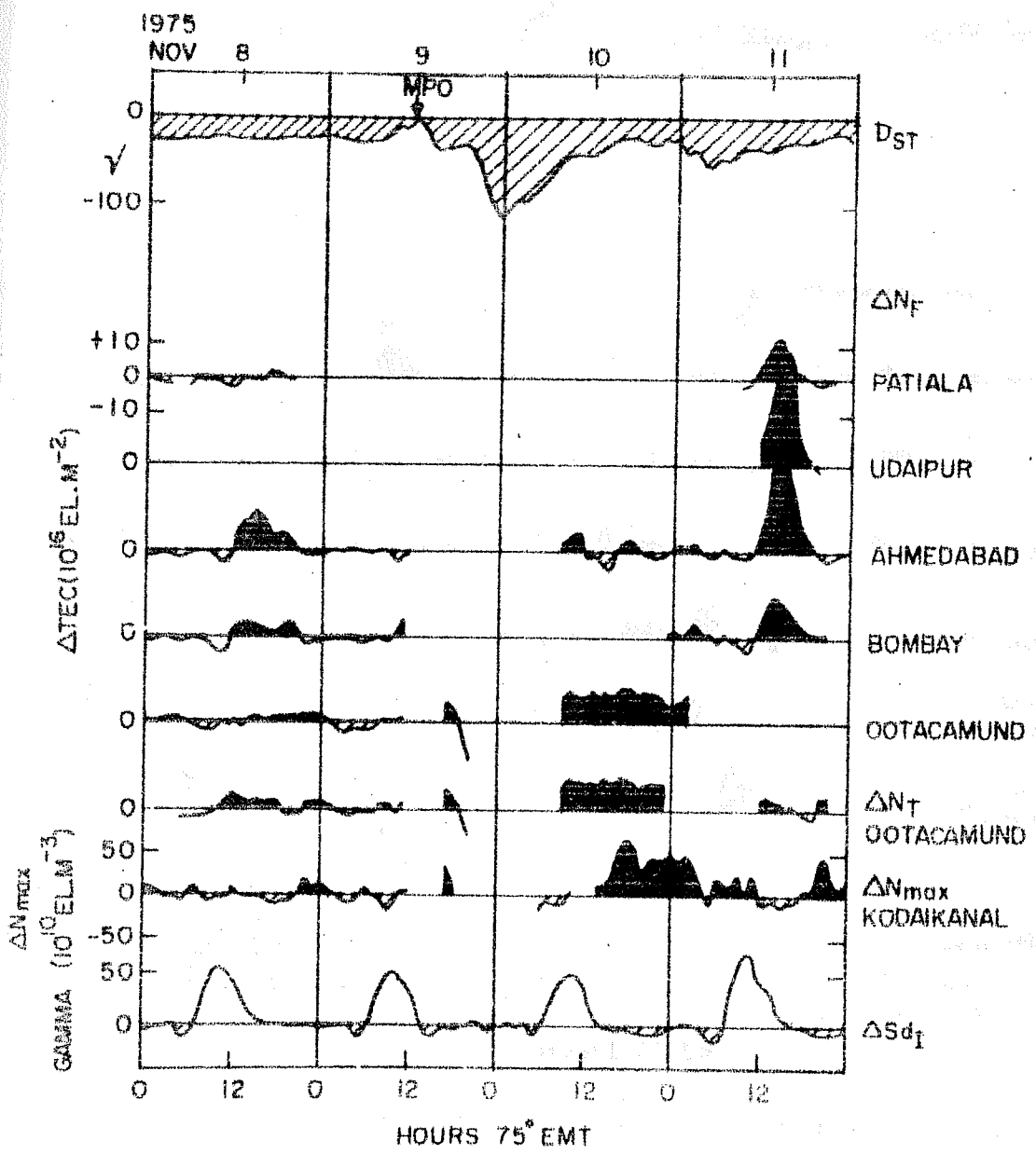

Fig.7.3 Similar to Fig.7.2, for storm period Nov.8-11, 1975.

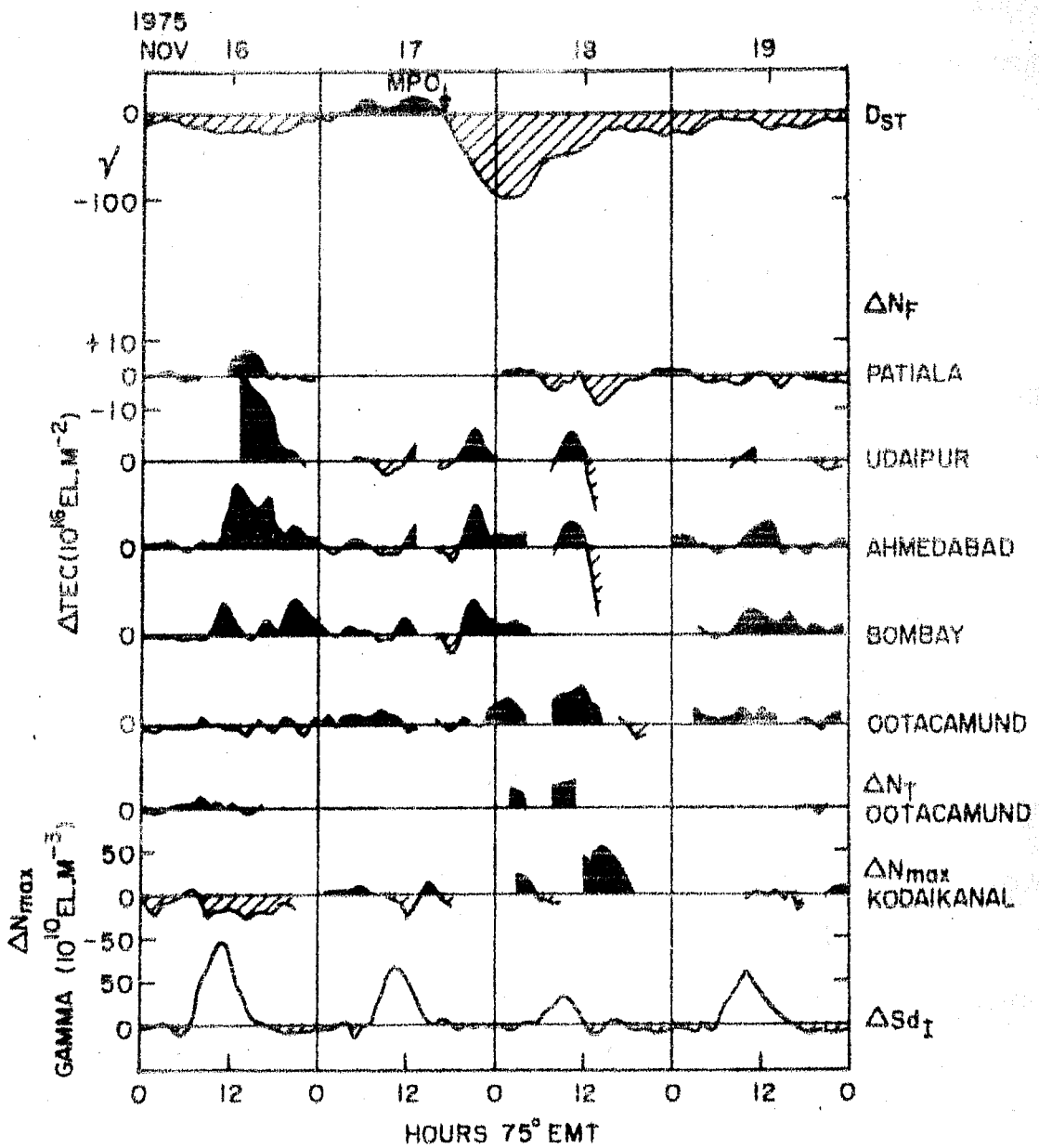

Fig.7.4 Similar to Fig.7.2, for storm period November 16 to 19, 1975.

high (indicating a lack of hite-out) as expected. However, TEC data at the crest are mostly missing, though there is a partial indication of large negative TEC change there. On Nov.19 electrojet is larger and TEC changes at the crest are positive; but N_{max} does not show any change.

Storm of Nov.21-24, 1975 (Fig.7.5):- This has already been depicted in Fig.7.1. The pre-storm day Nov.21 is not very quiet and D_{st} changes of -30 gamma did occur. The equatorial electrojet is strong and N_{max} is negative in the afternoon. So the whole picture is consistent with a strong Fountain effect. On Nov.22, the electrojet is abnormally weak, N_{max} and TEC changes at equator are positive and TEC changes at the crest are large negative. Thus a strong inhibition of the Fountain effect is indicated. If this is to be related to the geomagnetic storm which had an MPO at about 1200 LT on Nov.22, then this would be an example of a negative phase without an earlier positive phase at low latitudes. On the next day, the electrojet is still weak and N_{max} and TEC at equator were positive. But TEC at the crest is also positive, contrary to the expectation of an inhibition of Fountain effect. In contrast, Nov.24 has a strong electrojet, negative N_{max} and TEC change at equator and positive TEC change at the crest.

Storm of Nov.28 - Dec.1 (Fig.7.6):- This is also depicted in Fig.7.1. The TEC changes are large and negative on the afternoon of the pre-storm day Nov.28, not only at the crest but even at

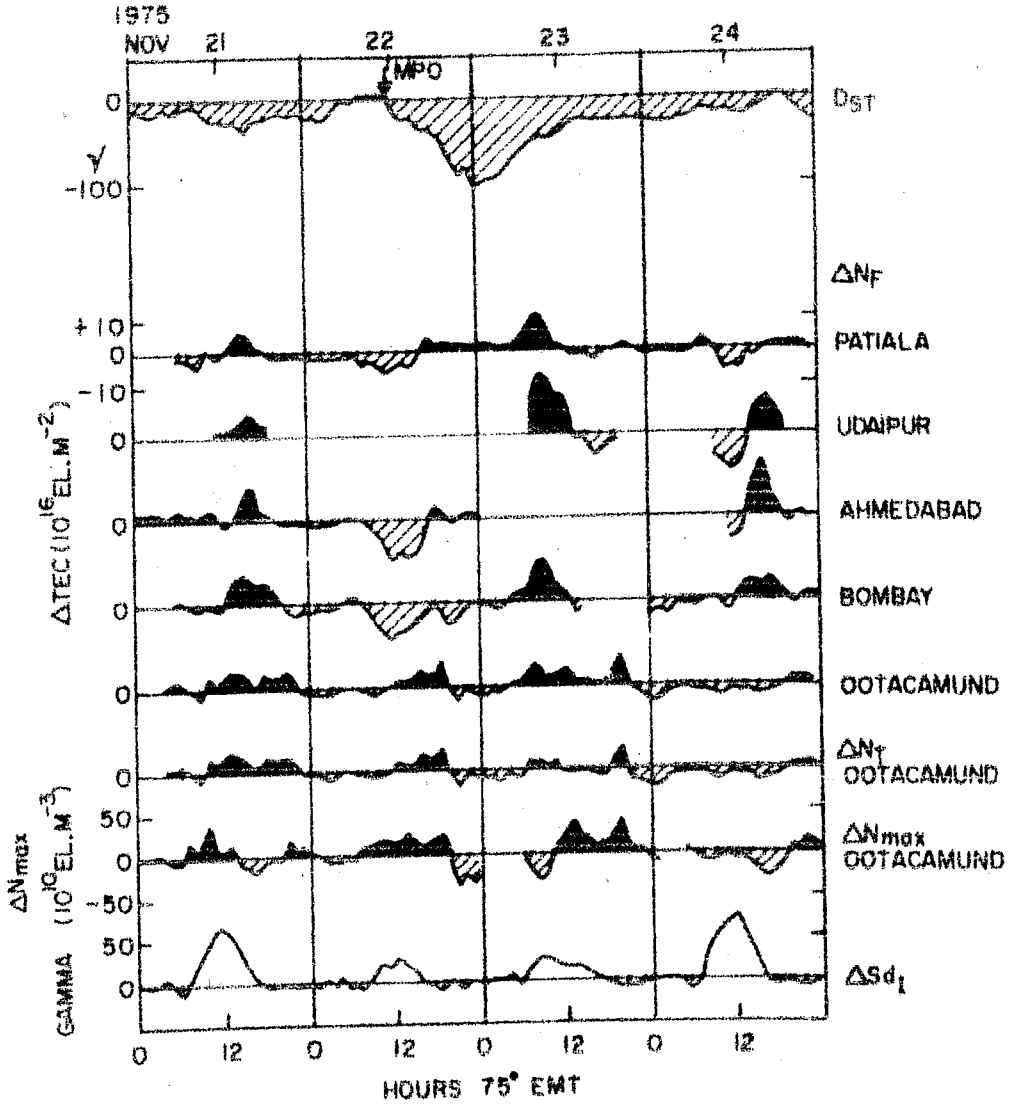

Fig.7.5 Similar to Fig.7.2, for storm period Nov.21-24, 1975.

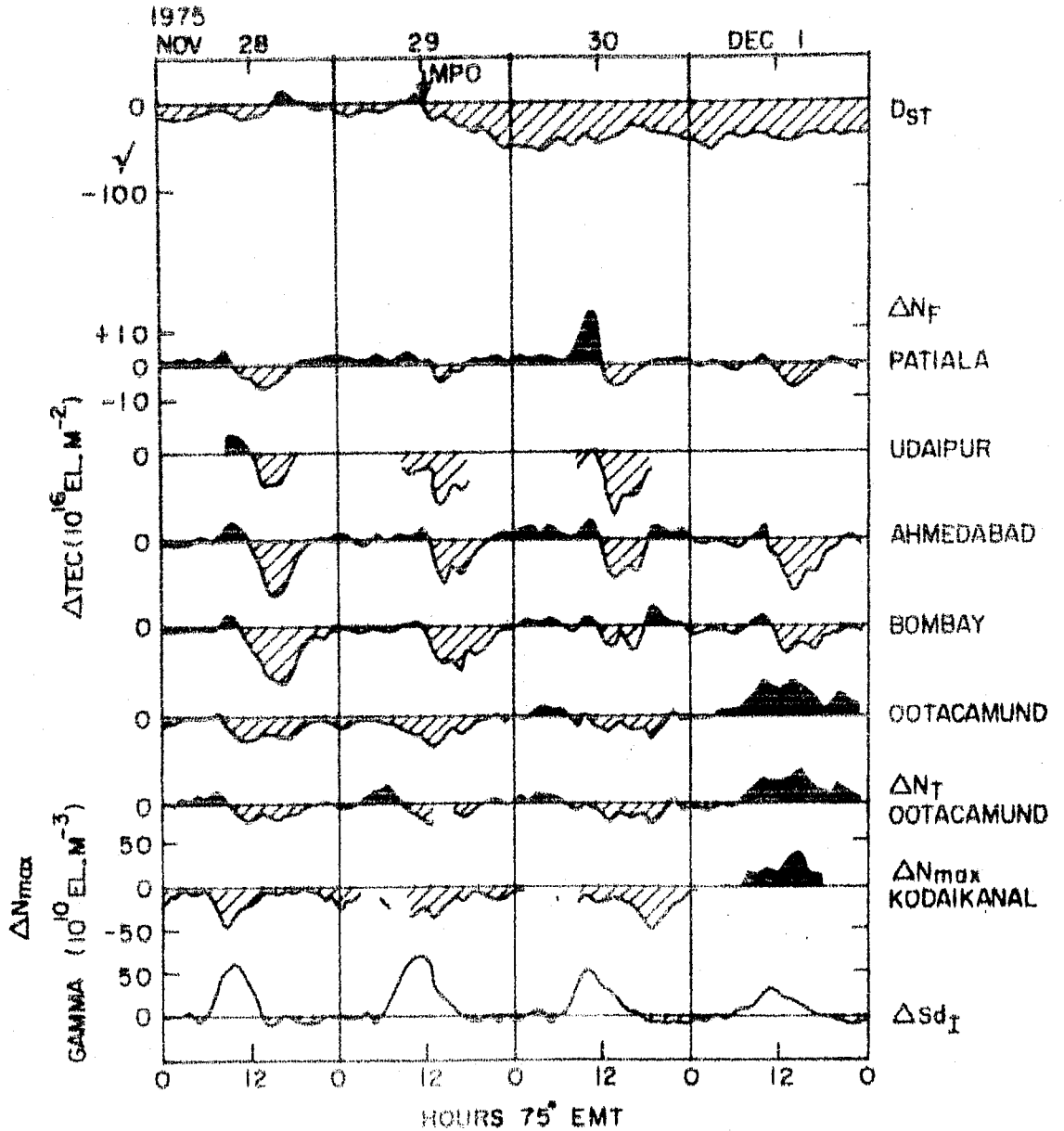

Fig.7.6 Similar to Fig.7.2 for storm period November 28 to December 1, 1975.

equator. On Nov.29, the MPO is at about 1200 LT. TEC changes on Nov.29 were similar to those on Nov.28. The equatorial electrojet is large on both the days. So, Fountain effect should have been operative giving negative N_{max} (and probably TEC) changes at equator which are seen and positive TEC changes at the crest, which are not seen. On Nov.30 too, a similar discrepancy is noticed. On Dec.1, the N_{max} and TEC changes at equator are largely positive, indicating an inhibition of the Fountain effect and the TEC changes at the crest are highly negative as expected. The electrojet on Dec.1 is abnormally weak as expected. On Nov.30, the TEC at Patiala showed a very large positive charge slightly before noon. This feature is not seen at other locations. A check of the data showed no errors.

Storm of Dec.7-10, 1975 (Fig.7.7):- This is a mild geomagnetic storm with D_{st} reaching about -40 gamma only. On Dec.7, a pre-storm day, the electrojet is weak and N_{max} changes at equator are positive as expected. At the crest, negative TEC changes are expected but data are missing. On Dec.8 when a very mild storm has occurred, the electrojet is normal and N_{max} changes are normal at equator. However, TEC changes at equator as well as at the crest are positive, more so at Bombay which is somewhat to the south of the crest. Thus, a movement of the crest towards equator is indicated. On Dec.9, the main storm seems to have started with a MPO before dawn. The electrojet is abnormally weak, N_{max} changes are very large positive at equator as expected and so are the

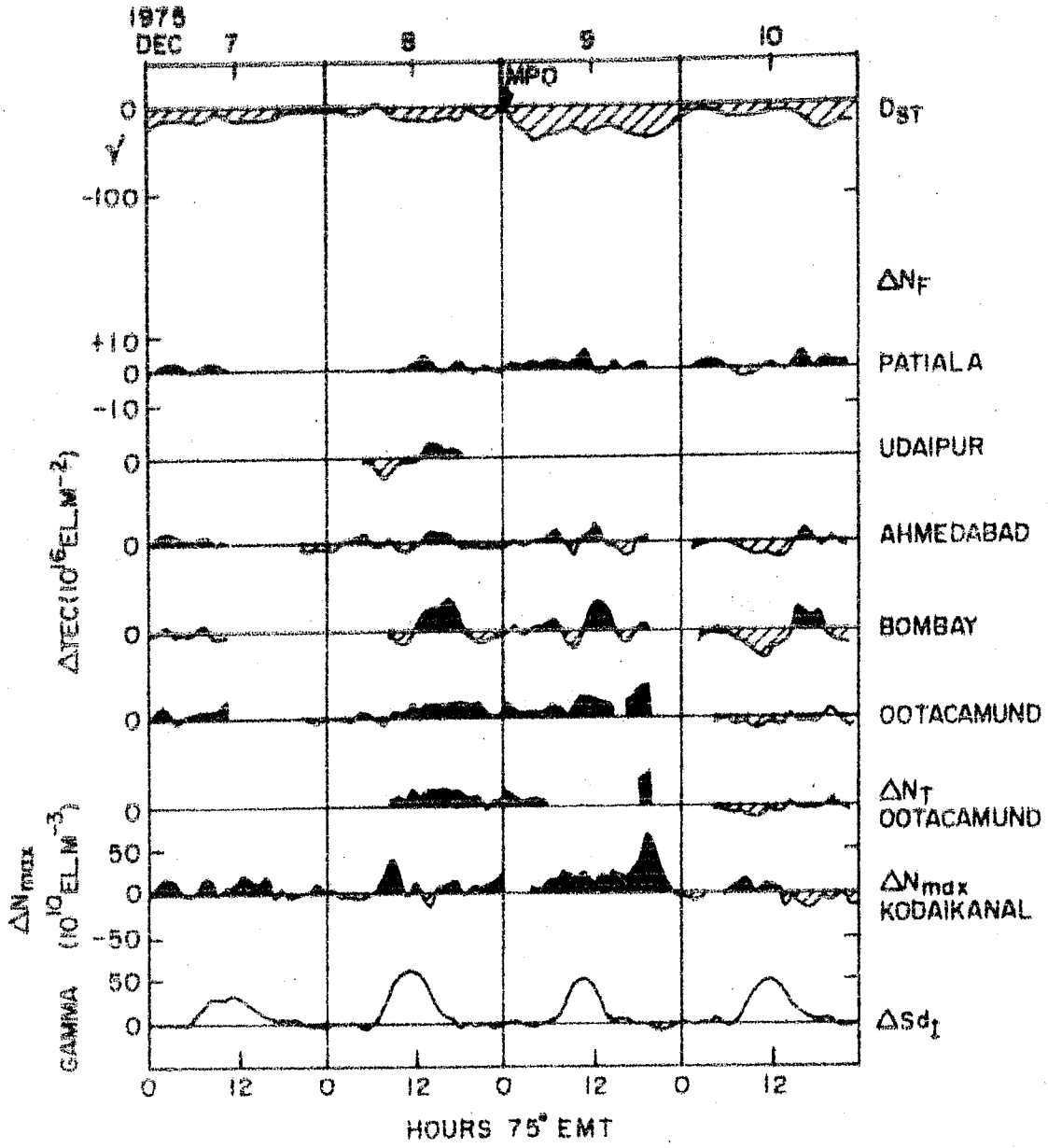

Fig.7.7 Similar to Fig.7.2 for storm period December 7 to 10, 1975.

equatorial TEC changes. However, at the crest, one expects large negative TEC changes. Instead, a peculiar oscillatory structure is noticed. Thus, the normal Fountain effect and/or its inhibition are not seen perfectly. On Dec.10, the main storm has recovered; but a new minor storm seems to have started. The electrojet is strong near noon but was unusually weak in the afternoon. N_{max} and TEC changes at equator are slightly negative; but the TEC patterns at the crest are not just positive as expected but are negative at and before noon and positive in the afternoon. Also, the electrojet pattern is not normal on this day. In the morning, the intensity shows fluctuations and some indication of an inhibition at about 0800 LT. This might have reflected in the TEC changes at the crest as a negative effect. It is to be noted that effects at the crest generally lag behind the equatorial effects by about 2-3 hours (Walker 1973, Iyer et al. 1976).

Storm of Dec. 25-28, 1975 (Fig.7.8):- Dec.25 is a fairly quiet day. The electrojet is normal. No N_{max} data are available; but TEC changes at equator are negative. If these were indications of a strong Fountain effect, the TEC changes at the crest should have been largely positive. Instead, large negative effects are noticed at all low latitudes. This is a case of the Fountain effect pattern not being followed. On the next day (Dec.26), the TEC patterns are again negative at the crest; but this is

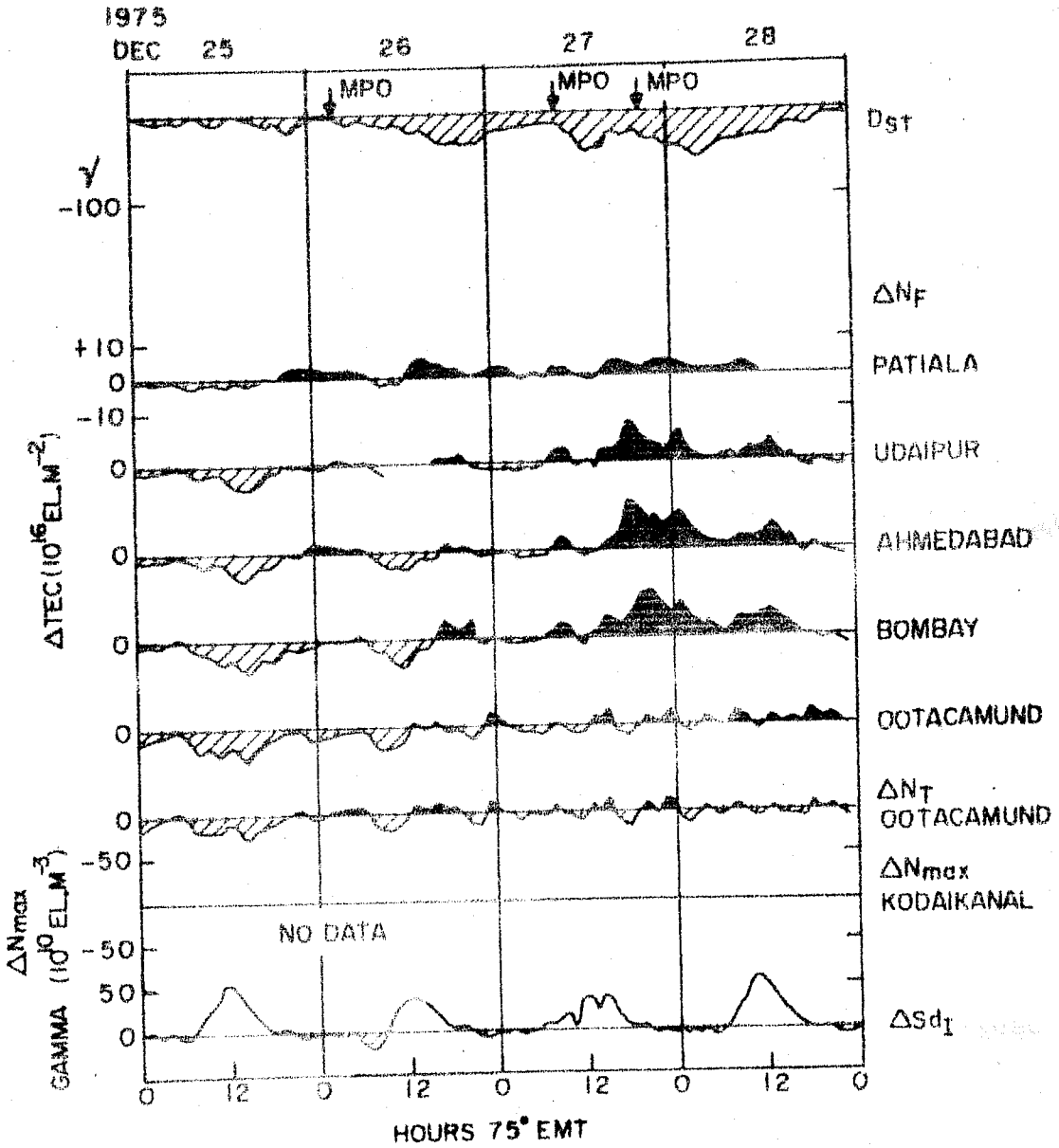

Fig.7.8 Similar to Fig.7.2, for storm period Dec.25-28, 1975.

accompanied by a weakening of the electrojet (in fact, there was a counter-electrojet in the morning). This is in accordance with the Fountain effect. In geomagnetic D_{st}, the period Dec.26-28 seems to show a succession of three small storms. The electrojet is weak and distorted on Dec.27. TEC changes at equator are characterised by small positive and negative fluctuations. But TEC changes at the crest are large positive in the afternoon hours, while these are expected to be large negative due to inhibition of the Fountain effect. Also, the large positive TEC changes extend well upto midnight on Dec.27. On Dec.28, the geomagnetic storm is weak and the small positive TEC changes at the crest are consistent with the strong electrojet.

Storm of Jan. 9-12, 1976 (Fig.7.9):- This is probably the cleanest geomagnetic storm for which TEC data are available. The major storm has an MPO at about 1700 UT on Jan.10. On Jan.9 (pre-storm day), the electrojet is normal. N_{max} data for equator are missing; but TEC changes at equator are negligibly small. If the Fountain effect is supposed to be normal, TEC changes at the crest should have been negligible, or positive. Instead, these are somewhat negative before noon. On Jan.10, the electrojet is normal and TEC changes at equator are negative. The Fountain effect is expected to be normal. But TEC at the crest shows small positive and negative fluctuations. Specifically at Bombay, the TEC changes are definitely negative.

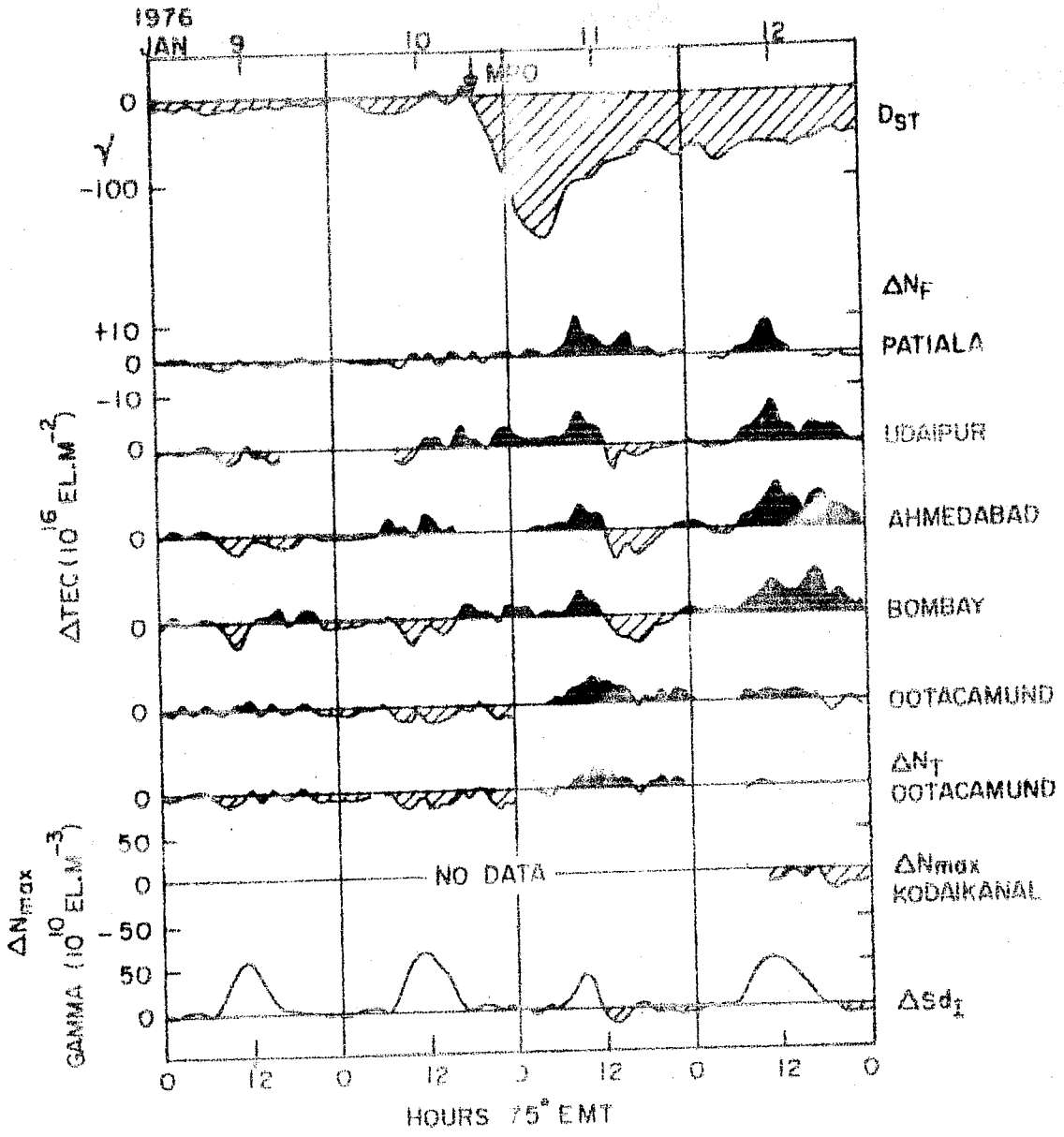

Fig.7.9 Similar to Fig.7.2, for storm period Jan.9-12, 1976.

On Jan.11, the equatorial electrojet is weak and has a counter-electrojet in the afternoon. Thus, the Fountain effect is expected to be inhibited. N_{max} data are not available; but TEC at equator does show positive effects. ΔTEC at the crest is expected to show negative effects. Actually, there is a strong positive phase before noon and a negative phase in the afternoon. On Jan.12, which is in the recovery of the geomagnetic storm, the electrojet is strong and TEC changes at the crest are largely positive as expected.

Storm of May 1-4, 1976 (Fig.7.10):- In contrast to all the earlier storms which are in winter, this is a summer storm. May 1 is a quiet day but probably at the tail-end of the recovery of a small earlier storm in April end. The TEC changes at the crest are large and positive, TEC changes at equator are small (slightly positive) and N_{max} changes are negative before noon and positive afternoon. Almost a similar pattern is observed on May 2 also. The electrojet is strong on both the days but has a counter-electrojet in the afternoon. So, the Fountain effect is seen properly. On May 3, the main storm has started with an MPO at about 0500 LT. TEC at the crest shows very large negative changes while N_{max} and TEC at equator show very large positive changes. The Fountain effect should have, therefore, been highly inhibited. The electrojet does show large counter-electrojets in the morning and afternoon, but the noontime value is not as small as one would

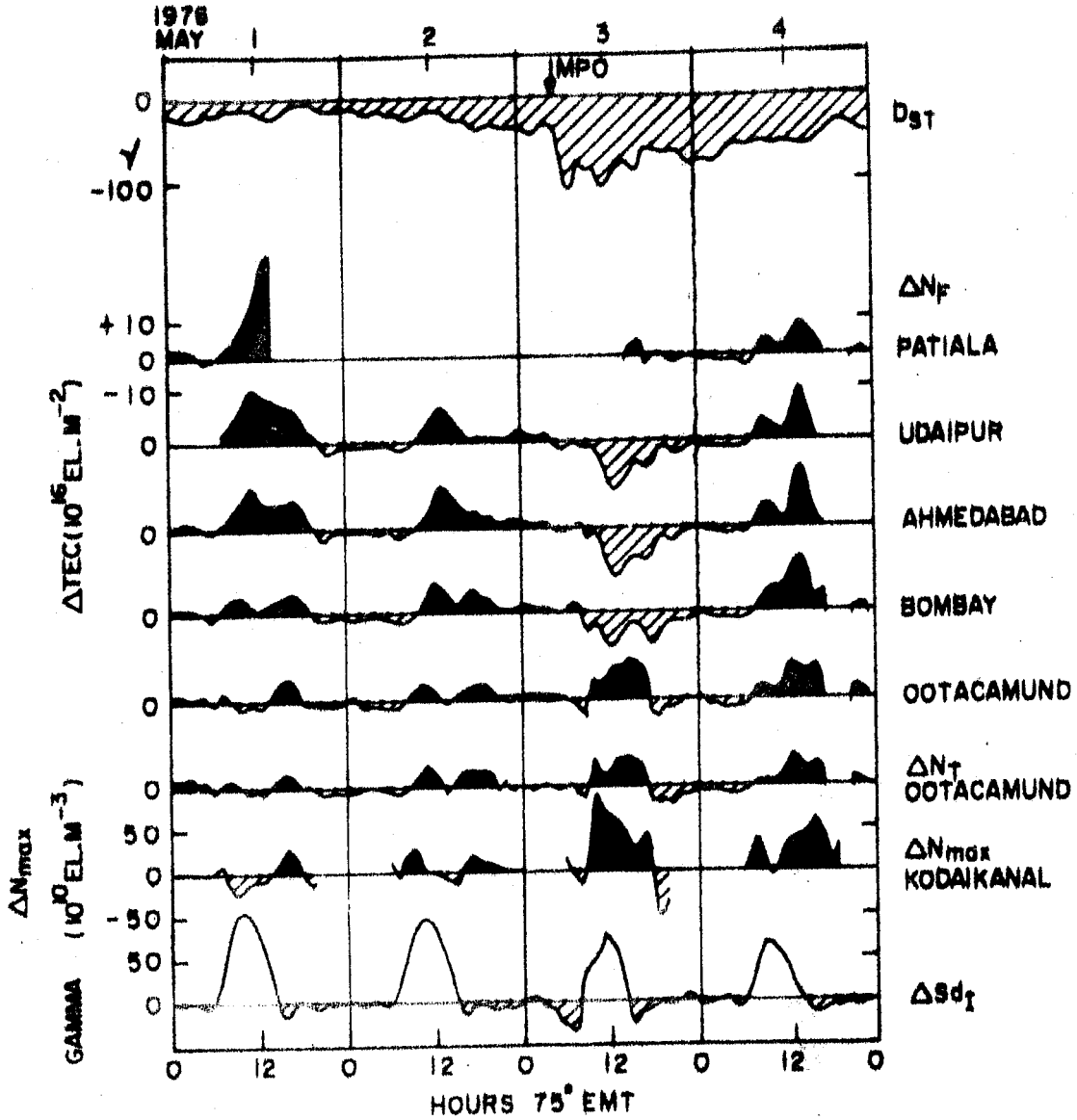

Fig.7.10 Similar to Fig.7.2 for storm period May 1-4, 1976.

have expected. In fact, it is almost as large as on the next day (May 4); but the TEC changes at the crest on May 4 are highly positive, i.e. opposite to those on May 3. It would thus seem that on May 3 in the main phase of the geomagnetic storm, some other complicating factors were interfering with the Fountain effect.

7.2.2 Discussion

There is known to be a large day to day variability in the magnitude and profile of the equatorial electrojet, the f_oF_2 (and hence N_{max}) at equator and TEC at low latitudes (anomaly crest). The precise cause of this variability is not yet been ascertained; but there is a Fountain effect which connects these three; viz. whenever the equatorial electrojet is strong, the vertical Hall polarization field is large, the equatorial f_oF_2 (and N_{max}) shows a noon-time bite-out (negative changes from average) in its daily variation pattern, electrons are convected upwards at equator and later fall back along the magnetic fields to the regions corresponding to the low and middle latitudes anomaly crest, giving positive TEC changes there (the TEC changes at equator may or may not show the f_oF_2 bite-out). If the equatorial electrojet is weak, this Fountain effect is inhibited (i.e. reversed), f_oF_2 (or N_{max}) bite-out disappears, equatorial TEC may or may not show any positive changes, but the TEC at the crest is expected to show a negative change.

This relationship before and during a few selected geomagnetic storms has been investigated in the present study. It is generally believed that during geomagnetic storms, TEC shows an evening increase for stations lying on L shells within the plasmasphere and this is interpreted in the early theories in terms of (i) diffusion of ionization from the magnetosphere into the ionosphere (Mendillo et al. 1970), (ii) convergency of ionization in the dusk sector due to E-W drifts (Papagiannis et al. 1971, Evans 1973) and (iii) lifting of the layer into regions of low recombination rates either by electric fields (Evans 1970, Somayajulu et al. 1971) or equatorward thermospheric winds (Jones and Rishbeth 1971, Obayashi 1972). Presently, it is believed that the lifting of the layer by substorm electric fields is the main cause of this increase (Tanaka and Hirao 1973, Davies and Ruster 1976, Soicher 1976b, Evans 1977). For the large decreases that are often seen, Mendillo et al. (1974) suggested that for middle latitudes, the rapid fall of TEC around sunset could be due to the southward motion of the mid-latitude trough. There are, however, other mechanisms too. Thus, Rishbeth (1975) proposed a storm-circulation theory where auroral zone heating would produce equatorward neutral winds which would initially cause an upward drift of ionization in middle latitudes, thus reducing the loss rates and giving an increase of f_0F_2 (and TEC) but sooner or later, these winds could also change the composition of air and bring in a larger percentage

of molecules and thus increase the loss coefficients which would result in decreases of TEC. However, none of these models can explain how one sees a negative effect without seeing first a positive effect at middle latitudes.

For the equatorial region, several processes are likely to affect the electron density. Firstly, the neutral winds originating from the polar regions would eventually converge on the magnetic equator and would thus oppose the Fountain effect and hence reduce the magnitude of the equatorial anomaly (Burg et al. 1973), and equatorial locations would show positive N_{max} (and probably TEC) changes. The convergence of the winds may also give plasma compression, resulting in increase of equatorial N_{max}. Both these effects would be a positive phase at equator. On the other hand, changes in air composition, in particular an increased molecular/atomic ratio may eventually reach equator too, would increase the loss coefficients and thus reduce the equatorial electron density N_{max} and perhaps TEC also. In addition, if the quiet-time electric field structure at equator is altered during storms, because of some magnetospheric or polar connection, this would affect the Fountain effect in a complicated way.

Earlier results on low and equatorial storms are as follows. Walker (1973) reported for Hong Kong (geomag. lat. 10.9°) that MPOs occurring during daytime are sometimes preceded by a slight increase but often followed by a sharp decrease in TEC and N_{max}.

Kaushik and Madan (1975) reported for Sao Paulo, Brazil (Mag. lat. -20°) a considerable negative effect on storm day. Basu et al. (1975) reported for Honolulu (Mag. lat. 20°) an initial positive phase followed by a long enduring negative phase for TEC as well as N_{max} during summer and only a marked positive phase during summer. Yeboah-Amankwah (1976) reported for Legon for equinox and winter storms a general rise (positive phase) sometimes persisting long after the geomagnetic storm.

From the results presented here the following features are to be noted:--

(1) Results for Faraday rotation method and Group delay method are found to be similar at Ootacamund. It is noticed that large changes in ionospheric TEC at low and equatorial latitudes are often observed even in the pre-storm period and can be at least as large as those observed during storms sometimes even more.

(2) These changes can be positive as well as negative at the crests and when considered in conjunction with the equatorial N_{max} and TEC changes and the changes in the equatorial electrojet strength, give a plausible pattern in many cases, consistent with the Fountain effect. In some cases, other effects seem to interfere with the Fountain effect or its inhibition (i.e. negative Fountain effect).

(3) Negative effects without seeing first the positive effects, are quite common and if interpreted in terms of composition changes (molecular enrichment of air), would imply either a very

rapid transit of neutral winds from poles to equator or a local equatorial turbulance.

In short, SSC, Main phase and recovery which are the striking features of a geomagnetic storm may not be related to an ionospheric storm in a straight forward way. Complex neutral wind motions and penetration of magnetospheric and polar electric fields to equatorial ionospheric region seem to be involved in the ionospheric changes. Normally, the polar regions are supposed to be the source of large scale neutral winds blowing towards equator during storms. It seems that the neutral winds have a considerable random component which causes complications in the ionospheric dynamics of the equatorial region. It would be interesting to study the evolution of ionospheric storms at closeby spaced locations right from poles to equator preferably in the same longitude zone as this would throw considerable light on the actual movements of neutral winds.

7.3 Geomagnetic Storm Time Studies of the Residual Component N_R at Ootacamund

The response of the ionosphere to geomagnetic storms is well documented (Rishbeth 1975 and references therein), although the complex interaction of the various physical mechanisms is not yet fully explained. However, the response of the overlying pleamasphere to geomagnetic activity, a topic important to the understanding of ionosphere-magnetosphere coupling has not been widely studied. In the present section we examine the storm time

behaviour of N_R, taken as a crude estimate of plasmasphere electron content, at Ootacamund for six storms for which we have adequate data.

7.3.1 Storm Time Changes in N_R

Out of the six storms studied, only one occurred in summer and other five in winter. The plots of geomagnetic D_{st} and ΔN_R i.e. deviation of N_R from the monthly median daily variation pattern for all the six storms have been shown separately in Figs.7-11 to 7.13. Each figure contains plots for two storms. For each of the six storms ΔN_R and D_{st} data for two pre-storm and three post-storm days have been examined for the storm effects.

Storm I (Nov.1 - Nov.5, 1975) (Fig.7.11 upper two curves):-

The main phase onset (MPO) is on Nov.2 at about 1600 LT as shown by D_{st} in the top curve. On Nov.1, D_{st} is not fully quiet. There is probably a recovery of a previous storm. MPO is followed by large positive phase in N_R, around midnight hours and then starts the negative phase in ΔN_R, which becomes as large as 4 TEC units (1 TEC unit = 10^{16} el m^{-2}) on Nov.5. N_R has almost recovered on Nov.5 to its monthly mean values whereas the storm is still in the recovery phase as indicated by D_{st}.

Storm II (Nov.21 - Nov. 25, 1975) (Fig.7.11 lower two curves):-

The MPO is around noon on Nov.22. In this storm MPO is not followed by a clear positive phase in N_R but a negative phase in ΔN_R is clearly noticed on Nov.23 and during prenoon hours of Nov.24.

D_{st} as well as N_R have almost recovered in the afternoon hours of Nov.24, but soon after that the storm restarts and almost simultaneously one observes a negative phase in N_R.

Storm III (Nov.28 - Dec. 2) (Fig.7.12 upper two curves):- Large positive phase is observed in ΔN_R on Nov.28 and Nov.29. The storm starts on Nov.29, around noon but no conspicuous changes in N_R follow the MPO on this day. On Dec.1 and Dec.2, large negative phase in ΔN_R is observed; the negative phase being as large as positive phase observed on Nov.28 and Nov.29.

Storm IV (Dec.25 - Dec.29) (Fig.7.12 lower two curves):- This is a complex storm with a number of MPOs. Large positive phase in N_R is observed on Dec.25-26. Negative phase in N_R is observed on Dec.27-29.

Storm V (Jan.9 - Jan.13, 1976) (Fig.7.13 upper two curves:- For this storm, MPO is preceded by a positive phase in N_R and is followed by a negative phase in ΔN_R. The data for post-storm days are discontinuous.

Storm VI (May 1 - May 5, 1976 (Fig.7.13 lower two curves):- This is the only storm which occurred in summer, for which N_R data were available. Small negative as well as positive phases are observed in ΔN_R on May 1 and 2. On May 3, the main storm started with an MPO at about 0500 LT. MPO is immediately followed by a small positive phase and then large negative phase in ΔN_R. The negative phase continues upto May 4 and probably upto May 5.

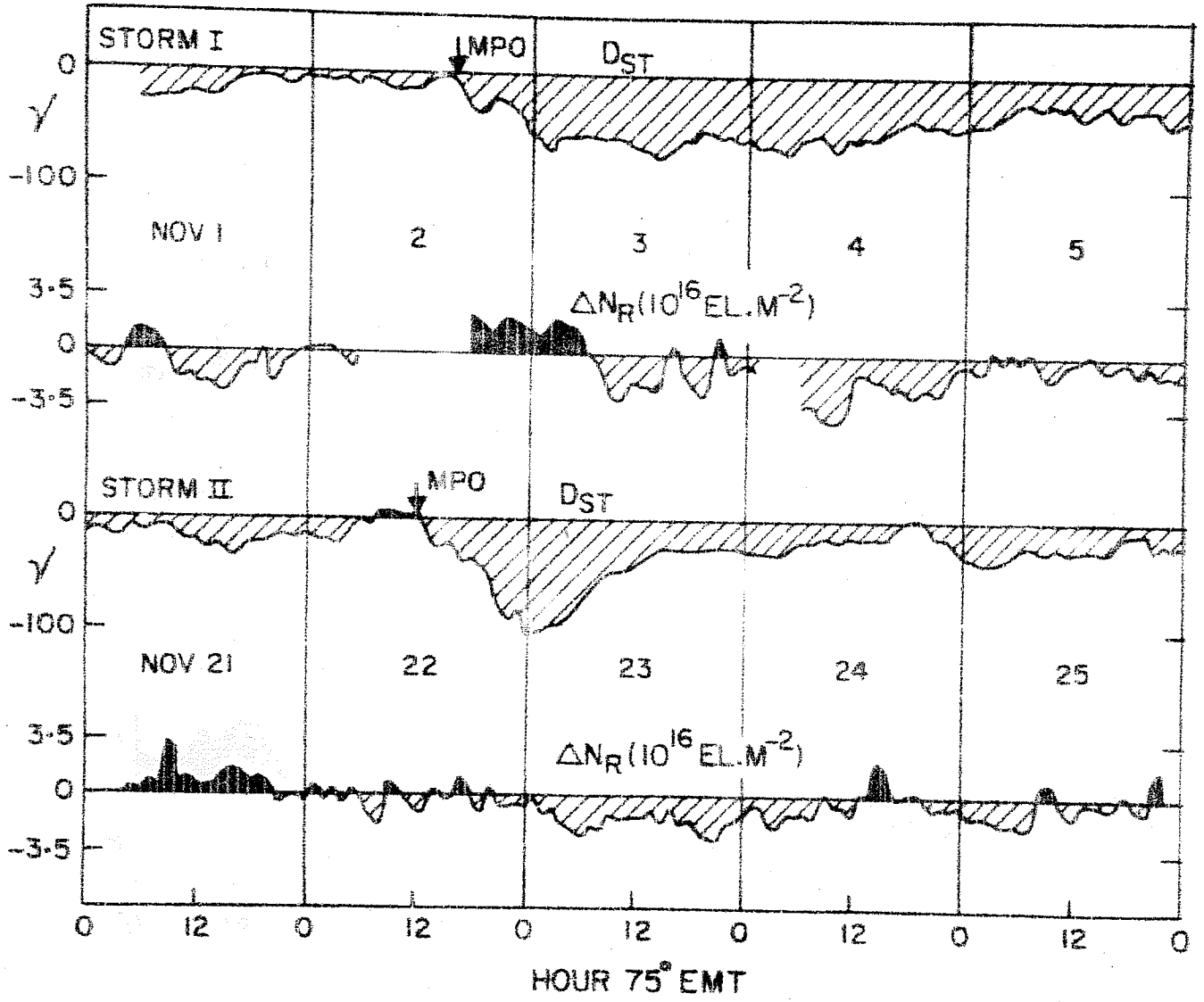

Fig.7.11 The plots of D_{st} and N_R deviations for storm I (Nov.1 to 5, 1975) and storm II (Nov. 21 to 25, 1975).

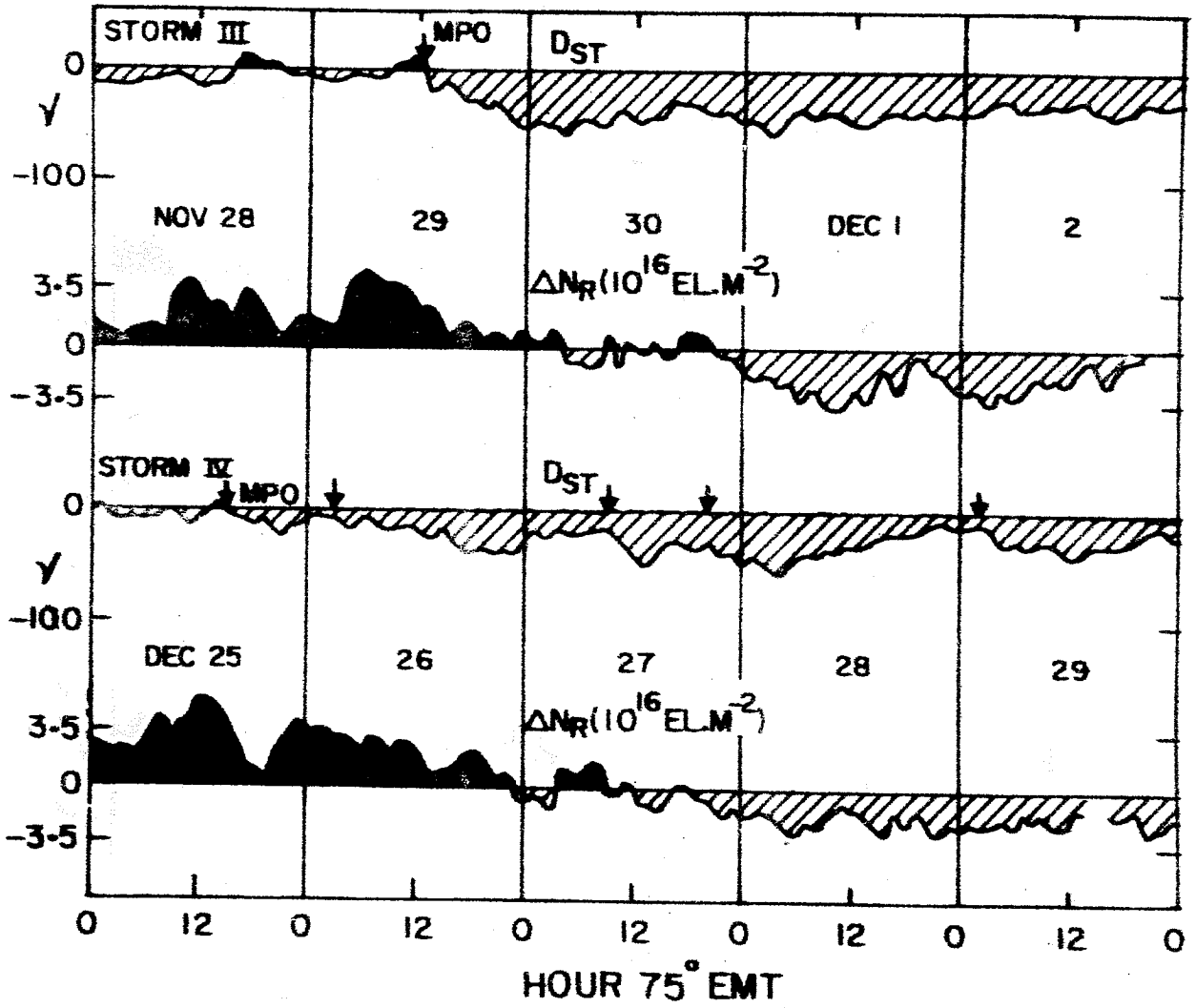

Fig.7.12 Similar to Fig.7.11 for storm III (November 28 to Dec.2,1975) and storm IV (Dec.25 to 29, 1975).

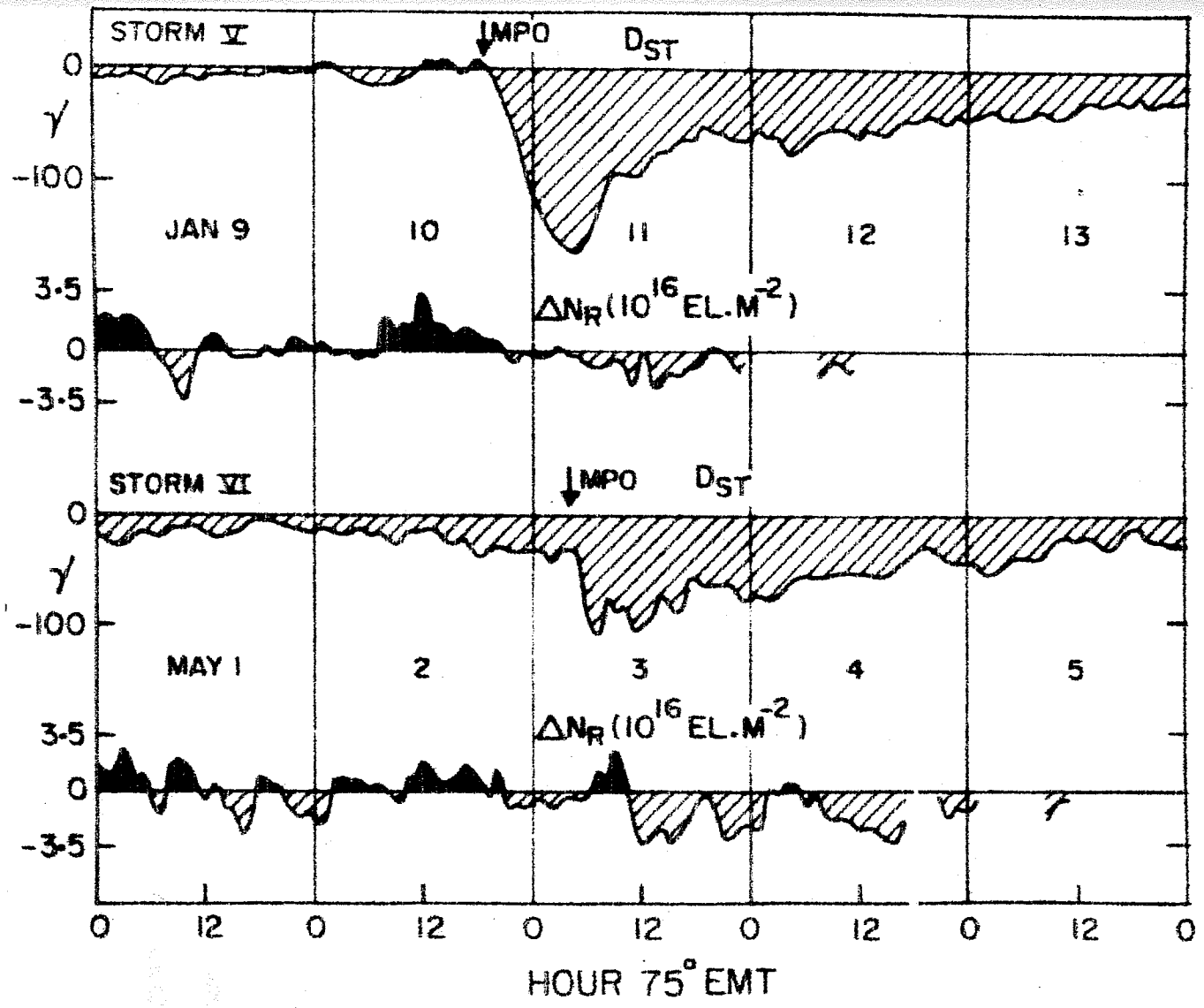

Fig.7.13 Similar to Fig.7.11 for storm V (Jan.9 to 13 1976). and storm VI (May 1 to 5, 1976).

7.3.2 Solar Wind Dependence of N_R During Storm Time

Magnetospheric plasma convection has been reviewed in detail by Axford (1969). A viscous-like interaction between solar wind plasma and magnetic field and magnetic-field-line merging have been suggested as mechanisms producing magnetospheric convection. In either model convection is sustained by down-dusk convection electric field which has been shown to depend on solar-wind speed V_{sw} (Vasyliunas 1968, Mendillo and Papagiannis 1971, Kivelson 1976). Vasyliunas suggested a linear dependence, but Mendillo and Papagiannis estimated that the convection electric field varies nearly quadratically with solar wind speed - this conclusion was supported by Kivelson. The convection electric field and hence solar wind speed have important roles in determining the location of plasmapause (Brice 1967, Nishida 1966). Model calculations assuming enhancement of the solar wind speed showed the plasmapause everywhere to be located at smaller L coordinates (Grebowsky 1971) (L is the McIlwain (1961) magnetic shell number). The location of the dusk-side bulge of the plasmapause has been shown to be inversely related to the solar wind speed (Mendillo and Papagiannis 1971). The residual electron content (N_R) is supposed to increase with increase in L (the plasmapause position) the rate of increase being dependent on the density distribution assumed and the L values under consideration (Webb and Lanzerotti 1977). Thus one expects an increase in N_R to be associated with a decrease in V_{sw} and vice versa. This possibility has been examined using N_R data during two magnetic

storms associated with large changes in V_{sw} and for which N_R and V_{sw} data are available simultaneously. The daily mean N_R values for the pre-storm and during storm days are compared with the corresponding solarwind speeds in Table 7.1. For the first storm the pre-storm solar wind data are not available for the first day. Solar wind speeds have been plotted against mean daily N_R for the corresponding day in Fig.7.14. All three pre-storm days have large mean N_R values but low solar wind speeds ($\sim$400 kms^{-1}) whereas during storm solar wind speeds were greater by a factor of 1.5 with mean daily N_R correspondingly decreased. This is the first experimental evidence confirming an inverse relationship between residual electron content N_R and solarwind speed V_{sw}. The correlation coefficient between N_R and the V_{sw} is -0.92 ± 0.05. A linear relationship between N_R and V_{sw} is obtained by the least square method and is given by:

$$N_R = 12.5 \left(1 - \frac{V_{sw}}{1000} \right) \qquad (7.1)$$

where V_{sw} is the solar wind speed in kms^{-1} ($V_{sw} < 750$ km).

7.3.3 Geomagnetic Activity Dependence of N_R

It is known that the night-side of the plasmasphere reacts very quickly (in 2-6 hours) and very predictably to changes in magnetic activity, so that day-side plasmapause position is thought to be determined by the level of magnetic activity present during its earlier corotation through the formative night-side region (Chappell 1972, Carpenter and Park 1973, and the references

Table 7.1

Comparison of pre-storm and during-storm residual electron content and solar wind speed

Storms	MPO	Maximum D_{st}( )	Days	V_{sw} (kms^{-1})	Daily mean $N_R \times 10^{16}$ electrons m^{-2}
1-5 Nov. 1975	2 Nov. 1100 UT	-76	1* Nov.	-	4.5
			2*	430	7.0
			3	650	4.6
			4	750	2.5
			5	640	4.2
28 Nov.- 2 Dec. 1975.	29 Nov. 0700 UT	-53	28* Nov.	350	6.7
			29*	475	7.3
			30	625	4.7
			1 Dec.	675	3.8
			2	725	4.2

MIO is the main phase onset; D_{st} is the ring current intensity index.

*Pre-storm days.

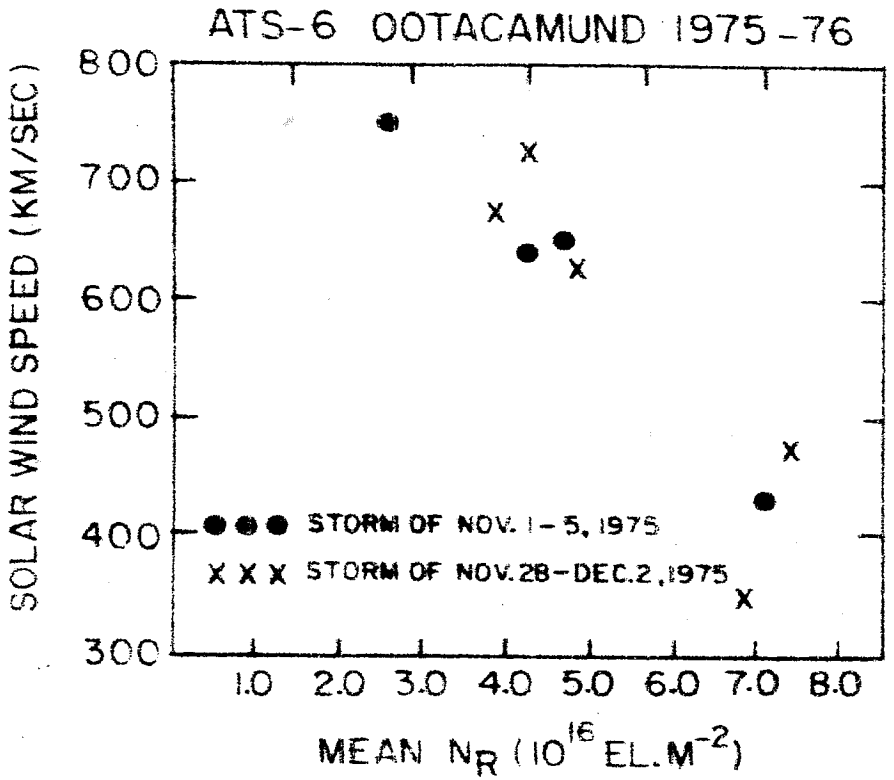

Fig.7.14 Solar wind speed plotted against daily mean N_R for the two storms.

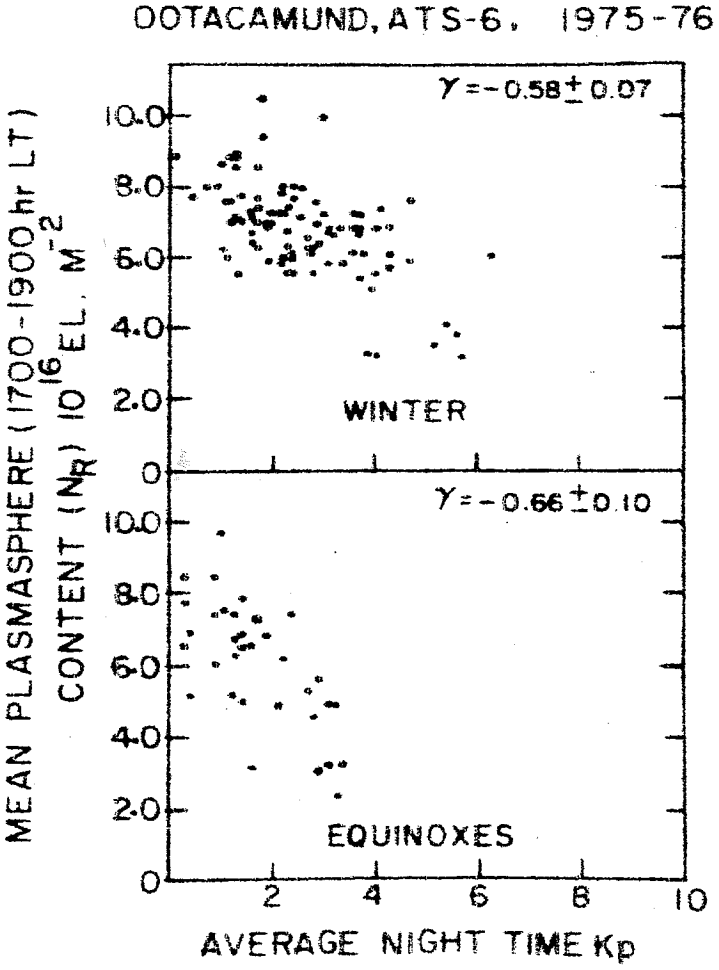

Fig.7.15 The mean peak values of N_R plotted against average night time three hourly K_p for winter and equinoxes.

therein). An attempt was therefore made to correlate the daytime values of N_R for different hours and the average night-time K_p. It is found that the peak value of N_R around 1800 hr LT_{sp} (sub-plasmasphere local time) correlates negatively (with correlation coefficient around 0.6) with average three hourly values of K_p of the previous night whereas N_R at other hours shows negative correlation of less than 0.5. The mass plots for the mean peak value of N_R and the average night-time three hourly K_p for winter and equinoxes are shown in Fig.7.15. The peak value of N_R has been taken as the mean N_R during 1700-1900 hr LT_{sp}. The correlation coefficients are -0.58 and -0.66 for winter and equinoxes respectively. For summer months beacon was off during 1800-2100 hr LT. The linear relationships between K_p and N_R are obtained by the least square method and are given by the equations:

$$\text{Winter}: \quad N_R = 8.5 \left(1 - \frac{K_p}{12.2} \right) \quad (K_p = 0\text{-}6) \qquad (7.2a)$$

$$\text{Equinoxes}: \quad N_R = 7.8 \left(1 - \frac{K_p}{7.0} \right) \quad (K_p = 0\text{-}4) \qquad (7.2b)$$

In the past, various statistical correlations have been made between magnetic activity and the equatorial plasmapause positions. Carpenter (1967) and Rycroft and Thomas (1970) both used whistler observations of the plasmapause and attempted correlations with geomagnetic activity at the times of measurements. Orr and Webb (1975) have considered the plasmapause position to be determined by the geomagnetic activity (K_p = 0-4)

in the night-time region; the boundary formed there corotates into the day-side where geomagnetic activity has little effect (Chappell et al. 1971). Using data from satellite studies of the plasmapause by Chappell et al. (1970), Orr and Webb (1975) took values of the average night-time K_p index (2100-0600 hr LT) and found a relationship between this index and the plasmapause at 0200 hr LT given by:

$$L_{pp} = 6.52 - 1.44\ K_p + 0.18\ K_p^2 \qquad (7.3)$$

where K_p is the range 0-4 and the data are scattered over $\pm$ 0.4 R_E (the rms value of the residuals).

The position of the plasmapause at any other local time was then taken to be directly related to the average daily variation of the plasmapause position as given by Chappell et al. (1971).

In the present investigations K_p ranges between 0 and 4 for equinoxes (see equation 7.2b), hence one can eliminate K_p using (7.2b) and (7.3) so as to obtain a relationship between N_R and L_{pp}, which is found to be as:

$$L_{pp} = 5.26 - 0.97\ N_R + 0.14\ N_R^2 \qquad (7.4)$$

where L_{pp} is plasmapause position at 0200 hr LT and N_R is the mean peak value of residual electron content in units of 10^{16} el m^{-2}, around 1800 hr LT.

7.3.4 Discussions

The storm time behaviour of N_R has recently been studied by Soicher (1976a), Kersley et al. (1978b), Poletti-Liuzzi et al. (1977) and Degenhardt et al. (1977). In these studies, it was observed that N_R shows a positive phase following SC (storm commencement) and then after some hours, it shows a negative phase followed by slow replenishment. Soicher (1976) interpreted the positive phase in terms of lifting of the ionization to the regions of reduced recombination, so as to increase N_F as well as N_T, but N_F at a slower rate since some of the ionization moves to the plasmaspheric regions, and is not accounted by N_F. The negative phase of N_R during magnetic storm is understood in terms of drop in ionospheric electron content and peak density as reported by many workers. With the reduced values of the ionospheric densities, the plasmasphere is depleted by downward fluxes, which seek to maintain hydrostatic equilibrium in the topside ionosphere (Soicher 1976). The role of enhanced magnetospheric convection in moving the plasmapause inward, and thereby decreasing N_R, was also suggested by Poletti-Liuzzi (1977) and Kersley et al. (1978). This possibility has been re-examined in light of solar wind speed dependence of N_R, as described in section 7.3.2. For two (I and III) of the storms, for which simultaneous solar wind measurements were available, it was noticed that decrease in N_R is associated with enhancement in solar wind speed and vice versa.

CHAPTER - VIII

NUMERICAL MODELS FOR LOW LATITUDE IONOSPHERE TEC (N_F)

8.1 Introduction

The exact amount of the time delay caused by the free electrons in the earth's ionosphere is essential for many disciplines viz. those who require error correction for UHF radars, geostationary satellite navigation systems, satellite tracking stations using VHF beacons, and radio astronomers who are attempting to measure accurate positions and distances by means of very long base line interferometry. As a result of all this interest several models of TEC have been made by different groups (Wright 1967, Klobuchar and Allen 1970, Klobuchar 1973). Most of these models have been constructed using a limited data base, hence the applicability both in geographical extent and in time in the solar cycle is limited.

Numerical models of ionospheric TEC (N_F) for low latitudes have recently been constructed by Klobuchar et al. (1977) using data from the orbiting satellites. In such models, the temporal resolution is limited hence an attempt has been made to model the ionospheric TEC using data from the geostationary satellite ATS-6 as described in section 3.3.3. The data used are of the period Oct. 1975 - July 1976 which is a low solar activity period with solar flux around 70-75 units.

8.2 Model Construction

The seasonal TEC contours, which have been prepared on a local time (75° EMT) versus latitude grid, extend from 2°N to about 25°N dip latitude, and are given in Fig.3.5 (a,b,c) of Chapter-III. The hourly values of TEC are scaled from these contours at 2°N dip latitude interval and a Fourier time series expansion of harmonic number 4 was made to each latitude set. A least square third degree polynomial was then fitted to each Fourier coefficient over the latitude range from 2° to 25°. The resultant coefficients equal 36 in number; one set of 4 polynomial coefficients to represent the latitude dependence of each of the 9 Fourier terms. Thus, a set of 36 numbers specify the seasonal mean TEC behaviour over the latitude range 2°-25°N. These coefficients for all the three seasons are given in Table 8.1. All that is necessary to obtain a value of TEC is to use the coefficients for the season desired, and to specify a latitude and local time. The model can be expressed in the following form (Klobuchar, 1973):

$$TEC = DC + 2 \sum_{i=1}^{4} C_i \cos (it - 2\pi \phi_i/24) \qquad (8.1)$$

where DC, C and $\phi = Ko + \sum_{j=1}^{3} K_j \, (lat)^j$

for the appropriate DC, C_i or ϕ_i term.

The rms deviation of the values so obtained from the observed values from which the model is constructed, is less than one TEC unit (10^{16} el.m^{-2}). The seasonal contours using the model

Table 8.1

Seasonal Coefficient set

Winter

	Constant	X	X^2	X^3
DC	0.115E 02	0.841E 00	-0.714E-01	0.117E-02
C1	0.759E 01	0.111E 01	-0.699E-01	0.907E-03
C2	0.202E 03	0.308E 01	-0.162E 00	0.131E-02
C3	0.218E 01	-0.583E-01	0.154E-01	-0.557E-03
C4	-0.510E 01	0.709E 01	-0.187E 00	-0.179E-02
PHI 1	0.131E 01	-0.156E-01	-0.365E-02	0.102E-03
PHI 2	0.325E 02	0.163E 02	-0.176E 01	0.439E-01
PHI 3	0.794E 00	-0.107E 00	0.940E-02	-0.230E-03
PHI 4	0.115E 03	0.147E 02	-0.965E 00	0.187E-01

Summer

	Constant	X	X^2	X^3
DC	0.114E 02	0.165E 00	-0.310E-02	-0.211E-03
C1	0.119E 02	0.500E-01	0.886E-02	-0.608E-03
C2	0.205E 03	0.102E 01	-0.415E-02	-0.113E-02
C3	0.706E 00	-0.281E-01	0.190E-01	-0.626E-03
C4	0.116E 03	-0.564E 01	0.352E 00	-0.929E 02
PHI 1	0.236E 01	-0.181E 00	0.882E-02	-0.167E-03
PHI 2	0.255E 02	0.120E 02	-0.124E 01	0.296E-01
PHI 3	0.872E 00	-0.828E-01	0.404E-02	-0.546E-04
PHI 4	0.310E 03	0.384E 02	-0.460E 01	0.110E 00

Equinoxes

	Constant	X	X^2	X^3
DC	0.168E 02	0.107E 00	-0.184E-03	-0.499E-03
C1	0.152E 02	0.546E-01	0.417E-01	-0.188E-02
C2	0.212E 03	0.136E 01	-0.874E-01	0.765E-03
C3	0.326E 01	-0.485E 00	0.718E-01	-0.199E-02
C4	0.135E 02	0.660E 01	-0.239E 00	0.947E-03
PHI 1	0.308E 01	-0.369E 00	0.183E-01	-0.270E-03
PHI 2	0.124E 03	-0.448E 02	0.503E 01	-0.119E 00
PHI 3	0.485E 00	-0.307E-01	0.129E-02	0.146E-04
PHI 4	0.198E 03	0.106E 02	-0.154E 01	0.387E-01

coefficients are shown in Fig.8.1 (a to c). One notices an excellent reproduction of the experimental contours.

8.3 Comparison with Previous Models Obtained from Orbiting Satellite Data

The data used for the present model construction are for the period 1975-76, which is a low solar activity period. The 10.7 cm flux for the different months and their seasonal averages are given in Table 8.2. The flux is found to be around 70-75 units. Hence one can compare the present model with the model for the low solar activity period (1964-66) with solar flux values around 70 units, reported by Klobuchar et al. (1977). The daytime TEC values for summer, winter and equinoxes are of the order of 30, 30 and 50 TEC units respectively whereas the present contours give the values 25, 25 and 40 TEC units respectively. The night-time values are also found to be more by 5 TEC units in the studies of Klobuchar et al. (1977). It is to be noted that, on the average, the number of observations for each hour for each season is about 5 in their contour building (Rastogi et al. 1975, 1977) whereas in the present study the number of observations is atleast 10 times more and therefore, the values are much more reliable. The error in the model fitting of the original data was estimated to be around 10% in the studies of Klobuchar et al. (1977) but in the present study, the errors involved are considerably less ($< 3\%$).

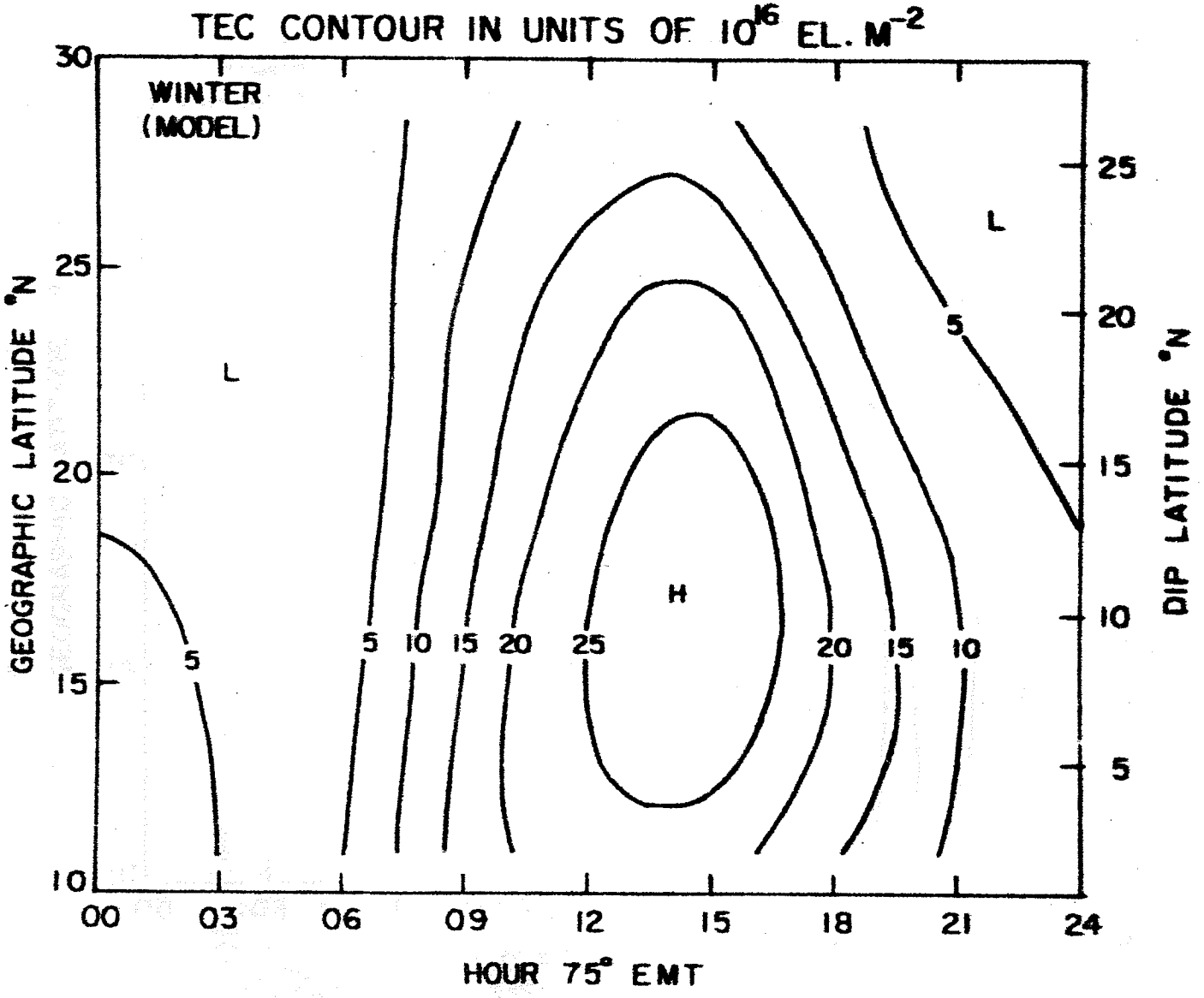

Fig.8.1a The N_F contour using model coefficients for winter (low solar activity period).

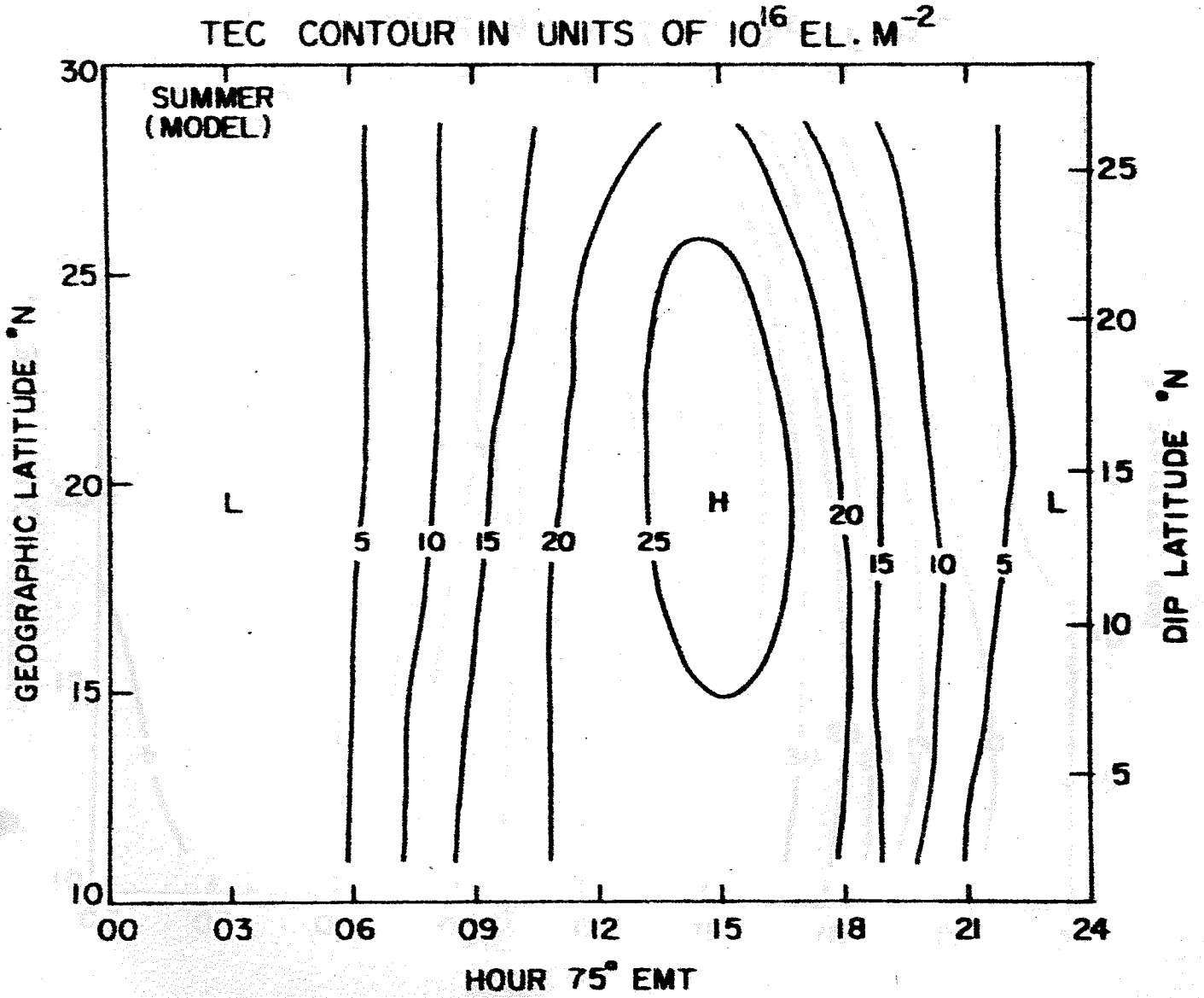

Fig.8.1b Similar to Fig.8.1a for summer.

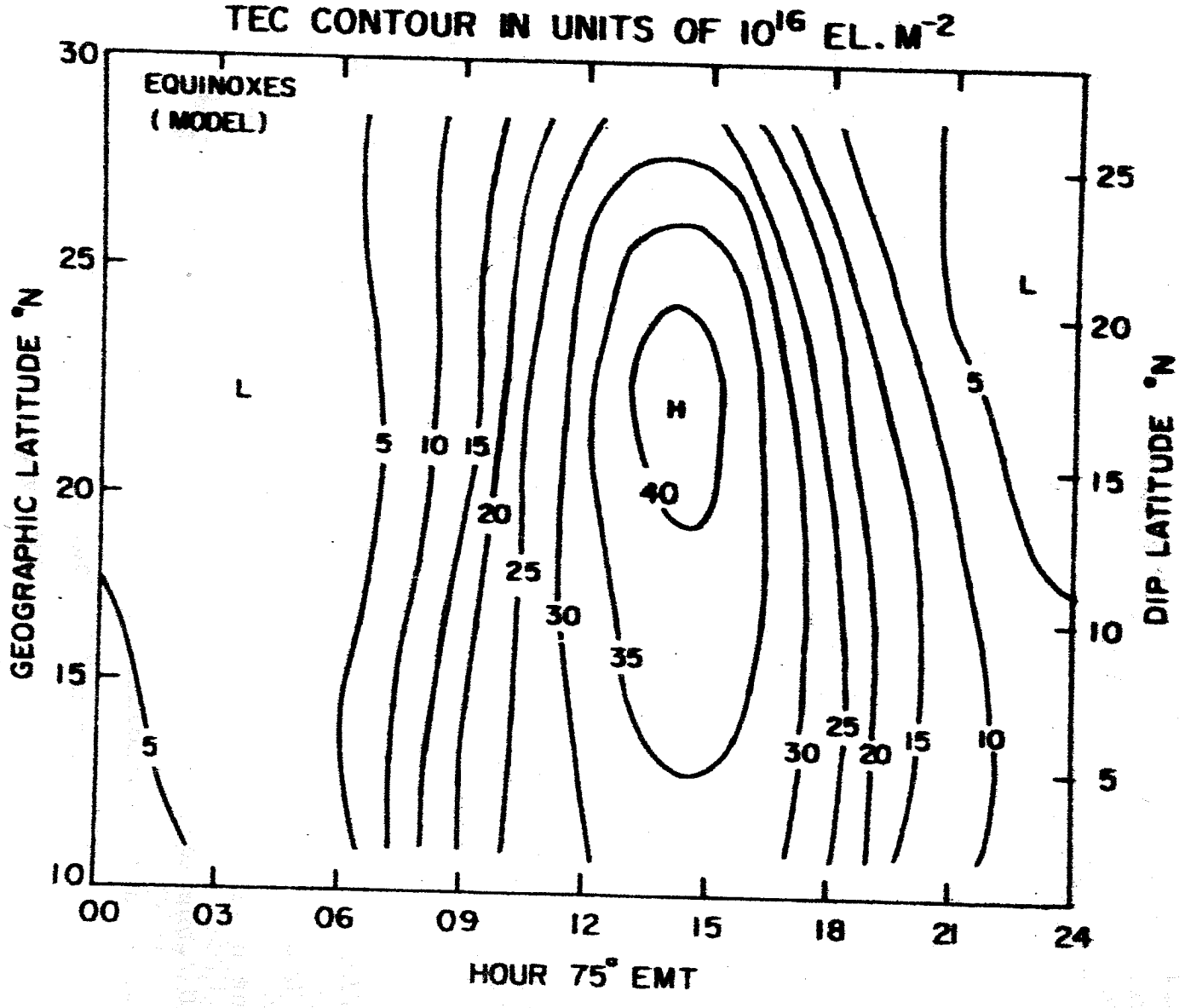

Fig.8.1c Similar to Fig.8.1a for equinoxes.

Table 8.2

Seasonal Solar Flux

Season	Month	10.7 cm solar flux.	Mean seasonal solar flux.
Winter 1975-1976	Nov.	80.8	75.1
	Dec.	74.6	
	Jan.	74.7	
	Feb.	70.5	
Summer 1976	May	70.6	69.6
	June	70.6	
	July	67.5	
Equinoxes 1975-1976	Oct.	75.6	76.1
	Mar.	76.6	
	April	76.2	

8.4 Extension of the Model for Medium and High Solar Activity Periods

The numerical models for ionospheric TEC for low as well as high solar activity periods, were given by Klobuchar et al. (1977) using orbiting satellite data. These contours can be used to get the slope with which the TEC varies with solar flux in a season for given values of the local time and the dip latitude. Using the slopes, so obtained, the seasonal contours of the present study are extended for medium (solar flux value 100 units) and high (200 units) solar activity periods. These are shown in Fig.8.2 (a-c) and Fig.8.3 (a-c). These contours can be utilised for estimating the errors for the satellite tracking systems. The details have been described in the following section.

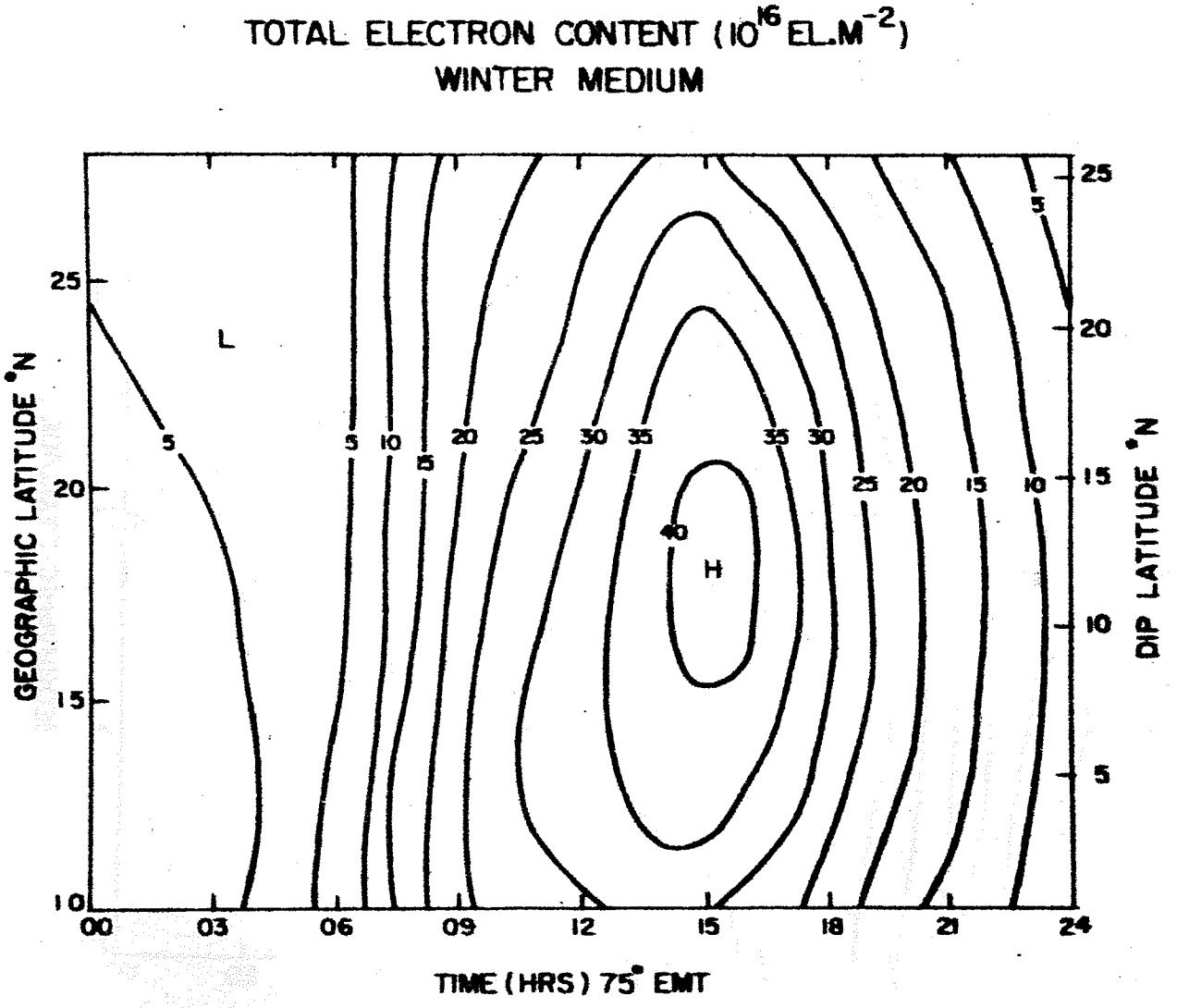

Fig.8.2a The N_F contour using the extended model for winter (medium solar activity period).

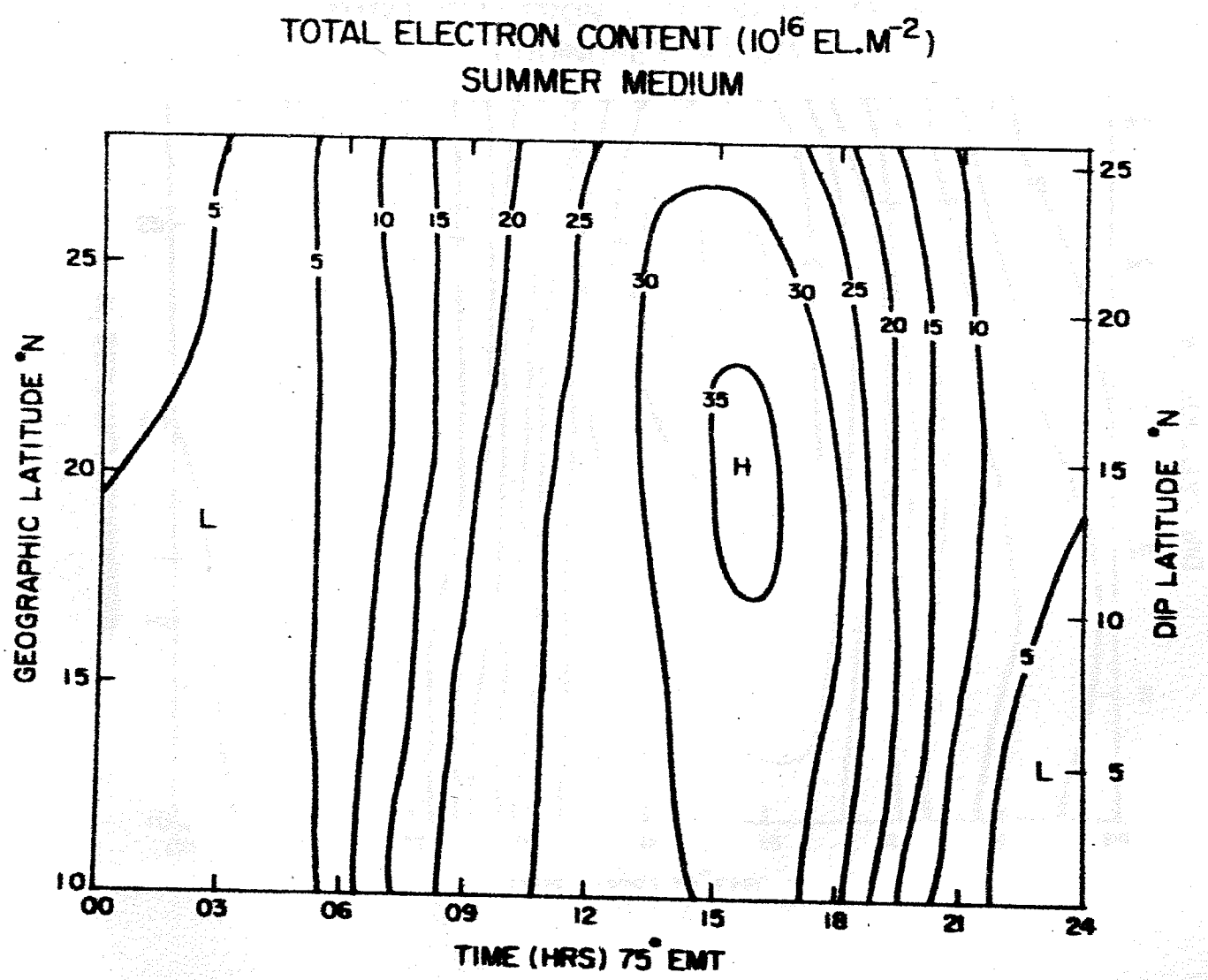

Fig.8.2b Similar to Fig.8.2a for summer.

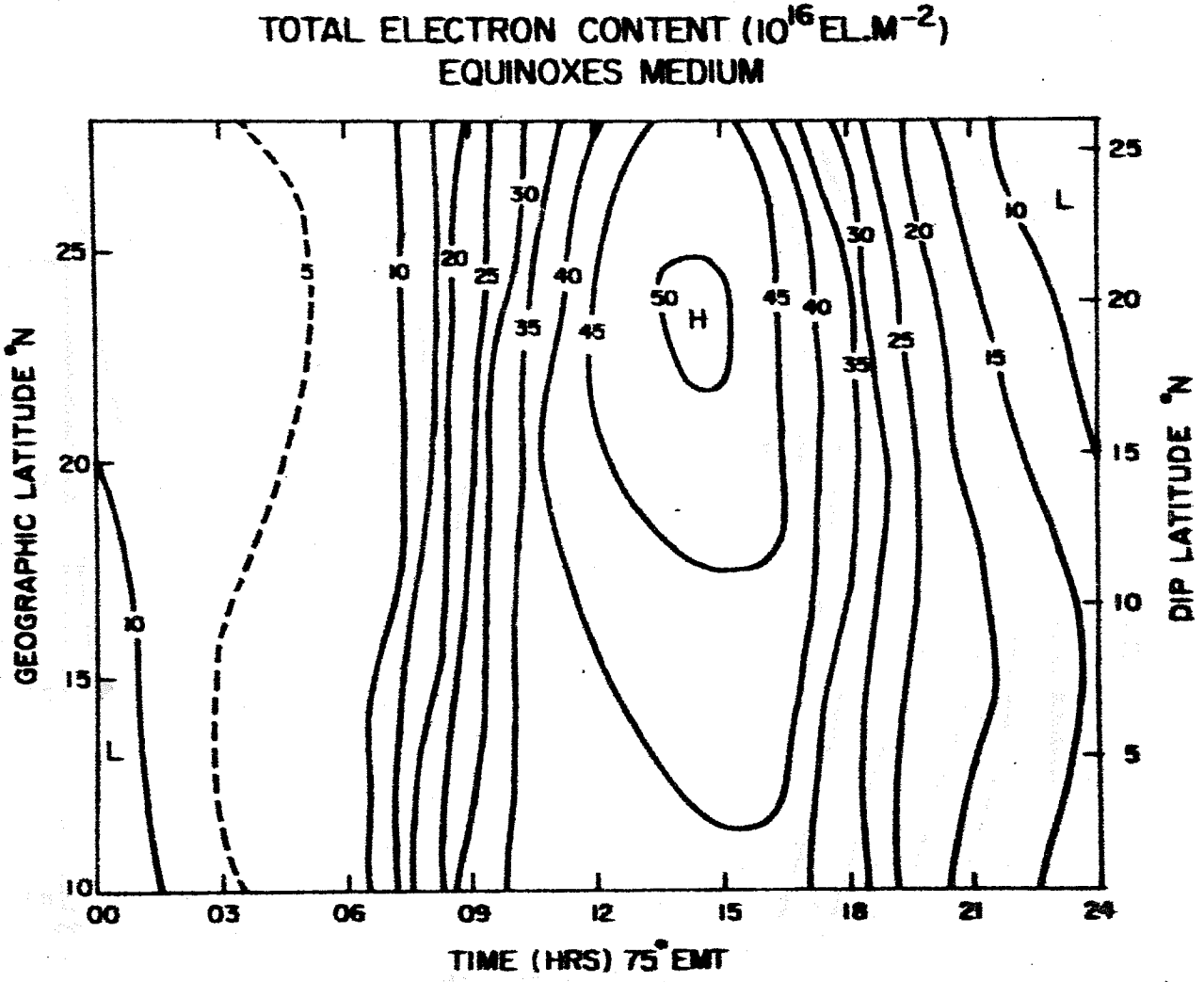

Fig.8.2c Similar to Fig.8.2a for equinoxes.

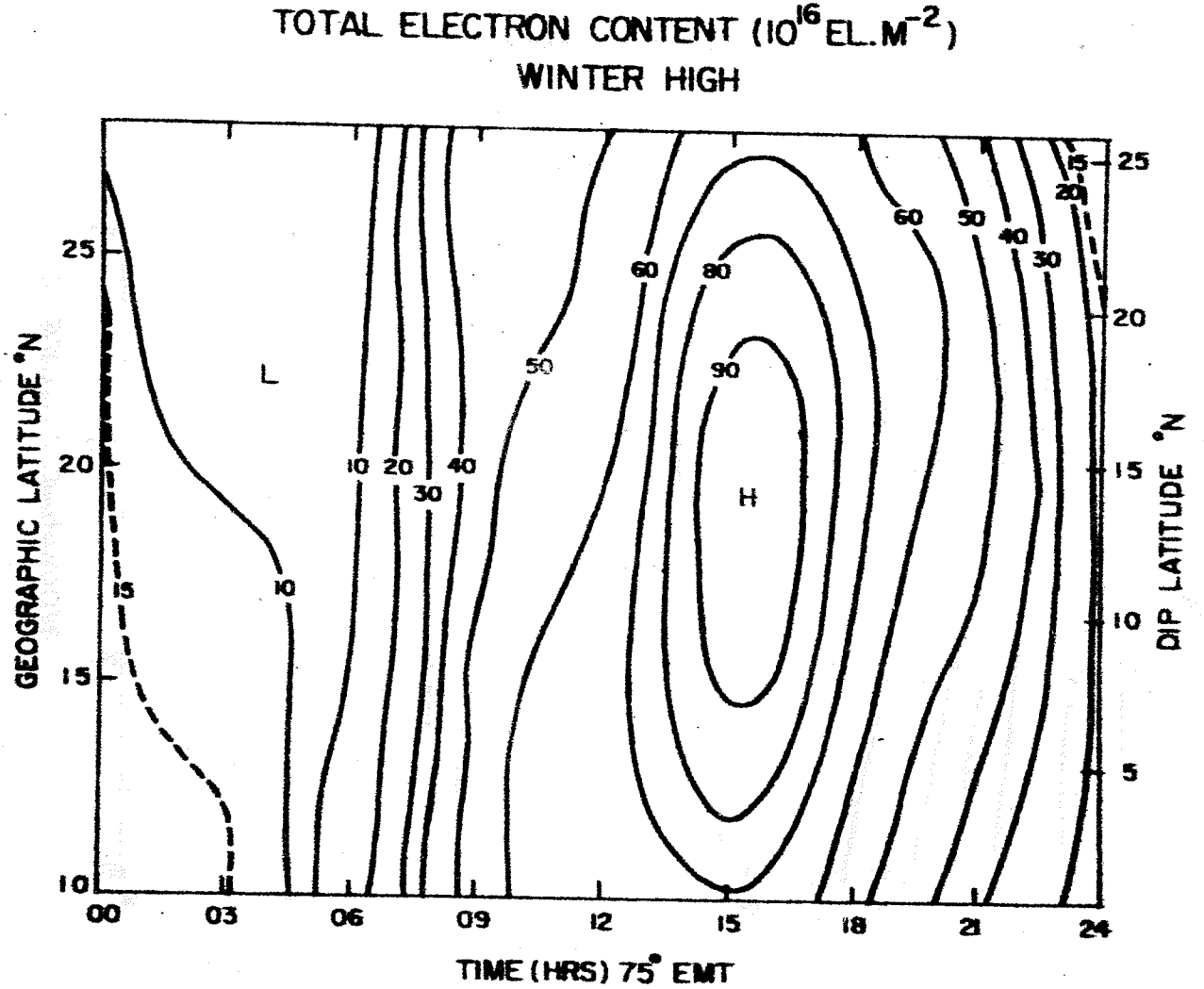

Fig.8.3a The N_F contour using the extended model for winter (high solar activity period).

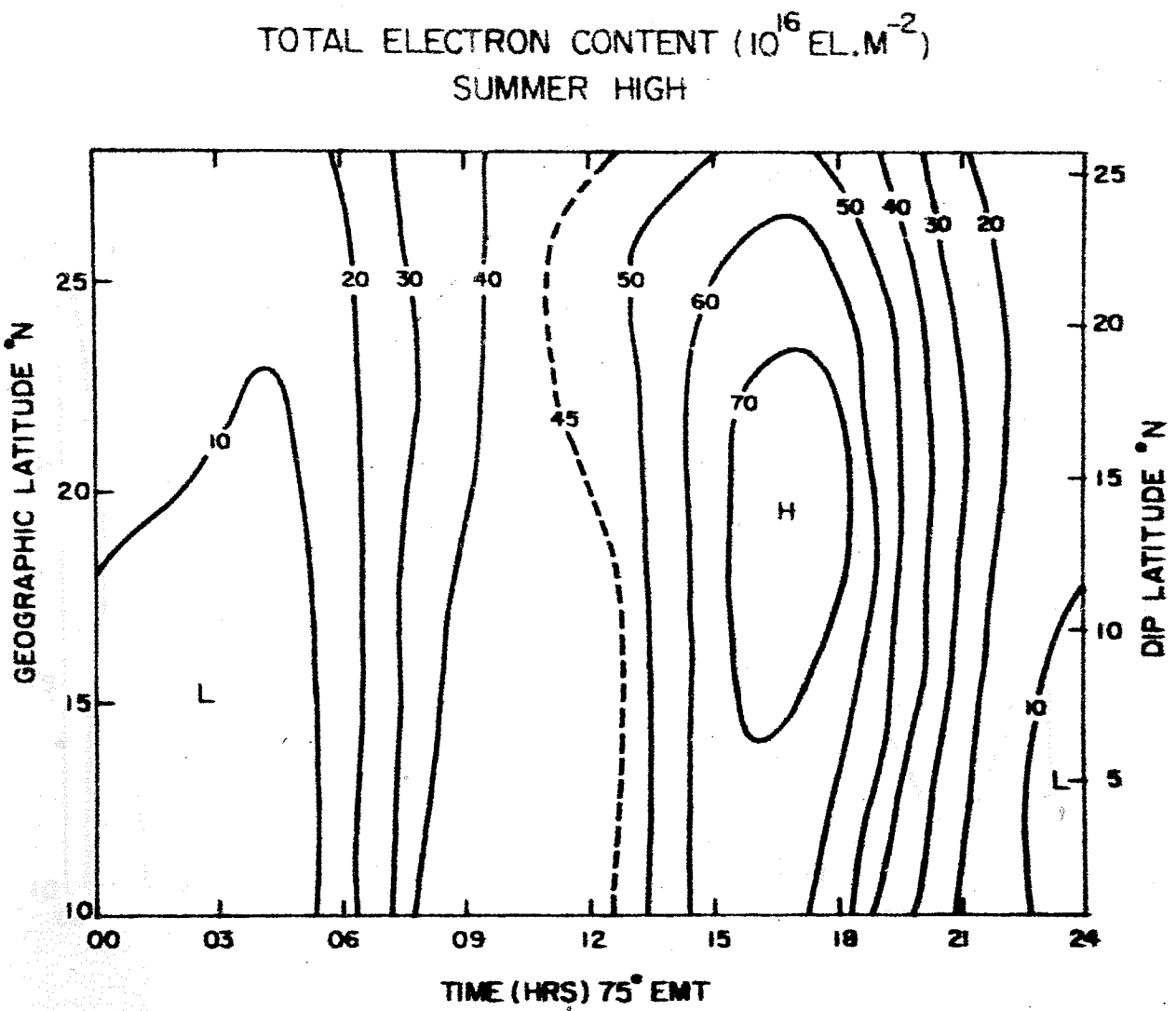

Fig.8.3b Similar to Fig.8.3a for summer.

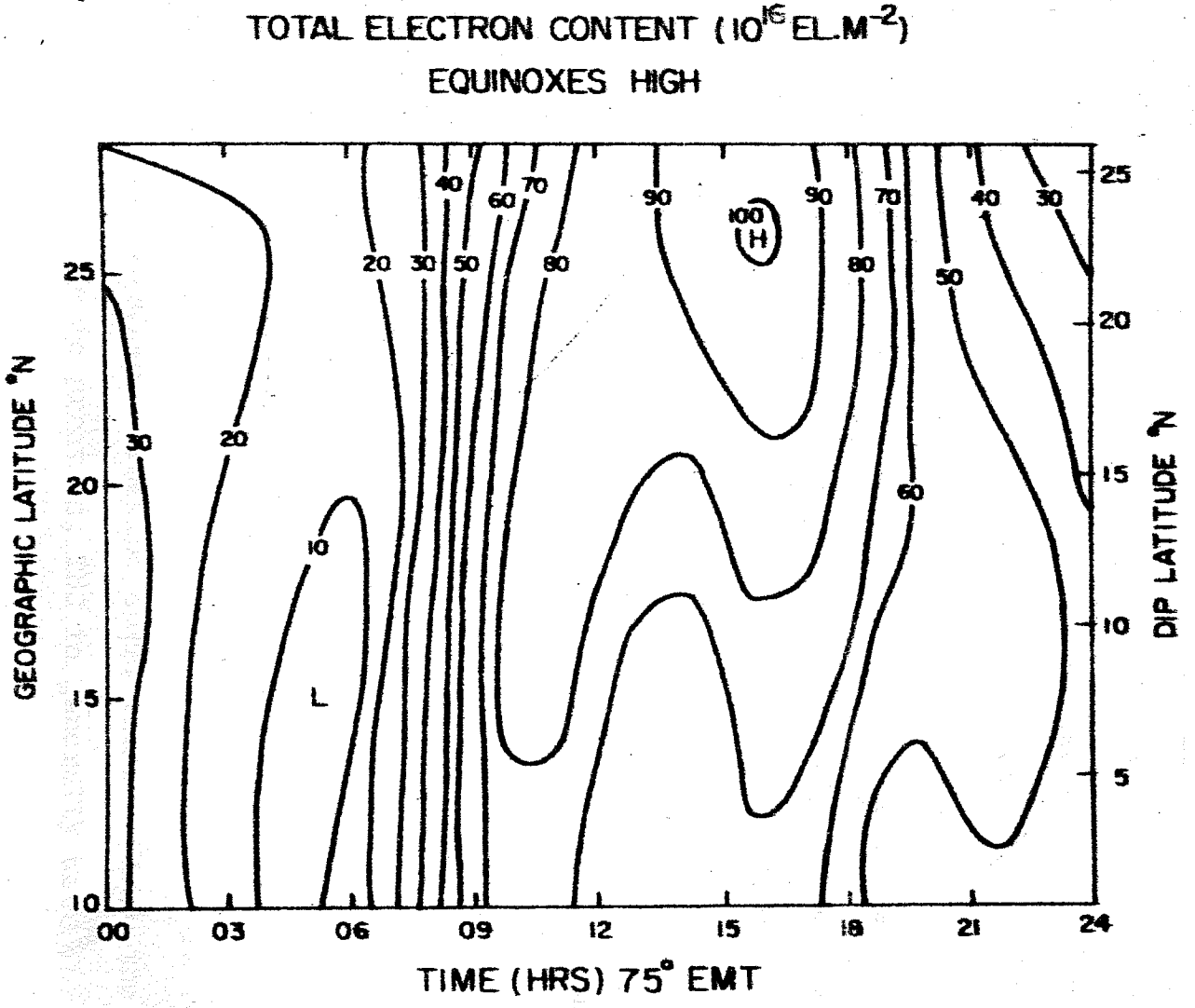

Fig.8.3c Similar to Fig.8.3a for equinoxes.

8.5 Application to Satellite Tracking

Satellite tracking systems suffer range, range rate, and angular refraction errors due to the electrons in the earth's ionosphere. To a first order accuracy these effects may be corrected if TEC along the path from the satellite to the observing station is known. The numerical model described in this chapter can be used to estimate the errors quickly. The amount of the time delay produced by the ionosphere on radio waves used for satellite tracking is directly proportional to the TEC along the path from the satellite to the tracking station which is given by:

$$T_g = \frac{1.34 \times 10^6}{f^2} \text{ TEC (nano second)} \qquad (8.2)$$

where TEC is expressed in units of 10^{16} el/m^2 column and f is system operating frequency in MHz. The range error R is given by:

$$R = C\, T_g \qquad (8.3)$$

where C is the velocity of light. Range rate errors are directly proportional to the time derivative of N_T and angular refraction errors can be approximated by the TEC, although a height profile of electron density along the path is required for precise angular refraction corrections. Since the profile is seldom known in practice, TEC is generally used for angular corrections also.

In determining TEC from a user location to a satellite, several geometrical calculations must be made. The TEC must be found at the

geographic point where the ray path intersects the mean ionospheric height, rather than at the user location. This point is taken here at a mean height of 350 km. For a satellite at an elevation angle of about 5°, this point is approximately 14 degrees of earth angle away from the user location. The obliquity, or slant factor, also must be calculated for the mean ionospheric location. Finally since the TEC is best ordered in magnetic rather than geographic coordinates, the assumption is made that the TEC is only a function of dip lat and local time at the sub-ionospheric location. If the exact form of all the necessary geometry calculations is used, the computer time used would be greater than that required for the TEC algorithm itself. Klobuchar (1975) made some simplifying assumptions to reduce the calculation complexity. The exact as well as the simplified expressions are as follows:

(i) Earth Angle:

The exact earth angle representation for a given elevation angle el is:

$$A = 90 - el - \sin^{-1}\left(\frac{R_E}{R_E+h}\cos el\right)$$

$$= 90 - el - \sin^{-1}(.948 \cos el) \qquad (8.4a)$$

for mean ionospheric height of 350 km.

The above expression is best estimated by:

$$A = \frac{445}{el+20} - 4 \qquad (8.4b)$$

This approximation is less than 0.2 degrees in error for all elevations greater than 10 degrees. It is off by only 0.4 degrees and 0.3 degrees at elevations of 5 and 0 degrees respectively.

(ii) Sub-ionospheric Coordinates:

Given the station coordinates, elevation angle and earth angle to the ionospheric point, its coordinates may be found by the following:

$$\phi_I = \sin^{-1} (\sin \phi_o \cos A + \cos \phi_o \sin A \cos az) \qquad (8.5a)$$

$$\lambda_I = \lambda_o + \sin^{-1} \left(\frac{\sin A \sin az}{\cos \phi_I} \right) \qquad (8.5b)$$

where ϕ_o is the station latitude and λ_o is the station longitude. If a flat earth approximation is used the following simplification can be made to the above two equations:

$$\phi_I = \phi_o + A \cos az \qquad (8.6a)$$

$$\lambda_I = \lambda_o + \frac{A \sin az}{\cos \phi_I} \qquad (8.6b)$$

For the latitude range of the present interest, the maximum error of these approximations is nearly 1°.

(iii) Conversion from Geographic to Dip Latitude:

$$\phi_{DL} = \phi_I + [- 3.42 + 10.6 \cos (\lambda_I - 261) + 4.1 \cos (2\lambda_I - 210) + 2.6 \cos (3\lambda_I - 182) + 1.5 \cos (4\lambda_I - 140)] \qquad (8.7a)$$

if $\lambda_I > 320$ or $\lambda_I < 140$

$$\phi_{DL} = \phi_I + [- 3.42 + 10.6 \cos (\lambda_I - 261) + 4.1 \cos (2\lambda_I - 210) + 2.6 \cos (3\lambda_I - 182) + 1.5 \cos (4\lambda_I - 140)] + 0.267 \cos (\lambda_I - 50) \phi_I \qquad (8.7b)$$

(iv) Finding the Local Time:

Given the universal time and the approximate longitude of the ionospheric point λ_I, the local time at the ionospheric point is simply:

$$t = UT + \frac{\lambda_I}{15} \quad \text{(hours)} \tag{8.8}$$

If t is greater than 24, make t = t-24 hours.

(v) The Obliquity Factor:

The vertical time delay at the sub-ionospheric point must be multiplied by an obliquity factor defined as the secant of the zenith angle at the mean ionospheric height. An average ionospheric height of 350 km is assumed. The exact obliquity or slant factor is:

$$SF = \text{Sec} \left[\sin^{-1} (.948 \cos el)\right] \tag{8.9a}$$

An approximation which is within 2 percent of the exact value for the elevation angle 5° to 90° is:

$$SF = 1+2 \left[\frac{96-el}{90}\right]^3 \tag{8.9b}$$

Above mentioned simplified formulae have been used to minimise the computation time required for the time delay and the range error calculations. The range errors for different locations of the satellite (i.e. different azimuth and elevation angles) as observed from Sriharikota (SHAR) and Ahmedabad have been calculated for equinoctial solar maximum conditions. The contour maps of the range error for SHAR on a grid of elevation angle vs. azimuth angle, for different local times have been shown in Fig.8.4(a-d).

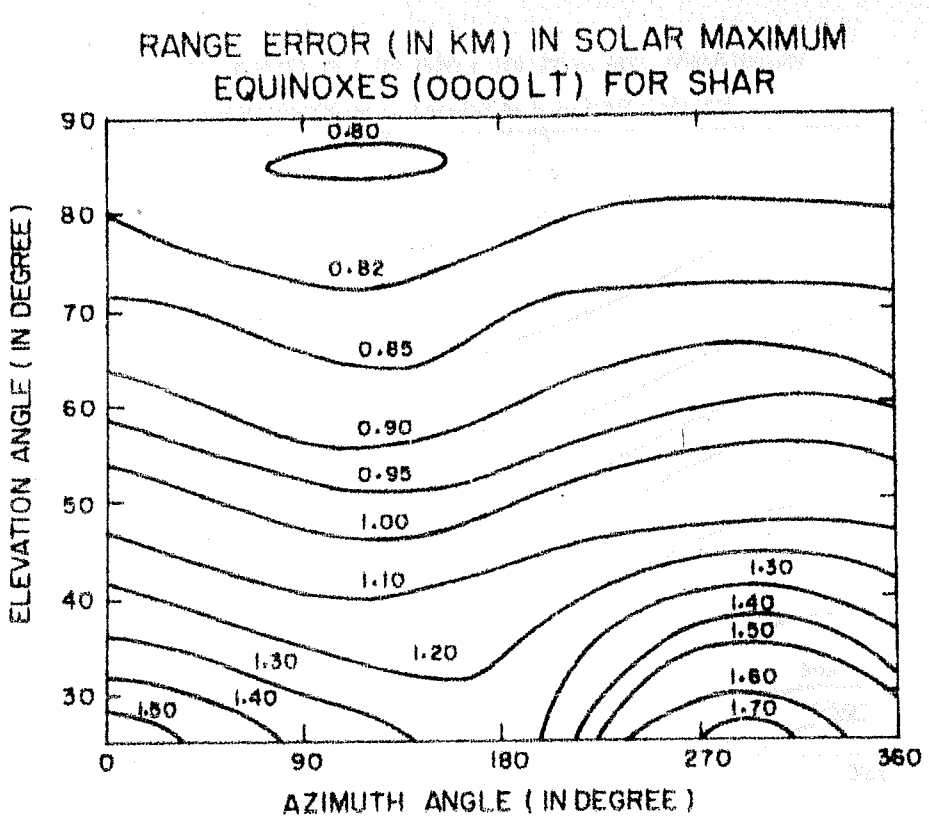

Fig.8.4a The contour maps of the range error for SHAR on a grid of elevation angle versus azimuth angle for 0000 LT.

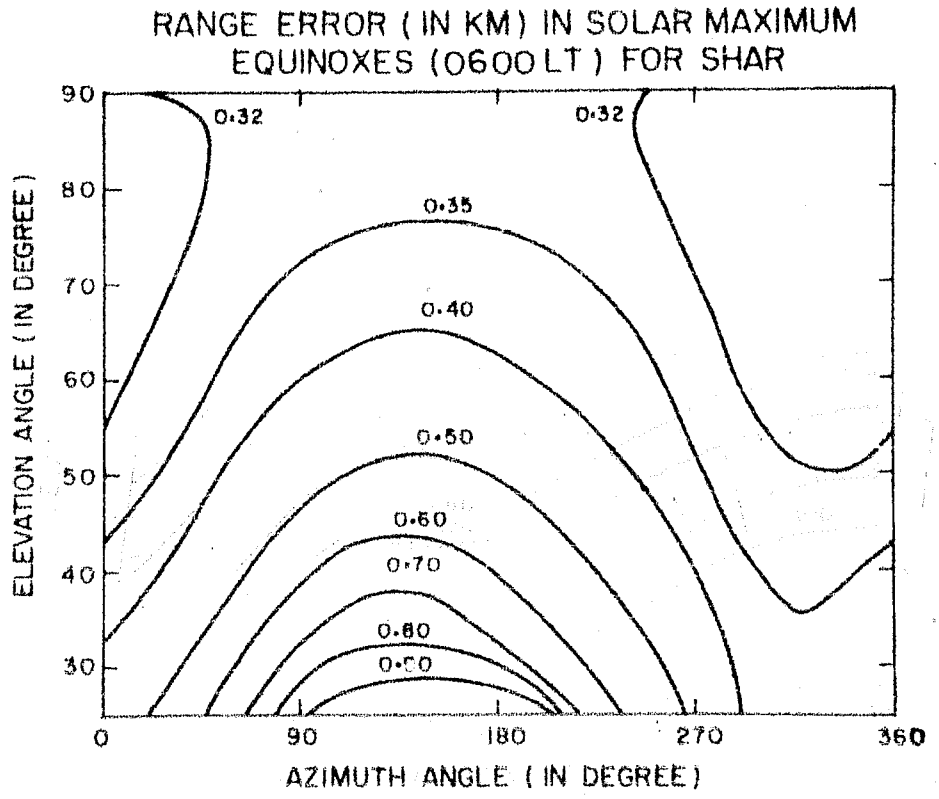

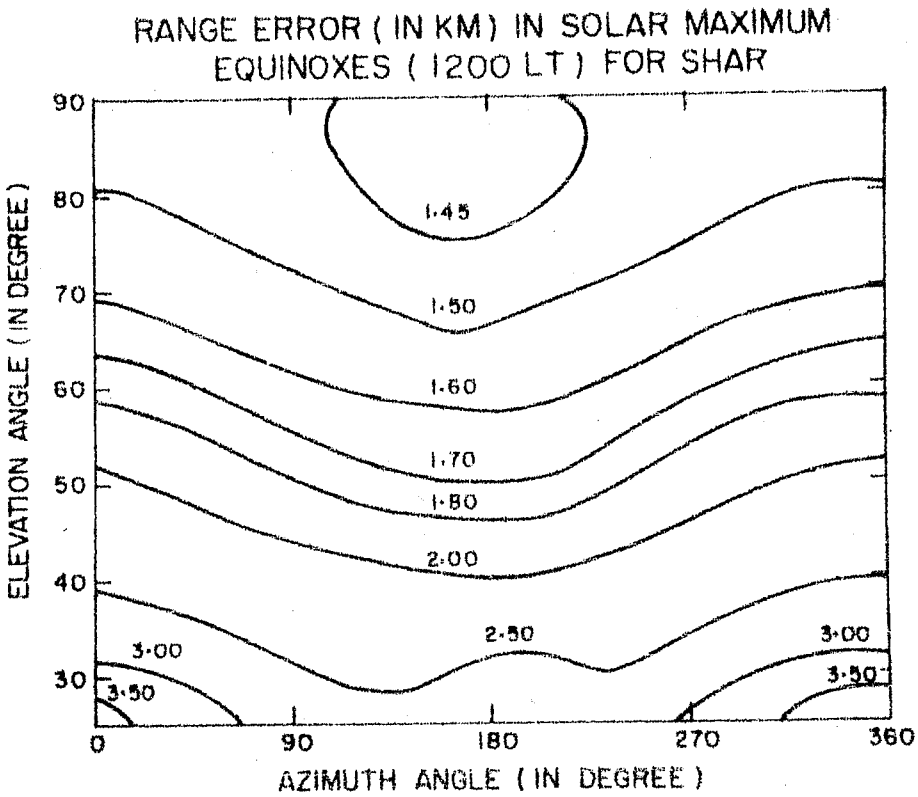

Fig.8.4c Same as Fig.8.4a for 1200 LT.

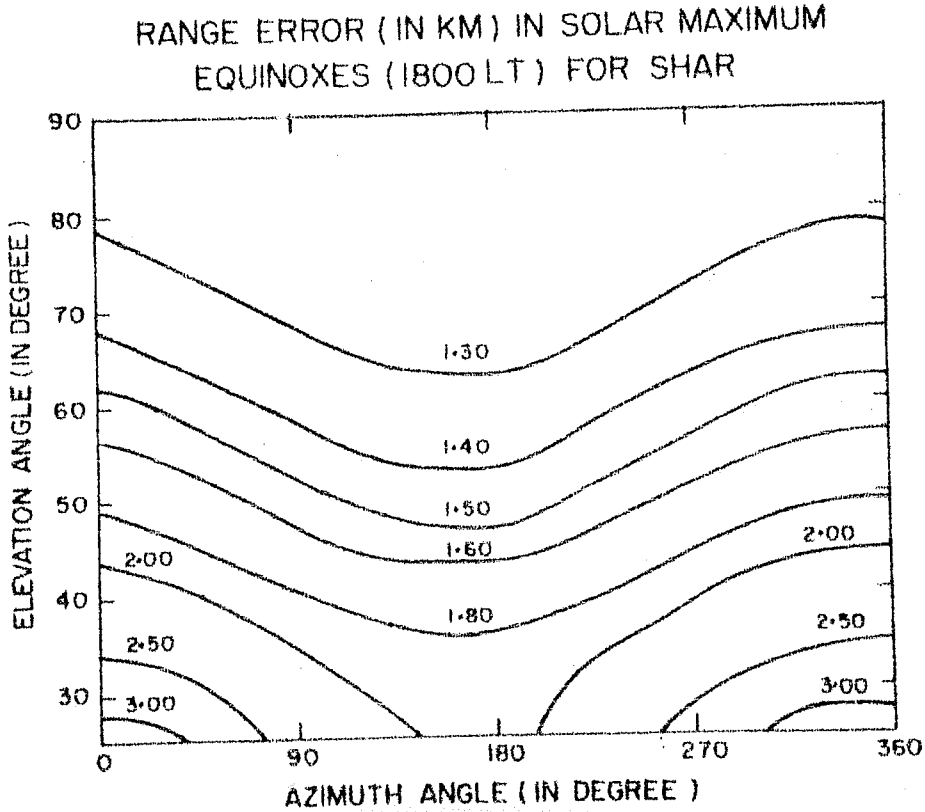

The similar contour maps have been built up for Ahmedabad and are shown in Fig.8.5 (a-d). In Fig.8.6(a,b) range errors for SHAR and Ahmedabad respectively from HF to S band have been shown for solar maximum equinox daytime conditions. For an elevation angle of 30°, the range errors at 40 MHz is about 30 km for SHAR and about 40 km for Ahmedabad. As one progresses into high frequency bands the error reduces e.g. for an elevation angle of 30°, the range errors at S band is about 7 meters for SHAR and about 9 meters for Ahmedabad.

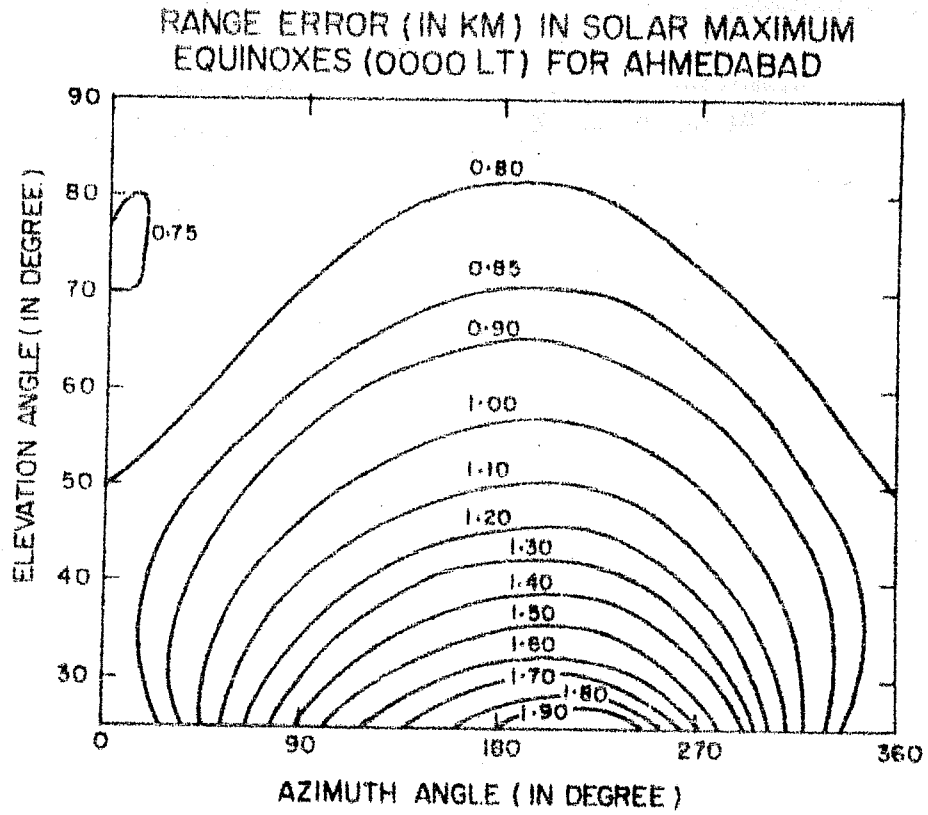

Fig.8.5a The contour maps of the range error for Ahmedabad on a grid of elevation angle versus azimuth angle, for 0000 LT.

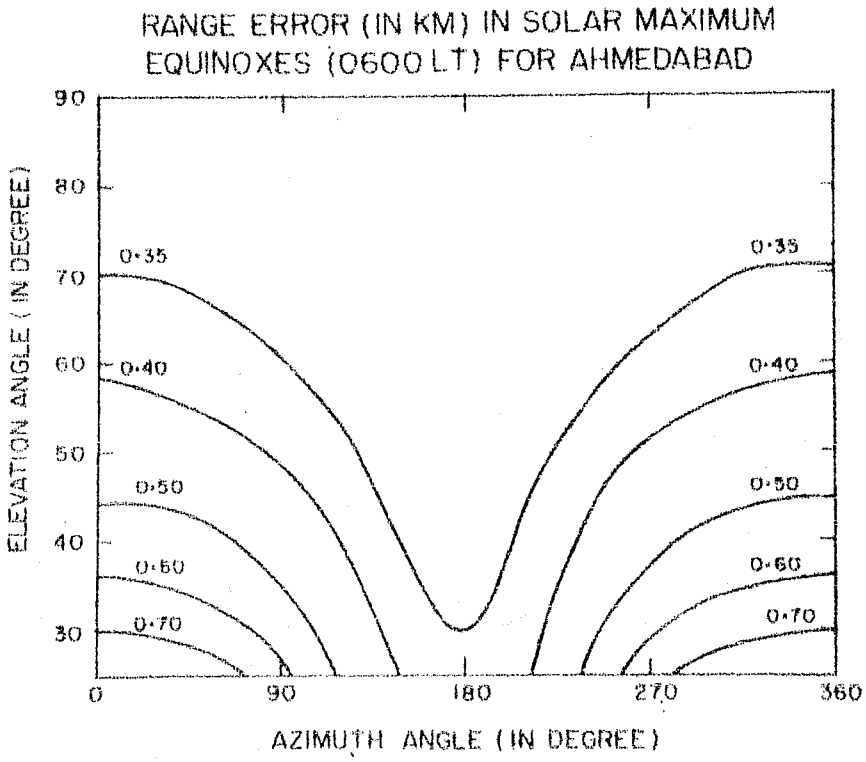

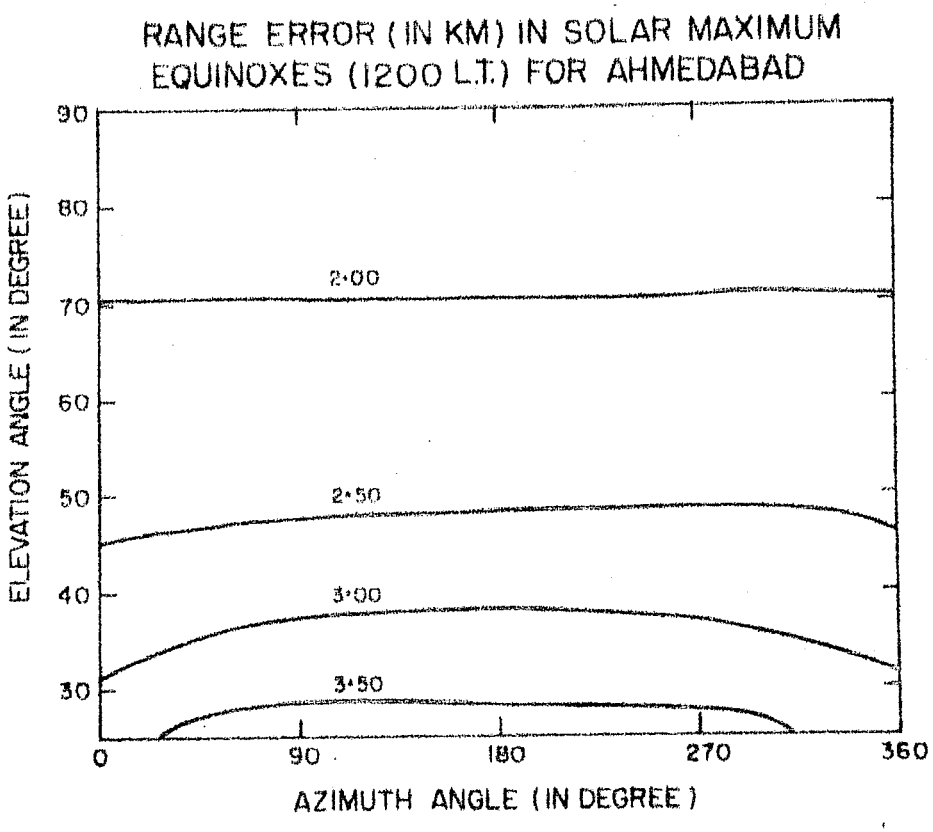

Fig.8.5c Same as Fig.8.5a for 1200 LT.

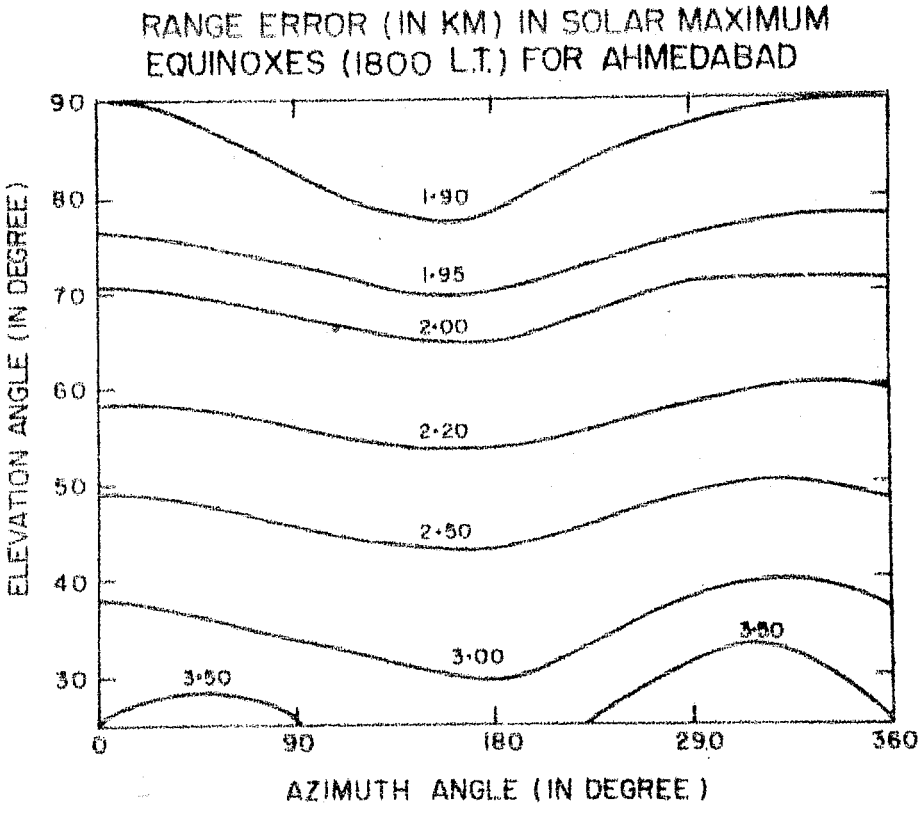

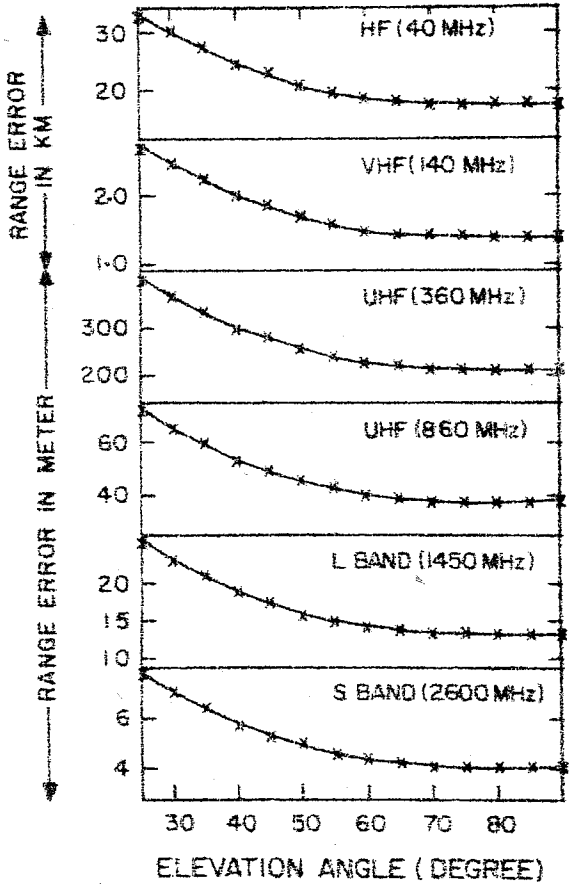

Fig.8.6a Range error in solar maximum equinoxes during daytime (1200 LT) for Ahmedabad when azimuth angle of satellite is 90°.

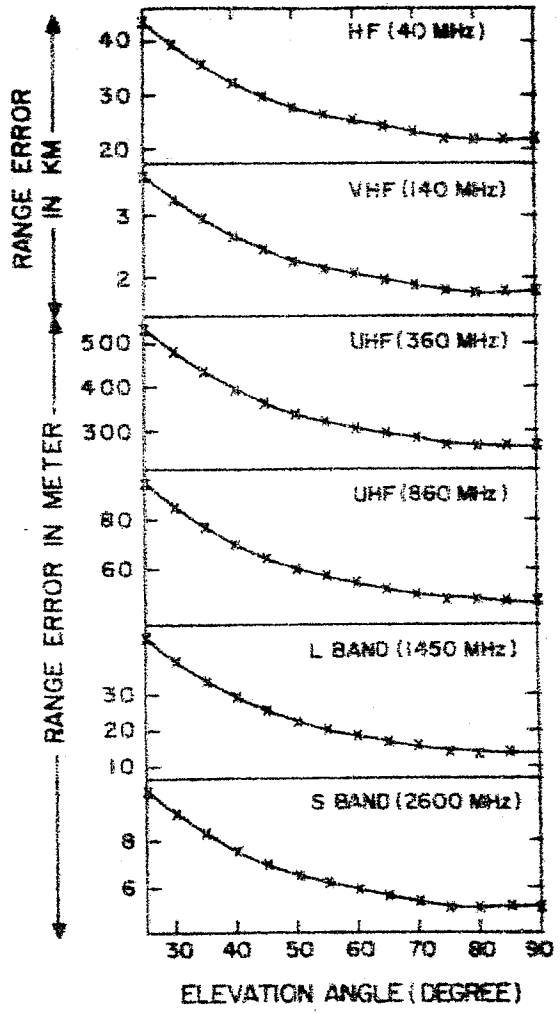

Fig.8.6b Same as Fig.8.6a for SHAR.

CHAPTER - IX

SUMMARY AND SUGGESTIONS

The present investigations deal with the studies of some of the physical properties of the ionosphere and the plasmasphere, at low and equatorial latitudes. The study is based on the (a) ionosphere electron content derived from Faraday rotation measurements, made at a chain of stations covering almost entire Indian sub-continent during the period October 1975 - August 1976 using radio beacons from the geostationary satellite ATS-6 and (b) the plasmasphere electron content derived from simultaneous Faraday rotation and the group delay measurements made at a low latitude station Ahmedabad (dip. lat. 18.6°N) during June, July 1976 and at a near equatorial station Ootacamund (dip. lat. 3°N).

In this chapter, the main conclusions of the present work have been summarised and also some suggestions for future work in this field, have been given.

The main conclusions are as follows:-

(i) For Ootacamund, a near equatorial station, the electron content N_F, obtained from Faraday rotation technique corresponds to electron content upto an altitude of 1500 km, with errors of the order of $\pm$ 5%, for the electron density profiles used in the present study.

(ii) No noon bite-out is observed in the equatorial total electron content (TEC), nevertheless one does observe a sharp decrease in the rate of increase of TEC during the period when F_2 region peak electron density (N_mF_2) shows a clear bite-out.

(iii) The daytime values of the ratio of top to bottomside electron content (N_a/N_b) are found to be in good agreement with the value calculated for a Chapman layer. During presunrise hours, N_a/N_b and slab-thickness (τ) show large peaks.

(iv) Although, TEC at all the stations in the present study show a semi-annual variation with maximum in equinoxes, the months within equinoxes show anomalous behaviour. Also the presence of "winter anomaly" is noted at the stations situated to the south (equatorward) of the crest of the equatorial anomaly. These features are found to be correlated with the seasonal variations of the electrojet strength.

(v) During geomagnetically disturbed period, the equatorial anomaly is found to be weakened with high values of the daytime equatorial TEC.

(vi) The storm time effects on electron contents obtained from Faraday rotation and the group delay measurements respectively are found to be in general similar. The variations in the equatorial electrojet intensity are found to be qualitatively responsible for the significant storm time effects in TEC. Some abnormal changes in TEC are suggested to be due to the effects of neutral winds.

(vii) TEC at all the stations of the chain, and also the equatorial F_2 region peak electron density (N_mF_2) and slab-thickness show significant lunar tidal effects. The lunar perturbations are found to be of the order of (1-4) x 10^{16} el.m^{-2} in TEC, 1 x 10^{11} el m^{-3} in N_m and about 40 km in τ. The semi-monthly (M_2) tides in N_mF_2 are found to be very nearly in phase apposition to that of slabthickness.

(viii) The lunar daily variation in TEC, near the crest is found to be predominantly semi-diurnal (L_2) which in turn is thought to be due to the additional "Fountain effect" caused by the L_2 variation of the electric field at the equatorial region. The amplitudes of L_2 and M_2 oscillations are found to be higher at the crest as compared to at either side of the crest. The amplitudes of the lunar oscillations are in general found to be larger in daytime than in night-time.

(ix) In contrast to previous studies using f_oF_2 data, the latitudinal variation of the phase of the L_2 oscillation in N_F does not show any phase reversal except that the phase at Ootacamund (9.5 l.hr) differs from the phase at the stations near the crest (11.5 l.hr) by about two hours.

(x) A numerical model of TEC at low latitudes has been constructed from the Faraday rotation measurements, made during October 1975 - July 1976 which corresponds to a low solar activity period. The model has also been extended for medium and high

solar activity periods and these have been used to estimate range errors for the Indian satellite tracking station Sriharikota (SHAR) and also for Ahmedabad for different solar activity periods.

(xi) The low latitude plasmasphere electron content (N_P), measured at Ahmedabad, increases from sunrise until nearly midnight, after which it decays to a near sunrise minimum. The post-midnight decay in N_P is accompanied by nearly constant, low values of local ionospheric electron content N_F.

(xii) The mean daily variation of the residual component N_R (group delay content minus Faraday content) at Ootacamund shows two maxima, one around dusk (1800 hr LT) and the other during prenoon hours (0900 hr LT). The prenoon maximum is found to be preceded by a dip around dawn. During geomagnetic storms N_R decreases and the decrease is found to be associated with enhancement in solar wind speed (V_{sw}). The empirical relationships between N_R and K_p and also between N_R and V_{sw} have been obtained.

Suggestions for Future Work:-

In the present study, the electron content data corresponds to a low solar activity period (1975-76) and a numerical model based on these data, has been extended for medium and high solar activity periods. It would be highly desirable to have the actual electron content data from a geostationary satellite for high solar activity period so as to make such numerical models more reliable.

As it was noted in the storm time studies of TEC, the neutral winds play an important role in the ionospheric changes. It would be interesting to study the evolution of ionospheric storms at closeby spaced locations right from poles to equator as this would throw considerable light on the actual movement of neutral winds. As we have seen that there are difficulties in converting the equatorial Faraday rotation measurements into electron content with high accuracy. This problem can probably be tackled if actual electron density profiles for different typical conditions are available. Such profiles can be utilised to recalibrate the magnetic field factor so as to improve the accuracy. Lastly it would also be interesting to have simultaneous and in the same longitude zone, the observations of whistler measurements and of plasmasphere electron content measurements. This would enable better understanding of the ionosphere-plasmasphere coupling during different conditions.

REFERENCES

Ahmed Iqhbal and Rao B.R. (1967) J. Instn. Telecom. Engrs., 13, 54.

Almeida O.G. (1973) J. Atmos. Terr. Phys., 35, 1657.

Anderson D.N. (1971) NCAR Co-operative Thesis No.24, University of Colorado and High Altitude Observatory, NCAR.

Anderson D.N. (1973a) Planet. Space Sci., 21, 409, 421.

Anderson D.N. (1973b) J. Atmos. Terr. Phys., 35, 753.

Appleton E.V. and Barnett M.A.F. (1925) Nature, 115, 333.

Appleton E.V. and Ingram L.J. (1935) Nature (Lond), 136, 548.

Appleton E.V. et al. (1937) Phil. Trans. Roy. Soc., A236, 191.

Appleton E.V. (1946) Nature, 157, 691.

Axford W.I. and Hines C.O. (1961) Can. J. Phys., 39, 1433.

Axford W.I. (1969) Rev. Geophys. Space Phys., 7, 421.

Bailey D.K. (1948) Terr. Mag. Atmos. Elec., 53, 41.

Bandyopadhyay P. (1970) Planet. Space Sci., 18, 129.

Banks P.M. and Kockarts G. (1973) 'Aeronomy' Part A, B, Academic Press Inc. (New York and London).

Bartels J. and Fanselau G. (1938) Abh. Geophys. Inst. Postdam Nr.2.

Bartels J. and Johnston H.F. (1940) Terr. Mag. Atmos. Elec., 45, 269.

Basu S. and Das Gupta A. (1967) J. Geophys. Res., 72, 5555.

Basu S. and Das Gupta A. (1968) J. Geophys. Res., 73, 5599.

Basu S. et al. (1974) Indian J. Rad. & Space Phys., 3, 207.

Basu S. et al. (1975) Ann. Geophys., 31, 497.

Berkner L.V. and Wells W.H. (1934) Terr. Magn. Atmos. Elec., 39, 215.

Berkner L.V. and Seaton S.L. (1940) Terr. Magn. Atmos. Elec., 45, 419.

Bernhardt P.A. et al. (1976) J. Geophys. Res., 81, 5957.

Binasack J.H. (1967) J. Geophys. Res., 72, 5231.

Blumle L.J. (1962) J. Geophys. Res., 67, 4601.

Bramley E.N. and Peart M. (1965) J. Atmos. Terr. Phys., 27, 1201.

Bramley E.N. and Young M. (1968) J. Atmos. Terr. Phys., 30, 99.

Breit G. and Tuve M.A. (1925) Nature, 116, 357.

Brice N.O. (1967) J. Geophys. Res., 72, 5193.

Brown R.A. (1956) J. Atmos. Terr. Phys., 9, 144.

Browne I.C. et al. (1956) Proc. Phys. Soc., B69, 901.

Burg J.D. et al. (1973) J. Atmos. Terr. Phys., 35, 617.

Burkard O. (1951) J. Atmos. Terr. Phys., 1, 349.

Carpenter D.L. (1963) J. Geophys. Res., 68, 1675.

Carpenter D.L. (1966) J. Geophys. Res., 71, 693.

Carpenter D.L. (1967) J. Geophys. Res., 72, 2969.

Carpenter D.L. and Stone K. (1967) Planet. Space Sci., 15, 395.

Carpenter D.L. (1970) J. Geophys. Res., 75, 3837.

Carpenter D.L. et al. (1972) J. Geophys. Res., 77, 2819.

Carpenter D.L. and Park C.G. (1973) Rev. Geophys. Space Phys., 11, 133.

Carpenter D.L. and Seely N.T. (1976) J. Geophys. Res., 81, 2728.

Chandra S. and Herman J.R. (1969) Planet. Space Sci., 17, 841.